Solidification en présence de champs magnétiques intenses

Xi Li

INSTITUT NATIONAL POLYTECHNIQUE DE GRENOBLE

N° attribué parla bibliothèque
|__|__|__|__|__|__|__|__|__|__|

T H E S E

pour obtenir le grade de

DOCTEUR DE L'INP Grenoble

Spécialité : Science et Génie de Matériaux

préparée au laboratoire SIMAP EPM/Madylam, ENSHMG BP 38402 St Martin d'Heres Cedex, France

dans le cadre de l'Ecole Doctorale « *Matériaux et Génie des Procédés* »

présentée et soutenue publiquement

par

Xi LI

le 16 Juillet 2007

Titre :

Solidification en presence de champs magnétiques intenses

Solidification behavior in the presence of a high magnetic field

Directeurs de thèse :

Professeur: Yves FAUTRELLE
Professeur: Zhongming REN

JURY

M. Jean-Charles JOUD	, Président
M. Gérard LESOULT	, Rapporteur
M. Michel RAPPAZ	, Rapporteur
M. Zhongming REN	, Examinateur
M. Yves FAUTRELLE	, Examinateur
M. Xiemin MAO	, Examinateur

Acknowledgment

To the largest degree, the author wishes to express his sincere gratitude to Professor **FAUTRELLE Yves**, from the Institute National Polytechnique de Grenoble, for his helpful guidance and continuous support for the work and life. And, the author is grateful to Professor **REN Zhongming** in Shanghai University of China for his help and guidance. These years that I spent working with Profs. **FAUTRELLE** and **REN** have given me a deep appreciation of their vast knowledge. Two respectable supervisors continuing interest in this work and valuable suggestions made this work possible.

I am indebted to Mrs. **FAUTRELLE Jocelyne** who helped me to translate and check French. Without her help, it ought to be difficult to finish this paper.

Acknowledgment is also to EGIDE, the European Space Agency through the IMPRESS project and the Natural Science Foundation of China for the opportunity and financial support to perform the work.

Stimulating discussion with Professor R. Moreau, Professor T. Duffar and Doctor Kader Zaïdat in EPM laboratory in MADYLAM are gratefully acknowledged. Many thanks are, too, to those who were concerned with the research work in Laboratory EPM MADYLAM in Grenoble. and EPM laboratory of Shanghai University.

My special thanks are due to the love of my parents and wife who always believe in me and encourage me to carry on my dreams through uncountable prayers. Without their love and understanding, my studying could not be realized.

Xi LI

TABLE DES MATIERES

[A1] Xi Li, Yves Fautrelle, Zhongming Ren
Influence of an axial high magnetic field on the liquid–solid transformation in Al–Cu hypoeutectic alloys and on the microstructure of the solid, Acta Materialia 55 (2007) 1377–1386.
[A2] Xi Li, Yves Fautrelle, Zhongming Ren
Influence of thermoelectric effects on the solid-liquid interface shape and cellular morphology in the mushy zone during the directional solidification of Al-Cu alloys under the magnetic field, Acta Materialia 55 (2007) 3803-3813.
[A3] Xi Li, Yves Fautrelle, Zhongming Ren
Influence of a high magnetic field on the columnar dendrite growth during the directional solidification, Acta Materialia 55(2007) 5333-5347.
[A4] Xi Li, Zhongming Ren,Yves Fautrelle
Effect of a high axial magnetic field on the microstructure in a directionally olidified Al–Al2Cu eutectic alloy, Acta Materialia 54 (2006) 5349–5360.
[A5] Xi Li, Zhongming Ren,Yves Fautrelle
The spiral growth of lamellar eutectics in a high magnetic field during the directional solidification process, Scripta Materialia 56 (2007) 505–508.
[A6] Xi Li, Zhongming Ren,Yves Fautrelle
Effect of high magnetic fields on the microstructure in directionallysolidified Bi–Mn eutectic alloy, Journal of Crystal Growth 299 (2007) 41–47.
[A7] Xi Li, Zhongming Ren,Yves Fautrelle
Effect of a high magnetic field on the phase transformation, morphology and magnetic properties of the MnBi and $Mn_{1.08}$Bi compounds.
[A8] Xi Li, Zhongming Ren,Yves Fautrelle
The alignment, aggregation and magnetization behaviors in MnBi/Bi composites solidified under a high magnetic fiel, Intermetallics 15 (2007) 845-855.
[A9] Xi Li, Zhongming Ren,Yves Fautrelle
Effects of the simultaneous imposition of electromagnetic and magnetic forces on the solidification structure of pure Al and Al-4.5wt.%Cu alloy, Journal of Materials Processing Technology (In press).

CHAPITRE 1: INTRODUCTION

1.1 Développement des recherches sur les procédés d'élaboration des matériaux sous champ magnétique statique intense

En 1982 l'Union Internationale de Mécanique Théorique et Appliquée (IUTAM) organisait à Cambridge (Angleterre) le premier symposium sur les phénomènes de Magnétohydrodynamique (MHD). Cette date marqua le point de départ d'une véritable prise de conscience de la part de chercheurs tant en Asie qu'en Europe de l'urgence de travailler sur les applications de ces phénomènes. C'est dans cette perspective que fut créé le Comité EPM (Electromagnetic Processing of Materials ou Elaboration par Procédés Magnétiques) qui organisa son premier congrès à Nagoya (Japon) en 1994. Le deuxième se tint à Paris en 1997, puis le congrès eut lieu tous les trois ans alternativement en Asie et en Europe. Durant cette période, des laboratoires centrés sur la thématique EPM furent créés au Japon, en France et en Chine. A présent les procédés électromagnétiques d'élaboration des matériaux sont reconnus comme un moyen d'améliorer les propriétés des matériaux et de développer de nouvelles technologies. La qualité de surface et la structure de solidification des métaux de fonderie ont été améliorées par l'imposition d'un champ magnétique au cours du procédé d'élaboration. Grâce à l'amélioration de la technologie des bobines supraconductrices le champ électromagnétique pourrait à l'avenir jouer un rôle majeur en permettant de mieux contrôler le phénomène de solidification des métaux, d'obtenir une meilleure qualité de l'électrodéposition et d'empêcher la corrosion des métaux.

Récemment, avec le développement des aimants supraconducteurs, il est possible de disposer d'un champ magnétique intense et celui-ci est appliqué dans différents domaines scientifiques. La découverte de nombreux phénomènes intéressants liés au champ magnétique intense ont ouvert la voie à la création d'un nouveau champ scientifique, celui des champs magnétiques intenses. Ainsi le nouveau domaine de l'élaboration des matériaux sous champ magnétique intense est en train de se développer sous le vocable EPM. L'action principale d'un champ magnétique intense sur les procédés d'élaboration des matériaux concerne l'alignement, la texturation de la structure, son influence sur les transformations de phase, l'effet sur l'évolution des joints de grain etc. Les principaux résultats de la littérature sont résumés ci-après.

1.1.1 Effet du champ magnétique sur l'orientation des cristaux et la phase d'alignement

L'orientation des cristaux est un facteur qui influence de manière cruciale les propriétés électriques, magnétiques et mécaniques des matériaux. C'est la raison pour laquelle des recherches sur les possibilités d'aligner des cristaux ont été développées.

Jusqu'à présent l'alignement pendant la solidification, l'électrodéposition, le dépôt en phase vapeur et la transformation à l'état solide a été obtenu sous champ magnétique intense. En 1981, Mikelson et Karklin [1] ont obtenu la première structure de solidification alignée avec des alliages Al-Ni, Al-Cu, Bi-Cd et Cd-Zn sous un champ magnétique de 0.5-1.5T. Par la suite, Stavitsky et al.[2] ont trouvé que la phase primaire MnBi s'alignait le long de la direction d'un champ magnétique de 2.5T pendant la solidification des alliages Bi-(0.9-10)wt.%Mn (Figure 1.1). De Rango et al. [3] ont pu réaliser la texturation interne d'un matériau supraconducteur $YBa_2Cu_3O_7$ pendant le processus de solidification sous un champ magnétique intense de 5T. Katsuk [4] a montré que le benzophénone diamagnétique cristallisé à partir de n-hexane ainsi que les chlorures de potassium KCl et de barium $BaCl_2$ cristallisés en solution s'alignaient sous un champ magnétique de 10T. La croissance d'un cristal texturé de Bi-2201 [5] et de Bi-(Pb)2212 [6] a également été obtenue sous un champ magnétique intense. Asai [7] a mis en évidence l'alignement perpendiculaire de la phase primaire pendant la solidification de l'alliage Al-Si-Fe sous un champ magnétique intense. De plus, il a été montré qu'au cours des processus d'électrodéposition et de dépôt en phase vapeur sous champ magnétique, les cristaux de Zinc et de Bismuth [8] alignaient leur direction préférentielle de magnétisation selon le champ magnétique. Il a été également montré que le degré d'alignement croissait avec l'augmentation de l'intensité du champ magnétique. Les résultats ci-dessus indiquent que l'application d'un champ magnétique est capable de texturer les microstructures.

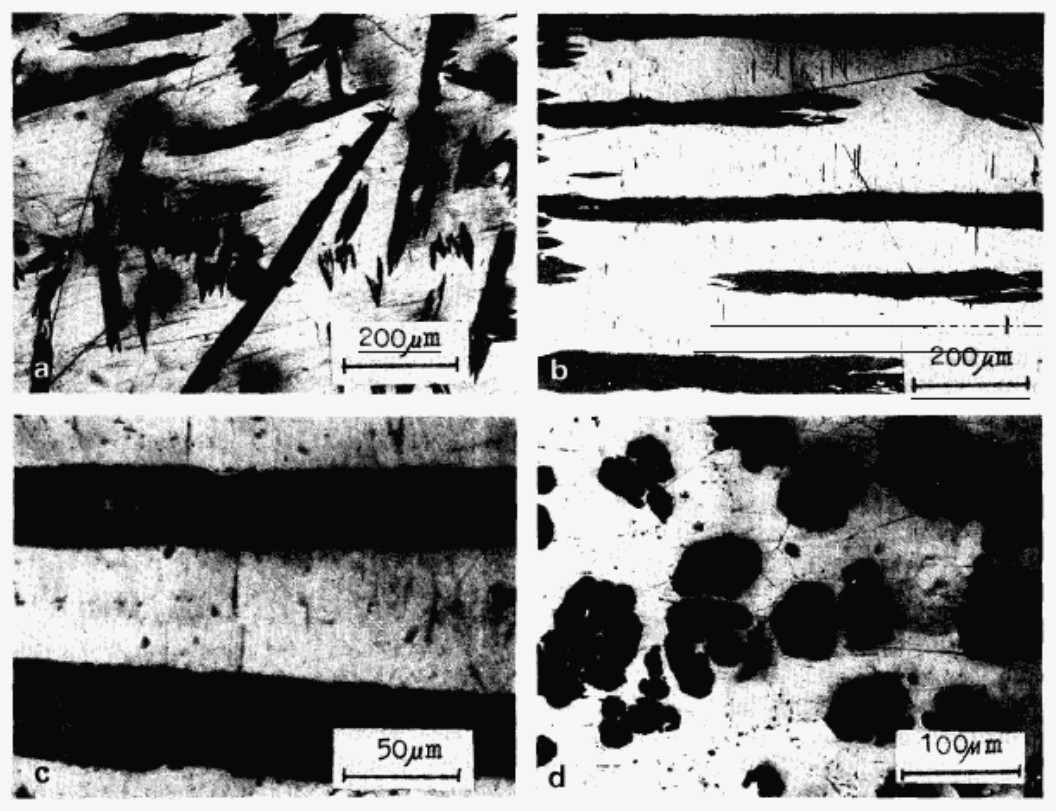

Fig. 1.1. The microstructure of Bi-10wt.%Mn alloy: (a) crystallization without external magnetic field; (b,c) section parallel to applied magnetic field; (d) section normal to applied magnetic field.

L'effet d'alignement des cristaux se produit sans apparition de transformation de phase. L'alignement des cristaux pendant la phase de transformation à l'état solide a été mis en évidence lorsque l'on appliquait un champ magnétique intense. La première observation de microstructures alignées dans des aciers, fut faite sur des alliages Fe-0.1C et Fe-0.6%C au cours de la transformation $\alpha \rightarrow \gamma$ sous un champ magnétique de 8T [9]. Les microstructures forment une chaîne ou des colonnes de phase γ qui se développent le long du champ magnétique dans la matrice de la phase α comme la montre la Figure 1.2. Le mécanisme de formation de la structure alignée est attribué à l'interaction dipolaire entre les noyaux de la phase γ jouant le rôle de trous au milieu de la phase ferromagnétique α. Par la suite, le même auteur en référence [10] est parvenu à former une microstructure alignée dans les aciers pendant la phase de transformation de l'austénite en ferrite sous un champ magnétique de 12T. Dans cette même étude, le mécanisme de formation des structures alignées sous champ magnétique est analysé selon le point de vue de la nucléation et croissance des grains de ferrite dans la phase austénite.

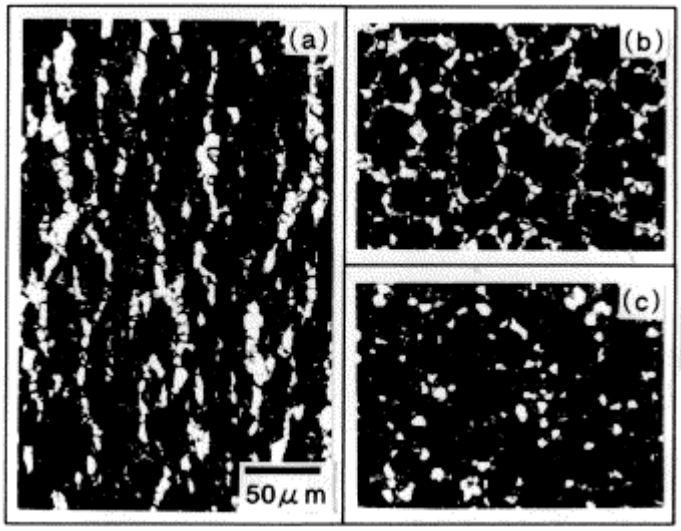

Fig. 1.2. Microstructures of Fe-0.6wt.%C specimens kept at 745°C for 45 min: (a) the cross section parallel to a magnetic field of 8T; (b) perpendicular to the field; and (c) the same treatment in zone magnetic field [9].

Le mécanisme d'alignement pourrait être attribué à la rotation d'un grain anisotrope et au changement de l'anisotropie de croissance sous l'effet d'un champ magnétique.

En général, un monocristal a différentes susceptibilités magnétiques qui dépendent du cristal (i.e., anisotropie magnétique) comme il est montré dans la Figure 1.3. Lorsqu'un cristal possédant une anisotropie magnétique est placé dans un champ magnétique, le cristal tend à s'orienter vers le champ magnétique. L'effet d'orientation du champ magnétique homogène sur un cristal anisotrope caractérisé par une anomalie de la susceptibilité $\Delta\chi$ le long de deux

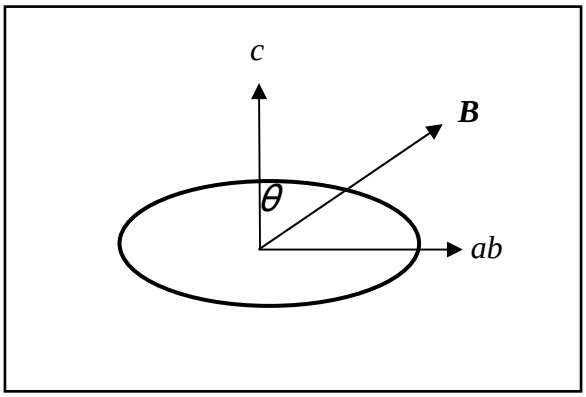

Fig. 1.3. An anisotropic grain in a magnetic field. *H* is the magnetic field direction. *c* and *ab* are the crystallographic axes, respectively.

axes mutuellement perpendiculaires sans prendre en considération l'influence de la forme du cristal, peut être décrit par l'équation suivante [11] :

$$K = \frac{\Delta\chi}{2\mu_0} B^2 V \sin 2a \qquad (1.1)$$

où α est l'angle entre le champ magnétique B et l'axe correspondant à la susceptibilité maximale. A partir de l'équation précédente, on peut en déduire que le cristal paramagnétique dans le champ magnétique homogène aura tendance à aligner son axe de magnétisation préférentielle le long du champ magnétique, tandis que pour un cristal diamagnétique ce même axe se positionnera perpendiculairement au champ magnétique. En principe, l'action d'orientation du champ magnétique affecte toujours un cristal possédant une anisotropie magnétique. Cependant, à cause de la présence de forces de viscosité, de la convection dans le bain et de l'interaction des cristaux entre eux et les parois du creuset, l'alignement peut ne pas se produire.

D'autre part, d'un point de vue thermodynamique, la magnétisation d'un cristal est un processus impliquant la prise en compte d'une énergie de magnétisation dans le système. L'énergie magnétique peut être exprimée de la façon suivante [12]:

$$G_M = -\int_0^{H_{ex}} \mu_0 M dH_{ex} \qquad (1.2)$$

Pour une substance non ferromagnétique

$$M = \chi H_{\mathrm{ex}} \qquad (1.3)$$

Insérant l'équation (1.3) dans l'équation (1.2) cela donne

$$G_{\mathrm{M}} = -\int_0^{H_{ex}} \mu_0 \chi H_{\mathrm{ex}} dH_{\mathrm{ex}} = -\frac{1}{2}\mu_0 \chi H_{\mathrm{ex}}^2 \qquad (1.4)$$

où G_M est l'entropie de magnétisation, $\mu_0 = 4\pi \times 10^{-7}$ H.m^{-1} la perméabilité magnétique du vide, H_{ex} le champ magnétique imposé et χ la susceptibilité magnétique. Pour un cristal, les valeurs de χ sont différentes selon les directions du cristal. C'est pourquoi, selon la formule (1.4), l'entropie de magnétisation varie en correspondance. La différence d'entropie de magnétisation entre les directions du cristal *c* et *a,b* est :

$$\Delta G_M^{c-ab} = G_M^c - G_M^{ab} < 0 \qquad (1.5)$$

Cela signifie que la diminution de l'énergie libre dans la direction de l'axe *c* est plus importante que dans la direction de l'axe *a, b*. C'est pourquoi le champ magnétique favorise la croissance dans la direction de l'axe *c*. L'application d'un champ magnétique intense pendant

le processus de solidification nous permet donc de développer des méthodes d'alignement des cristaux.

1.1.2 Effet d'un champ magnétique intense pendant la transformation de phase

Ainsi, quand on applique un champ magnétique intense, l'équilibre de phase change à cause de la contribution de l'énergie magnétique de Gibbs. En conséquence, la température ainsi que la durée de la phase de transformation peuvent être considérablement modifiées. De même que la température ou la pression, le champ magnétique est l'un des paramètres importants en thermodynamique qui est utilisé pour changer l'énergie interne des matériaux.

Dans le cas par exemple de la transformation d'austénite en martensite, l'énergie libre de Gibbs des matériaux sera considérablement abaissée en raison de la plus forte magnétisation de la martensite comparée à celle de l'austénite. Cette dernière est paramagnétique et son énergie libre de Gibbs change peu en présence d'un champ magnétique. Comme il est montré dans la Figure 1.4, puisque le champ magnétique abaisse l'énergie libre de Gibbs de la martensite de G_α à G_α^M et que celle de l'austénite ne change que faiblement passant de G_γ à G_γ^M . La température d'équilibre des deux phases T_0 augmente jusqu'à T_0^M et M_s croît dans la même sens. Puisque la force motrice de la transformation est déterminée par la différence d'énergie libre de Gibbs entre les deux phases, la transformation peut être considérablement favorisée en présence d'un champ magnétique. Il est bien connu que le champ magnétique augmente la température de début de la réaction martensitique et que cette augmentation ΔT_M est proportionnelle au champ magnétique [13]

$$\Delta T_M = \frac{\Delta M}{\Delta S} B = \frac{\Delta M}{\Delta H} T_0 B . \qquad (1.6)$$

où ΔM , ΔS and ΔH représentent respectivement les variations de magnétisation, d'entropie et d'enthalpie entre les deux phases considérées. Cependant, Ladislav Valko et Marian Valko [14] ont donné des formules différentes dans leur analyse de l'influence du champ magnétique sur du fer pur pendant sa phase de transformation de liquide à solide, soit :

$$T - T_0 = \Delta T = \frac{T_0}{\Delta H_s^0} H^2 \qquad (1.7)$$

où ΔH_s^0 est l'enthalpie et H l'intensité du champ magnétique.

Cet effet fut d'abord étudié sur le plan théorique et expérimental en utilisant plusieurs alliages ferreux subissant une transformation de martensite non-diffusive [15-17]. Les résultats ont montré que le champ magnétique pouvait permettre un accroissement de la

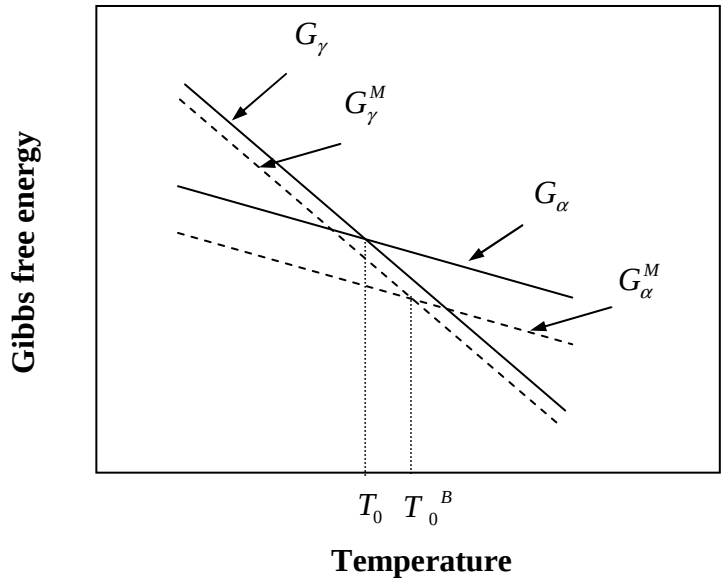

Fig. 1.4. Variation of Gibbs free energy of austenite and martensite versus temperature in the case without and with the magnetic field, α - *martensite;* γ - *austenite*; M- *magnetic field.*

température M_s d'environ 3K pour un champ magnétique de 1 Tesla. En 1964, Sadovsky [18] trouva de petites augmentations de température M_s en utilisant un champ magnétique faible. Kakeshita et al. [19] ont étudié les effets du champ magnétique sur les modifications à la fois de l'isotherme et de la cinétique thermique de la transformation martensitique dans les alliages Fe-Ni-Mn. Ils ont trouvé qu'en présence de champs magnétiques inférieurs à la valeur critique, la cinétique de la transformation martensitique isotherme était effectivement modifiée. La « pointe » du diagramme TTT apparaissait à une température plus basse et dans un temps d'incubation plus court que lorsqu'il n'y avait pas de champ magnétique comme on le voit sur la figure 1.5.

Les transformations dans les aciers contrôlées par la diffusion sont également influencées par un champ magnétique. Pustovoit et Yu [20] ont appliqué un champ magnétique de 1.2T pendant la décomposition de l'austénite dans le cas d'aciers à haut carbone et ont trouvé une augmentation de la quantité de ferrite hypoeutectique. Selon Palmai [21] le champ magnétique de 0.45T retarde la transformation inverse dans un acier de composition 0.6wt.%C. Peters et Miodownik [22] ont observé que la limite d'équilibre de phase entre

l'austénite et la ferrite dans un alliage Fe-Co était décalée. Récemment, des recherches sur l'influence d'un champ magnétique intense de 7.5T sur la cinétique de la transformation ferritique proeutectique dans des alliages de base Fe-C ont permis de clarifier le fait qu'un

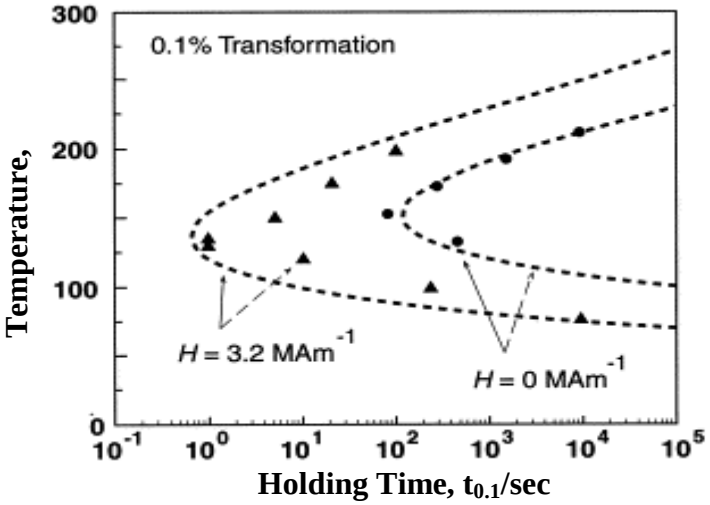

Fig. 1.5. TTT diagrams of the isothermal martensitic transformation in a Fe-24.9Ni-3.9Mn alloy with and without an applied magnetic field. (Ref.[5])

champ magnétique accélérait la transformation au-dessous et également au-dessus de la température de Curie[23]. Joo et al. [24] ont simulé de manière théorique l'effet du champ magnétique sur l'équilibre de phase ferrite/austénite et austénite/ferrite et les résultats montrent que le diagramme de phase est décalé vers le haut de telle manière que les températures Ac_1 et Ac_3 augmentent en présence d'un champ magnétique. De plus, Galkin et al. [25] ont trouvé que des champs magnétiques affectaient également la transformation de phase induite par pression entre les phases B81 et B31 de l'alliage MnAs. En conséquence, l'application d'un champ magnétique de 10T engendre une brusque transformation de la phase stabilisée B31 vers la phase B81. Selon Liu et al. [26], pour des particules de $Zr0_2$ dans un alliage MnZn ferrite, on passe d'une transformation tétragonale à une transformation monoclinique à partir d'un champ magnétique critique (entre 4T et 6T). Le champ magnétique n'affecte pas directement les particules $Zr0_2$ car elles sont paramagnétiques, mais crée une transformation de phase induite par contrainte à cause de la magnétostriction engendrée par le champ magnétique dans la matrice MnZn ferritique magnétique. Les effets du champ magnétique sur la transformation de phase α/γ dans les aciers ont été amplement étudiés pour des champs supérieurs à 30T [27-34], montrant d'importants changements cinétiques induits. Les températures Ae_3 et Ae_1 augmentent d'environ 2K/T lorsque la ferrite devient plus stable.

1.1.3 Effet d'un champ magnétique sur l'interface liquide-solide et la microstructure solide

L'application d'un champ magnétique pendant la phase de solidification directionnelle des matériaux peut réduire de façon significative les vitesses de convection dans le bain [35]. Ceci a comme effet de modifier les fluctuations de la température et la distribution de la composition, comme le montre la figure 1.6 [36]. L'efficacité du champ magnétique à amortir les écoulements convectifs dépend de la valeur du nombre d'Hartmann

$$Ha = \mu B_0 L\sqrt{\sigma/\eta} \qquad (1.8)$$

où μ représente la perméabilité magnétique relative, B_0 l'amplitude du champ magnétique, σ la conductivité électrique, η la viscosité cinématique et L la longueur caractéristique du système (par exemple le diamètre du creuset). Cependant, quelques résultats inattendus ont été obtenus dans le cas d'alliages métalliques solidifiés de manière directionnelle. Youdelis et Dorward [37] ont soumis, en cours de solidification, un alliage AlCu de composition variée (entre 0.5 et 4.5wt.%Cu) à un champ magnétique de 3.4T et ont mesuré le coefficient de partition effectif $k_{eff} = \frac{C_s}{C_0}$, C_s désignant la concentration de soluté dans le solide formé et C_0 la concentration dans le liquide interne.

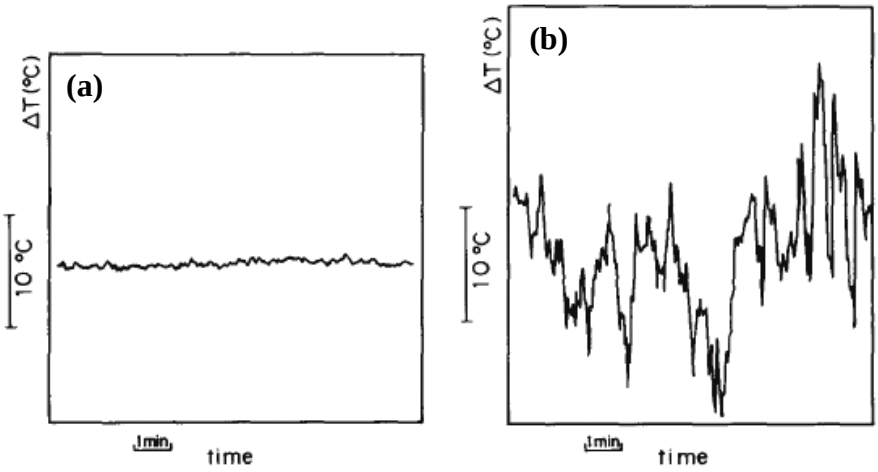

Fig. 1.6. Effect of a static magnetic field on the temperature fluctuations in molten AsGa [36]. (a) B= 0.34T; (b) B=0T.

A vitesse de tirage réduite et à faibles concentrations, le coefficient de partition augmente avec le champ magnétique, suggérant que la convection naturelle a été freinée. Mais à plus grande vitesse il décroît comme si le transport de soluté avait été accru par le

champ magnétique. Ces résultats ont été interprétés comme la conséquence de la variation du coefficient de diffusion de la solution avec le champ magnétique. Quelques années plus tard, les mêmes auteurs ont démontré que cette interprétation ne coïncidait pas avec les ordres de grandeur attendus. Aucune influence sur la microstructure ou sur la macroségrégation longitudinale n'a été relevée en présence d'un champ magnétique qu'il soit transversal ou axial (0.1T) pendant la solidification directionnelle de l'alliage Pb-57wt.%Sn proche de la composition eutectique, qui contenait seulement une faible fraction volumique de dendrites primaires [39]. Pour pousser plus loin l'analyse, Tewari et al. [40] ont étudié l'effet d'un champ magnétique transversal intense (0.45T) sur la solidification directionnelle de deux alliages Pb-Sn, à savoir 38.7wt.%Sn et 17.7wt.%Sn. Le premier a un maximum de macroségrégation longitudinale en l'absence de champ magnétique et le second un minimum de ségrégation. Ces degrés de macroségrégation suggèrent une importante convection thermosolutale dans l'alliage 33.3wt.%Sn et une convection minimale dans l'alliage 17.7wt.%Sn. Le champ magnétique de 0.4T n'avait aucune influence sur le réseau dendritique mais occasionnait une sévère distorsion du réseau cellulaire de l'alliage fortement chargé en étain (voir par exemple la figure 1.7). La macroségrégation qui s'était formée le long de l'échantillon n'était cependant pas influencée par le champ magnétique.

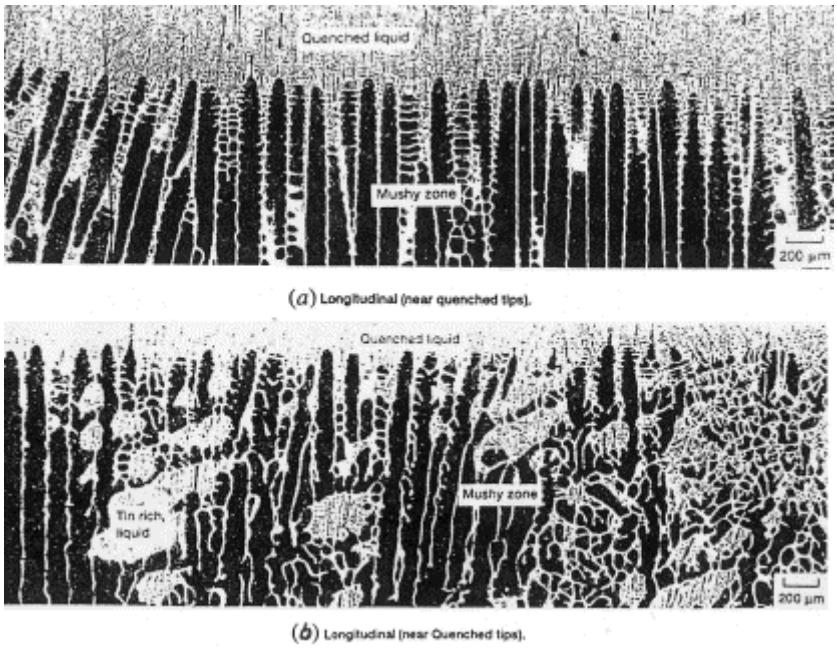

Fig. 1.7. Cellular microstructures of directionally solidified Pb–17.7wt.%Sn alloy: (a) without magnetic field and (b) with a transverse magnetic field of 0.45T. [40].

Selon Tewari et al. [40], un courant électrique induit, dans la direction perpendiculaire à la fois au champ magnétique et à l'écoulement, résulte du mouvement du bain conducteur de l'électricité. Ce courant conduit à une force de Lorentz ($\vec{j} \times \vec{B}$) s'opposant au mouvement et à une convection thermosolutale anisotrope. Tewari et al. attribuèrent la distorsion de l'arrangement cellulaire à l'anisotropie de la convection thermosolutale produite par le champ magnétique.

Alboussière et al. [41] et Laskar [42] ont réalisé des expériences de solidification avec application d'un champ magnétique (transversal ou axial) sur des alliages Bi-60wt.%Sn et Cu-45wt.%Ag. Il en ressort que d'importants canaux ségrégés apparaissent, comme le montre la figure 1.8, mettant en évidence l'existence d'un nouveau mouvement. Alboussière et al. [41] ont suggéré que cette nouvelle convection était induite par l'interaction entre le champ magnétique et l'effet thermoélectrique, qui engendre la convection dite thermoélectromagnétique dite TEMC. La TEMC est basée sur le principe selon lequel, quelque soit le matériau, un gradient de température, $\vec{\nabla} T$, produit une force électromotrice de type Seebeck $S\vec{\nabla} T$ où S représente la pouvoir thermoélectrique du matériau, fonction de la nature du matériau, de sa composition etc. Si les gradients de S et de T ne sont pas parallèles, un courant thermoélectrique est alors généré dans le système [43]. L'application d'un champ

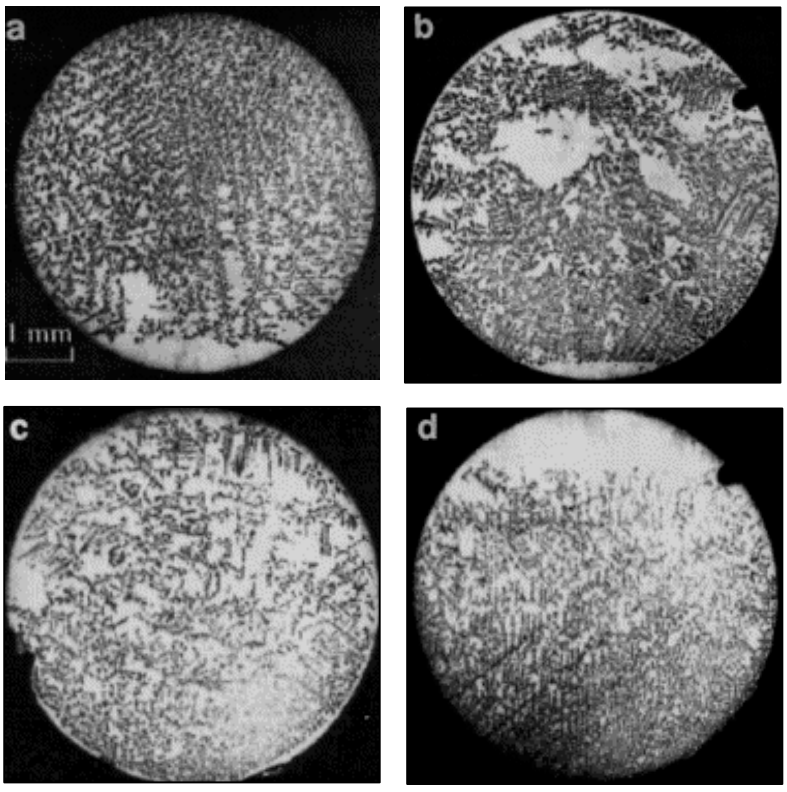

Fig. 1.8. Transverse metallographies of the CuAg alloy. (a) No field, (b) B=30mT, (c) B=50mT, (d) B=200mT.[41]

magnétique à un tel système produit une force de volume thermoélectromagnétique et un écoulement correspondant dans le bain.

La description la plus détaillée des effets liés à la TEMC a été faite par Shercliff [44]. Bien qu'il se fut principalement intéressé à des écoulements de métaux liquides pour des dispositifs de refroidissement et non au domaine de la croissance cristalline, il a donné un excellent aperçu de la théorie de la TEMC ainsi qu'une estimation en ordre de grandeur de la variation des vitesses d'écoulement correspondantes en fonction des champs magnétiques appliqués. L'une des premières évidences de la TEMC dans le domaine de la croissance cristalline fut donnée par Gel'fgat et Gorbunov (45). Ils ont montré de manière impressionnante l'intensité des écoulements d'origine thermoélectromagnétique lors de la croissance des cristaux de InSb par la méthode Czochralski. Une forte déformation de la forme du cristal provoquée par l'apparition des écoulements d'origine thermo-électromagnétique se produisait lorsqu'ils appliquaient un champ magnétique axial statique. Ils ont réalisé des expériences sur la croissance dans des creusets conducteurs de l'électricité (graphite) aussi bien que dans des creusets non-conducteurs (verre de quartz). Bien que la TEMC fut plus forte dans le cas du creuset conducteur d'électricité, le même phénomène a été observé dans le creuset en verre de quartz. En fonction du champ magnétique appliqué une rotation du bain jusqu'à 5 tours par minute a été également observée. Dans leurs expériences, l'écoulement du bain a atteint un maximum d'environ 0.1m/s et a décru pour des champs magnétiques plus élevés. Pour des nombres de Hartmann faibles, *Ha*, la vitesse d'écoulement induite est directement proportionnelle au champ magnétique. Pour des nombres de Hartmann élevés, l'effet d'amortissement du champ magnétique, quelque soit le type d'écoulement, devient le facteur dominant et une proportionnalité inverse est observée entre la vitesse d'écoulement et le champ magnétique. Une analyse plus détaillée a été donnée par Khine et Walker [46]. La composante azimutale de la vitesse caractéristique v_{az} en présence d'un champ magnétique s'exprime comme suit :

$$Ha<1 : \upsilon_{az} = \sigma(S_B - S_A)\Delta TBr/\mu ; \quad Ha>1 : \upsilon_{az} = (S_B - S_A)\Delta T/Br \qquad (1.9)$$

où σ représente la conductivité électrique, S_B-S_A la différence des pouvoirs thermoélectriques, ΔT la différence de température entre le centre et la périphérie du bain, B le champ magnétique, r le rayon du bain et μ la viscosité du bain. Les vitesses azimutales calculées par les auteurs ont atteint plusieurs mm/s. Un tel écoulement azimutal peut générer des striations de composition (microségrégation) de forme circulaire dans le cristal en cours de croissance,

et ceci plus particulièrement s'il existe une déviation entre le champ magnétique et le gradient de température, ce qui est en réalité toujours le cas. De plus ils ont relevé que d'intenses écoulements azimutaux pouvaient créer des instabilités de type Rayleigh-Taylor, ce qui se traduit par des distorsions de la composition du cristal à l'échelle microscopique. Le transport de masse n'est pas directement influencé par l'écoulement azimutal mais par l'écoulement méridien (i.e. les composantes axiales et radiales). Pour $Ha > 1$, Khine et Walker [48] ont donné une expression du champ de vitesse méridien v_m comme suit :

$$\upsilon_m = (\rho \upsilon_{az})(r\sigma B^2) \qquad (1.10)$$

ρ représentant la masse volumique du bain. Le champ de vitesse méridien est d'environ 3 à 4 ordre de grandeur inférieur au champ de vitesse azimutal correspondant. Ils ont obtenu par le calcul un champ de vitesse méridien de 0.76 mm/s pour la solidification de HgCdTe et 1.8 mm/s pour la croissance du silicium dopé. Croll et al. [47] ont mis en évidence la génération de microségrégation dans un procédé de croissance de cristaux de silicium dopé en zone flottante. Les inhomogénéités induites par la TEMC ont fait apparaître une configuration distincte assez différente de celles induites par la convection gravitaire ou la convection thermocapillaire. Yesilyurt et al. [48] ont simulé numériquement la croissance verticale du germanium-silicium en procédé Bridgman. Ils ont mis en évidence une influence des écoulements TEMC sur la forme de l'interface solide-liquide. Plus récemment, Dold et al. [49] ont étudié l'effet de la TEMC sur la croissance verticale de cristaux de germanium-silicium avec une concentration moyenne de silicium de 2at%-Si sous champ magnétique axial jusqu'à 5T. Ils ont trouvé que la croissance sous un champ magnétique statique de $B \geq 0.5$T et $B \leq 4$T se traduisait par une forte microségrégation. Ils ont trouvé des fluctuations de composition dont l'intensité croissait avec le champ magnétique mais atteignait une valeur maximum pour un champ égal à 2T. Ces inhomogénéités induites par un champ magnétique sont amorties pour des champs plus intenses et ne peuvent presque pas être éliminées avec un champ magnétique de 5T. Lehmann et Moreau [50] ont étudié la TEMC à l'échelle interdendritique et ont relevé que les champs magnétiques inférieurs à 1T sont trop faibles pour amortir la convection interdendritique. L'existence d'un courant électrique local de type Seebeck dans le réseau dendritique entraîne la création d'une force de Lorentz d'origine thermoélectrique, ce qui produit un écoulement convectif supplémentaire dans la zone pâteuse.

1.1.4. Effet du champ magnétique sur les joints de grain pendant le traitement thermique

Depuis les années 80, un certain nombre d'effets significatifs du recuit magnétique sur la recristallisation ont été étudiés pour du fer [51], des alliages Fe-Co [52] et Fe-Si [53]. La retard de la recristallisation par l'application d'un champ magnétique est une caractéristique commune du recuit magnétique. Il a été également relevé que la fréquence des joints à faible désorientation augmentait avec l'intensité du champ magnétique [54}. Un champ magnétique de 8T est capable d'affecter la migration du joint de grain ainsi que le développement de la texture même dans un état paramagnétique supérieur à la température de Curie [55]. Il était déjà connu auparavant que la fréquence d'apparition des frontières de type low-Σ avec des énergies faibles tendait à augmenter avec la finesse de la texture [56-58] et que des microstructures uniques se développaient. Par exemple, un champ magnétique intense de 14T transforme une structure lamellaire périodiquement alignée de couches de solide α et de perlite pour des vitesses de refroidissement de 10K/minute [59]. Le degré de l'allongement du grain de ferrite prend une valeur maximale à la température de Curie (770°C) dans un alliage Fe-0.4wt.%C même pendant la phase de transformation isotherme α/γ à 10T [60]. De plus, on a observé la formation de perlite extrêmement fine dans un acier de teneur moyenne en carbone, refroidi de 850°C à 30T [61,62]. L'espace interlamellaire d'environ 50nm a été confirmé par la TEM. L'effet du champ magnétique a été attribué a un accroissement de la température de départ de la martensite autour de 70 à 90K. Ceci est du à l'accélération de la cinétique de la réaction perlitique et à la réduction de l'énergie libre de Gibbs dans un champ magnétique intense. On a trouvé qu'un champ magnétique était capable de supprimer la croissance anormale de grain de nickel nanocristallin pendant le processus de recuit [63, 64]. L'application d'un champ magnétique statique augmente la croissance précoce de grain et produit une structure de grain plus homogène, tandis que la croissance anormale de grain persiste uniquement pendant le recuit thermique. Le recuit magnétique produit toujours une structure de grain homogène et ceci même pendant la croissance rapide du grain. Le moment critique où le recuit commence sa croissance de grain rapide, dépend de l'instant d'application d'un champ magnétique.

Un alliage $Fe_{78}Si_9B_{13}$, élaboré par coulée sur roue, a été cristallisé dans un champ magnétique de 6T à des températures allant de 753K à 853K (i.e., supérieures aux températures de Curie et de cristallisation). Une texture fortement orientée {110} de la phase de cristallisation s'est développée seulement en présence d'un champ magnétique appliqué parallèlement à la surface du ruban pendant la recristallisation du recuit à 853K mais pas sous d'autres conditions. Il a été confirmé que l'orientation {110} de la texture provenait de la phase

ferritique ferromagnétique nanocristalline. La cristallisation magnétique de cet alliage a produit une grande diversité de propriétés magnétiques internes. En raison de la présence d'une très grande densité de joints de grain, il est raisonnable de penser que l'on puisse trouver d'autres interactions significatives entre les parois du domaine et les joints de grain dans les matériaux nanocristallins [65, 66]. On a de plus observé [67] comme dans le cas d'un alliage Fe-50mol%Co que les parois du domaine pouvaient interagir avec le grain et les joints d'interphase même à la température de 1253K.

1.1.5. Dépôt en phase vapeur et électrodéposition

On appelle magnéto-electrodéposition [68-70] le dépôt d'un métal ou d'un alliage par un courant électrique en présence d'un champ magnétique. De nombreux métaux tels que le nickel, l'argent, le cuivre et le zinc, ainsi que leurs alliages élaborés par électrodéposition.en présence d'un champ magnétique, ont été étudiés pour leurs propriétés structurelles et morphologiques grâce à différentes techniques de caractérisation de surface. On a par exemple observé que la croissance dendritique du zinc ou du plomb pouvait être fortement modifiée en imposant un champ magnétique externe et que, dans quelques cas, la croissance dendritique pouvait être totalement inhibée en raison de l'augmentation du taux de dépôt du métal, entraînant ainsi un dépôt lisse [71, 72]. Mogi [73, 74] a trouvé qu'un champ magnétique statique intense changeait considérablement la forme de croissance pendant le processus de dépôt. Sous un champ magnétique intense de 8T, on a pu observer au cours du dépôt d'argent et de plomb par la réaction chimique

$$2Ag^{+}\,Cu \rightarrow A\ AgCu^{2+} + Ag, \quad \text{et} \quad ZnPb^{2+} \rightarrow Zn^{2+}Pb + Pb,$$

une modification profonde de la structure, comme le montre la figure 1.9. Le champ magnétique avait changé la forme de croissance dendritique en une forme de type DLA. Ce changement est à attribuer à l'augmentation de la force de Lorentz dans un courant de faible amplitude. De plus, Coey et Hinds [75] ont établi que le champ magnétique pouvait être utilisé pendant l'électrodéposition pour augmenter le taux de dépôt des espèces magnétiques et également pour induire un écoulement turbulent. Ils ont trouvé que la morphologie des dépôts réalisés en croissance radiale était très sensible à la présence de champ magnétique. Plusieurs travaux sont publiés concernant l'effet d'un champ magnétique sur l'électrodéposition du nickel [76-84]. A partir d'une étude utilisant la méthode de diffraction par réflexion d'électron à haute énergie (Reflexion of High-Energy Electron Diffraction : RHEED), Yang [76] a rapporté qu'un champ magnétique imposé n'avait que peu d'effet sur

les orientations préférentielles. Cependant, il a pu observer une augmentation de la rugosité du dépôt avec des effets de digitation dans la direction perpendiculaire au champ magnétique. Perakh [77], au contraire, a fait état d'une importante différence dans les macro-contraintes concernant des couches de nickel et d'alliage fer-nickel en raison de la présence d'un champ magnétique appliqué parallèlement au substrat. Chiba et al. [78] en utilisant l'analyse par diffraction des rayons X (XRD) ont conclu que le champ magnétique pouvait modifier les orientations de la croissance du cristal en corrélation avec l'axe préférentiel de magnétisation. En outre, cet effet est plus important pour les cas des faibles densités de courant où l'effet du champ magnétique prévaut sur celui du champ électrique. Shannon et al. [79, 80] ont étudié à

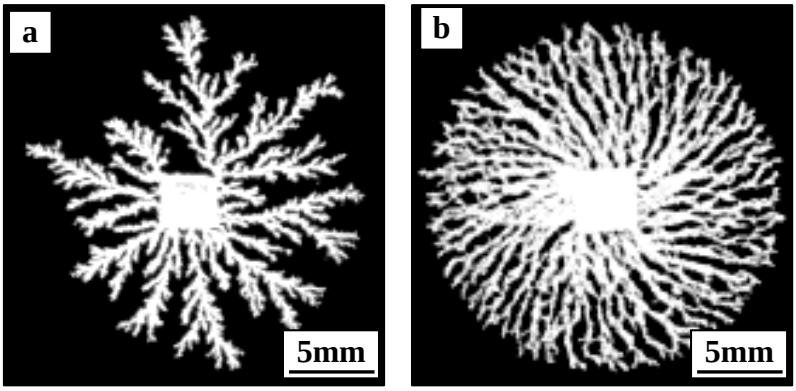

Fig. 1.9. Magnetic field dependence of the metal-leaves patterns in electroless deposition: (a) 0T; (b) 8T. [73]

la fois l'effet du champ magnétique imposé horizontal et l'effet du champ magnétique imposé vertical sur la rugosité des dépôts de nickel cathodiques, au moyen d'un microscope à laser (CSLM). A partir de l'analyse des profils d'épaisseur de surface et le test de Bartlett sur l'homogénéité, les auteurs ont pu vérifier que la rugosité du dépôt dépendait fortement de la position relative à l'intérieur de la surface de dépôt ainsi que de l'orientation du champ magnétique. Généralement le processus de magnéto-électrolyse donne une surface plus lisse que celle obtenue en absence de champ magnétique. Brillas et al. [81] ont trouvé que l'imposition d'un champ magnétique extérieur sur une électrodéposition de nickel , soit parallèlement, soit perpendiculairement aux électrodes, conduisait à une augmentation du caractère compact des grains de nickel qui croissaient en dimension et en formes géométriques de manière plus régulière. Les auteurs concluaient que la morphologie de surface est grandement influencée par le champ magnétique. En utilisant les techniques SEM et TEM, Devos et al. [82, 83] ont observé quelques changements morphologiques de surface avec des modifications au niveau de la direction de croissance préférentielle des grains de nickel, quand un champ magnétique est appliqué parallèlement au substrat lors de

l'électrodéposition du nickel. Les auteurs ont attribué ces changements à l'augmentation du flux de diffusion de certaines espèces telles que les ions H^+ dans un bain de Watts pur ou dans une solution de Watts modifiée à 2-butyne-1,4-diol. La réduction de ces espèces sur la surface cathodique entraîne une légère augmentation de la valeur interfaciale du pH, générant ainsi la formation d'hydroxyde de nickel tout près de la surface. Les espèces adsorbées ont passivé la partie de la surface cathodique active de l'électrodéposition pour le nickel, ce qui a conduit à une faible diminution de la densité de courant dans l'électrolyse avec l'augmentation du champ magnétique appliqué. Ceci avait également été vérifié grâce à des techniques de caractérisation électrochimiques. Bund et al. [84] ont étudié l'influence d'un champ magnétique perpendiculaire sur le comportement électrochimique du cuivre et du nickel en présence de systèmes $(IrCl_6)^{2-/3-}$. L'augmentation de la densité du courant limite avec le champ magnétique s'explique par l'augmentation de la convection du à l'effet MHD. On attribue la formation d'un matériau composé de grains plus fins en présence d'un champ magnétique dans le cas de l'électrodéposition de nickel à l'augmentation du courant de convection, ce qui conduit à une augmentation du taux de dépôt. Plus récemment, Hirota et al. [85] ont étudié l'effet morphologique de champs magnétiques sur le dépôt d'argent par l'observation microscopique in situ d'une dendrite d'argent au moyen d'un système de périscope mis au point à partir d'un microscope à laser sous un champ magnétique de 12T appliqué perpendiculairement au plan de l'échantillon. Une branche droite en argent s'est d'abord formée pendant un instant. Puis, tout près de l'extrémité, une partie de la branche a commencé à bouger rapidement et s'est complètement ployée. A la fin du processus, une dendrite d'argent dense s'était formée en forme de vortex. Quand on restreint l'espace de l'échantillon, la branche ne se plie pas à cause du frottement statique entre la branche et le substrat de verre. A partir de ces observations, on a estimé que le mécanisme de formation d'une dendrite dense en forme de vortex résultait de l'effet de la force de Lorentz agissant sur la branche, du au courant électrique passant à travers la branche elle-même, et accompagné par la dépôt d'argent ainsi que par les réactions de dissolution du cuivre.

Le champ magnétique intense est également appliqué pendant le dépôt de vapeur chimique (CVD). Le champ magnétique n'affecte pas seulement l'orientation mais aussi la nucléation et le taux de croissance des grains. Awaji et al. [86] ont étudié des films YBCO sur des substrats monocristallins MgO et des substrats polycristallins d'argent élaborés par CVD en présence de champs magnétiques supérieurs à 10T et ont trouvé qu'un champ magnétique intense réduisait la dimension des grains et augmentait la valeur du courant critique J_c. Ma et al. [87] ont trouvé que le mode de croissance de $YBa_2Cu_3O_7$-x évoluait, d'une forme spirale à

champ nul vers une forme dispersée bi ou tridimensionnelle en présence d'un champ magnétique extérieur.

1.1.6. Lévitation magnétique et séparation de phase

La lévitation se révèle être d'un grand intérêt pour l'élaboration sans contact de matériaux purs et peut être réalisée grâce à de nombreuses techniques. L'une d'entre elles consiste à utiliser un champ magnétique intense inhomogène. Depuis que Beaugnon et Tournier ont réussi en 1991 à faire léviter de l'eau ainsi que certains matériaux diamagnétiques sous un champ magnétique intense [88], la lévitation magnétique est devenue l'un des sujets majeurs de la science des champs magnétiques intenses [89-91]. L'application d'un champ magnétique à haut gradient est prévue pour réaliser des expériences similaires à celles réalisées dans l'espace. Motokawa et al. [89] ont réussi à observer, in situ, des gouttes d'eau en lévitation en cours de solidification, grâce à une vue de coté en utilisant un miroir et une micro-caméra CDD installée dans l'entrefer de l'aimant [92, 93]. Hamai et al. [94] ont étudié la croissance d'un cristal de chlorure d'ammonium dans des conditions de lévitation magnétique et ont mis en évidence la réduction de la nucléation hétérogène dans des conditions de lévitation. Un autre sujet important concerne la séparation de phase. Il est de notoriété que l'application d'un gradient de champ magnétique peut affecter la convection naturelle. Braithwaite et al. [95] ont rapporté dans des publications que l'application d'un champ magnétique intense pouvait supprimer ou accroître la convection thermogravitaire dans une solution de nitrate de gadolinium, le signal de l'effet dépendant de l'orientation relative du champ magnétique par rapport aux gradients de température. Cet effet pourrait être utilisé dans des dispositifs de transferts thermiques ou bien pour contrôler les microstructures dans la croissance cristalline.

1.2. Problèmes en suspens et objectifs à atteindre

Si l'on se réfère aux travaux cités précédemment, il reste encore de nombreux problèmes à résoudre. Le premier d'entre eux, jusqu'à présent, réside dans l'insuffisance d'études approfondies sur le comportement de l'alignement du cristal et plus précisément sur la croissance de l'eutectique et des dendrites pendant la solidification directionnelle sous champ magnétique intense. En conséquence, il paraît important de poursuivre les recherches sur la croissance du cristal en y incluant les régimes eutectique et dendritique et d'élaborer une théorie complète de la croissance du cristal sous champ magnétique intense.

En second lieu, en ce qui concerne l'effet d'un champ magnétique sur l'écoulement à l'interface liquide-solide quelques travaux ont déjà été publiés. Outre l'effet d'amortissement du champ magnétique, la convection thermo-électromagnétique (THMC) a fait l'objet de recherches approfondies, mais peu d'études ont été menées en TEMC à l'échelle de la dendrite primaire et des bras secondaires. Plus précisément nous manquons de preuve expérimentale directe. D'ailleurs, peu de recherches sur la forme et l'évolution de l'interface liquide-solide, ont été entreprises.

Enfin et surtout, de nombreux travaux dans le domaine de la transformation de phase à l'état solide sous champ magnétique intense ont été publiés, mais aucun dans la phase de transformation pendant le processus de solidification. Il existe tout particulièrement un manque évident d'observation in situ de la transformation de phase sous champ magnétique.
En se basant sur les différents points cités précédemment, nos recherches ont porté sur les effets du champ magnétique sur le réseau de dendrite et le réseau cellulaire ainsi que sur la forme et l'évolution de l'interface. Nous avons, pour cela, étudié le comportement de la solidification des alliages hypo et hypereutectiques Al-Cu, Al-Ni, Bi-Mn pendant le processus de solidification directionnelle. Des recherches approfondies ont également été entreprises sur la croissance d'alliages eutectiques lamellaires (Al_2Cu-Al et Pb-Sn) et fibreux (Bi-MnBi) sous champ magnétique intense. Une méthode a été proposée pour observer in situ les arrangements de la transformation de phase de MnBi/Mn1.08Bi pendant le processus de solidification sous champ magnétique intense. L'organisation de l'exposé du travail de thèse, qui correspond au déroulement des recherches, est décrite dans le paragraphe qui suit.

1.3. Organisation et contenu du mémoire

Le présent mémoire se compose de huit chapitres décrits brièvement ci-après.

Dans le chapitre 2, nous présentons le dispositif expérimental et la méthode choisie.

Dans le chapitre 3, nous présentons nos études expérimentales concernant les effets d'un champ magnétique axial intense (supérieur à 12T) sur la morphologie de l'interface liquide-solide ainsi que sur la microstructure du solide pour un alliage hypoeutectique Al-Cu pendant la croissance de type Bridgman. Nous avons trouvé que le champ magnétique engendrait une déstabilisation de l'interface la rendant irrégulière et favorisait la transformation du front plan en front cellulaire et du front cellulaire en front dendritique. Le champ magnétique a une

grande influence sur la morphologie dendritique et sur la morphologie cellulaire. En effet, le champ magnétique entraîne de fortes distorsions dans l'arrangement cellulaire et augmente les ramifications. En ce qui concerne l'arrangement dendritique, le champ magnétique complexifie la morphologie dendritique. Avec l'augmentation des intensités du champ magnétique et la diminution des vitesses de croissance, les dendrites se fracturent et s'orientent selon la direction <111>, le long de la direction de solidification, au lieu de s'orienter selon la direction <100>. En outre, le champ magnétique accroit également l'espace interdendritique primaire et favorise le phénomène de ramification des dendrites pour former des bras d'ordre supérieur. En étudiant le mécanisme de croissance dendritique et le comportement de croissance de la phase MnBi dans l'alliage Bi-0.85wt.%Mn et Al_3Ni dans l'alliage Al-12wt.%Ni, nous parvenons aux résultats selon lesquels le champ magnétique augmente la croissance de la phase MnBi le long de la direction du champ magnétique et incite le cristal Al_3Ni à s'orienter de telle façon que le plan de la phase Al_3Ni soit perpendiculaire à la direction de solidification et forme une structure régulière « en sandwich ». Par la suite nous avons abordé les phénomènes relatifs aux effets du champ magnétique sur le coefficient de partition k et sur la pente du liquidus, la production de contraintes provoquée par le champ magnétique, l'écoulement engendré par la convection thermo-électromagnétique (TEMC) et l'anisotropie de croissance magnétique du cristal.

Dans le chapitre 4 nous présentons nos études expérimentales sur l'effet d'un champ magnétique axial intense (supérieur à 12T) sur la microstructure de solidification de l'eutectique lamellaire des alliages Al-Al_2Cu et Pb-Sn et l'eutectique fibreux de l'alliage Bi/MnBi. Les résultats montrent qu'un champ magnétique intense dégénère la structure lamellaire en une structure ondulée à vitesse de croissance faible. Les diagrammes XRD, SAD et HREM indiquent que le champ magnétique a changé l'orientation préférentielle et orienté le cristal Al_2Cu selon la direction de cristal de <001> le long de la direction de solidification (la direction du champ magnétique). A une vitesse de 0.5 μm/s, le champ magnétique ($B \geq 4T$) entraîne une ségrégation. Il se forme alors des striations sur la section longitudinale et une zone riche en Al dans la section transversale. On peut attribuer aux effets du champ magnétique l'orientation des cristaux Al_2Cu et Al ainsi que la diminution du coefficient de diffusion. Pour l'eutectique fibreux de MnBi/Bi, nous avons trouvé qu'un champ magnétique intense favorisait la formation de fibres MnBi et rendait plus régulière la structure de solidification directionnelle de l'eutectique. L'espacement intercellulaire MnBi et les diamètres de cellule augmentent graduellement avec l'intensité du champ magnétique. En

outre, le champ magnétique augmente la croissance facetée de la phase MnBi ainsi que les coercivités magnétiques de l'alliage.

Dans le chapitre 5, nous présentons l'effet d'un champ magnétique intense sur la transformation de phase ainsi que les propriétés morphologique et magnétique. En premier lieu, nous proposons une nouvelle méthode pour déterminer la température de transformation de phase. Celle-ci consiste à mesurer la température pour laquelle la force magnétique change brutalement dans le gradient de champ magnétique. La température de transformation de phase de MnBi/Mn1.08 sous un champ magnétique intense est mesurée grâce à cette méthode et les résultats indiquent que le champ magnétique augmente la température de la transformation de phase. Nous observons alors qu'un champ magnétique de 10T a élevé la température de transformation de phase d'environ 20K. La morphologie et les propriétés magnétiques de la phase MnBi ont également été étudiées et nous avons trouvé que le champ magnétique fracturait le cristal MnBi le long du plan <001> et que les fragments de cristaux de MnBi s'agrégeaient et s'alignaient le long de la direction du champ magnétique. En parallèle avec le changement de la morphologie de la phase MnBi, la propriété magnétique subit elle aussi des changements importants. Ceci a pour effet d'augmenter la magnétisation de saturation M_s et la susceptibilité magnétique χ et de diminuer le champ coercitif H_c ainsi que la magnétisation rémanente M_r. Cela implique que le champ magnétique entraîne la transformation de la propriété magnétique de la phase MnBi en magnétisme doux. En termes d'énergie magnétique et de force créées par le champ magnétique, nous nous proposons ensuite de discuter et d'analyser les résultats obtenus.

Dans le chapitre 6, nous présentons les effets de l'imposition simultanée d'un courant alternatif et d'un champ magnétique statique sur les structures de solidification de l'aluminium pur et de l'alliage Al-4.5wt.%Cu. Les résultats montrent qu'une structure affinée a été obtenue grâce à l'application de champs magnétiques complexes cités précédemment. A cause de la chute libre des nucleii pendant le processus de vibration électromagnétique (i.e. la formation d'une pluie de cristal) la structure affinée a été obtenue uniquement au bas de l'échantillon. Une méthode pour contenir les cristaux a été trouvée. Elle consiste à imprimer une force magnétique ascendante. Selon les résultats expérimentaux, le champ magnétique entraîne des changements significatifs dans la sédimentation des grains affinés. Nous avons également trouvé qu'il existait une force magnétique capable d'affiner l'échantillon dans son intégralité et en conséquence, d'obtenir une structure affinée uniforme. Nous avons étudié

l’effet de la force électromagnétique sur la structure dans le cas de l’élimination complète des pluies de cristal et nos résultats indiquent que lorsque la densité de la force électromagnétique croit, la taille des grains d’aluminium diminue et la profondeur de la zone d’affinement augmente. Nous avons choisi l’alliage Al-4.5wt.%Cu pour étudier l’influence des forces électromagnétique et magnétique sur la croissance des dendrites. Nous avons pu observer qu’avec l’augmentation de la densité de la force magnétique la structure dendritique colonnaire se transformait en structure équiaxe. Comme dans le cas de l’aluminium pur, les pluies de cristal se forment pendant la vibration électromagnétique et peuvent être contenues en utilisant la force magnétique.

Dans le chapitre 7, nous présentons l’influence du gradient de champ magnétique sur la distribution de phase et sur la structure de phase. Nous avons trouvé que l’application d’un champ magnétique à gradient était capable de contrôler la distribution de la phase primaire dans les alliages. En conséquence, nous pouvons établir que le gradient de champ magnétique axial provoque la ségrégation de la phase primaire MnBi dans l’alliage Bi-6wt.%Mn et de la phase primaire Si dans l’alliage Al-18wt.%Si. De plus, l’application d’un gradient de champ magnétique radial produit une couche riche en MnBi en forme d’anneau. L’application d’un gradient de champ magnétique axial peut produire la même structure affinée pendant le processus de vibration électromagnétique pour l’aluminium pur en limitant la formation de pluies de cristal. Le gradient de champ magnétique affecte également la microstructure en alignant la phase et en contrôlant le processus d’agrégation de phase. En outre, une étude sur l’influence d’un gradient de champ magnétique axial sur la distribution de l’élément indique que le champ magnétique provoque la séparation du soluté de manganèse de la matrice dans l’alliage Bi-6wt.%Mn.

Enfin, dans le chapitre 8, nous présentons les conclusions de ce travail.

OUTLINE

[A1] Xi Li, Yves Fautrelle, Zhongming *Ren*
Influence of an axial high magnetic field on the liquid–solid transformation in Al–Cu hypoeutectic alloys and on the microstructure of the solid, Acta Materialia 55 (2007) 1377–1386.

[A2] Xi Li, Yves Fautrelle, Zhongming Ren
Influence of thermoelectric effects on the solid-liquid interface shape and cellular morphology in the mushy zone during the directional solidification of Al-Cu alloys under the magnetic field, Acta Materialia 55 (2007) 3803-3813.

[A3] Xi Li, Yves Fautrelle, Zhongming Ren
Influence of a high magnetic field on the columnar dendrite growth during the directional solidification, Acta Materialia 55(2007) 5333-5347.

[A4] Xi Li, Zhongming Ren,Yves Fautrelle
Effect of a high axial magnetic field on the microstructure in a directionally olidified Al–Al2Cu eutectic alloy, Acta Materialia 54 (2006) 5349–5360.

[A5] Xi Li, Zhongming Ren,Yves Fautrelle
The spiral growth of lamellar eutectics in a high magnetic field during the directional solidification process, Scripta Materialia 56 (2007) 505–508.

[A6] Xi Li, Zhongming Ren,Yves Fautrelle
Effect of high magnetic fields on the microstructure in directionally solidified Bi–Mn eutectic alloy, Journal of Crystal Growth 299 (2007) 41–47.

[A7] Xi Li, Zhongming Ren,Yves Fautrelle

Effect of a high magnetic field on the phase transformation, morphology and magnetic properties of the MnBi and $Mn_{1.08}Bi$ compounds.

[A8] Xi Li, Zhongming Ren,Yves Fautrelle

The alignment, aggregation and magnetization behaviors in MnBi/Bi composites solidified under a high magnetic fiel, Intermetallics 15 (2007) 845-855.

[A9] Xi Li, Zhongming Ren,Yves Fautrelle

Effects of the simultaneous imposition of electromagnetic and magnetic forces on the solidification structure of pure Al and Al-4.5wt.%Cu alloy, Journal of Materials Processing Technology (In press).

Chapter 1: Introduction

1.1. Research development of material processing under a high static magnetic field

In early 1982, a symposium on Magnetohydrodynamics (MHD) phenomena was held by the International Union of Theoretical and Applied Mechanics (IUTAM) at Cambridge University, England. Since then, in Asia and France, etc, the research workers began to realize that application of Magnetohydrodynamics (MHD) became urgent. To do this, The Committee of Electromagnetic Processing of Materials (EPM) was founded and held the first EPM conference in Japan (Nagoya) in 1994. The second in Paris in 1997 and then the conference every three years is held in Asia and Europe alternately. During this period, EPM laboratories were found in Japan, France, China, etc. Now Electromagnetic Processing of Materials has become an important method of improving the properties of material and developing new technology of materials processing. The surface quality and solidification structure of cast metal were improved by imposing the electromagnetic field during the material processing. With the improvements in the technology of super-conducting coils, an important role could be played by electromagnetic field regarding the control of metal solidification, improving electrodeposit quality and preventing metal corrosion.

In recent year, with the development of superconducting magnets, a high magnetic field has readily been available and is being applied in various fields of science. Many interesting phenomena relating to a high magnetic field have been found, and a new academic field named High Magnetic Field Science is going to open a gate. The new field of Materials Processing by use of a high magnetic field is growing under the umbrella of EPM. The main influence of a high magnetic field on material processing involves the alignment or textured structure, the influence on the phase transformation process, effect of the magnetic filed on the growth of grain boundary, etc. The related reports on above several aspects will be summarized in the next section below.

1.1.1. Effect of the magnetic field on crystal orientation and phase alignment

The crystal orientation is one of the most crucial factors to determine the electric, magnetic and mechanical properties, etc. That is the reason why the development of crystal

alignment method has been desired. So far, the alignment during solidification, electrodeposition, vapor-deposition and solid transformation, etc, has been carried out in a high magnetic field. In early 1981, Mikelson and Karklin [1] firstly obtained the aligned solidification structure in Al-Ni, Al-Cu, Bi-Cd and Cd-Zn alloys under a 0.5-1.5T magnetic field. Subsequently, Savitsky et al. [2] found that the primary MnBi phase in Bi-(0.9-10)wt.%Mn alloys aligned along the direction of a magnetic field of 2.5T during solidification (Fig. 1.1). De Rango et al. [3] firstly prepared the bulk texture of $YBa_2Cu_3O_7$ superconductor during solidification process under a high magnetic field of 5T. Katsuk [4] reported that diamagnetic benzophenone crystallized from n-hexane and KCl and $BaCl_2$ crystallized from solution aligned under a 10T magnetic field. Texture crystal growth of Bi-2201 [5] and Bi (Pb)2212 [6] have been also obtained in a high magnetic field. Asai [7] put forth the perpendicular alignment of the primary phase during solidification of Al-Si-Fe alloy in a strong magnetic field. Moreover, during the electrodeposition and vapour-deposition process under the magnetic field, Zinc and Bismuth crystals [8] were found to be oriented with the easy magnetic axis parallel to the magnetic direction and with the increase of the magnetic field intensity, the alignment degree increased. The above results indicate that an application of a magnetic field is capable of texturing the microstructure.

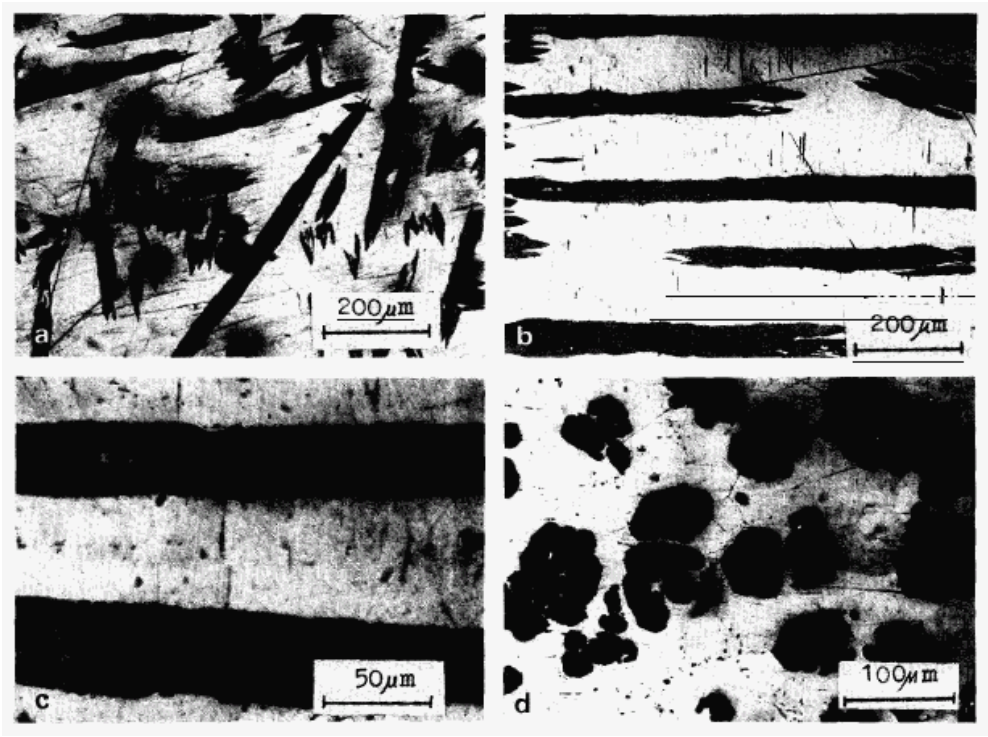

Fig. 1.1. The microstructure of Bi-10wt.%Mn alloy: (a) crystallization without external magnetic field; (b,c) section parallel to applied magnetic field; (d) section normal to applied magnetic field.

The above alignment behavior of the phase occurred in the case without the occurrence of the phase transformation. The crystal alignment during the solid phase transformation was also found under a high magnetic field. The first observation of aligned microstructures in steels was made on Fe-0.1%C and Fe-0.6%C alloys undergoing α to γ transformation in a magnetic field of 8T [9]. The microstructures are chain or columns of the γ phase developed along the magnetic field in the matrix of α phase as shown in Fig. 1.2. The formation mechanism of the aligned structure is attributed to the dipolar interaction between the nuclei of γ phase regarded as magnetic holes in the background of ferromagnetic medium of α phase. Subsequently, the same author in Ref. [10] formed successfully an aligned microstructure during the austenite to ferrite transformation in steels under a magnetic field of 12T. At the same time, the formation mechanism of the aligned structures is discussed from the viewpoint of the nucleation and growth of ferrite grains in austenite phase under a magnetic field.

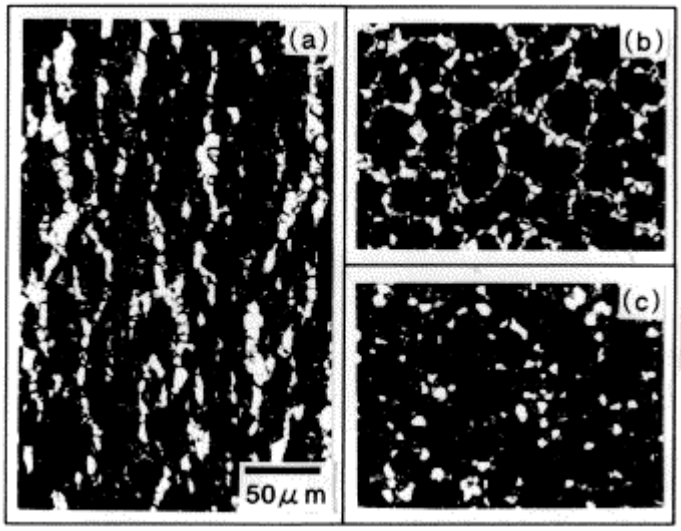

Fig. 1.2. Microstructures of Fe-0.6wt.%C specimens kept at 745℃ for 45 min:
(a) the cross section parallel to a magnetic field of 8T;
(b) perpendicular to the field; and (c) the same treatment in zone magnetic field [9].

The alignment mechanism should be attributed to the rotation of an anisotropic grain and the change of growth anisotropy of the crystal under the magnetic field. As in general, a unit crystal has different magnetic susceptibilities depending on the crystal (i.e. magnetic anisotropy) as shown in Fig. 1.3. When a crystal is put into a magnetic field, owing tomagnetic anisotropy of the crystal will tend to rotate toward the magnetic field. The orienting effect of the homogenous magnetic field on an anisotropic crystal characterized by an anomaly of magnetic susceptibility $\Delta\chi$ along two mutually-perpendicular axes without

taking into consideration the influence of the crystal shape, can be expressed from the following relation [11]:

$$K = \frac{\Delta\chi}{2\mu_0} B^2 V \sin 2a, \qquad (1.1)$$

where V is the volume, α the angle between B and the axis with the maximum $|\chi|$. From the above equation, it follows that paramagnetic crystal in the homogenous magnetic field will align itself with easy magnetization axis along the magnetic field direction, while the diamagnetic crystal will position itself perpendicularly with the magnetic field. In principle, the orienting action of the magnetic field must always affect a crystal having magnetic anisotropy; however, owing to the existence of viscous forces, convective flows in the melt and interaction of the crystals with each other and the walls of the crucible, the alignment may not occur.

On the other hand, from a thermodynamic viewpoint, the magnetizing of a crystal is a process involving an input of magnetization energy to the system. The magnetic energy can be expressed as[12]:

$$G_M = -\int_0^{H_{ex}} \mu_0 M dH_{ex} \qquad (1.2)$$

For a non-ferromagnetic substance

$$M = \chi H_{\mathrm{ex}} \qquad (1.3)$$

Inserting Eq. (1.3) into Eq. (1.2) gives

$$G_{\mathrm{M}} = -\int_0^{H_{ex}} \mu_0 \chi H_{\mathrm{ex}} dH_{\mathrm{ex}} = -\frac{1}{2}\mu_0 \chi H_{\mathrm{ex}}^2 \qquad (1.4)$$

where G_M is the magnetization Gibbs energy, μ_0 the magnetic permeability, $4\pi\times10^{-7}\ H\cdot m^{-1}$, H_{ex} the imposed magnetic field and χ the magnetic susceptibility. For a crystal, the χ -values are heterogeneous for different crystal directions. Therefore, from formula (1.4), the magnetizing entropy varies correspondingly. Then the difference in the magnetizing entropy between crystal direction *c* and *ab* is

$$\Delta G_M^{c-ab} = G_M^c - G_M^{ab} < 0 \qquad (1.5)$$

This means that the decrease of free energy along the c-axis direction is more than the one in the ab-axis direction. Therefore, the magnetic field enhances the growth in the c-axis direction; as a consequence, the growth alignment under a high magnetic field will occur.

Therefore, the application of a high magnetic field during material processing enables us to develop crystal alignment methods.

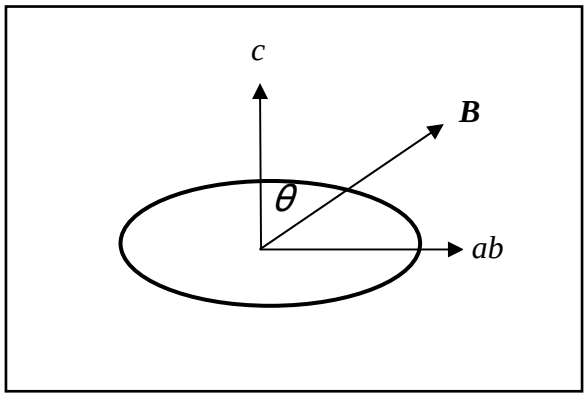

Fig. 1.3. An anisotropic grain in a magnetic field. *H* is the magnetic field direction. *c* and *ab* are the crystallographic axes, respectively.

1.1.2. Effect of a high magnetic field on the phase transformation

As the saturation magnetization of the parent and the product phases is different and the phase transformation temperature is determined by the Gibbs energy. Thus, when a high magnetic field is applied, the phase equilibrium will change due to magnetic Gibbs energy contribution. Consequently, the temperature and extend of phase transformation can be considerably affected. Like temperature or pressure, the magnetic field is one of the important thermodynamic parameters that are used to change the internal energy of materials. For example, in the case of transformation form austenite to martensite, the Gibbs free energy of materials would be greatly lowered as it has higher magnetization compared with that of austenite. The latter is paramagnetic, and its Gibbs free energy does not change too much with the applied magnetic field. As shown in Fig. 1.4, since magnetic field lowers the Gibbs free energy of martensite G_α to G_α^M and that of austenite change only weakly from G_γ to G_γ^M, the equilibrium temperature of the two phases T_0 is thus be elevated to T_0^M and then M_S will go up in the same direction. As the driving force of the transformation is determined by the Gibbs free energy difference between the two phases, the transformation can be greatly enhanced by the application of the magnetic field. It is well known that the magnetic field will increase the starting point of martensite reaction, and the increment of the start point is proportional to the magnetic field [13]

$$\Delta T_M = \frac{\Delta M}{\Delta S} B = \frac{\Delta M}{\Delta H} T_0 B . \qquad (1.6)$$

where ΔM , ΔS , ΔH are the difference in magnetization, entropy and enthalpy between the two phases considered, respectively. However, Ladislav Valko and Marian Valko[14] gave different formula in their analysis on the influence of magnetic field on melt-solid phase transformation of pure iron as follow:

$$T - T_0 = \Delta T = \frac{T_0}{\Delta H_s^0} H^2 \qquad (1.7)$$

where, ΔH_S^0 is the enthalpy and *H* the intensity of the magnetic field.

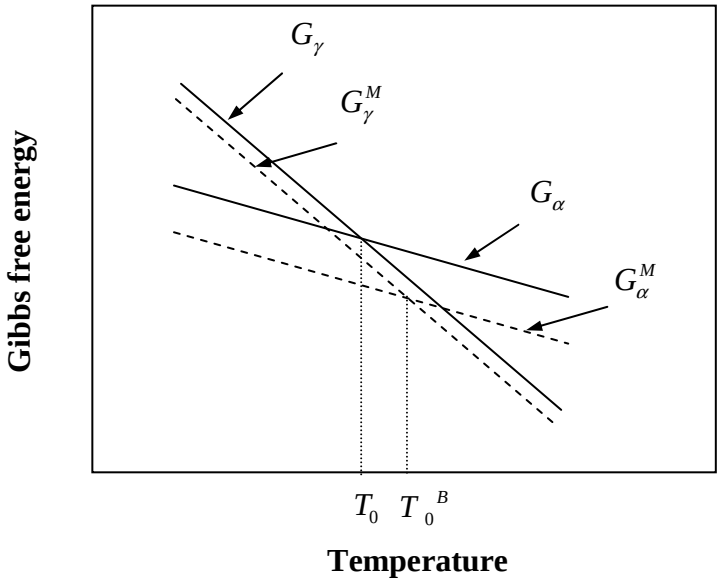

Fig. 1.4. Variation of Gibbs free energy of austenite and martensite versus temperature in the case without and with the magnetic field, α - *martensite;* γ - *austenite*; M- *magnetic field.*

This effect was first investigated theoretically and experimentally using several ferro-alloys undergoing non-diffusional martensitic transformation [15-17], and the research results showed that the magnetic field was able to cause a rise in the *Ms* temperature by approximately 3K per magnetic field in unit of T (Tesla). In early 1964, Sadovsky [18] found small increases in the M_s temperature with the modest magnetic field used. Kakeshita et al. [19] studied the effects of the magnetic field on the both the isothermal and a thermal kinetics of martensite transformation in Fe-Ni-Mn alloys and found that when magnetic fields were less than the critical value, the kinetics of the isothermal martensitic transformation were changed. The 'nose' of the TTT curve occurred at a lower temperature and shorter incubation time than that for the case no-applied field as shown in Fig. 1.5.

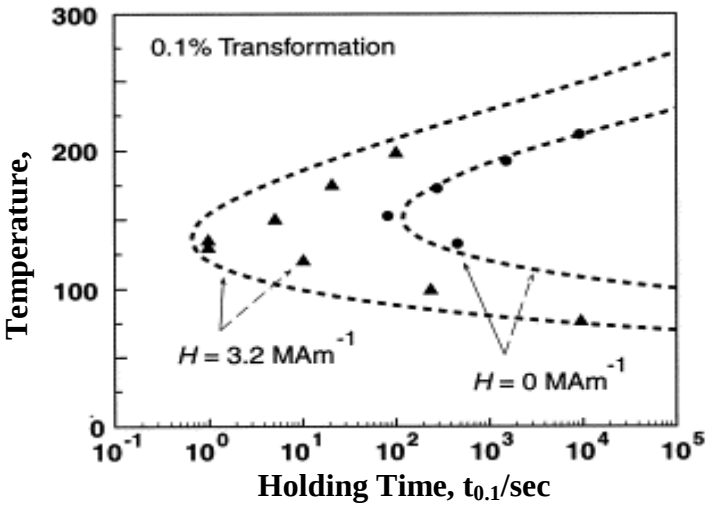

Fig. 1.5. TTT diagrams of the isothermal martensitic transformation in a Fe-24.9Ni-3.9Mn alloy with and without an applied magnetic field. (Ref.[5])

Diffusion-controlled transformations in steels are also influenced by a magnetic field. Pustovoit and Yu [20] applied a magnetic field of 1.2T during the austenite decomposition of high carbon steels and found the amount of hypoeutectic ferrite to increase. Palmai [21] reported that the magnetic field of 0.45T retarded the inverse transformation in 0.6wt.%C steel. Peters and Miodownik [22] observed the phase boundary between the austenite and ferrite of Fe-Co alloy to be shifted to a higher temperature. Recently, the influence of a high magnetic field of 7.5T on the kinetics of pro-eutectic ferrite transformation in Fe-C base alloys was investigated [23], and it was clarified that a magnetic field accelerates the transformation below and also above the Curie temperature. Joo et al. [24] simulated theoretically the effect of the magnetic field on the ferrite/austenite and austenite/ferrite phase equilibrium and the result shows that the phase diagram is shifted upward so that the Ac_1 and Ac_3 temperatures increase as the magnetic field is applied. Moreover, Galkin et al. [25] found that magnetic fields also affected the pressure-induced phase transformation between $B8_1$ and B31 phases of MnAs. As a consequence, the application of a magnetic field of 10T causes an abrupt transformation from the stabilized B31 to the $B8_1$ phase. Liu et al. [26] reported that a critical magnetic field (between 4T and 6T) induced the tetragonal to monoclinic transformation in ZrO_2 particle in a MnZn-ferrite. The magnetic field did not directly affect the ZrO_2 particles, since they are paramagnetic, but created the stress-induced transformation due to the magnetostriction caused by the magnetic field in the magnetic MnZn-ferrite matrix. Field effects on the α/γ phase transformation in steels have been studied extensively for up to 30 T [27–34], with large kinetic changes induced. The Ae3 and Ae1 temperatures are raised by about 2 K/T as the ferrite becomes more stable.

1.1.3. Effect of magnetic field on the liquid-solid interface and solid microstructure

It is well known that the application of magnetic field during the directional solidification of materials can significantly reduce convection flow in melt [35]. As a consequence, the temperature fluctuation and composition distribution will be affected as shown in Fig. 1.6 [36]. The efficiency of the magnetic field in damping convective flows depends on the value of the non-dimensional Hartmann number ($Ha = \mu\beta L\sqrt{\sigma/\eta}$). Where μ is the relative magnetic permeability, β the magnetic field strength, σ the electrical conductivity, η the viscosity and L the characteristic length of the system (e.g. the diameter of the crucible). However, some unexpected results have been obtained in directionally solidified metallic alloys. Youdelis and Dorward [37] processed an AlCu alloy of various composition (between 0.5 and 4.5 Cu) under a 3.4T magnetic field and measured the effective

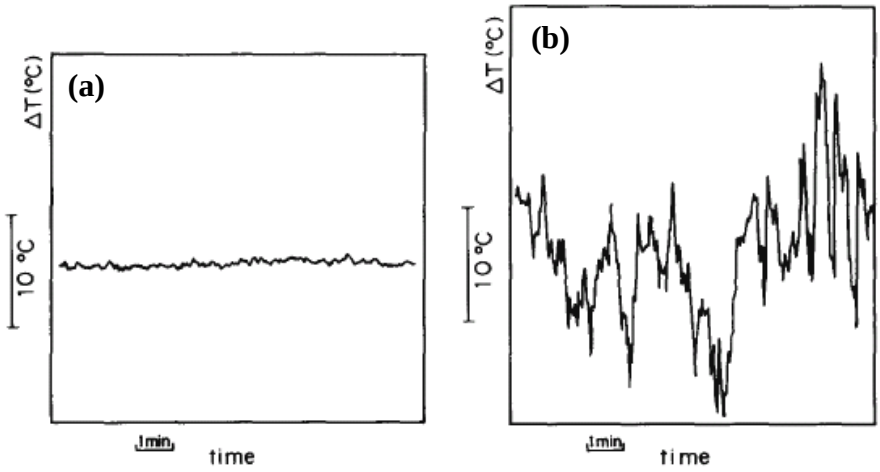

Fig. 1.6. Effect of a static magnetic field on the temperature fluctuations in molten AsGa [36]. (a) B= 0.34T; (b) B=0T.

partition coefficient $k_{eff} = \frac{C_S}{C_0}$, C_s being the solute concentration in the formed solid and C_0 the concentration in the bulk liquid. At low pulling rates and low concentrations, the partition coefficient increased with the field suggesting that natural convection had been braked. But at higher pulling rates it decreased, just as if solute transport had been enhanced by magnetic field. These results were interpreted as the consequence of the variation of the solution diffusion coefficient with the applied field. A couple years later, the same author [38] demonstrated that this interpretation does not agree with the expected orders of magnitude.

No influence on the microstructure or longitudinal macrosegregation was detected upon application of either a transverse or axial field (0.1T) during the directional solidification of the near eutectic Pb-57wt.%Sn alloy, which contained only a small volume fraction of primary dendrites[39]. To investigate this further, Tewari et al.[40] studied the effect of a higher transverse magnetic field (0.45T) on the directional solidification in two Pb-Sn alloys, namely 38.7wt.%Sn and 17.7wt.%Sn, the former having maximum longitudinal macrosegregation without the field and the latter minimal segregation. These degrees of macrosegregation suggested extensive thermosolutal convection in the 33.3 wt.%Sn alloy and minimal convection in 17.7 wt.%Sn alloy. The magnetic field of 0.4T had no influence on the morphology of dendrite arrays, but did cause severe distortion in the cellular array morphology of the high Sn alloy; see for example Fig. 1.7. Macrosegregation along the length

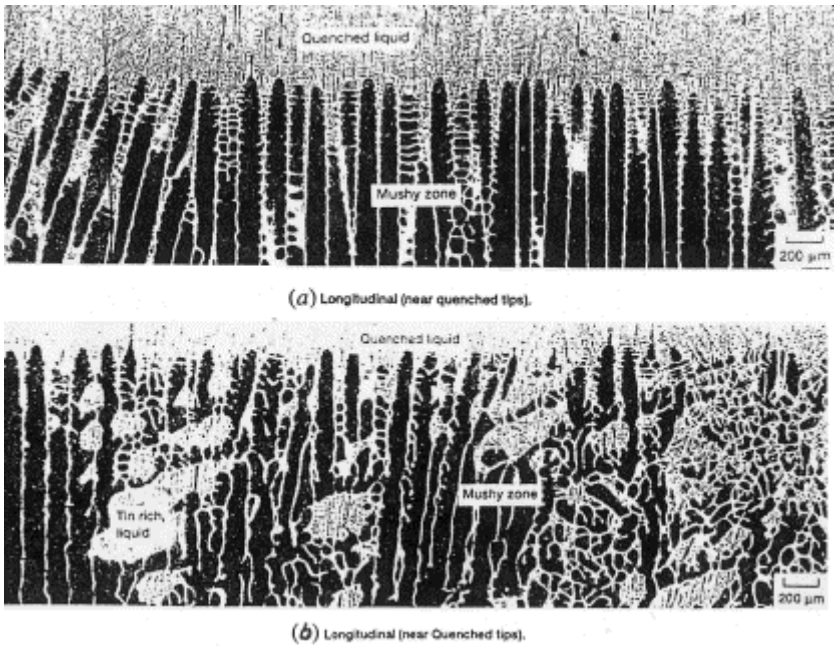

Fig. 1.7. Cellular microstructures of directionally solidified Pb–17.7wt.%Sn alloy: (a) without magnetic field and (b) with a transverse magnetic field of 0.45T. [40].

of the specimen was, however, not influenced by the field for either the dendritic or cellular arrays. Tewrai [40] thought that an induced electric current $\vec{j}$ in the direction normal to the fluid velocity and to the applied magnetic field $\vec{B}$ result from the motion of the electrically conductive melt. This current leads to a Lorentz force ($\vec{j}\times\vec{B}$) opposing the motion and promoting an anisotropic thermosolutal convection. Tewari attributed the distortion in the cellular array morphology to the anisotropy in the thermosolutal convection produced by the

magnetic field. Alboussière et al. [41] and Laskar [42] had performed the experiments on Bi-60wt.% Sn and Cu-45wt.% Ag alloys, solidified with a magnetic field (transverse or axial). It has been found that large freckles appeared in this case as shown in Fig. 1.8, showing that a new movement has been created. Alboussière et al. [41] suggested that this new convection was induced by the interaction between the magnetic field and the thermoelectric effect, which produced the thermoelectromagnetic convection (TEMC). TEMC is based on the principle that in any material a temperature gradient, ∇T , produces a Seebeck electromotive force $S\nabla T$, where S is the thermoelectric power of the material. If the gradients of S and T are not parallel, then a thermoelectric current is generated in the system [43]. Application of a

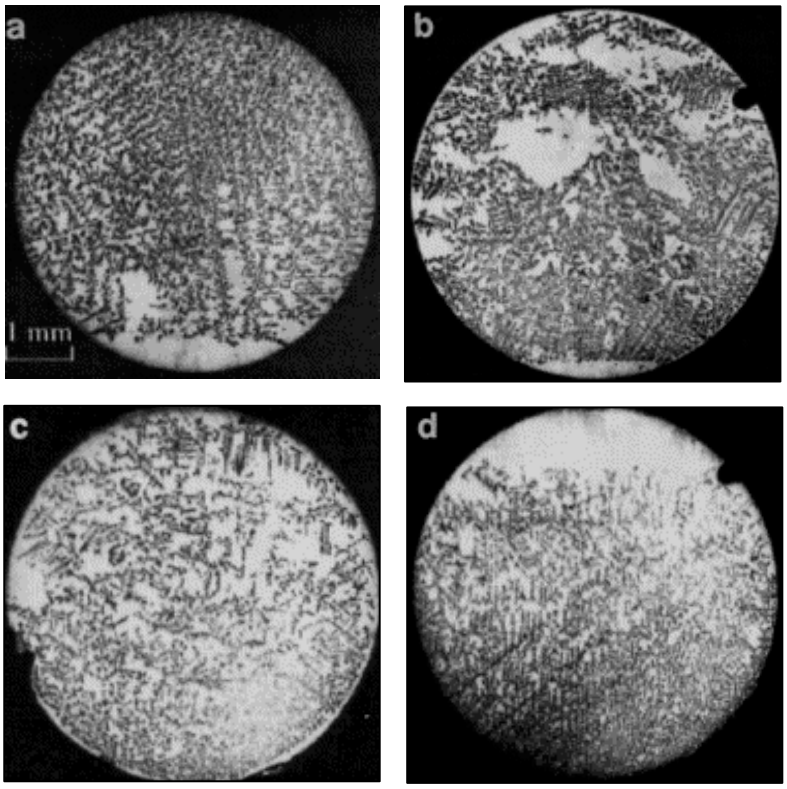

Fig. 1.8. Transverse metallographies of the CuAg alloy[41]. (a) No field, (b) B=30mT, (c) B=50mT, (d) B=200mT.

magnetic field to such a system produces a thermo-electromagnetic body force and an associated flow in the melt. The most detailed description of TEMC-related effects was provided by Shercliff [44]. Although he was mainly interested in flows of liquid metals for cooling devices and not in crystal growth itself, he gave an excellent outline of the theory of TEMC as well as an order of magnitude estimation of corresponding flow velocities as a function of applied magnetic fields. One of the earliest proofs of TEMC in crystal growth arrangements was given by Gel'fgat and Gorbunov [45]. They demonstrated impressively the

strength of TEMC flows in InSb grown by the Czochralski method. A strong deformation of the crystal shape occurred due to the appearance of TEMC flows when they applied a static axial magnetic field. They performed growth experiments in electrically conductive crucibles (graphite) as well as non-conductive ones (quartz glass). Although TEMC was stronger in the case of the electrically conductive crucible, it was observed for the quartz glass crucibles, too. As a function of the applied magnetic field, a melt rotation of up to 5 rpm was observed. In their case, the melt flow reached a maximum around 0.1T and decreased for higher magnetic inductions. For low Hartmann numbers, *Ha*, the induced flow velocity is directly proportional to the magnetic field. For high Hartmann numbers, the damping effect of the magnetic field on any kind of flow motion becomes the dominant factor and an inverse proportionality is found between the flow velocity and the magnetic field. A detailed analysis was given by Khine and Walker [46]. The characteristic azimuthal flow velocity component v_{az} in the presence of an axial magnetic field scales as follows:

$$Ha<1: \upsilon_{az} = \sigma(S_B - S_A)\Delta TBr/\mu; \quad Ha>1: \upsilon_{az} = (S_B - S_A)\Delta T/Br \qquad (1.9)$$

where σ is electrical conductivity, S_B-S_A difference of the thermoelectric powers, ΔT temperature difference between center of the melt and periphery, *B* magnetic induction, *r* melt radius and μ melt viscosity. The azimuthal flow velocities which they calculated reached several mm/s. Such an azimuthal flow may generate rotational-like compositional striations (microsegregation) in the growing crystal, especially if there is a deviation from a perfectly axisymmetric alignment of the crucible and the temperature field, which in reality is always the case. They further point out that strong azimuthal flows might generate Rayleigh–Taylor-like flow instabilities, which can result in disturbances of the crystal composition in the microscale. The mass transport is not influenced directly by the azimuthal flow but by the meridional one (i.e. the axial and radial flow components). For *Ha* >1, Khine and Walker [48] scaled the meridional flow velocity v_m as

$$\upsilon_m = (\rho\upsilon_{az})(r\sigma B^2) \qquad (1.10)$$

with ρ being the density of the melt. Meridional flow velocities are some 3-4 orders of magnitude smaller than the corresponding azimuthal one. They calculated a meridional flow velocity of 0.76 mm/s for the solidification of HgCdTe and 1.8 mm/s for the growth of doped silicon. The generation of microsegregation in FZ grown doped silicon crystals grown under strong static magnetic fields was reported by Croll et al. [47]. The TEMC-induced inhomogeneities showed a distinctive pattern quite different from the ones induced by buoyancy or surface tension driven convection. Numerical simulations of the vertical

Bridgman growth of germanium–silicon have been performed by Yesilyurt et al.[48]. They showed an influence of TEMC flows on the shape of the solid–liquid interface. More recently, Dold et al. [49] have investigated the effect of TEMC on the vertical Bridgman growth of germanium–silicon crystals with an average silicon concentration of 2at%-Si under axial static magnetic fields of up to 5T. It has been found that the growth under the static magnetic field of $B \geq 0.5$T and $B \leq 4$T resulted in strong microsegregation. These magnetic field induced inhomogeneities are damped with higher fields and can almost be eliminated with a magnetic field of 5T. Lehmann and Moreau had [50] investigated TEMC in interdendritic scale and pointed out that the magnetic fields less than 1T is difficult to damp the interdendritic convection. Since a local current density due to Seebeck effect occurs in the dendrite network, a thermoelectric Lorentz force is created, which gives an additional convective flow in the mushy zone.

1.1.4. Effect of the magnetic field on grain boundary during heating treatment

Since the 1980s, some significant effects of magnetic annealing on recrystallization were reported for deformed iron [51], Fe–Co [52] and Fe–Si alloys [53]. The retardation of recrystallization by the application of the magnetic field is a common feature of magnetic annealing. It was also found that the frequency of low-angle boundaries and low-R coincidence boundaries was increased with the increase of the magnetic field strength [54]. It has been reported that a magnetic field of 8T was capable of affecting grain boundary migration and texture development even in the paramagnetic state above the Curie temperature [55]. It was already revealed that the frequency of occurrence of low-Σ-coincidence boundaries with low-energies tends to increase with increasing sharpness of texture [56-58] and unique microstructures have also been seen to develop. For example, periodically aligned lamellar structure of elongated α layer and the pearlite layer for a medium-carbon steel (42CrMo steel) transformed in a high magnetic field of 14T at the cooling rate of 10 K/min [59]. The degree of ferrite grain elongation showed a maximum value at the Curie temperature (770°C) in an iron-0.4wt.% alloy even during “isothermal” α/γ phase transformation at 10T [60]. Furthermore, the formation of extremely fine pearlite was observed in a medium-carbon steel cooled from 850°C at 30T [61, 62]. The interlamellar spacing of about 50nm was confirmed by TEM. The effect of a magnetic field was ascribed to an increase of the martensite-start temperature by 70–90 °C. This was due to the acceleration of the kinetics of the pearlite reaction and the reduction of the Gibbs free energy in a high

magnetic field. It is found that a magnetic field was able to suppress abnormal grain growth of nanocrystalline nickel during annealing process [63, 64]. The application of a static magnetic field enhanced early grain growth and produced a more homogeneous grain structure, while abnormal grain growth persisted during solely thermal annealing. Magnetic annealing always produced a homogeneous grain structure even during rapid grain growth. The critical annealing time at which rapid grain growth starts depends on whether a magnetic field is applied.

Melt-spun amorphous $Fe_{78}Si_9B_{13}$ was crystallized in a magnetic field of 6T at temperatures ranging from 753K to 853K (i.e., exceeding the Curie and crystallization temperatures). An extremely sharp {110} texture of crystallized phase was developed only when the field was applied parallel to the ribbon surface during crystallization annealing at 853 K, but not under other conditions. It was confirmed that the sharp {110} texture came from the nanocrystalline ferromagnetic ferrite phase. A large variety of bulk magnetic properties of this alloy were produced by the magnetic crystallization. It is reasonable to think that more significant interactions between domain walls and grain boundaries are expected in nanocrystalline material [65, 66], because of the presence of an extremely high density of grain boundaries. Moreover, it was found that magnetic domain walls could interact with grain and interphase boundaries even at the high temperature of 1253K as observed in Fe–50mol %Co alloy [67].

1.1.5. Vapor- and electro- deposition

The deposition of a metal or an alloy by electric current in the presence of an applied magnetic field is known as magnetoelectrolytic deposition [68-70]. Many of the metals and its alloys such as nickel, silver, copper and zinc, prepared by electrodeposition in the presence of a magnetic field had been examined for their structural and morphological properties by various surface characterization techniques. For example, it was observed that the dendritic growth of zinc or lead can be strongly modified by imposing an external magnetic field, and in some cases the dendritic growth may be totally inhibited due to an increase of the rate of metal deposition resulting in a smooth deposit [71, 72]. Mogi [73, 74] had found that a static high magnetic field considerably changed the growth pattern during the deposition process. It has been found that during Ag and Pb metal-leaves deposited by a chemical reaction of

$$2Ag^{+}Cu \rightarrow 2AgCu^{2+} \text{ and } ZnPb^{2+} \rightarrow Zn^{+2}Pb \qquad (1.11)$$

under a high magnetic field of 8T, respectively, a different structure was obtained as shown in Fig. 1.9. It can be observed that the magnetic field had changed the dendrite growth pattern into the DLA-like one. This was ascribed to the enhancement of Lorentz force even though the weakness of the elctric current. Moreover, Coey and Hinds [75] reported that the magnetic

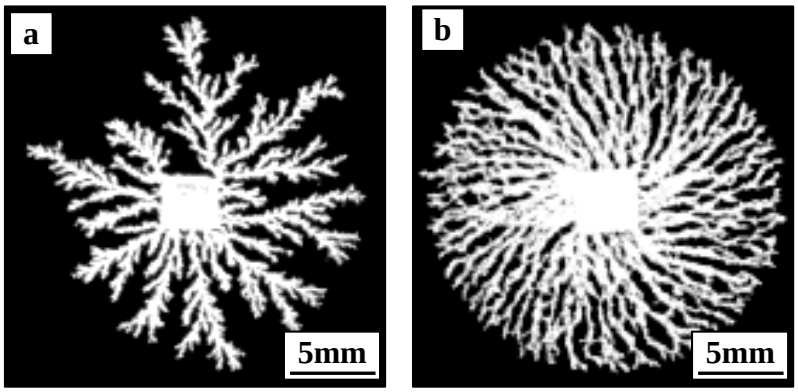

Fig. 1.9. Magnetic field dependence of the metal-leaves patterns in electroless deposition: (a) 0T; (b) 8T. [73]

field could be used during electrodeposition to enhance the deposition rate of magnetic species and also to induce turbulent flow. They found that the morphology of radially grown electrodeposits was much sensitive to the applied magnetic field. There were a several reports in the literature on the effect of a magnetic field on the electrodeposition of nickel [76-84]. Based on reflection high-energy electron diffraction (RHEED) study of Ni, Fe and Co, Yang [76] reported that an imposed magnetic field had little effect on their preferred orientations. But an increase in the roughness of the deposit with projections protruding in the direction of the applied perpendicular field was observed. On the contrary, Perakh [77] reported a large difference in macro-stresses for nickel and iron-nickel alloy films due to a magnetic field applied parallel to the substrate. Chiba et al. [78] using X-ray diffraction (XRD) analysis concluded that the magnetic field could modify the crystal growth orientations in relation to the easy magnetization axis, and this effect is more dominant at low current densities where the magnetic field effect dominates over that of the electric field. Shannon et al. [79, 80] investigated the effect of both horizontal and vertical imposed magnetic fields on the surface roughness of cathodic nickel deposits by means of confocal scanning laser microscopy (CSLM). Based on surface depth profile analysis and Bartlett's test of homogeneity, these authors reported that the deposit roughness depends strongly on relative position within the deposit surface and the orientation of magnetic field. In general, magneto-electrolysis process leads to a smoother surface compared to the deposition in the absence of magnetic field.

Brillas et al. [81] found that the imposition of an external magnetic field on nickel electrodeposition, either parallel or perpendicular to the electrodes, led to an enhancement in the compactness of Ni grains which growed with more regular sizes and geometrical shapes. They concluded that the surface morphology was greatly influenced by the magnetic field. Using scanning electron microscopy (SEM) and transmission electron microscopy (TEM) techniques, Devos et al.[82,83] observed some surface morphological changes with modifications on the preferential growth direction of nickel grains when a magnetic field was applied parallel to the substrate during nickel electrodeposition. These authors attributed the changes to increase of the diffusion flux of certain species such as H^+ in a pure Watts bath or 2-butyne-1,4-diol in modified Watts solution. The reduction of these species on the cathode surface leads to a small increase of the interfacial pH value, thus generating the nickel hydroxide formation in the close vicinity of the surface. This adsorbed species hinder the active part of the cathode surface for Ni electrodeposition that leads to a weak decrease in the electrolysis current density with the increase in applied magnetic field. This had also been proved by electrochemical characterization techniques. Bund et al. [84] investigated the influence of a perpendicular magnetic field on the electrochemical behaviour of Cu, Ni and $[IrCl_6]^{2-/3-}$ systems. The increase of limiting current density with the magnetic field had been explained based on the increase in the convection flow due to MHD effect. Observation of the formation of more fine-grained material in the presence of a magnetic field in the case of Ni electrodeposition had been attributed to increased convection current that led to an increase in the deposition rate. More recently, Hirota et al. [85] investigated the mechanism of the morphological effect of magnetic fields on electroless silver deposition through in situ microscopic observation by using a periscope system that was developed on the basis of a confocal scanning laser microscope. At the growth front of a silver dendrite, under a 12T magnetic field applied perpendicularly to the sample plane, a silver branch was grown straightly for a while; then, a certain length of the branch at the neighbor of the tip started moving rapidly and was bent in an integrated manner. As a result of the process, a dense silver dendrite in the shape of a vortex was formed. When the sample space was narrowed, the branch did not bend due to the increase in the static friction between the branch and the glass plates. Judging from these observations, the mechanism of the formation of a dense vortex dendrite was thought to be the effect of a Lorentz force acting on the branch due to the electric current flowing through the branch itself accompanied by the silver deposition and the copper dissolution reactions.

The high magnetic field also is applied during the chemical vapor deposition (CVD). The magnetic field affects not only orientation, and it has been reported that nucleation and grain growth rate are also affected by the magnetic field. Awaji et al. [86] have investigated YBCO film on single-crystalline MgO substrates and polycrystalline Ag substrates prepared by CVD in magnetic fields up to 10T and found that a high magnetic field has reduced the grains in size and improved J_c. Ma et al. [87] has found that the growth-mode change of $YBa2Cu_3O_{7-x}$ from the spiral growth mode at zero field to the two-dimensional or (3D) island mode under an external magnetic field.

1.1.6. Magnetic levitation and phase separation

Levitation of bodies is of great interest for contactless elaboration of pure materials and can be achieved by numerous techniques. One of them is the use of a strong inhomogenous static magnetic field. Since Beaugnon and Tournier succeeded in levitating water and some diamagnetic materials in 1991 under a high magnetic field [88], magnetic levitation has become one of the topics in high magnetic field science [89-91]. An application of a high gradient magnetic field is planned for doing similar experiments as those space projects. Motokawa et al. [89] had succeeded in the in situ observation of freezing of levitated water from the side using a mirror and a micro-CCD camera installed in the magnet bore [92, 93]. Hamai et al. [94] had investigated the crystal growth of ammonium chloride in magnetic levitation conditions and it had been found the reduction of heterogeneous nucleation in levitation condition. Another topic under a gradient magnetic field is phase separation. It is well known that an application of the gradient magnetic field can separate the phase. Moreover, it has been found that an application of a gradient magnetic field can affect buoyancy convection. Braithwaite et al. [95] has published that an application of a high magnetic field could suppress or enhance buoyancy-driven convection in a solution of gadolinium nitrate, the sign of the effect depending on the relative orientation of the magnetic field and temperature gradients. This effect might be exploited in heat-transfer devices or to control microstructure in crystal growth.

1.2. The existing problem and valuable direction

Basing on the above review, there exist many pending problems and questions worthwhile to be solved. First of all, up to now, there is still short of detail investigation on

the alignment behavior of crystal, especially on the growth of eutectic and dendrite during the directional solidification under a high magnetic field. Therefore, it is valuable to investigate the growth of crystal including dendrite and eutectic and built the complete growth theory of crystal under a high magnetic field.

Secondly, concerning the effect of a magnetic field on the flow at the liquid-solid interface, some works have been done. Besides the damping effect of magnetic field, thermo-eletromagnetic convection (THMC) has been investigated extensively, but there exists few works devoted to investigate TEMC on the scales of primary dendrite and secondary dendritic arm. Especially there is a lack of direct experimental proof. Moreover, few investigations have been done on the solid-liquid interface transformation and shape.

Last but not the least; in the field of the phase transformation under high magnetic field, many works have been published on the solid state phase transformation. However, there exists no works concerning the study of the phase transformation during the solidification process. Especially there are few in situ observations of the phase transformation under the magnetic field.

Basing on the above several points, the present work has studied the effects of the magnetic field on the dendrites and cellular array, and interface transformation and shape by investigation of the solidification behavior of Al-Cu, Al-Ni, Bi-Mn hypo and hypereutectic alloys during the directional solidification process. Investigations on growths of the lamellar eutectic (Al_2Cu-Al and Pb-Sn) and rod eutectic (Bi-MnBi) alloy under a high magnetic field have also been done intensive. Moreover, A method has been proposed to in situ observe that the phase transformation of MnBi/$Mn_{1.08}$Bi compounds during the solidification process under a high magnetic field. The detailed organization and content of this thesis are described in the subsequent paragraphs.

1.3. The organization and content of the present thesis

The present thesis entails eight chapters. In the chapter 2, the experimental device and method are introduced.

In the chapter 3, influences of an axial high magnetic field (up to 12T) on the liquid-solid interface morphology and the microstructure of the solid have been investigated experimentally during Bridgman growth of Al-Cu hypoeutectic alloys. It is found that the magnetic field causes the interface to be destabilized and irregular and promotes the planar-cellular and the cellular-dendritic transformation. The field has also a great influence on the

cellular and dendritic morphology. Indeed, the field causes severe distortion in the cellular array and enhances the cell branching. For the dendrite array, the field makes the dendrite morphology more complex. With the increase of the magnetic field intensities and the decrease of the growth velocities, the dendrites become broken and orientate with the <111>-direction along the solidification direction instead of the <100>-direction. Furthermore, the field also enlarges the primary dendrite spacing and promotes the branching of the dendrites to form higher order arms. In order to investigate the dendrite growth mechanism, the growth behaviour in the MnBi in Bi-0.85wt.%Mn alloy and Al_3Ni in Al-12wt.%Ni alloy have also been investigated. The results indicate that the field enhances the growth of MnBi phase along the magnetic field direction and causes the Al_3Ni crystal to be oriented in such a way that the plane of Al_3Ni phase is square with the solidification direction and form the regular sandwich structure. Then, we discuss the effect of the magnetic field on the equilibrium partition coefficient k and the liquidus slope m_L, the production of stress caused by the field, the flow created by the thermo-electromagnetic convection (TEMC) and the magnetic and growth anisotropy of crystal.

In the chapter 4, the effect of a high axial magnetic field (up to 12T) on the microstructure in directionally solidified lamellar eutectic of Al-Al_2Cu and Pb-Sn and rod eutectic of Bi/MnBi has been investigated experimentally. The results show that a high magnetic field degenerates lamellar structure into a wavy one at low growth speed. The XRD, SAD and HREM patterns indicate that the field has changed the preferred orientation and oriented the Al_2Cu crystal with the <001>-crystal direction along the solidification direction (i.e., the magnetic field direction). At 0.5μm/s, the magnetic fields ($B \geq 4\mathrm{T}$) cause the segregation; as a result, the Al-striations on the longitudinal section and Al-rich zone on the transverse section form. The effects of the field may be attributed to the orientation of the Al_2Cu and Al crystals and the decrease of the diffusion coefficient caused by the magnetic field. For the rod eutectic of MnBi/Bi, it has been found that a high magnetic field promotes the formation of MnBi fiber and makes the directional solidification structure of the eutectic more regular. The MnBi inter-rod spacing and rod diameters gradually increase with the magnetic field intensity. Furthermore, the magnetic field enhances the faceted growth of MnBi phase and the magnetic coercivities of the alloy.

In the chapter 5, the effect of a high magnetic field on the phase transformation, morphology and magnetic property have been investigated. Firstly, a new method is suggested to determine the phase transformation temperature by measuring the temperature at

which the magnetic force changes abruptly in a gradient magnetic field. The MnBi/$Mn_{1.08}$Bi phase transformation temperature under a high magnetic field is measured by this method and the result indicates that the magnetic field has increased the phase transformation temperature. As a result, a 10T-magnetic field has raised the phase transformation temperature about 20K. The morphology and magnetic properties of the MnBi phase are also investigated. It is found that the field has cracked the MnBi crystal along the <001>-crystal plane, and the split MnBi crystals align and aggregate along the magnetic field direction. Along with the change of the MnBi phase morphology, the magnetic property changes greatly. Consequently, the saturation magnetization M_s and the magnetic susceptibility χ increase, and the coercive field H_c as well as the remnant magnetization M_r decrease. This implies that the field causes the magnetic property of the MnBi phase to transform towards soft magnetism. From the magnetic energy and the force caused by the magnetic field, the above results are discussed and analysed.

In the chapter 6, the effects of the simultaneous imposition of an alternating current and a static magnetic field on the solidification structures of the pure Al and the Al-4.5wt.%Cu alloy were investigated. The results show that the structure is refined by the application of the above complex fields. Owing to the fall of the refined grains during the electromagnetic vibration process (i.e., the formation of crystal rains), the refined structure is normally gained only at the bottom region of the sample. A method is proposed to restrain crystal by using an upward magnetic force, and the results indicate that by using this method, the distribution of the refined grains is changed significantly. It is found that there exists a proper magnetic force able to make the whole sample refined. As a consequence, the uniformly refined structure is gained. In the case of the completely suppressed crystal rains, the effect of the electromagnetic force on the structure is investigated, and result indicate that with the increase of the electromagnetic force density, the size of Al grains decreases and the depth of refinement zone increased. Moreover, the Al-4.5wt.%Cu alloy was chosen to investigate the influence of the electromagnetic and magnetic forces on the growth of dendrite. It was observed that with the increase of the electromagnetic force density, the columnar dendritic structure changed into equiaxed ones that continued to disintegrate to isolated grains. Similar to the behaviour of the pure Al, crystal rains formed during the electromagnetic vibration and could be restrained by using the magnetic force.

In the chapter 7, influence of a high gradient magnetic field on the phase distribution and phase structure has been investigated. It was found that the application of a gradient magnetic field was capable of controlling the distribution of the primary phase in alloys. As a consequence, an axial gradient magnetic field causes the primary MnBi phase in Bi-6wt.%Mn

alloy and the primary Si in Al-18wt.%Si alloy to segregate from the matrix. The application of a radial gradient magnetic field produces a ring-like MnBi phase-rich layer. The application of an axial gradient magnetic field can produces the refined structure on the whole sample during the electromagnetic vibration process of pure Al through restraining the formation of crystal rains. The gradient magnetic field also affects microstructure by aligning the phase and controlling the phase aggregation process. Moreover, investigation on the influence of an axial gradient magnetic field on the distribution of the element indicates that the field causes the Mn solute in Bi-6wt.%Mn alloy to separate from the Bi matrix.

In the chapter 8, we provide concluding remarks.

Reference

[1] A. E. Mikelson, Ya. Kh. Karklin, J.Crystal Growth 52 (1981) 524.

[2] E.M.Savitsky, R.S.Torchinova, S.A.Turanov, J.Crystal Growth 52 (1981) 519.

[3] P.Rango, M.Lees, P.Lajay, A.Sulpice, R.Tournier, M.Ingold, P.Germi, M.Pernet, Nature 349 (1991) 770.

[4] A. Katsuki, R. Tokunaga and S.I. Watanabe, Chem. Lett. 8 (1996) 607.

[5] X. Y. Lu, A. Nagata, K. Watanabe, T. Nojima, K. Sugawara and S. Kamada, Physica C: Superconductivity, Volume 382, Issue 1, 15 October 2002, p.27.

[6] W. P. Chen, H. Maeda, K. Kakimoto, P. X. Zhang, K. Watanabe, M. Motokawa, H. Kumakura and K. Itoh, J. Crystal Growth 20 (1999) 69.

[7] H.Morikawa, K.Sassa, S.Asai, Materials Transactions JIM 139 (1998) 814.

[8] Y. Ootake, K. Sassa, T. Yamada, S. Asai, Journal of the Japan Institute of Metals. 67(2003)1.

[9] M. Shimotomai, K. Maruta, Scripta Mater. 42 (2000)499.

[10] M. Shimotomai, K. Maruta, K. Mine and M. Matsui, Acta Materialia 51(2003) 2921.

[11] I.Kittel, Introduction to solid-state physics. Moscow: GIFML Publ. House; 1963. p. 326.

[12] H. Morikawa, K. Sassa and S. Asai, Materials Transaction JIM, 39 (1998) p.814.

[13] J.W. Martin, R.D.Doherty and B.Cantor, Stability of microstructure in metallic systems. Cambridge University press 2nd Ed. 1997, p.391.

[14] L. Valko and M. Valko, IEEE Transactions on Magnetics 30 (2) (1994) 1122.

[15] V.D.Krivoglaz, N.M.Rodigin, L.V.Smirnor, G.M.Filonchik, I.G.Fakidov, Fiz Metalloved;12(1961) 302.

[16] Ye.A .Fokina, E.A. Zavadskiy, Fiz Metalloved 12(1963)311.

[17] K.R. Satyanarayan, W. Eliasz, A.P. Miodownik, Acta Metall 16(1968)877.

[18] V.D.Sadovsky L.V.Smirnov, Y.A.Fokina, P.A.Malinen, I.P.Soroskin, Fiz Metal Metall 24 (1964) 502.

[19] T. Kakeshita, K. Shimizu, T. Saburi, in: W.C. Johnson, J.M.Howe, D.E. Laughilin, W.A.Soffa (Eds.), Solid→solid Phase Transformations TMS,Warrendale, P.A,1994, PP.817.

[20] V.N. Pustovoit, Y. M. Dombrovskii, S.A.Grishin, Metalloved Term Obrab Met 1979:22.

[21] Z. Palmai, Gepgyartastechnologia 22(1982) 463.

[22] C.T. Peters, A.P. Miodownik, Scr MET 71(973)955.

[23] M.Enomoto, H.Guo, Y.Tazuke, Y.R.Abe, M.Shimotomai, Metall Mater Trans;32A(2001)445.

[24] H.D.Joo, S.U.Kim, N.S.Shin, Y.M.Koo, Materials letters 43 (2000)225.

[25] A.A.Galkin,E.A.Zavadskii, Y.I.Yalkov, Phys. Stat.Sol.(b) 46(1971)K23.

[26] Y. C.Liu, D.Gau, P. Shen, J.Am.Ceram.Soc.79(1996)559.

[27] J.K. Choi, H. Ohtsuka, Y. Xu and W.Y. Choo, Scripta Mater 43 (2000) 221.

[28] M. Enomoto, H. Guo, Y. Tazuke, Y.R. Abe and M. Shimotomai, Metall Mater Trans 32A (2001) 445.

[29] W. Liu, D.R. Ou, H.H. Zhou, G.Y. Tang and F. Wu, J Mater Res 16 (2001) 2280.

[30] M. Shimotomai, K. Maruta, K. Mine and M. Matui, Acta Mater 51 (2003) 2921.

[31] Y. Zhang, N. Gey, C. He, X. Zhao, L. Zuo and C. Esling, Acta Mater 52 (2004) 3467.

[32] Y. Zhang, C. He, X. Zhao, L. Zuo, C. Esling and J. He, J. Magn Magn Mater 284 (2004) 287.

[33] G.M. Ludtka, R.A. Jaramillo, R.A. Kisner, D.M. Nicholson, J.B. Wilgen and G. Mackiewicz-Ludtka et al., Scripta Mater 51 (2004), p. 171.

[34] R.A. Jaramillo, S.S. Babu, G.M. Ludtka, R.A. Kisner, J.B. Wilgen and G. Mackiewicz-Ludtka et al., Scripta Mater 52 (2005) 461.

[35] D.H.Mattheson, M.Wargo, S.Motakef, D.Carlson, J.Nakos, A.Witt, J. Cryst Crowth 85(1987) 557.

[36] G.D.Robertson, D.OConnor, J.Crystal. Growth.76 (1986)100.

[37] W.V. Youdelis, R.C.Dorwad, Can. J .Phys., 44(1966)139.

[38] W.V. Youdelis, J. R.Cahoon. Can. J .Phys., 48(1970)805.

[39] W.J.Boettinger, F.Biancaniello, S.Corell, Met.Trans.A 12A (1981)321.

[40] S.N.Tewari, R.Shah, H.Song, Met.Trans.A 25A(1994) 1535.

[41] T. Alboussiere, R. Moreau, and D Camel, Compte Rendu de l'Acad. Sci., 313(1991)749.

[42] O. Lakar, Thesis INPG, France, 1994.

[43] H.B. Callen. Phys. 73(1948)1349.

[44] J.A.Shercliff, J.Fluid Mech.91 (2) (1979) 231.

[45] Y. Gel'fgat, L. Gorbunov, Sov. Phys. Dokl. 34 (5) (1989) 470.

[46] Y.Y. Khine, J.S. Walker, J. Crystal Growth 183(1998) 150.

[47] A. Cröll, F.R. Szofran, P. Dold, K.W. Benz and S.L. Lehoczky, J. Crystal Growth 183 (1998) 554.

[48] S. Yesilyurt, L. Vujisic, S. Motakef, F.R. Szofran and M.P. Volz, J. Crystal Growth 207(1999) 278.

.

[49] P. Dold, F.R.Szofran, K.W. Benz, J. Crystal Growth 291(2006) 1.

[50] P. Lehmann, R. Moreau, D. Camel, R. Bolcato, Acta Mater 46 (1998) 4067.

[51] H.O. Martikainen and V.K. Lindroos, Scand J Metall 10 (1981) 3.

[52] T.Watanabe, Y.Suzuki, S.Tanii and H.Oikawa, Philos Mag Lett. 62 (1990) 9.

[53] N.Masahashi, M. Matsuo and K. Watanabe, J. Mater Res 13 (1998) 457.

[54] T. Watanabe, Y. Suzuki, S. Tanii and H. Oikawa, Philos Mag Lett 62 (1990) 9.

[55] C.M.B. Bacaltchuk, G.A. Castello-Branco, M. Ebrahimi, H. Garmestani and A.D. Rollet Scripta Mater 48 (2003)1343.

[56] T. Watanabe, Text Microstruct 20 (1993) 195.

[57] A.G. Garbatz and M.W. Grabski, Acta Metall Mater 41 (1993) 457.

[58] L. Zuo, T. Watanabe and C. Esling, Z Metallkde 85 (1994) 554.

[59] Y. Zhang, C. He, X. Zhao, L. Zuo, C. Esling and J. He, J. Magn Magn Mater.54 (2004) 287.

[60] X.J. Hao, H. Ohtsuka, H.Wada, Mater Trans.44(2003)2532.

[61] G.M. Ludtka, R.A. Jaramillo, R.A. Kisner, D.M. Nicholson, J.B. Wilgen and G. Mackiewicz-Ludtka et al., Scripta Mater 51 (2004) 171.

[62] R.A. Jaramillo, S.S. Babu, G.M. Ludtka, R.A. Kisner, J.B. Wilgen and G. Mackiewicz-Ludtka et al., Scripta Mater. 52 (2005) 461.

[63] S.Tsurekawa and T.Watanabe, Mater Sci Forum 426–432 (2003) 3819.

[64] S. Tsurekawa, K. Harada, T. Sasaki, T. Matsuzaki and T. Watanabe, Trans JIM 41 (2000) 991.

[65] K. Kawahara, Y. Ando, K. Nogiwa, Y. Yagyu, S. Tsurekawa and T. Watanabe, Ann Chim Sci Mater. 27 (2002) 269.

[66] S. Yamaura, Y. Furuya and T. Watanabe, Acta Mater 49 (2001) 3019.

[67] K. Kawahara, D. Iemura, S. Tsurekawa and T. Watanabe, Mater Trans 44 (2003) 2570

[68] T.Z. Fahidy, Prog. Surf. Sci. 68 (2001) 155.

[69] T.Z. Fahidy, J. Appl. Electrochem 13 (1983) 553.

[70] R.A. Tacken and L.J.J. Janssen, J. Appl. Electrochem 25 (1995) 1.

[71] A. Chiba and T. Ogawa, Chem. Abstr. 108 (1988) 175888.

[72] G. Hinds, J.M.D. Coey and M.E.G. Lyons, J. Appl. Phys. 83 (1998) 6447.

[73] I. Mogi, S. Ookubo, Boundary 4(1994) 37.

[74] I. Mogi, S. Okubo and Y. Nakagawa, J. Crystal Growth 128 (1993) 258.

[75] J.M.D. Coey and G. Hinds, J. Alloys Comp. 326 (2001) 238.

[76] L. Yang, J. Electrochem. Soc. 101 (1954) 456.

[77] M. Perakh, J. Electrochem. Soc. 122 (1975) 1260.

[78] A. Chiba, K. Kitamura and T. Ogawa, Surf. Coat. Technol. 27 (1986) 83.

[79] J.C. Shannon, Z.H. Gu and T.Z. Fahidy, J. Electrochem. Soc. 144 (1997) 314.

[80] J.C. Shannon, Z.H. Gu and T.Z. Fahidy, J. Appl. Electrochem. 29 (1999) 577.

[81] E. Brillas, J. Rambla and J. Casado, J. Appl. Electrochem. 29 (1999) 1367.

[82] O. Devos, A. Olivier, J.P. Chopart and G. Maurin, J. Electrochem. Soc. 145 (1998) 401.

[83] O. Devos, O. Aaboubi, J.P. Chopart, E. Merienne, A. Olivier and J. Amblard, J. Electrochem. Soc. 145 (1998) 4135.

[84] A. Bund, S. Koehler, H.H. Kuehnlein and W. Plieth, Electrochim. Acta 49 (2003), 147.

[85] N. Hirotaa, Soma Harab, H. Uetakeb, H. Nakamurab, K. Kitazawab, J. Crystal Growth 286 (2006) 465.

[86] S. Awaji, K. Watanabe, Y. Ma, M. Motokawa, Physical B 294 (2001) 482.

[87] Y. Ma, K. Watanabe, S. Awaji, M. Motokawa, Physical Review B 2002(65) 174528.

[88] E. Beaugnon, R. Tournier, Nature 349 (1991) 470.

[89] M.A. Weilert, D.L. Whitaker, H.J. Maris, G.M. Seidel, Phys. Rev. Lett. 77 (1996) 4840.

[90] M.V. Berry, A.K. Geim, Eur. J. Phys. 18 (1997) 307.

[91] Y. Ikezoe, N. Hirose, J. Nakagawa, K. Kitazawa, Nature 393 (1998) 749.

[92] M.Motokawa, I. Mogi, M. Tagami, M. Hamai, K. Watanabe, S. Awaji, Physica B 256}258 (1998) 618.

[93] M.Tagami, M. Hamai, I. Mogi, K. Watanabe, M. Motokawa, J. Crystal Growth 203 (1999) 594.

[94] M. Hamai, I. Mogi, M. Tagami, S. Awaji, K. Watanabe, M.Motokawa, J.of Crystal Growth 209 (2000) 1013.

[95] D.Braithwaite, E.Beaugnon and R.Tournier, Nature 354(1991) 134.

Chapter 2: Experimental equipment and method

2.1. Experimental device

In the present work, the experimental device consists of a superducting magnet, a free solidification apparatus under a high magnetic field, a directional solidification apparatus

Fig. 2.1. High superconductor magnet.

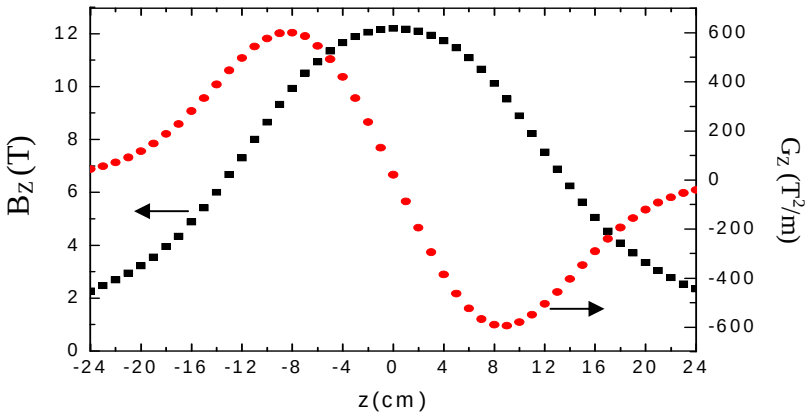

Fig. 2.2. Profiles for a magnetic field operating at 12T. B_z is the vertical component of the field on the axis of the coil. G_z is the vertical component of grad $(B_z^2/2)$ on the axis of the coil (i.e. $B_z dB_z/dz$), z is the distance above the coil.

under a high magnetic field, a phase transformation measurement equipment and an electromagnetic vibration device under complex fields.

2.1.1. Superconducting magnet

The superconducting magnet was made by the Oxford Instrument Company with a columnar working space as shown in Fig. 2.1. The diameter and high of the columnar space are 98mm and 1174mm, respectively. The magnet is capable of producing a static magnetic field up to 14T with a precision of 1Oe. Field profiles in the magnetic field along the axial direction operating at 12T are as shown in Fig. 2.2.

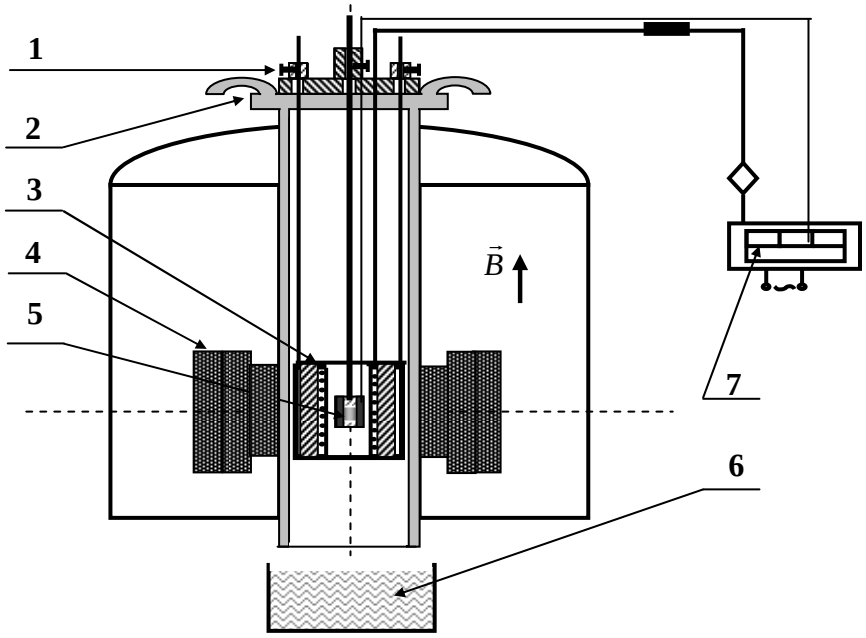

Fig. 2.3. Schematic diagram of the experimental device of metal solidification under the magnetic field. 1 Sample frame, 2 water-cool cover, 3 heat furnace, 4 superconductor magnet, 5 sample, 6 quenching water-pond, 7 controlling temperature system.

2.1.2. Free solidification apparatuses under a high magnetic field

Under the above magnet, the solidification experiment is performed to investigate the influence of the magnetic field on the solidification structure. The experiment apparatus is schematically shown in Fig. 2.3. It consists of heating furnace, temperature controller, a

water-cool cover (to protect the magnet), the sample, the sample frame and quenching water-pond.

2.1.3. Directional solidification apparatus under a high magnetic field

The directional solidification apparatus is shown in Fig. 2.4**.** It consists of a static superconductor magnet and a typical Bridgman-Stockbarge type furnace equipped with pulling system and temperature controllers. The furnace, consisting of nonmagnetic material,

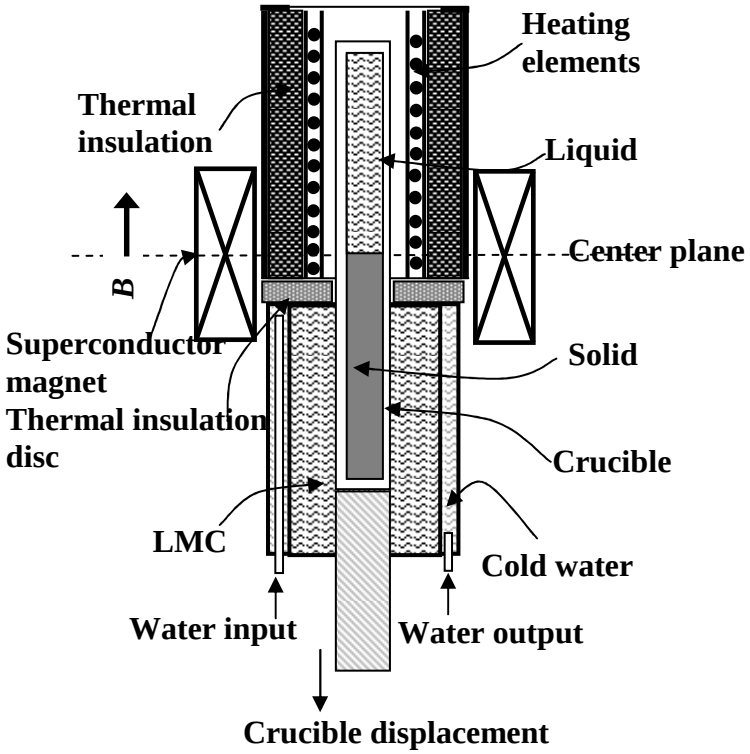

Fig. 2.4. Schematic illustration of the Bridgman solidification apparatus in a superconducting magnet.

has a negligible effect on field uniformity. A water-cooled cylinder containing liquid Ga-In-Sn metal (LMC) is used to cool down the specimen. The temperature gradient within the specimen is controlled by adjusting the temperature of the furnace hot zone, which is insulated from the LMC by a refractory disc. The apparatus is designed such that the specimen moves downward while the furnace remains stationary. Growth speeds, R, lie in the range $0.5\mu m/s \leq R \leq 5000\mu m/s$. In order to observe the morphology of the liquid /solid interface during the growth of the crystal, quenching experiments were carried out by quickly withdrawing the specimen into the LMC cylinder to cool the specimen immediately to room temperature. During the experiment, the specimens contained in the corundum crucibles are

melted and directionally solidified in the Bridgman apparatus by drawing the crucible assembly at various speeds into the LMC cylinder.

2.1.4. Measuring phase transformation equipment

In order to in situ investigate the phase transformation under a high magnetic field, a method was proposed to determine the phase transformation by measuring the change in the magnetic force. It is well known that under a gradient magnetic field, the vertical magnetic

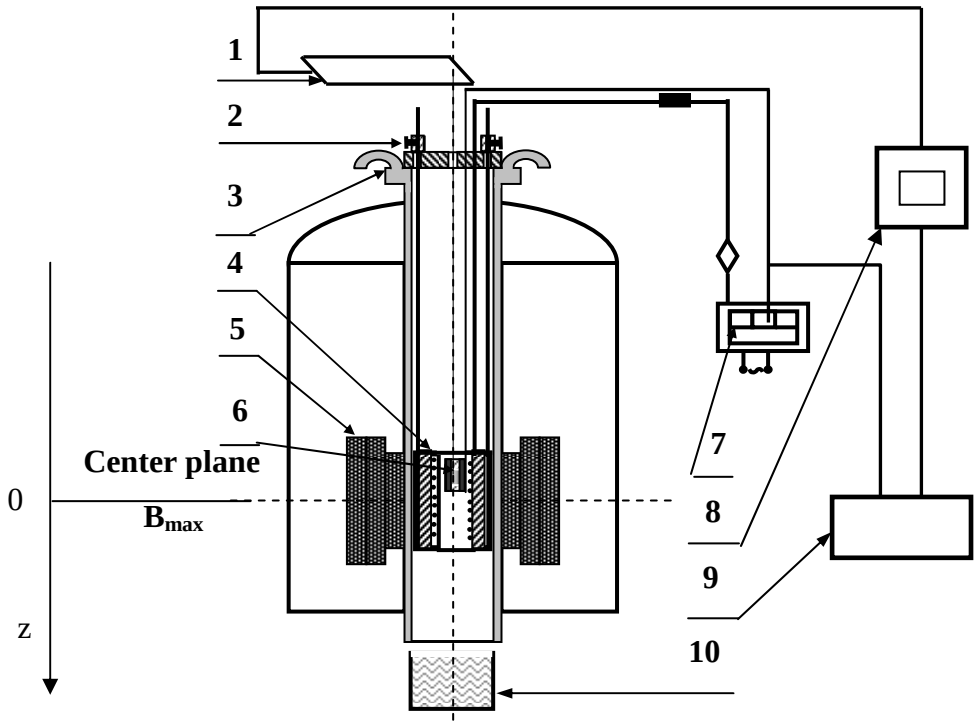

Fig. 2.5. Schematic diagram of the experimental device to fabricate samples and measure the phase transformation. 1 Force sensor; 2 furnace frame; 3 water-cool cover; 4 heating furnace; 5 superconductor magnet; 6 sample; 7 controlling temperature system; 8 dynamic resistance strain meter; 9 *X*-*Y* recorder; 10 quenching tank.

force F_z is:

$$F_z = (\chi/\mu_0) B_z \, \mathrm{d}B_z/\mathrm{d}z \qquad (2.1)$$

where χ is the susceptibility of the substance, μ_0 the permeability of free space, B_z the magnetic field induction or magnetic flux density on vertical direction. In S.I. unites, F is in N/kg. The value of μ_0 is $4\pi\times10^{-7}$ H/m. Usually, the phase transformation can lead to the change in the magnetic susceptibility. From formula (2.1), it can be learned that the magnetic

force will change during the phase transformation. Therefore, the phase transformation temperature can be determined by measuring the temperature at which the magnetic force changes abruptly in a gradient magnetic field. The experimental procedure is as follow: an alumina crucible containing the sample was hung by a copper wire in a gradient magnetic field and the copper wire was connected to a self-designed magnetometer with a force sensor. The samples were heated to a certain temperature (higher than the phase transformation temperature) and then cooled to below the phase transformation temperature. Meanwhile, the force and temperature values were measured simultaneously. A sharp increase (decrease) in force indicated the occurrence of phase transformation. The error is around 5%.

2.1.5. Electromagnetic vibration device under complex fields

The experimental apparatuses of electromagnetic vibration are shown in Fig. 2.6. A static magnetic field was imposed during all the experiment process by using super-conducting magnet, and the distribution of the field is shown in Fig. 2.2. The sample was placed in the alumina tube of almost the same inner diameter and set in a sample holding assembly, the assembly being positioned at the different position of the magnet. A removable resistance furnace was used to heat and melt the sample. In these experiments, samples were heated

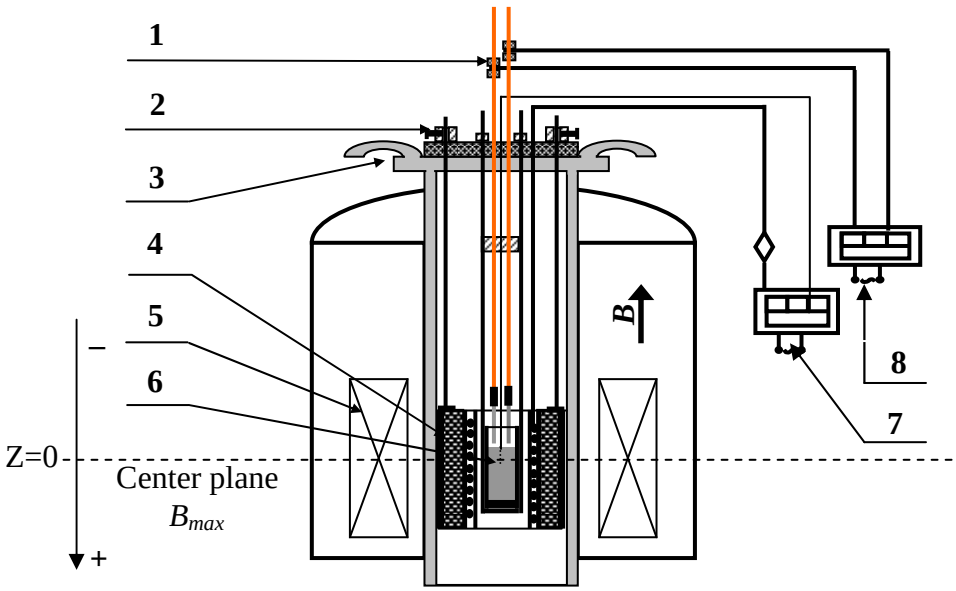

Fig. 2.6. Schematic diagram of the metal solidification experimental device in complex fields: 1 Electric pole, 2 Sample frame, 3 Water-cool cover, 4 Heat furnace, 5 Superconductor magnet, 6 Samples, 7 Controlling temperature system, 8 AC electric source.

above melting point and kept at this temperature for 30 minutes which were enough to melt

the sample completely, and then an alternating electrical current with the frequency of 50Hz was supplied to the metal by inserting a couple of stainless steel electrodes at the top surface of the metal. The current was stopped when samples were cooled completely. Temperature of the sample was measured by a K-type thermocouple that was put in direct contact with sample and controlled by the controlling temperature equipment, and the average cooling rate of sample was 20K/min.

2.2. Experiment materials and alloy preparation

In this work, Al-Cu, Al-Ni and Bi-Mn alloys and pure Al were used. Bi-Mn alloys including Bi-20wt.%Mn, Bi-6wt.%Mn, Bi-0.85 wt.%Mn and Bi-0.72. wt.%Mn ones were prepared with high purity Bi(99.99 wt.%) and Mn (99.99 wt.%). The alloys in a high-purity graphite crucible of 10cm in diameter were heated to 600°C in a vacuum induction and magnetically stirred for 0.5hour, and then poured into a graphite mold to cast specimens. The Al-Cu alloys (i.e., Al-0.85wt.%Cu and Al-4.5wt.%Cu alloys) used in this study were prepared with high purity Al (99.99 wt.%) and Cu (99.99 wt.%). The alloy, being put in a high-purity graphite crucible of 10cm diameter, was heated to 900°C, magnetically stirred for 0.5hour and poured into a graphite mold to cast specimens. In a similar way, Al-12 wt. %Ni samples were prepared. Then, the cast specimen was enveloped in the corundum tube of high purity to prepare for the experiment. The detailed experimental process is presented in the following chapters and appendices.

Chapter 3: Influence of an axial high magnetic field on the growth of the single phase alloy during directional solidification

3.1. Introduction

It is traditionally suggested that the static magnetic field damps the convection in the liquid bulk during the solidification process. However, some unexpected results have been observed, depending on the composition of the alloy and the experimental conditions as described in chapter 1. Alboussière et al [1] suggested that a new convection was induced by the interaction between the magnetic field and thermoelectric effect, and further produced the thermoelectromagnetic convection (TEMC). Yesilyurt et al [2]. presented numerical solutions for the buoyant convection and TEMC flows in an actual crystal-growth process with an axial magnetic field. However, many previous studies usually were related to TEMC only with a moderate or weak magnetic field (B<1T) and few studied in strong magnetic field (B>2T), and especially there are few studies on the effect of magnetic field on the liquid-solid interface morphology. Moreover there is lack of investigation on the cell and dendrite array under a high magnetic field. This chapter investigates the effect of a high magnetic field on the morphology of liquid-solid interface and the microstructure of solid in Al-Cu hypoeutectic alloy during directional solidification process. It will be shown that the magnetic field deforms shape of the growth interface and promote the interface transformation. Moreover, the field also affects the cell and dendrite array significantly.

3.2. Effect of the magnetic field on the interface transformation and shape

Al-0.85wt.%Cu alloy is chosen to investigate the influence of a high magnetic field on the planar-cellular and cellular-to-dendritic interface transformation. Fig. 3.1 shows the longitudinal microstructures at the liquid-solid interface solidified at a temperature gradient in liquid (G_L) of 62.8K/cm. Fig. 3.1(a) and Fig. 3.1(b) demonstrate the microstructures solidified at the speed of 1.5μm/s without and with the magnetic field, respectively. It can be observed

that the application of a 10T-magnetic field has destabilized the interface. At 5μm/s, comparison of the microstructures without and with the field [Fig. 3.1(c) and Fig. 3.1(d)] indicates that a 10T field causes the transition from the cell to dendrite by promoting the branching. Moreover, it can be found that the interface becomes more irregular.

The effect of a high magnetic field on the equilibrium partition coefficient *k* has been

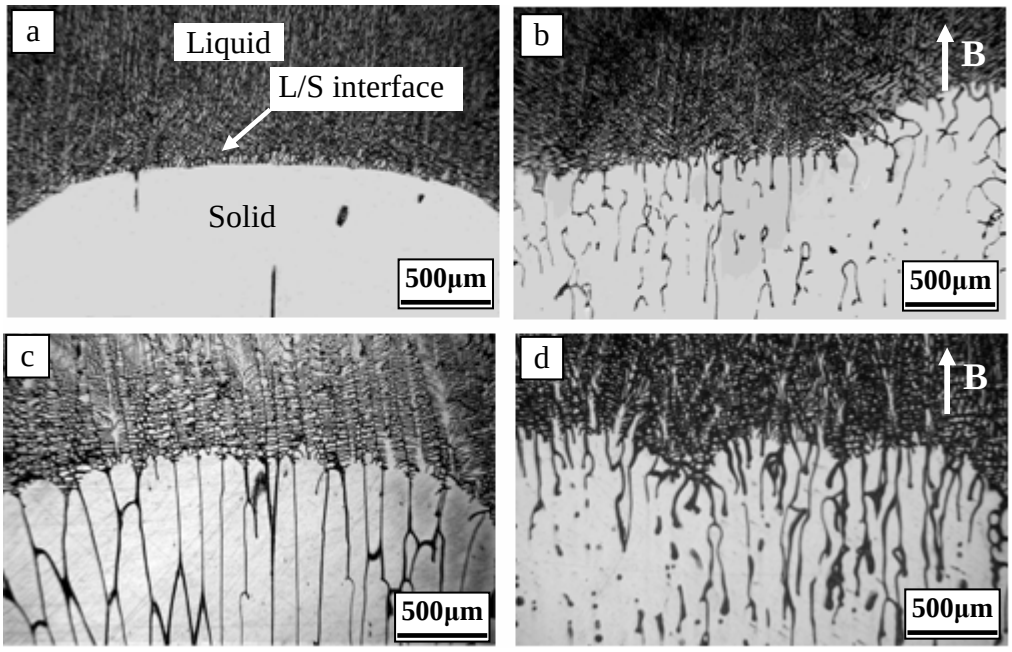

Fig. 3.1. Longitudinal solidification structure at the quenched liquid-solid interface (parallel to the growth direction) of Al-0.85wt%Cu alloy solidified at a temperature gradient in liquid (G_L) of 62.8K/cm for various growth speeds.
(a) 0T, 1.5μm/s; (b) 10T, 1.5μm/s; (c) 0T, 5.0μm/s; (d) 10T, 5.0μm/s.

investigated (see e.g .(8) of A2). Here, the value of $\frac{k'}{k}$ has been evaluated as follow:

The maximal value of $\frac{k'}{k}$ can be written as

$$(\frac{k'}{k})_{\max} = 1 + \mu_0 \frac{\left|\chi_S^{Cu}\right| V_S^{Cu}}{2RT_M^{Al}} \mathrm{H}^2 \qquad (3.1)$$

where μ_0 is the permeability of free space, $4\pi\times10^{-7}$ H/m, χ_S^{Cu} partial molar susceptibilities of Cu in the solid, its value can be written as $\chi_S^{Cu} = \chi_V^{Cu} = 10^{-5}$; V_S^{Cu} the partial molar volumes of

Cu in the solid, $V_S^{Cu} \approx V_{mol}^{Cu} = \frac{64\times10^{-3}}{8.9\times10^{3}} = 7.2\times10^{-6}\ \mathrm{m}^3/\mathrm{mol}$, R gas constant, 8.314 J/K/mol.

Thus, under a high magnetic field of 10T,

$$(\frac{k^{/}}{k})_{\max} \approx 1+(4\pi\times10^{-7}\times\frac{7.2\times10^{-6}\times10^{-5}}{2\times8.31\times933}\times10^{2}) = 1+5.8\times10^{-18} \quad (3.2)$$

From the above evaluation value, it can be learned that effect of high magnetic field on the value of *k* is very small. This implies that there exist other factors to affect the interface instability. Nevertheless, it must be emphasized that the uncertainty on the magnetic susceptibility is very large. The detail results and analysis are investigated in **appendix [A1] and [A2].**

3.3. Effect of the magnetic field on the array of dendrite

Bi-0.85 wt.%Mn, Al-4.5 wt.%Cu and Al-12wt.%Ni alloys are applied to investigate effect of high magnetic field on the dendrite array. Fig. 3.2 shows the microstructures on the section parallel to the solidification direction (i.e., the magnetic field direction) in directionally solidified Bi-Mn, Al-Cu and Al-Ni hypereutectic alloys with and without a 10T magnetic field, respectively. Comparison of the microstructures with and without the magnetic field shows that the field has influenced the primary dendrite arm growth significantly. As a consequence, for the Bi-0.85wt.% Mn alloy solidified at 5μm/s [Fig. 3.2 (a)], the field has increased the ratio of length to diameter and made the alignment of the MnBi dendrite more regular. This means that the field has enhanced the growth of the MnBi dendrite along the solidification direction (i.e. the magnetic field direction). However, for the Al-4.5wt.%Cu alloy solidified at 50μm/s, the field deflects the primary dendrite arm from the solidification direction and the primary dendrite arm is aligned about 45° with the solidification direction [Fig. 3.2(b)]. For the Al-12wt.%Ni alloy solidified at 100μm/s, the field aligns Al_3Ni dendrite with the primary dendrite arm perpendicular to the magnetic field [Fig. 3.2 (c)]. Above results indicate that for different alloys, the influences of the magnetic field on the dendrites are different. **Appendix [A3] presents the detailed investigations**.

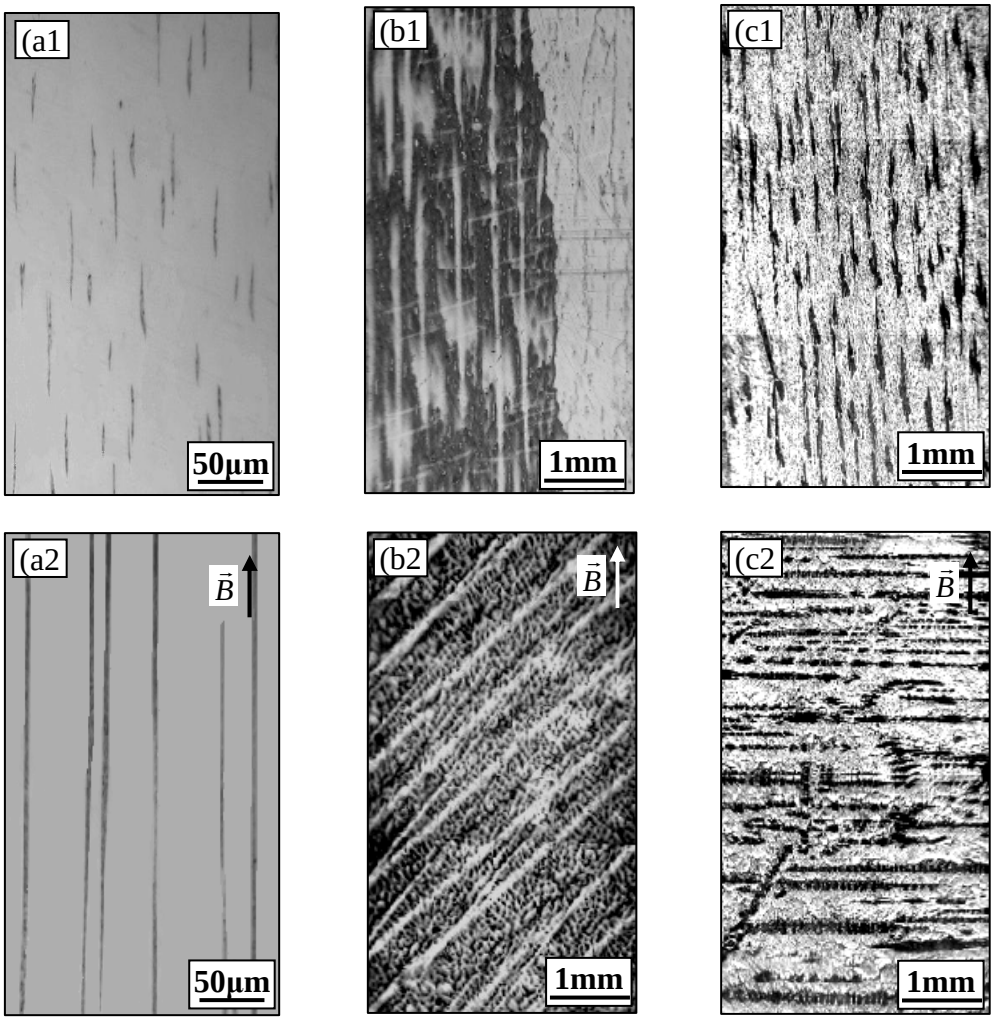

Fig. 3.2. Influences of a 10T magnetic field on the primary dendrite arm during the directional solidification: (a) Bi-0.85wt.%Mn; (b) Al-4.5wt.%Cu; (c) Al-12wt.%Ni. The primary phase in above alloys: MnBi, α-Al and Al_3Ni, respectively.

3.4. The columnar-to-equiaxed transition (CET) under a magnetic field

Fig. 3.3 shows the microstructures at the solid-liquid interface and mushy zone in directionally solidified Al-4.5wt.%Cu alloy at a lower growth rate of 5μm/s and 10μm/s, respectively. It can be observed that the field has caused the occurrence of the columnar-to-equiaxed transition (CET). Further investigation is done in **Appendix [A3]**.

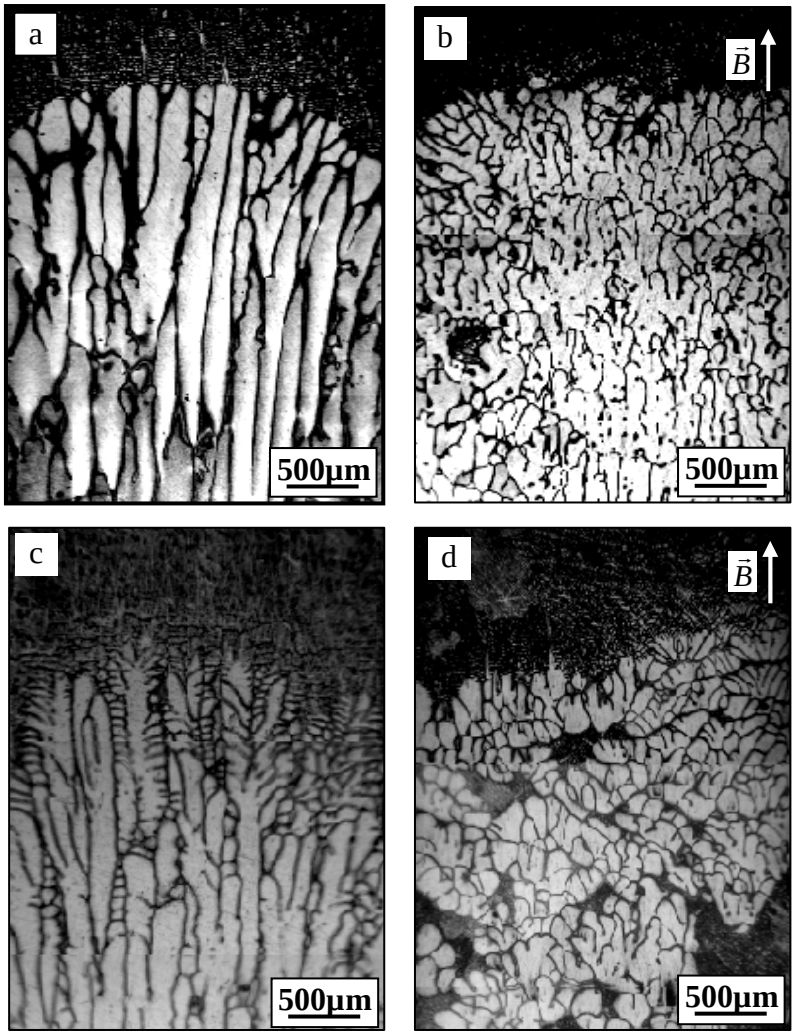

Fig.3.3. The columnar-to-equiaxed transition (CET) at the liquid/solid interface:
(a) 5µm/s, 0T; (b) 5µm/s, 10T; (c) 10µm/s,0T; (d)10µm/s, 10T.

Reference

[1] T. Alboussiere, R. Moreau, and D Camel, Compte Rendu de l'Acad. Sci., 313(1991)749.

[2] S. Yesilyurt, L. Vujisic, S. Motakef, F.R. Szofran and M.P. Volz, J. Crystal Growth 207(1999) 278.

Chapter 4: Effect of an axial high magnetic field on the eutectic microstructure during the directional solidification

4.1. Introduction

In the past, many works had focused on controlling directional solidification of binary eutectic in which the microstructure was related to conditions of solidification. In addition to the influence of solidification speed, composition, convection, gravity, the influence of magnetic field on the unidirectional solidification has also beeninvestigated. The microstructure directionally solidified eutectic Bi/MnBi was characterized by an aligned rod eutectic morphology with a faceted-nonfaceted phase interface. Thus, rod diameter, inter-rod spacing, and solidification temperature can be used to monitor solidification processing effects. Researches involving the directional solidification of Bi-Mn compounds have indicated significant gravity and transverse magnetic field related effects [1-3]. Moreover, Al/Al_2Cu and Pb/Sn eutectic alloys are typical lamellar eutectic and always act as ideal object to investigate the growth behaviour of the lamellar eutectic in such conditions. Up to now, however, few researches are reported about the effect of longitudinal magnetic field, especially high magnetic field, on rod eutectic MnBi/Bi and lamellar eutectic Al_2Cu/Al and Pb/Sn. So, in this chapter we choose the Al-Al_2Cu and Pb/Sn eutectic alloys as the objective to investigate the effect of a high magnetic field on lamellar and rod eutectic during the directional solidification process. The directional solidification equipment and method are shown in Fig. 2.3.

4.2. Lamellar eutectic

4.2.1. Al-Al_2Cu eutectic

Fig. 4.1 shows the microstructures of Al-Cu alloy directionally solidified at 0.5μm/s without and with a 12T magnetic field. Comparison of the microstructures without and with the field indicates that the application of the magnetic field has resulted in the structure degeneration and decrease of the lamellar spacing. Moreover, the single-phase striations appear. The detail experiment result and analysis are presented in **appendix [A4] and [A5].**

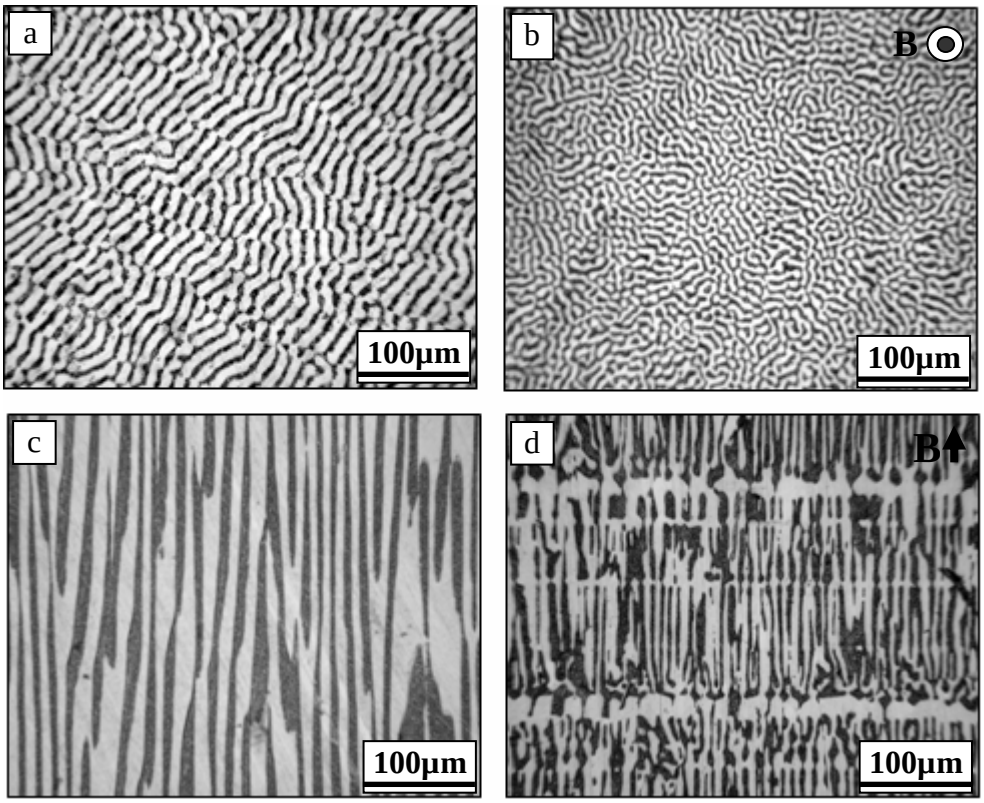

Fig. 4.1. Microstructure of Al-Al_2Cu eutectic alloy with and without magnetic field (G_L=66.8K/cm, R=0.5μm/s).
(a) 0T, transverse section; (b) 12T, transverse section;
(c) 0T, longitudinal section; (d) 12T, longitudinal section.

4.2.2. Pb-Sn eutectic

Fig. 4.2 shows the microstructure of the Pb-Sn alloy directionally solidified at 2μm/s without and with a 10T magnetic field. It can be observed that the field has changed the microstructure and caused the eutectic to be degenerated and deviate from the solidification direction. The detailed experimental result and the analysis are presented in **appendix [A5].**

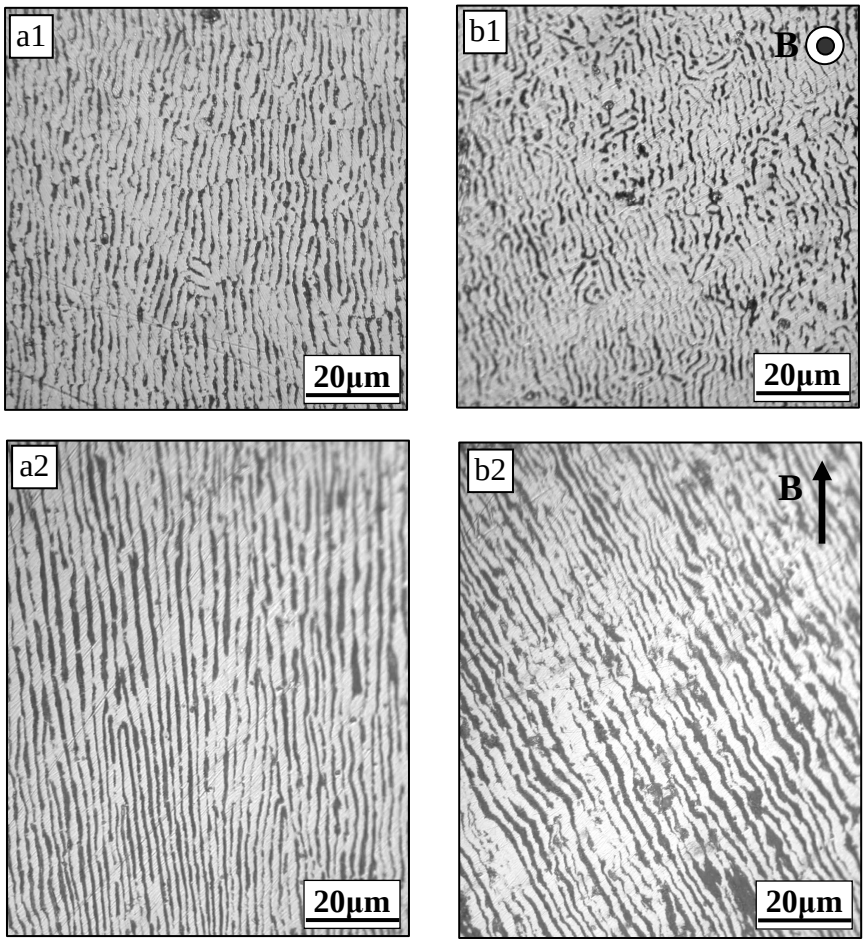

Fig. 4.2. Microstructures in directionally solidified Pb-Sn eutectic alloy without (a) and with a 10T magnetic field (b) (G_L=45K/cm, R=2μm/s) .

4.2. Rod eutectic (Bi-MnBi)

Fig. 4.3 shows the microstructure of the MnBi/Bi eutectic solidified at 5μm/s without and with a 4T magnetic field. Note that the application of the field coarsens MnBi fibers and enhances their growth in the solidification direction significantly [Fig. 4.3(d)]. The "V" shape MnBi appears on the transverse section [Fig. 4.3(b)] suggesting that the field enhances the growth of MnBi phase in the faceted form. The detailed experimental results and the analysis can be found in **appendix [A6].**

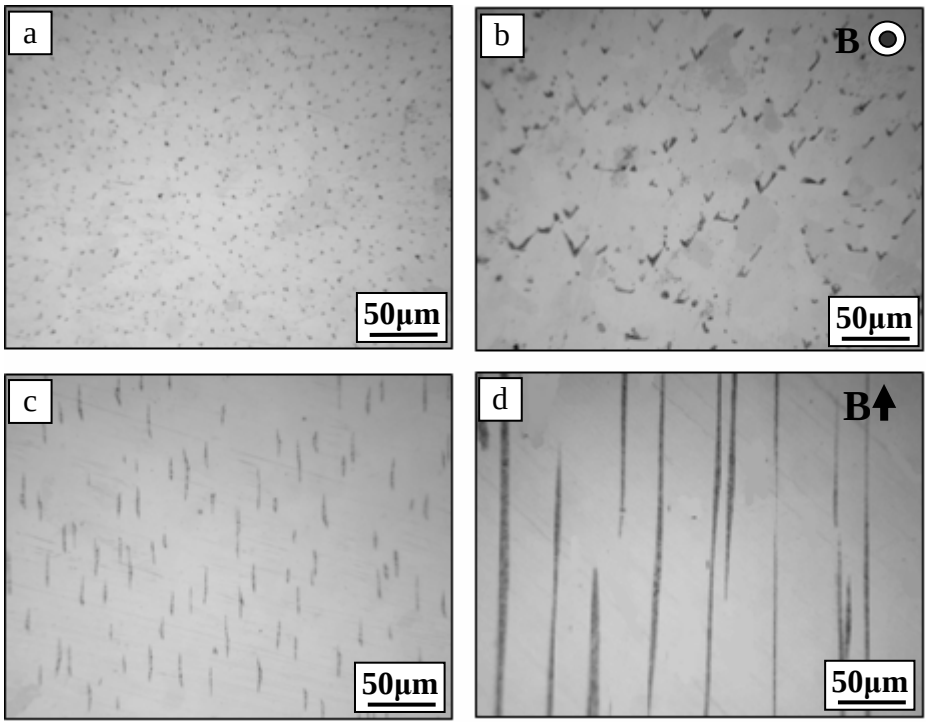

Fig. 4.3. Microstructure of MnBi/Bi eutectic solidified at 5μm/s without and with the magnetic field:
(a) 0T, transverse section; (b) 10T, transverse section;
(c) 0T, longitudinal section; (d) 10T, longitudinal section.

Reference

[1] R. G. Pirich, Mettal Trans. 15 A(1984)2139.

[2] J. L. Decarlo, R. G.:Pirich, Metallurgical Transactions A 15A(1984)2155.

[3] R. G. Pirich and D. J. Larson: Materials Processing in the Reduced Gravity Environment of space, Elsevier Science Publishing Co., New York, NY, 1982:523.

Chapter 5: Effect of a high magnetic field on the phase transformation, morphology and magnetic properties of the MnBi and Mn1.08Bi compounds

5.1. Introduction

Owing to the high uniaxial magnetic anisotropy of its low-temperature phase (LTP) and the favorable magnetooptical properties of its quenched high-temperature phase (QHTP), MnBi compounds have been investigated extensively. A high magnetic field may enhance the above properties, so it is valuable to investigate the physical properties and microstructure of binary compound MnBi. This chapter investigates firstly the effect of high magnetic fields (up to 10T) on the $Mn_{1.08}Bi$ /MnBi phase transformation temperature by measuring the difference of the magnetization force in a gradient magnetic field. Then, the morphology and property change of the primary phase during the phase transformation process under a high magnetic field were investigated in detail. The device to fabricate samples and measure the phase transformation and the experimental process are shown in Fig. 2.5**.**

5.2. Effect of a high magnetic field on the phase transformation temperature

MnBi compound undergoes a magnetic and structure transformation at 355℃ upon heating and 340℃ upon cooling. The transformation on heating is associated respectively with the transformation of the compound from an ordered NiAs structure of low temperature phase MnBi (LTP) to a NiIn-type structure of high temperature phase $Mn_{1.08}Bi$(HTP) and with ferro-to-paramagnetic transition and vice versa. High temperature phase (HTP) quenched forms the quenching high temperature phase (QHTP), which is ferromagnetic. Since the saturation magnetization difference between $Mn_{1.08}$ Bi and MnBi, the application of an external magnetic field can modify the Gibbs free energy of phases and then affects the phase equilibrium. Thus, the phase transformation temperature and transformation course are changed.

Fig. 5.1 shows the schematic illustration of the variation of Gibbs free energy versus temperature in the case without and with the magnetic field. *G* is function of temperature, *T*.

T_0 stands for the temperature at which parent (MnBi) and product phase (MnBi and Bi) have the same free energy in the absence of an applied field. If a magnetic field is applied, the free energy of ferromagnetic MnBi is decreased as shown by the dotted lone. The free energy of $Mn_{1.08}Bi$ and Bi is also changed, but is neglected because it is non-ferromagnetic, the change being very small. Therefore the temperature at which parent and product phase has the same energy shifts to $T_0^{/}$. As a result, the field will raise the $Mn_{1.08}Bi$/MnBi phase transformation temperature.

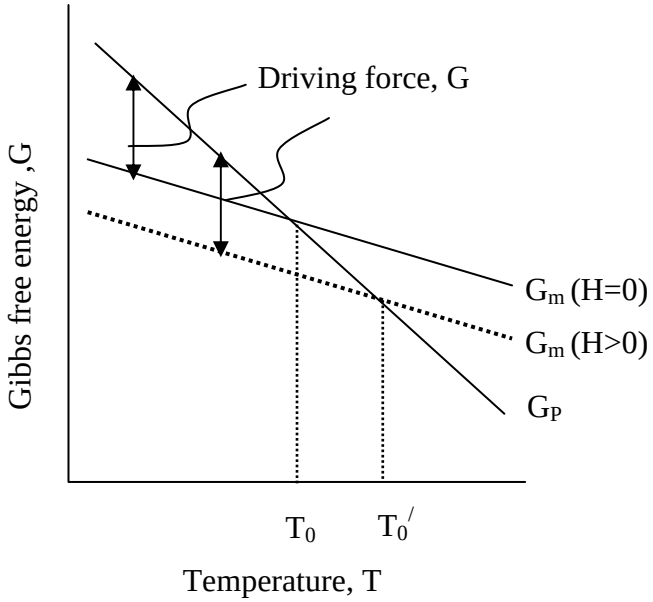

Fig. 5.1. Schematic illustration of free energy as the function of temperature with and without magnetic field.

5.3. In situ measurement of the phase transformation temperature

Usually, the phase transformation will lead to abrupt change in magnetic susceptibility, so, the magnetic force will change abruptly during the phase transformation. Because the $Mn_{1.08}Bi$ is paramagnetic and MnBi ferromagnetic, during the $Mn_{1.08}Bi$/MnBi phase transformation, the change of magnetic force is obvious. Therefore, by measuring the temperature of the sample at which the magnetic force changes abruptly, the phase transformation temperature can be determined. The experimental device and method as shown in Fig. 2.5 were applied to determine the phase transformation. Bi-21wt%Mn was used in this experiment (according to phase diagram [1], Bi-21%Mn alloy is composed of single MnBi phase). The experimental procedure for measuring the phase transformation temperature was

the following: the alumina crucible with the Bi-Mn alloy specimen in it was hanged at the position (z>0) and a downward magnetizing force was detected because the phase is ferromagnetic and paramagnetic with positive magnetic susceptibility. The specimen was heated up to 380℃ at a rate of 0.25K/min, then cooled to below 330℃ at a rate 0.5K/min, meanwhile the force and temperature values were measured. Fig. 5.2 shows the typical force and temperature curves in a gradient magnetic field of B=10T and $B_z \mathrm{d}B_z / \mathrm{d}z = 400\mathrm{T}^2/\mathrm{m}$. The temperature at which the force decreases abruptly is defined as the MnBi to $Mn_{1.08}Bi$ phase transformation temperature and the temperature at which the force increases abruptly as the one from $Mn_{1.08}Bi$ to MnBi. By using above method, the phase transformation temperature in different magnetic field intensity was measured and the measuring result is shown in Fig.5.3. This shows that the application of the magnetic field raises the equilibrium temperature, and in the 10T magnetic field, the MnBi to $Mn_{1.08}Bi$ phase transformation temperature during heating process increases to 375 ℃ from 355 ℃ and the $Mn_{1.08}Bi$ to MnBi phase transformation temperature increases to 362℃ from 340℃.

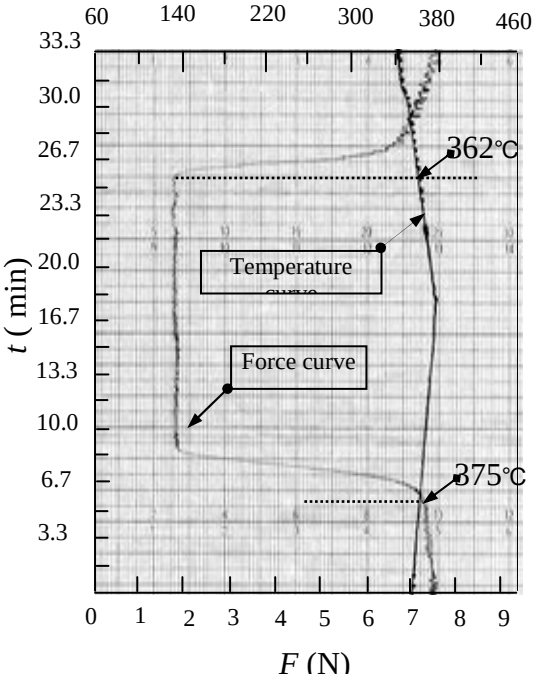

Fig. 5.2. The measured curves of force and temperature during heating and cooling of Bi-Mn alloy in magnetic field. B=10T.

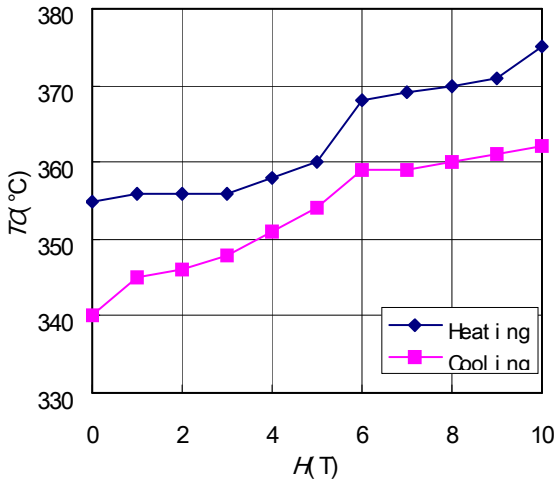

Fig. 5.3. The $Mn_{1.08}Bi$/MnBi phase transformation temperature T_C as a function of the external magnetic field H during heating and cooling, respectively.

5.4. Effect of a high magnetic field on the transformed structure

Fig. 5.4 shows the microstructure heated up at a rate of 10K/min to a certain temperature, then held for 30min and in the 10T high magnetic field cooled below the 262℃, the cooling rate being about 10K/min. Solidified from 350℃ (below 355℃ phase transformation temperature), the elongated MnBi crystals (dark gray) are oriented and grow preferentially along the direction of field in Bi matrix (white) [Fig. 5.4(b)]. The hexagonal sections of crystals only appear in the section perpendicular to the field [Fig. 5.4(a)]. Further XRD patterns show that the *c*-axis of hexagonal MnBi crystal (easy magnetization axis) is aligned parallel to the direction of field. However, solidified from 360℃ (above 355℃) in field, compared with the one solidified from 350℃, the great change of microstructure occurred. As a consequence, the microstructure is larger and the phase cracks along the (001) crystallographic plane.

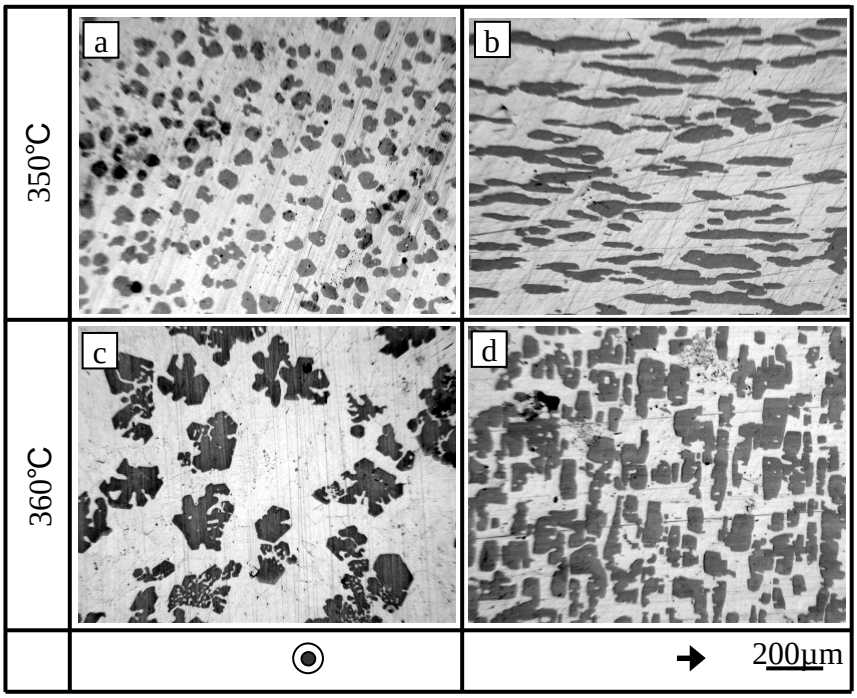

Fig. 5.4. Microstructure of Bi-6wt%Mn alloy solidified from a certain temperature after holding temperature for 60 min at this temperature in the 10T magnetic field.

5. 5. Effect of high magnetic field on the magnetic properties

To study the magnetic properties of MnBi compounds, the magnetization and hysteresis loops along and perpendicular to the direction of magnetic field imposed during the solidification were measured. Because Bi phase is diamagnetic, and its effect may be ignored, the magnetic properties of the alloy are determined mainly by the MnBi phase. Therefore, the properties of the alloy will reflect the ones of MnBi phase.

Fig. 5.5 shows the hysteresis loops of the same sample as in Fig. 5.4. It indicates that the strong anisotropy in the MnBi compound and the magnetic properties [magnetic permeability χ (the slope of the magnetizing curve) and saturation magnetization Ms] of the alloy are as large as the one of ferromagnetic substance. Comparison of the hysteresis loops of the samples solidified from 350℃ and 360℃ indicates that coercive field H_c and the remnant magnetization M_r of the sample solidified from 360℃ are much lower than the one of the sample solidified from 350℃. However, its saturation magnetization M_S is larger. This shows that the effect of the magnetic field on the magnetic properties of MnBi compounds is significant and different for various states.

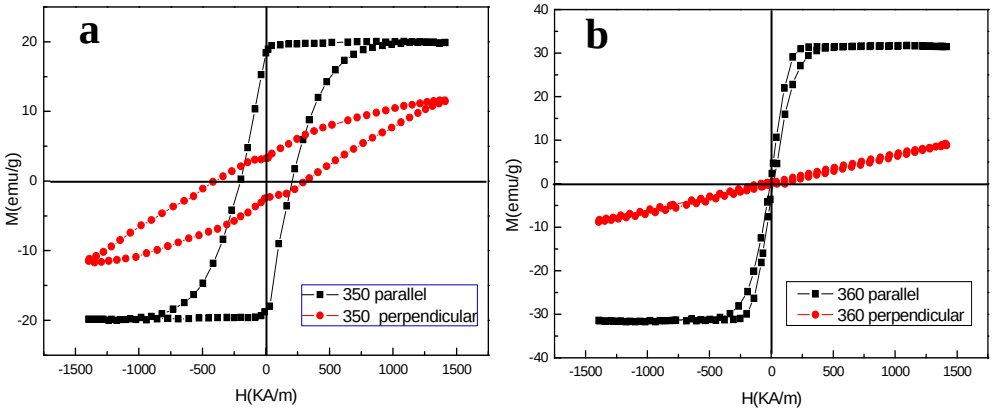

Fig. 5.5. Hysteresis loops of the same samples as shown in Fig. 5.4:
(a) 350℃, (b) 360℃. “parallel and perpendicular” indicate directions of the magnetic field imposed for the magnetization measurement with respect to the magnetic field imposed during the solidification.

The above results a high magnetic field has affected the MnBi/MnBi phase transformation, the morphology and magnetic properties. The detailed experimental results and analysis are presented in **appendix [A7] and [A8]**.

References

[1] W. G. Moffatt, The Handbook of Binary Phase Diagrams. USA: Genium, 1984.p.83.

Chapter 6 : Effects of the simultaneous imposition of a static high magnetic field and alternating current on the solidification structure of the pure Al and Al-4.5wt.%Cu alloy

6.1. Introduction

Many of the mechanical properties of metallic alloys depend on the size and distribution of grains in the structure. Therefore, the structure refinement and the distribution of the refined grains have been the subject of numerous researches in the field of metallurgy. The structure is almost determined in the solidification process, so it is essential to control the solidification structure. Many different methods have been used for this purpose, and the inoculation is a usual method. In early 1980, Vives [1] had studied the effect of electromagnetic vibrations induced by the interaction of alternating electric and static magnetic fields during the solidification of hypoeutectic Al-Si alloys and reported considerable microstructural refinement. Rsdjai [2] investigated the effect of electromagnetic vibrations in hypereutectic Al-Si alloys and found that suspended silicon particles were crushed into small pieces by the cavitation phenomenon. The purpose of this chapter is to study the effect of the simultaneous imposition of electromagnetic and magnetic forces on the structure of pure metal and metallic alloy. The pure Al and its Al-4.5wt.%Cu alloy were chosen to investigate effect of the electromagnetic force on the refinement and the break of the dendrite and effect of the magnetic force on the distribution of the refining grain. The directional solidification equipment and process are shown in Fig. 2.5.

6.2. The effect of the complex fields on the pure Al

Fig. 6.1 shows the structures simultaneous imposed of a 10T-magnetic field and various alternating electric currents with 50 Hz. Compared with the structure imposed of a single magnetic field [Fig. 6.1 (a)], the application of the complex fields has refined the structures significantly and with the increase of the density of the electromagnetic force "$F=J\times B$", the refinement is enhanced.

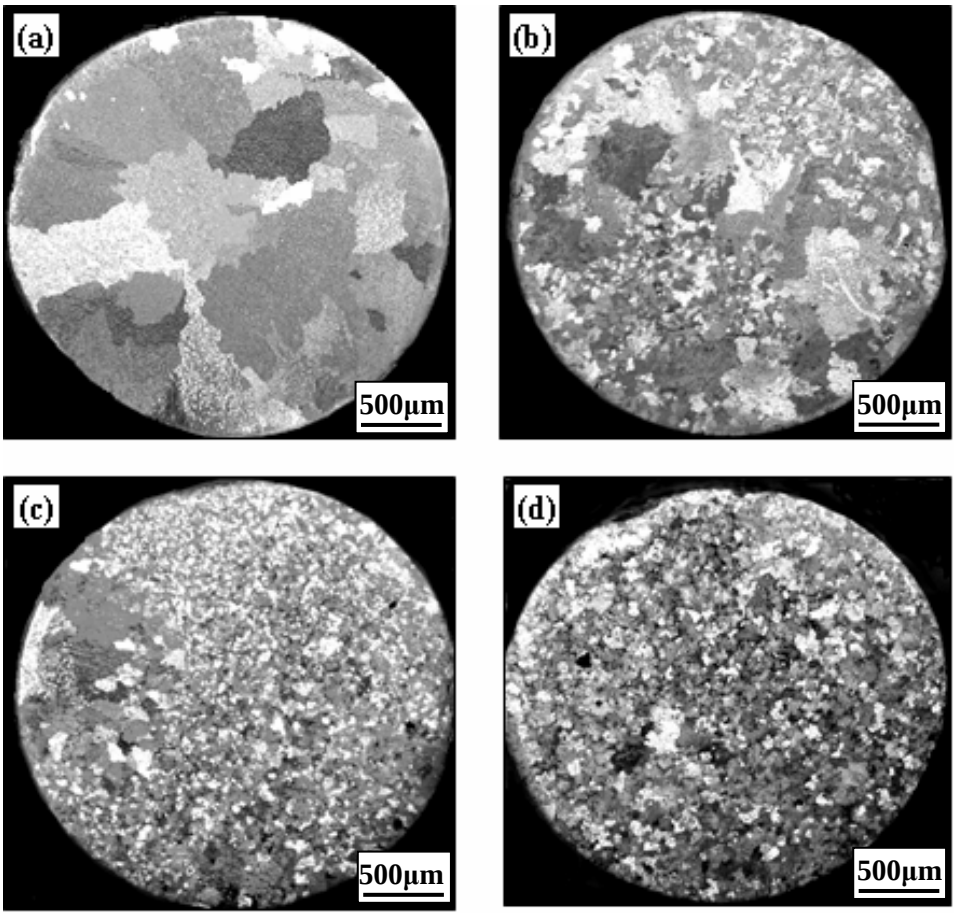

Fig. 6.1. Effect of simultaneous imposing of a 10T magnetic field and various alternating currents on the structure of Aluminum.
(a) B=10T, I=0A; (b) B=10T, I=1A; (c) B=10T, I=3A; (d) B=10T, I=10A.

6.3. The effect of the complex fields the Al-4.5wt.%Cu alloy

Fig. 6.2 shows the microstructures on the transverse section at 2 mm from the electric pole. It can be noticed that under a single field (i.e. the magnetic field of 10T or the current of 10A), there are not obvious effects on microstructure [Figs. 6.2(b) and 6.2(c)]. However, simultaneous imposition of the magnetic field and the electric field, the microstructure was refined obviously. It can be observed that at lower electromagnetic force densities, complex fields changed the originally columnar dendritic structure into equiaxed ones [Fig. 6.2(c)]. At higher intensities, the irradiated structure was disintegrated into isolated grains as the current density was increased further [Fig. 6.2(d)].

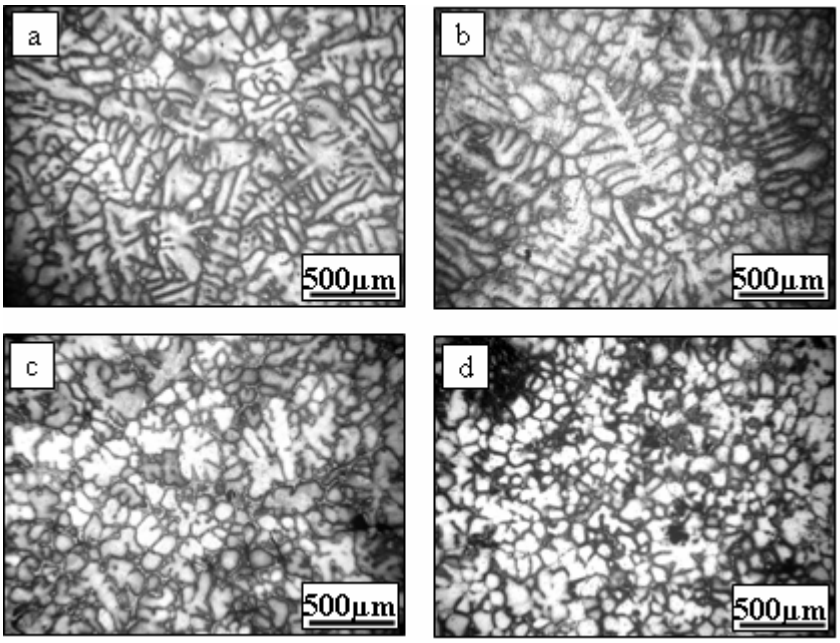

Fig. 6.2. Effect of an electromagnetic force on the solidification microstructure of Al-4.5wt%Cu alloy.
(a) B=0T, I=10A; (b) B=10T, I=0A;
(c) B=10T, I= 1A; (d) B=10T, I=10A.

6.4. Effect of magnetic force on the distribution of refined grains

Fig. 6.3 shows the structure with the same electromagnetic force density and various magnetic forces. Comparison of the structures indicates that with the increase of the magnetic force, the distribution of refining grains changes greatly. Under the complex fields of B=0.5T, $B_z dB_z / dz$ =0.95T^2/m and I=20A, the structure was refined only at the bottom of the sample as shown in Fig. 6.3(a). When we imposed of a field of B=1.5T, $B_z dB_z / dz$ =8.5T^2/m and a current of I=6.5A, the structure [Fig. 6.3(b)] was refined on the whole sample. Under the field of B=2T, $B_z dB_z / dz$ =16.2 T^2/m and I=5A, the structure [Fig. 6.3(c)] was not refined at the margin of the sample. The structure was refined only on the top of the sample by the application of the field of B=6T, $B_z dB_z / dz$ =150 T^2/m and I=1.6A [Fig. 6.3(d)]. The above results prove that the application of the magnetization force has changed the distribution of the refined grains significantly. The detailed experimental result and the analysis are present in **appendix [A].**

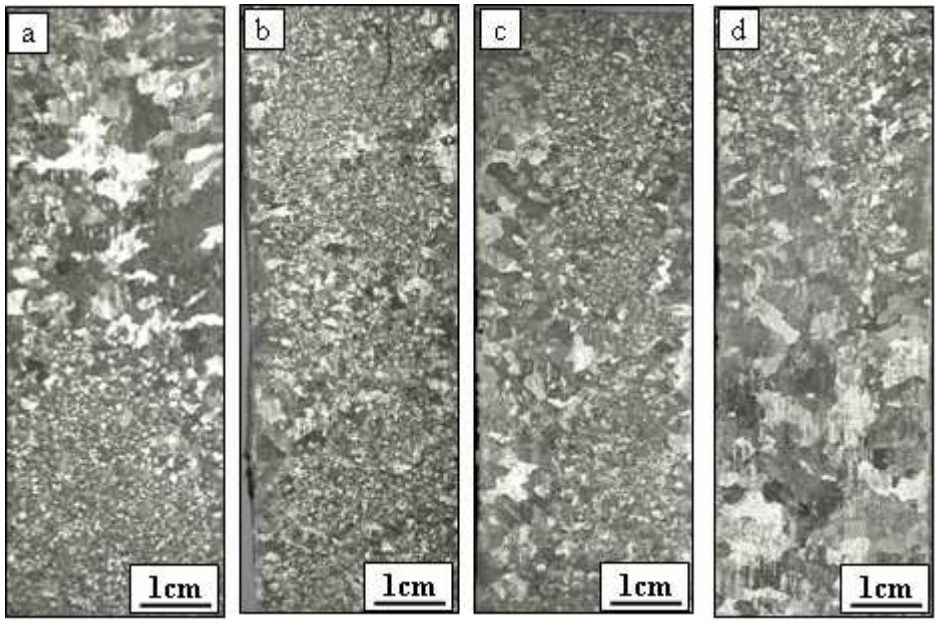

Fig. 6.3. Effects of a magnetic force on the structures of pure Al at the same electromagnetic force density. (a) B=0.5T and $B_z dB_z / dz$ =0.95T^2/m, I=20A; (b) B=1.5T and $B_z dB_z / dz$ =8.5T^2/m, I=6.5A; (c) B=2T and $B_z dB_z / dz$ =16.2 T^2/m, I=5A; (d) B=6T and $B_z dB_z / dz$ =150 T^2/m, I=1.6A.

Reference

[1] C.Vives, Metall.Trans.B. 27 (1996) 457.

[2] A.Radjai, Kamiah and T.Nishio, Metall.Trans.A.29 (1998) 1477.

Chapter 7: Phase distribution and phase structure control through a high gradient magnetic field during the solidification process

7.1. Introduction

Since many of the mechanical properties of material depend on the structure and distribution of phase and the structure is almost determined in the solidification process, so, it is essential to control the solidification structure. The imposition of external fields (including electric field, magnetic field and their complex fields) is often applied to improve the structure and the distribution of the phase and solute. It is well known that the electromagnetic field has a great influence on the segregation of elements and in alloys during electromagnetic stirring (EMS) solidification processes [1, 2] and the application of an electromagnetic force is capable of separating the no-metallic inclusion from the melt-metal and refines the grains [3-6]. Recently, a high magnetic field is extensively used during the solidification process and many interesting and valuable phenomena have been found. For example, it has been found that an application of a high magnetic field is capable of aligning and levitating the nonmagnetic substance [7, 8].

In this chapter, the phase separation under a high gradient magnetic field has been investigated. The results indicate that an application of a gradient magnetic field is capable of separating the phase and solute from the matrix. Moreover, it was also found that the application of a gradient magnetic field can change the microstructure and improve the refining structure.

7.2. Effect of a gradient magnetic field on the phase segregation

Fig. 7.1 shows the structure of Bi-6wt.%Mn alloy solidified from 345℃ at a cooling rate of 1℃/min under a positive gradient magnetic field of B=10T, $B_z dB_z / dz$ =400T^2/m. It can be observed that the phase segregation occurs. As a consequence, the primary MnBi phases segregate from Bi matrix and are located at the bottom region of the sample [Fig. 7.1(a)]. Moreover, it can be observed that elliptical MnBi phases are separated from the club-shaped MnBi and located at the upper region of the primary phase [Fig. 7.1 (b) and 7.1(c)]. Fig. 7.2

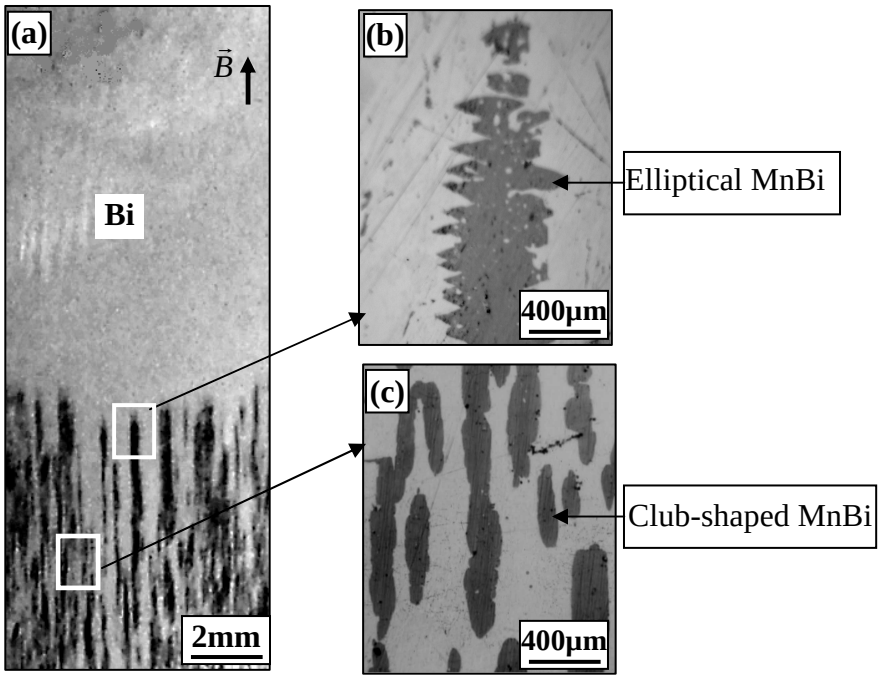

Fig. 7.1. Solidification structures of Bi-6wt.%Mn alloy solidified from 345℃ at a cooling rate of 0.1K/min under a positive gradient magnetic field: (a) longitudinal structure, no MnBi phases on the top region of the sample; (b) microstructure at the site denoted by the rectangle in Fig. 7.1(a); (c) microstructure at the site denoted by the rectangle in Fig. 7.1(a).

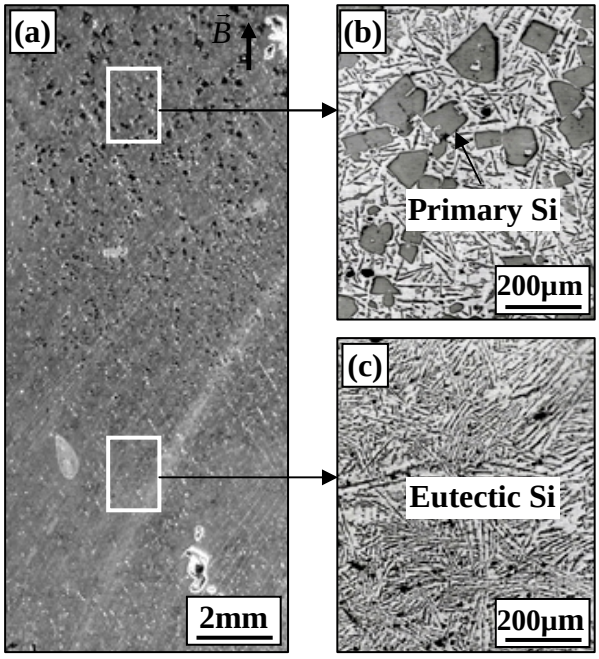

Fig. 7.2. Structures of Al-18wt.%Si alloy solidified from 800℃ at a cooling rate of 0.15K/min under a positive gradient magnetic field: (a) Macrostructure on the longitudinal section; (b) and (c) microstructure at the site denoted by the rectangle in Fig. 5(a).

shows the structure of Al-18wt.%Si solidified from 800℃ at a cooling rate of 10℃/min under

a positive gradient magnetic field of B=10T, $B_z dB_z / dz$ =400T^2/m. It can be observed that the primary Si separates from Al matrix and is located at the upper region of the sample.

Fig. 7.3 shows the structure of Bi-6wt.%Mn alloy solidified from 345℃ at a cooling rate of 1℃/min in the center of the magnetic field [i.e. under a radial gradient magnetic field]. It can be observed that the primary MnBi phases are separated from the Bi matrix and located at the periphery region of the sample. Moreover, it is also observed that the elliptical MnBi phases are separated from the club-shaped MnBi ones and located at the inner region of the ring-like structure.

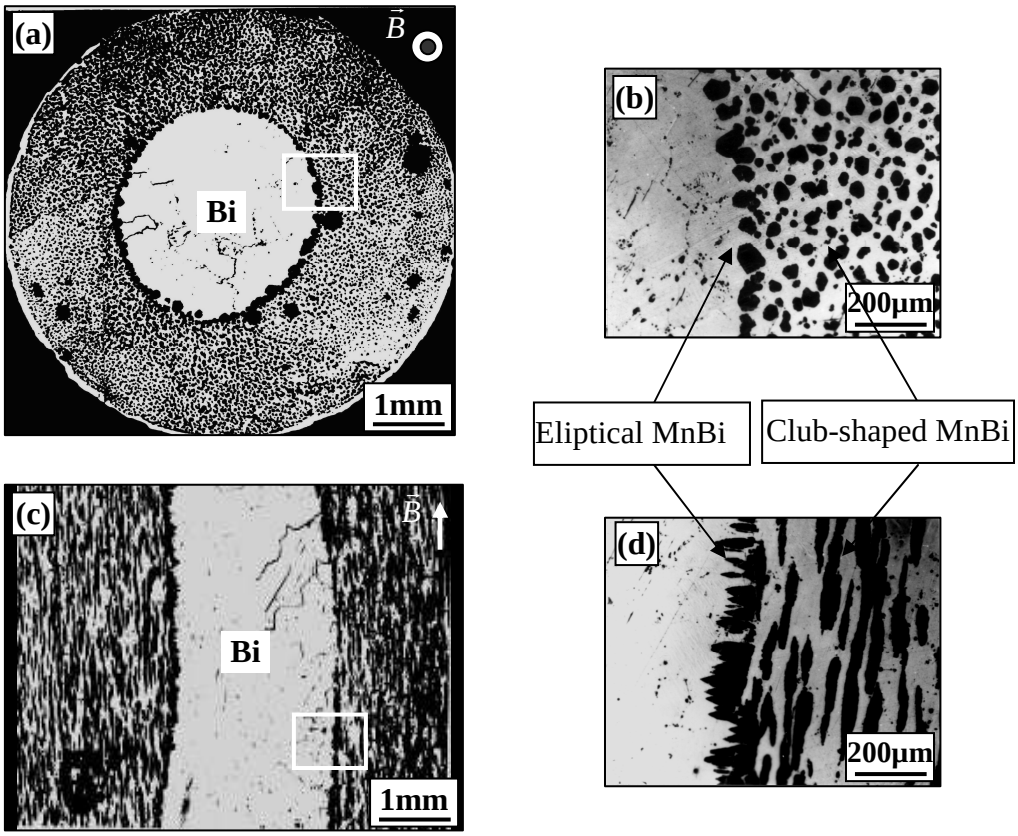

Fig. 7.3. Solidification structures of Bi-6 wt.%Mn alloy solidified from 345℃ at a cooling rate of 0.1K/min under a radial gradient magnetic field of B=10T: (a) Macrostructure on the transverse section, no MnBi phases in the center region of the sample; (b) microstructure at the site denoted by the rectangle in Fig. 7.1(a); (c) macrostructure on the longitudinal section; (d) microstructure at the site denoted by the rectangle in Fig. 7.1(c).

7.3. Effect of a gradient magnetic field on the microstructure

The Effect of a gradient magnetic field on the microstructure was investigated. Fig. 7.4 shows the microstructure of the Bi-6wt.%Mn alloy solidified from 380℃ at a cooling rate of 1℃/min under the magnetic field. Figs. 7.4 (b) (c) and (d) show microstructures located at different positions of a gradient magnetic field as shown in Fig. 7.4(a), respectively. It can be observed that the microstructure in the upper region of the gradient magnetic field (i.e. subjected to a smaller magnetic force) is composed of the elliptical MnBi phase, and the microstructure on the middle of the sample is composed of the polymer of elliptical MnBi phase. However, at the lower region of the gradient magnetic field (i.e. subjected to a smaller magnetic force), the polymer of the elliptical MnBi phase amalgamates and forms a rod-like

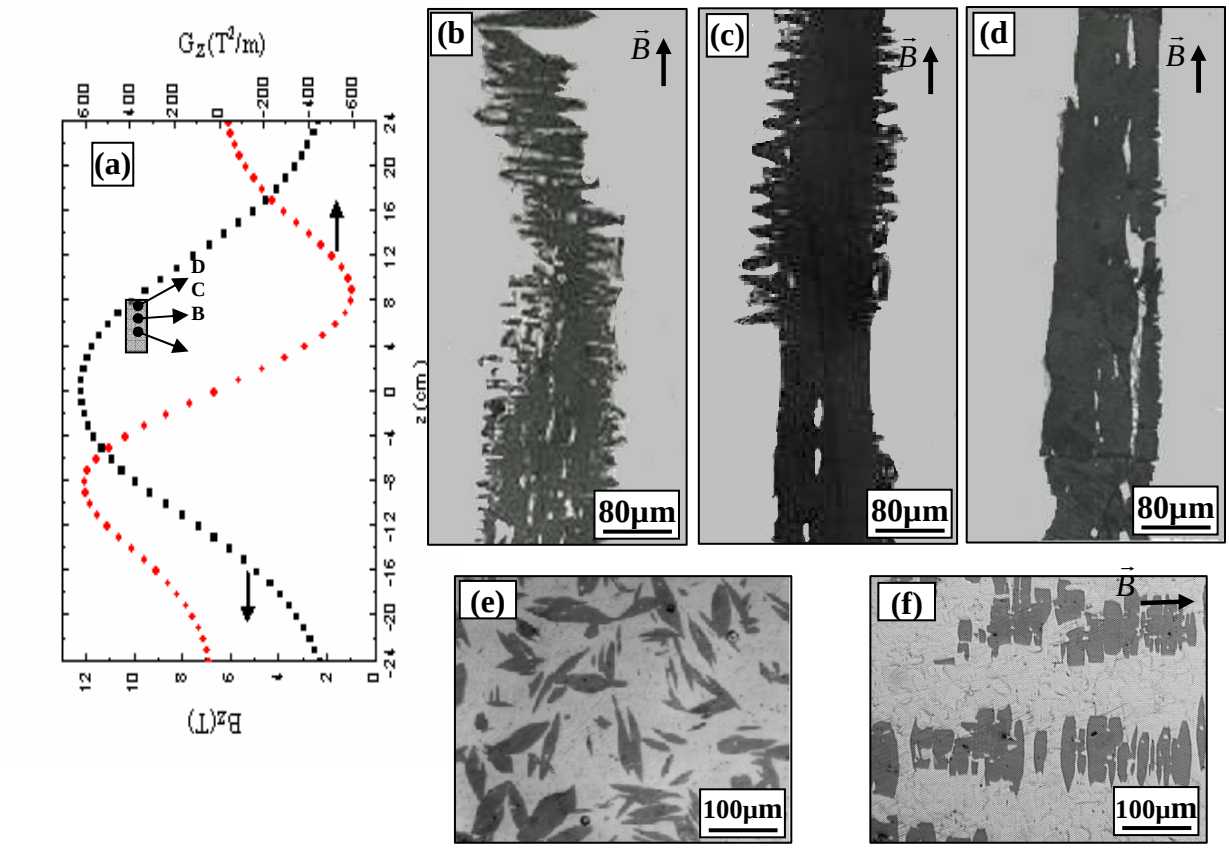

Fig. 7.4. Solidification structures of Bi-6wt.%Mn alloy solidified from 380℃ at cooling rate of 0.15 K/min under a 10T magnetic field.
Under a positive gradient magnetic field: (a) lower gradient field, (b) middle gradient field, (c) higher gradient field;
Under a uniform magnetic field: (e) without the magnetic field, (f) section parallel to the uniform magnetic field.

structure. Figs. 7.4 (e) and 7.4(f) show microstructure solidified without and with a 10T uniform magnetic field. It can be observed that the application of a 10T magnetic field is capable of aligning and aggregating the elliptical MnBi phase. However, comparison of the microstructure under a uniform and a gradient magnetic fields show that an application of a gradient magnetic field has enhanced the aggregating course.

7.4. Discussion

The above experimental results show that an application of a gradient magnetic field can control the distribution of the primary phase in alloys. This should be attributed to the application of the magnetic force under a gradient magnetic field. Generally, a unit volume of material in a one-dimensional magnetic field gradient experiences a magnetic force (F_m) defined as:

$$F_m = \frac{1}{\mu_0} \chi_V B_z \frac{dB_z}{dz}, \qquad (7.1)$$

where, B_z is magnetic field intensity, z a site-coordinate, χ_V the volume magnetic susceptibility. Thus, when an alloy is solidified under a gradient magnetic field, the primary phase and the matrix will experience a magnetic force at the same time. However, owing to the difference in the susceptibilities between the primary phase and the matrix, the magnetic forces are different. Thus, for the primary phase, the effective magnetic force F_m^f will be:

$$F_m^f = (\chi_V^P - \chi_V^M) \frac{1}{\mu_0} B_z \frac{dB_z}{dz}, \qquad (7.2)$$

where, χ_V^P and χ_V^M are the volume susceptibilities of the primary phase and the matrix, respectively. The effective magnetic force works as a “driving force” and tends to separate the primary phase from the matrix. Consequently, under a radial gradient magnetic field, if viscous forces and convective flows are ignored, the force (F_V^f) will cause the primary phase to separate from the matrix. Therefore, the formation of the ring-like MnBi phase layer should be attributed to the effective magnetic force under a radial gradient magnetic field. Since MnBi phase and matrix Bi are ferromagnetic and diamagnetic substances, respectively in a radial gradient magnetic field, the MnBi phase will be subjected to the outward force along the radial direction. As a consequence, the MnBi phase will transfer outward and form the ring-like structure at last.

Under an axial gradient magnetic field, the effective gravitational force $G_V = (\rho_P - \rho_M)g$ is applied at the same time. The total force F acting on the primary phase under a gradient magnetic field is

$$F = G_V + F_m^f = (\rho_P - \rho_M)g + (\chi_V^P - \chi_V^M)\frac{1}{\mu_0} B_z \frac{dB_z}{dz} , \qquad (7.3)$$

Thus, if ignoring viscous forces and convective flows, the total force F will decide whether the primary phase will separate or not from the matrix. The above experimental results show that the primary MnBi and Si phases are segregated from the respective matrixes, and this should be attributed to this total force. In the same mechanism, owing to the difference in the susceptibilities between solid and liquid of pure metal, an effective magnetic force is applied to the solid. Thus, it is possible to control the solidification behaviour of pure metal by using this force. The experimental result in Fig. 6.3 has shown that an application of an upward magnetic field can restrain crystal rains and improve the refining structure during the electromagnetic vibration.

Moreover, the above experimental results indicate that the application of a gradient magnetic field is capable of changing the microstructure (Fig. 7.4). This should be attributed to the effect of the magnetization force on the alignment and aggregation of the primary phase. It is well known that the magnetic field can align the phase with the easy magnetic axis along the magnetic field direction; and at the same time, owing to the interaction between magnetic phases, the aggregation will occurs. Since the magnetic force is capable of affecting the transfer of the phase, an application of a magnetic force changes the aggregating process; as a consequence, the microstructure is affected.

Reference

[1] M. Garnier. Proceedings of the International Symposium on Electromagnetic Processing of Materials, ISIJ, Nagoya, 1994, 1.

[2] H. Branover. Proceedings of the International Symposium on Electromagnetic Processing of Materials, ISIJ, Nagoya, 1994, 23.

[3] K. Takahashi, S. Taniguchi, ISIJ International 43 (6) (2003)820.

[4] Y. Miki, H.Kitaoka, T.Sakuraya, et al, ISIJ International 32 (1) (1992)142.

[5] C. Vives, Metall.Trans. B 27B(1996)457.

[6] A. Radjai, Kamiah and T. Nishio, Merall.Trans. A 29A(1998)1477.

[7] M. Shimotomai, K. Maruta, Scripta Mater 42(2000)499.

[8] E. Beaugnon, R. Tournier, Nature 349(1991) 470.

[9] E. Beaugnon, R. Tournier, J. Phys. III, France; 1(1991) 1423.

Chapter 8: Conclusion

In present work, effects of a static high magnetic field (up to 12T) on liquid-solid interface transformation of the single phase alloy, eutectic growth and the phase transformation have been investigated. Moreover, the effect of magnetic force on the distribution of the phase and refined structure during the electromagnetic vibration process is also investigated.

Al-0.85wt.%Cu alloy is used to investigate the effect of a high magnetic field on the interface transition and shape. Results indicate that the field causes the interface to be destabilized and irregular and promotes the planar-cellular and the cellular-dendritic transformation. Al-Cu, Al-Ni, Bi-Mn hypo and hypereutectic alloys are used to study the effects of the field on the dendrites and cellular array. It has been observed that the field has a great influence on the cellular and dendrite array morphology. Indeed, the field causes severe distortion in the cellular array and enhances the cell branching. For the dendrite array, the field makes the dendrite morphology more complex. As a consequence, the field breaks the dendrite of Al crystal at a lower growth speed and high magnetic field intensity. At a moderate growth speed and magnetic field intensity, the field orientates Al dendrite with the <111>-direction along the solidification direction instead of the <100>-crystal direction. For MnBi crystal, the field enhances the growth along the solidification direction. For Al_3Ni crystal, the field causes the preferred growth direction to be perpendicular to the solidification direction.

The TEMC has been evaluated for different scales, and the results show that for different scales, the effect of the magnetic field is different. The smaller the structure, the larger the magnetic field is needed to modify the structure by the thermoelectric effect. Therefore, for the crucible scale, a high magnetic field works as damping effect; however, for high-order dendrite arm, the TEMC will take place. The influence of high magnetic field on the interface stability and the branching of cell could be attributed to the effect of a high magnetic field on the equilibrium partition coefficient k and the liquidus slope m_L. The stress caused by the interaction thermoelectric current and the magnetic field may also be responsible for the above experimental results. The alignment and break of the dendrites could be attributed to the magnetic force. Moreover, the TE torque caused by the interaction between the thermoelectric current and the magnetic field is also responsible for the breaking of the dendrite/cell.

Investigations on growths of the lamellar eutectic (Al_2Cu-Al and Pb-Sn) and rod eutectic (Bi-MnBi) alloy under a high magnetic field have been investigated and the results show that the field affects the microstructure significantly. As a consequence, a high magnetic field has degenerated the lamellar structure into a wavy one at a low growth speed .XRD, SAD and HREM patterns indicate that the field has changed the preferred orientation. The Al_2Cu crystal is oriented with the <001>-crystal direction along the solidification direction (i.e., the magnetic field direction). At the pulling velocity of 0.5μm/s, the magnetic field ($B \geq 4\mathrm{T}$) is responsible for the segregation. This may be attributed to the orientation of the Al_2Cu and the Al crystals as well as the decrease of the diffusion coefficient caused by the magnetic field. For rod MnBi/Bi eutectic, the influence of the magnetic field on morphology and magnetic properties of the specimens have been studied, and the results indicate that a high magnetic field promotes the formation of MnBi fiber and makes the directional solidification structure of the eutectic more regular. The MnBi inter-rod spacing and rod diameters gradually increase with the magnetic field intensity. Furthermore the magnetic field enhances the faceted growth of MnBi phase and the magnetic coercivities of the alloy. This may be attributed to the magnetic anisotropy and the shift of the eutectic point by the magnetic field.

MnBi/$Mn_{1.08}$Bi compounds are chosen to investigate effects of the field on the phase transformation, structure and magnetic property. Firstly, a method to determine the phase transformation through measuring the change of magnetic force in the gradient magnetic field has been proposed. By this method, the phase transformation between MnBi/$Mn_{1.08}$Bi compounds has been observed in situ. It has been found that the magnetic field increased the phase transformation temperature. As a result, a 10T magnetic field has raised the phase transformation temperature about 20K. Moreover, the field has changed the MnBi phase morphology during the phase transformation. Along with the change of the MnBi phase morphology, the magnetic property changes significantly. As a consequence, the saturation magnetization M_s and the magnetic susceptibility χ increase and the coercive field H_c and the remnant magnetization M_r decrease. This implies that the field causes the magnetic property of the MnBi phase to transform towards soft magnetism.

Effects of complex fields between a high magnetic field and alternate current on the pure Al and the dendritic growth in Al-4.5 wt.%Cu alloy have been investigated, and it is found that the refined structure was gained by the application of the above complex fields. Moreover, by using an upward magnetic force, the distribution of the refined grains was changed significantly. It was found that a right magnetic force is able to make the whole sample refined. As a consequence, the uniformly refined structure was gained. Moreover,

investigations on influences of the electromagnetic and magnetic forces on the growth of dendrite indicate that with the increase of the electromagnetic force density, the columnar dendritic structure changed into equiaxed ones that continued to disintegrate to isolated grains. Moreover, the distribution of refined grain can be controlled during the electromagnetic vibration and could be restrained by using the magnetic force.

Moreover, this work also investigates simply the effect of magnetic force on the phase separation and the microstructure. The results indicate that an application of a gradient magnetic field is capable of separating the phase from the matrix. As a consequence, a radial gradient magnetic field has formed the ring-like structure; and an axial gradient magnetic field has caused primary MnBi in Bi-6wt.%Mn and Si in Al-18wt.%Si to separate from the respective eutectic. It was also found that the application of a gradient magnetic field can change the microstructure through enhancing the aggregation of the phase.

The above work has indicated that a high magnetic field caused the interface to be destabilized and irregular. However, the formation mechanism of the undulating solid/liquid interface under a high magnetic field is not yet so clear. It is necessary and valuable to investigate it further. Moreover, the experimental result has proved that the TEMC is present during the directional solidification under an axial magnetic field. However, the TEMC has only been evaluated simply. Therefore, it should be extended through a numerical investigation. Especially, it is very relevant to investigate the TEMC when considering the application of a radial and axial temperature gradient at the same time.

Chapter 9: Appendices

9.1. Physical properties of the alloys and some values

Al-Cu alloy

Diffusion coefficient, D=4×10^{-9}m^2/s

The equilibrium partition coefficient, k=0.17

The liquidus slope, $m_l = 3.4$

Electric power of Al-Cu alloy, $\eta_s(Al\text{-}4\%massCu, 600) = \text{-}3.2\mu V / K$

Thermoelectric power of liquid Al, $\eta_l(Al) = -2.24\times10^{-3}t - 0.61\mu V / K(tin)$

Thermoelectric power of Al-Cu alloy, $\eta_l(Al\text{-}20\%massCu) = \text{-}3.42\times10^{-3}t\text{-}0.93\mu V / K(tin)$

Density of Al at the melting point, $\rho_0(700) = 2357kg / m^3$

Electrical conductivity of solid Al, $\sigma_s = 13.7\times10^6/(\Omega m)(Al)$

Electrical conductivity of liquid Al, $\sigma_l = 3.8\times10^6/(\Omega m)(Al)$

Eutectic temperature, T_E=821K

Eutectic concentration, C_E=33.3%*mass*

Bi-Mn alloy

Eutectic temperature of Mn-Bi alloy, T_E=535K

Eutectic concentration, $C_E = 0.72\%mass$

Crystal structure of MnBi in different temperature

Phase	Structure	T_c(K)
MnBi(LTP)	hex. $P6_3/mmc$	628 Ferro
MnBi (HTP)	hex. $P6_3/mmc$	460 Para
MnBi(QHTP)	ortho. $P6_3/mmc$	440 Ferro
MnBi(NP)	hex. $P6_3/mm$	240 Ferro

9.2. List of symbols in this paper

Symbol	Meaning	Unit
T	Temperature field	*[K]*
B	Magnetic field	*[T]*
G	Temperature gradient	*[K/cm]*
V	Solidification velocity	*[μm/s]*
m_l	The slope of the liquidus line	*[K.(wt%)$^{-1}$]*
k	The partition coefficient	---
k_{eff}	Effective partition coefficient	---
D_L	The diffusion coefficient	*[m^2/s]*
C_0	The alloy composition	*[wt.%]*
χ	The magnetic susceptibility	*[m^3/kg]*
η	Thermoelectric power	*[V/K]*
σ	Electrical conductivity	*[Ω/m]*
λ	Eutectic space	*[μm]*
μ_0	Permeability of free space	----
ρ	Density	*[Kg/m^3]*
Re	Rayleigh number	---
Ha	Hartmann number	---
Pe	Peclet number	---
C_E	Weight eutectic composition	*[wt.%]*
G_M	Magnetic Gibbus free energy	*[j/mol]*
N	Demagnetization factor	---
ΔT	The temperature difference	*[K]*
$\Delta\chi$	magnetic susceptibility difference between different crystal direction	*[m^3/kg]*
α	The angle between the solidification direction and the prefer growth direction	---
j	Current density	*[A/ m^2]*
v	Kinematic viscosity of the fluid	*[m^2/s]*
E	Electric field	*[A]*
H_C	The coercive field	*[kOe]*
M_r	The remnant magnetization	*[kG]*
C_E	The eutectic composition	*[wt.%]*

9.3. Papers published and finished

[A1] Xi Li, Yves Fautrelle, Zhongming Ren
Influence of an axial high magnetic field on the liquid–solid transformation in Al–Cu hypoeutectic alloys and on the microstructure of the solid, Acta Materialia 55 (2007) 1377–1386.

[A2] Xi Li, Yves Fautrelle, Zhongming Ren
Influence of thermoelectric effects on the solid-liquid interface shape and cellular morphology in the mushy zone during the directional solidification of Al-Cu alloys under the magnetic field, Acta Materialia 55 (2007) 3803-3813.

[A3] Xi Li, Yves Fautrelle , Zhongming Ren
Influence of a high magnetic field on the columnar dendrite growth during the directional solidification, Acta Materialia 55(2007) 5333-5347.

[A4] Xi Li, Zhongming Ren,Yves Fautrelle
Effect of a high axial magnetic field on the microstructure in a directionally solidified Al–Al2Cu eutectic alloy, Acta Materialia 54 (2006) 5349–5360

[A5] Xi Li, Zhongming Ren,Yves Fautrelle
The spiral growth of lamellar eutectics in a high magnetic field during the directional solidification process, Scripta Materialia 56 (2007) 505–508

[A6] Xi Li, Zhongming Ren,Yves Fautrelle
Effect of high magnetic fields on the microstructure in directionallysolidified Bi–Mn eutectic alloy, Journal of Crystal Growth 299 (2007) 41–47.

[A7] Xi Li, Zhongming Ren,Yves Fautrelle
Effect of a high magnetic field on the phase transformation, morphology and magnetic properties of the MnBi and $Mn_{1.08}Bi$ compounds.

[A8] Xi Li, Zhongming Ren,Yves Fautrelle
The alignment, aggregation and magnetization behaviors in MnBi/Bi composites solidified under a high magnetic field, Intermetallics 15 (2007) 845-855.

[A9] Xi Li, Zhongming Ren,Yves Fautrelle
Effects of the simultaneous imposition of electromagnetic and magnetic forces on the solidification structure of pure Al and Al-4.5wt.%Cu alloy, Journal of Materials Processing Technology (In press).

[A1] Xi Li, Yves Fautrelle, Zhongming Ren

Influence of an axial high magnetic field on the liquid–solid transformation in Al–Cu hypoeutectic alloys and on the microstructure of the solid,

Acta Materialia 55 (2007) 1377–1386.

Available online at www.sciencedirect.com
ScienceDirect
Acta Materialia 55 (2007) 1377–1386
Acta MATERIALIA
www.actamat-journals.com

Influence of an axial high magnetic field on the liquid–solid transformation in Al–Cu hypoeutectic alloys and on the microstructure of the solid

Xi Li [a,b,*], Yves Fautrelle [b], Zhongming Ren [a]

[a] Department of Material Science and Engineering, Shanghai University, Shanghai 200072, China
[b] EPM-Madylam/CNRS, ENSHMG, BP 95, 38402 St. Martin d'Heres Cedex, France

Received 16 March 2006; received in revised form 2 October 2006; accepted 3 October 2006
Available online 11 December 2006

Abstract

The influence of an axial high magnetic field (up to 10 T) on the liquid–solid interface morphology and microstructure of the solid has been investigated experimentally during Bridgman growth of Al–Cu hypoeutectic alloys. It is found that the field causes the interface to become destabilized and irregular, and promotes planar–cellular and cellular–dendritic transformation. The field has a great influence on the cellular and dendrite array morphology. Indeed, the field causes severe distortion in the cellular array and enhances cell branching. The field makes the morphology of the dendrite array more complex and, with the increase of the magnetic field intensities and decrease of the growth velocities, the dendrites become broken and orientate with the ⟨1 1 1⟩-direction along the solidification direction instead of the ⟨1 0 0⟩-direction. Furthermore, the field also enlarges the primary dendrite spacing and promotes the branching of the dendrites to form higher-order arms. The above phenomena may be attributed to the change of the equilibrium partition coefficient k and the liquidus slope m_L caused by the field, the magnetic anisotropy of the α-Al crystal and the flow created by the thermoelectromagnetic convection.

Keywords: High magnetic field; Al–Cu hypoeutectic alloy; Liquid–solid interface transformation; Orientation

1. Introduction

Solidification in a high magnetic field is an interesting topic that has attracted much attention from researchers. However, the effect of a static magnetic field on the solidification is not well understood. It is traditionally suggested that the static magnetic field damps the convection in the liquid bulk during the solidification process. However, some unexpected results have been observed, depending on the composition of the alloy and the experimental conditions. Youdelis and Dorward [1] applied a 3.4 T transverse field on the directionally solidified Al–Cu alloy. The result showed that the value of the effective partition coefficient decreased with the presence of the field, as if the magnetic field enhanced mass transport in the bulk liquid. Tewari et al. [2] found that the cellular array was severely distorted, and the stripes of freckles on the plane perpendicular to the magnetic field formed when a Pb–Sn alloy was solidified vertically at very low growth speed under a 0.45 T transverse magnetic field. Alboussière et al. [3] and Laskar [4] also found that the freckles appeared in Bi–60 wt.% Sn and Cu–45 wt.% Ag, solidified vertically with a 0.6 T transverse or 1.5 T axial magnetic field. The above results indicated clearly that new convection had been created in the liquid bulk. Alboussière et al. [3] suggested that this new convection was induced by the interaction between the magnetic field and a thermoelectric effect, which produced thermoelectromagnetic convection (TEMC). Yesilyurt et al. [5] presented numerical solutions for the buoyant convection and TEMC in an actual crystal-growth process with an axial magnetic field. Their results indicated that thermoelectric currents at the growth interface during Bridgman

* Corresponding author. Address: Department of Material Science and Engineering, Shanghai University, Shanghai 200072, China.
E-mail address: xi@hmg.inpg.fr (X. Li).

1359-6454/$30.00
doi:10.1016/j.actamat.2006.10.007

growth promoted convection when a low-intensity axial magnetic field was applied. For high magnetic field strengths, typically, meridional flow slows down due to the Lorentz force, according to Khine and Walker [6]. The magnitude of TEMC is maximum when the Hartmann number, *Ha*, is about 10. Most previous studies have looked at thermoelectric magnetohydrodynamic flow with a moderate or weak magnetic field. However, there are a few studies on the effect of a high magnetic field, and especially the influence of the magnetic field on the liquid–solid interface morphology. This paper investigates the effect of a high magnetic field on the morphology of the liquid–solid interface and the microstructure of the solid in Al–Cu hypoeutectic alloy during the directional solidification process. The results show that the magnetic field promotes the interface transformation and deforms the shape of the interface. It is also found that the magnetic field causes severe distortion of the cellular and dendritic arrays. Furthermore, new effects of the magnetic field are presented to explain the above experimental results in light of the TEMC effect.

2. Description of the experiments

The Al–0.85 wt.% Cu and Al–4.5 wt.% Cu alloys used in this study were prepared with high-purity Al (99.99 wt.%) and Cu (99.99 wt.%) in an induction furnace. The alloy, being put in a high-purity graphite crucible of 10 cm diameter, was heated to 900 °C, magnetically stirred for 0.5 h and poured into a graphite mold to cast specimens with a diameter of 3 mm and length 200 mm. The cast specimen was enveloped in a tube of high-purity corundum of inner diameter 3 mm and length 200 mm.

The experimental apparatus is shown in Fig. 1. It consists of a static superconductor magnet and a Bridgman–Stockbarge-type furnace equipped with a pulling system and temperature controllers. The superconductor magnet can produce an axial static magnetic field with an adjustable intensity up to 14 T. The furnace, consisting of nonmagnetic material, has a negligible effect on field uniformity. A water-cooled cylinder containing liquid Ga–In–Sn metal (LMC) is used to cool down the specimen. The temperature gradient in the specimen is controlled by adjusting the temperature of the furnace hot zone, which is insulated from the LMC by a refractory disk. The apparatus is designed such that the specimen moves downward while the furnace remains stationary. The growth speed, R, lies in the range $0.5\ \mu m/s \leqslant R \leqslant 5000\ \mu m/s$. In order to observe the morphology of the liquid–solid interface during the growth of the crystal, quenching experiments are carried out by quickly withdrawing the specimen into the LMC cylinder to cool the specimen immediately to room temperature.

During the experiment the specimens contained in the corundum crucibles are melted and directionally solidified in the Bridgman apparatus by drawing the crucible assembly at various speeds into the LMC cylinder. The temperature gradient and the growth speed are adjusted to form a plane, cellular and dendritic regions, respectively. In all the experimental procedures the magnetic field is present. The longitudinal (parallel to the growth direction) and transverse microstructures are examined in the etched condition by an optical microscope and X-ray diffraction (XRD) with Cu Kα irradiation. Dendrite morphology (diameter and spacing) is evaluated by a computer-aided W T MiVnt particle analyzer system and the error is around 5–10%.

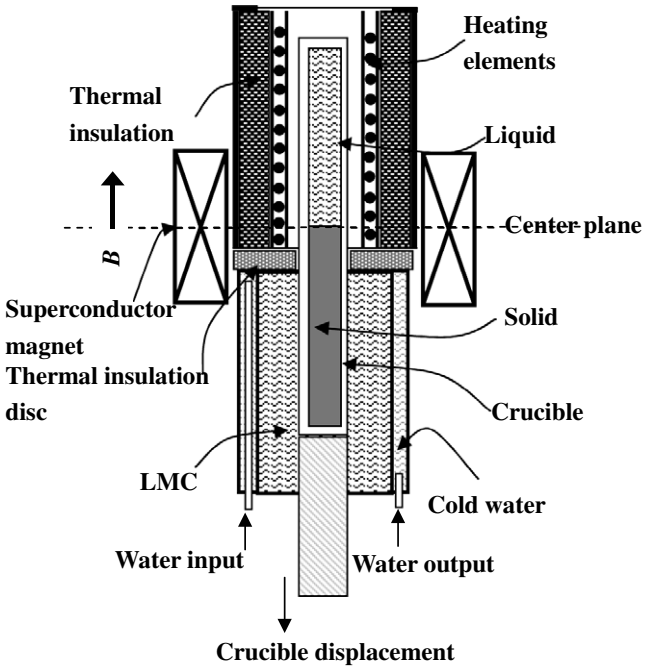

Fig. 1. Schematic illustration of the Bridgman solidification apparatus in a superconducting magnet.

3. Results

3.1. The interface transformation and cellular array

Al–0.85 wt.% Cu alloy is used to investigate the influence of a high magnetic field on the planar–cellular interface transformation and cellular array. Fig. 2 shows the longitudinal microstructures of Al–0.85 wt.% Cu alloy at the liquid–solid interface solidified at a temperature gradient in liquid (G_L) of 62.8 K/cm. Fig. 2a and b demonstrates the microstructures solidified at the speed of 1.5 μm/s without and with the magnetic field, respectively. It can be observed that the application of a 10 T magnetic field has destabilized the interface and broken the planar interface to cellular array. At 5 μm/s, comparison of the microstructures without and with the field (Fig. 2c and d) indicates that a 10 T field causes the transition from the cell to dendrite by promoting the branching. Further, the convex liquid–solid interface, which was typical in the case without the field, was flattened by the imposition of the magnetic field.

The influence of the magnetic field intensities on the planar interface is investigated by observing the microstructures solidified at 1.5 μm/s under 2, 6 and 9 T magnetic

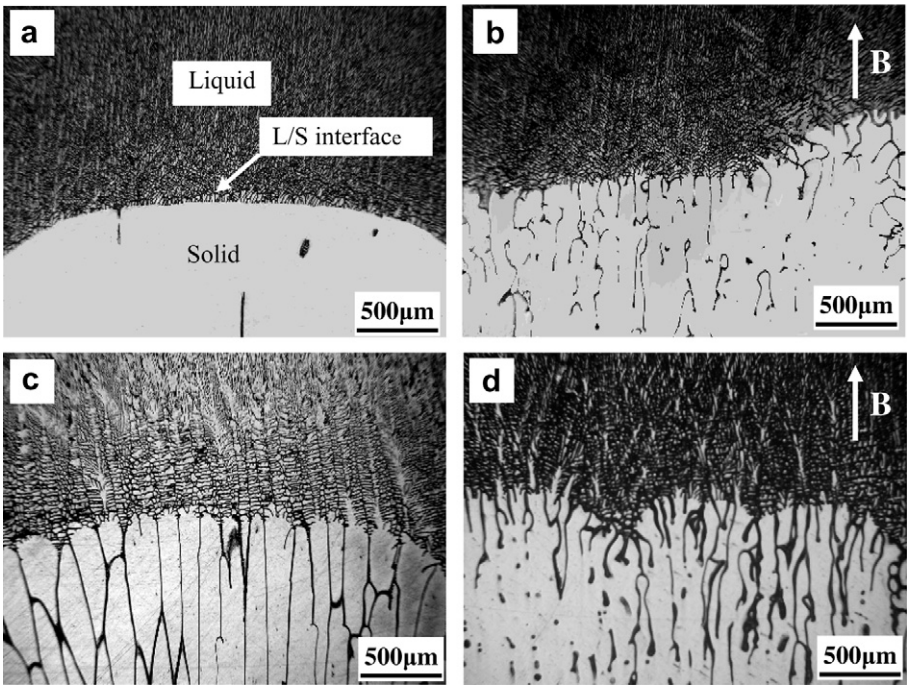

Fig. 2. Longitudinal solidification structure at the quenched liquid–solid interface (parallel to the growth direction) of Al–0.85 wt.% Cu alloy solidified at a temperature gradient in liquid (G_L) of 62.8 K/cm for various growth speeds. (a) 0 T, 1.5 μm/s; (b) 10 T, 1.5 μm/s; (c) 0 T, 5.0 μm/s; and (d) 10 T, 5.0 μm/s.

fields. The results are shown in Fig. 3. The experiments show that the application of a 2 T magnetic field leads to deformation of the liquid–solid interface from the regular convex to a wavy one (Fig. 3a). When the magnetic field intensity increased up to 6 or 9 T, the interface (Fig. 3b and c) begins to break down and complex cell morphology appears. The influence of the magnetic field intensities on the cellular array is investigated at 10 μm/s (Fig. 4). As can be seen in Fig. 4a and b, the microstructure without the field consists of regular cells. However, after the application of a 0.5 T magnetic field, the interface becomes very uneven, and some structure appears in the liquid. Under a 1 T magnetic field the cell spacing decreases apparently and some side branches appear. Under a 2 T magnetic field, branching on the cells is apparent, and with a 5 T magnetic field the microstructure becomes dendritic. When the magnetic field intensity is increased to 10 T, the dendrites become more developed. Fig. 5 shows the transverse microstructures below the eutectic isotherm. Comparison of the microstructures without and with the field indicates that the application of a 10 T magnetic field causes the reduction of the grain boundary and promotes the amalgamation of the grains, which suggests that a high magnetic field may promote the solid diffusion.

3.2. Dendritic array

The influence of the magnetic field on the dendrites is investigated by means of the Al–4.5 wt.% Cu alloy. Fig. 6 shows the longitudinal microstructures at the liquid–solid interface of the sample solidified at a temperature gradient of 38 K/cm in liquid (G_L) without and with a 10 T magnetic field. Without the magnetic field, the primary dendrites have a usual aligned nature in all experiments, as shown in Fig. 6a. The application of a 10 T magnetic field has a remarkable effect on the dendritic array. At the lower growth rate of 10 μm/s (Fig. 6b), the dendrites are distorted and broken, and the broken dendrites are tilted and melted together (Fig. 7b). The above results indicate that the application of a high magnetic field leads to a fluid motion as well as a force which causes the collapse of dendrites and the deviation of the primary axis of the main stem from the solidification direction. With the increase of growth speed, the primary dendrites are not broken but tilted, with a tilting angle of about 40–45° for the main stems from the solidification direction, as shown in Fig. 6c, suggesting that the field causes the reorientation of the dendrite. At the higher growth speed of 100 μm/s (Fig. 6d), the dendrites are neither distorted nor tilted. However, from the transverse microstructure below the isotherm-solidified eutectic, it can be found that the high-order arms of dendrite become much more developed and the dendrite spacing increases (Fig. 7d). The latter results suggest that the magnetic field promotes the branching of the dendrites.

The XRD of the specimens are shown in Fig. 8. Compared with the pattern of the samples without directional solidification shown at the bottom of the figure, the peak corresponding to the (1 0 0)-plane, as expected, increases in the case of the directional solidification without the field, because the ⟨1 0 0⟩-direction of α-Al is its preferred growth direction. However, the peak corresponding to the (1 1 1)-planes of the samples grown at the lower growth speeds

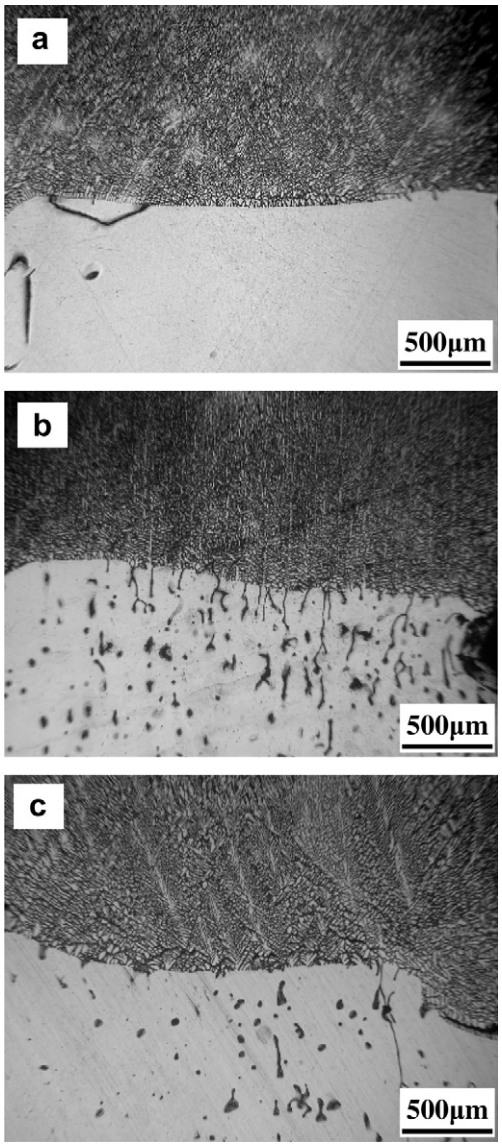

Fig. 3. Longitudinal solidification structure of Al–0.85 wt.% Cu at the liquid–solid interface in various magnetic field intensities ($G_L = 62.8$ K/cm and $R = 1.5$ μm/s). (a) 2 T; (b) 6 T; and (c) 9 T.

of 5 and 50 μm/s under a 10 T magnetic field (Fig. 8a and b) increases remarkably, whilst the peak corresponding to the (1 0 0)-plane decreases. Grown at the higher growth speed of 100 μm/s, the patterns are similar to those of the samples directionally solidified without the field, as shown in Fig. 8c. These results indicate that the high magnetic field tends to alter the growth direction of the dendrites from ⟨1 0 0⟩ to ⟨1 1 1⟩ at the lower growth speed. This agrees well with the tilting effect of the dendrites in Fig. 6.

The influence of the magnetic field intensities on the dendrites has been investigated by studying the microstructures on the liquid–solid interface obtained by quenching the specimen solidified directionally at 20 μm/s. The results are shown in Fig. 9. It can be observed from the figure that the application of a 0.2 T field enhances the dendritic branching and, accordingly, the dendrites becomes more developed (Fig. 9b). When the magnetic field intensity increases to 0.5 T, the dendrites begin to deviate their main stems from the solidification direction (Fig. 9c). Increasing the field further to 2 T leads to the breaking of the dendrites and the tilting of the main stems as well. It is interesting to note that, with the increase in the magnetic field intensity, the columnar dendrites gradually transform into equiaxed dendrites. It is also observed that the tilting of the main stems occurs at their tips at a certain growth speed range. The maximum tilting angle from the solidification direction is about 45°, no matter how strong the field is in the experiment (Fig. 9e and f).

The primary dendrite spacing was also measured, and the result is shown in Fig. 10. It can be learnt from this figure that the presence of the field leads to a substantial increase in primary dendrite spacing. At a lower growth speed of 10 μm/s, the dendrite spacing increases by 167% with an increase in the field from 0 to 2 T. Under a field larger than 2 T, the primary dendrite spacing at this speed is not measured because the dendrites are broken, and it is difficult to distinguish the primary dendrites from the high-order arms. At a higher growth speed, the increment in the dendrite spacing is reduced in line with the increase in growth speed. The above experiment results indicate that the magnetic field affects the dendrite array, and the extent of the alteration depends on the magnetic field intensity and growth speed.

4. Discussion

4.1. Influence of the magnetic field on the liquid–solid interface morphology

The above experimental results indicate that the field has reduced the critical growth speed at which the planar interface begins to destabilize and enhances the planar–cellular transformation. According to the constitutional supercooling theory, an interface is unstable when

$$\frac{G_L}{R} < \frac{m_l C_0 (1-k)}{k D_L} \tag{1}$$

where G_L is the temperature gradient in the liquid, R the growth speed of the crystal, D_L the diffusion coefficient of the solute in the liquid, m_l the liquidus slope, k the equilibrium partition coefficient and C_0 the alloy composition. The critical growth speed at which the planar interface plane begins to destabilize is $\frac{G_L k D_L}{m_l C_0 (1-k)}$. From the above formula and the experimental results, it can be predicted that the magnetic field may affect k, m_l or D_L. It is well known that the magnetic field is able to affect the Gibbs free energy and the chemical potential of the system, as well as the phase equilibrium, which may lead to a change in the equilibrium partition coefficient k and the liquidus slope m_l of an alloy phase diagram. Therefore, to account for the influence of the magnetic field on the interface transformation, the influence of the magnetic field on k and m_l is investigated.

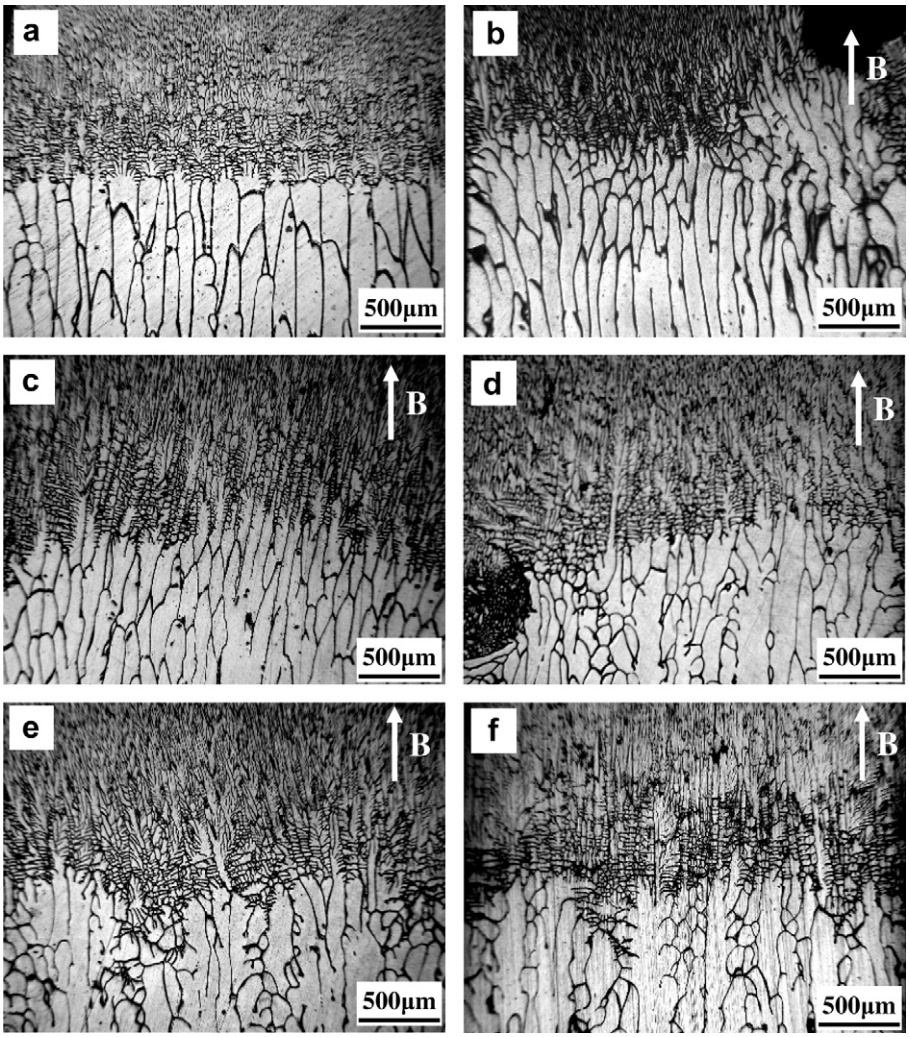

Fig. 4. Longitudinal solidification structure of Al–0.85 wt.% Cu at the liquid–solid interface under different magnetic filed intensities ($G_L = 62.8$ K/cm and $R = 10$ μm/s). (a) 0 T; (b) 0.5 T; (c) 1 T; (d) 2 T; (e) 5 T; and (f) 10 T.

In a binary alloy, the chemical potentials of elements A and B are written as [7]

$$\mu^A = \mu_0^A + S^A \Delta T^A + RT \ln(1 - C) \quad (2)$$

$$\mu^B = \mu_0^B + S^B \Delta T^B + RT \ln C \quad (3)$$

where μ_0^A and μ_0^B are constants representing the chemical potential of the pure components at unit composition. ΔT is the difference between reference temperature and the actual temperature T, and the subscripts A and B represent components A and B, respectively. C is the alloy composition. Eqs. (2) and (3) can be written for both the solid and liquid phases as follows:

$$\mu_L^A = \mu_0^A + S_L^A \Delta T^A + RT \ln(1 - C_L) \quad (4)$$

$$\mu_S^A = \mu_0^A + S_s^A \Delta T^A + RT \ln(1 - C_S) \quad (5)$$

$$\mu_L^B = \mu_0^B + S_L^B \Delta T^B + RT \ln C_L \quad (6)$$

$$\mu_S^B = \mu_0^B + S_S^B \Delta T^B + RT \ln C_S \quad (7)$$

At the two-phase equilibrium, we have $\mu_L^A = \mu_S^A$ and $\mu_L^B = \mu_S^B$. We use the designation C_L^* for the equilibrium liquid composition and C_S^* for the equilibrium solid composition. For ideal solutions, the equilibrium partition coefficient, $k = C_S^*/C_L^*$, can be calculated independently. This is done by equating Eqs. (6) and (7) at equilibrium and taking the melting point of pure solute B as the temperature of the standard state. The result, for a dilute solution in B is

$$k = \exp\left[\frac{\Delta H^B (T_M^A - T_M^B)}{RT_M^A T_M^B}\right] \quad (8)$$

where ΔH^B is the heat of fusion of pure solute B, T_M^A the melting point of pure A and T_M^B the melting point of pure B. When a system is placed in the magnetic field H, the change in the magnetic energy of the system with the change in the magnetic field can be written as

$$dU_m = -\mu_0 VM\, dH = -\mu_0 V \chi H\, dH \quad (9)$$

where M is the magnetic moment per unit volume, H the imposed magnetic field, μ_0 the vacuum magnetic permeability ($4\pi \times 10^{-7} H/A$), χ the molar magnetic susceptibility and V the molar volume. Taking the effect of the magnetic

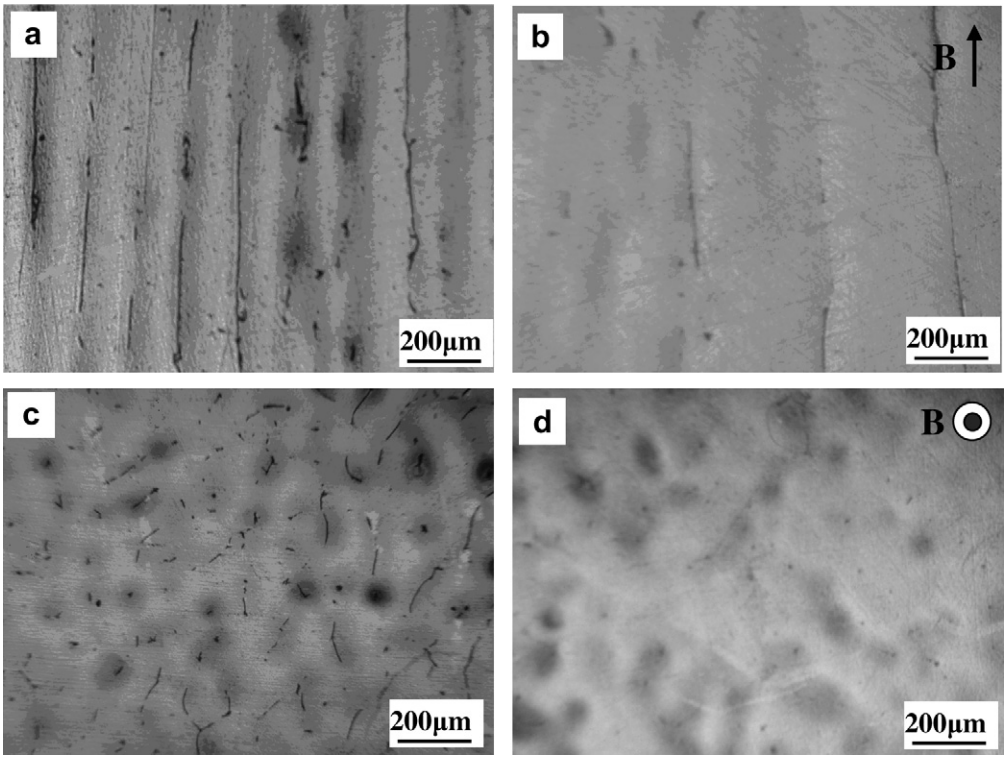

Fig. 5. Microstructures below the eutectic isotherm of Al–0.85 wt.% Cu alloy solidified at 10 μm/s and a temperature gradient in liquid (G_L) of 62.8 K/cm. (a) Longitudinal, 0 T; (b) longitudinal, 10 T; (c) transverse, 0 T; and (d) transverse, 10 T.

field into consideration, we obtain the new formulae for the chemical potentials of the liquid and solid phases:

$$\mu_L^A = \mu_0^A + S_L^A \Delta T^A + RT\ln(1 - C_L) - \frac{\mu_0 V_L^A \chi_L^A}{2} H^2 \quad (10)$$

$$\mu_S^A = \mu_0^A + S_s^A \Delta T^A + RT\ln(1 - C_S) - \frac{\mu_0 V_S^A \chi_S^A}{2} H^2 \quad (11)$$

$$\mu_L^B = \mu_0^B + S_L^B \Delta T^B + RT\ln C_L - \frac{\mu_0 V_L^B \chi_L^B}{2} H^2 \quad (12)$$

$$\mu_S^B = \mu_0^B + S_S^B \Delta T^B + RT\ln C_S - \frac{\mu_0 V_S^B \chi_S^B}{2} H^2 \quad (13)$$

where χ_L^A and χ_L^B are partial molar susceptibilities of A and B in the liquid, respectively; χ_S^A and χ_S^B partial molar

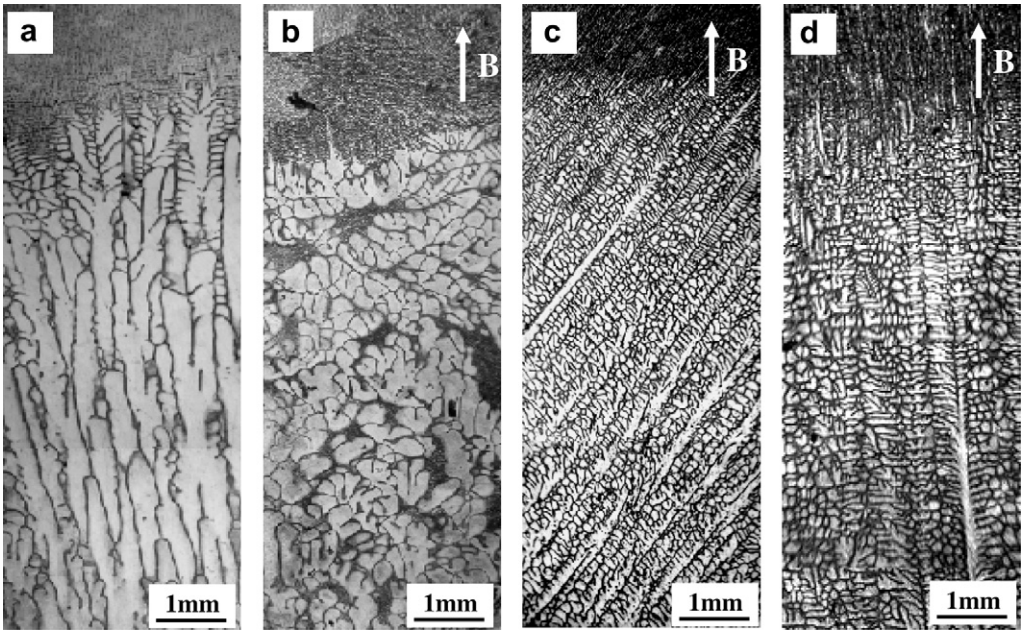

Fig. 6. Longitudinal solidification structure at the quenched liquid–solid interface of Al–4.5 wt.% Cu alloy solidified at a temperature gradient in liquid (G_L) of 38 K/cm for various growth speeds (a) $B = 0$ T, $R = 10$ μm/s; (b) $B = 10$ T, $R = 10$ μm/s; (c) $B = 10$ T, $R = 50$ μm/s; and (d) $B = 10$ T, $R = 100$ μm/s.

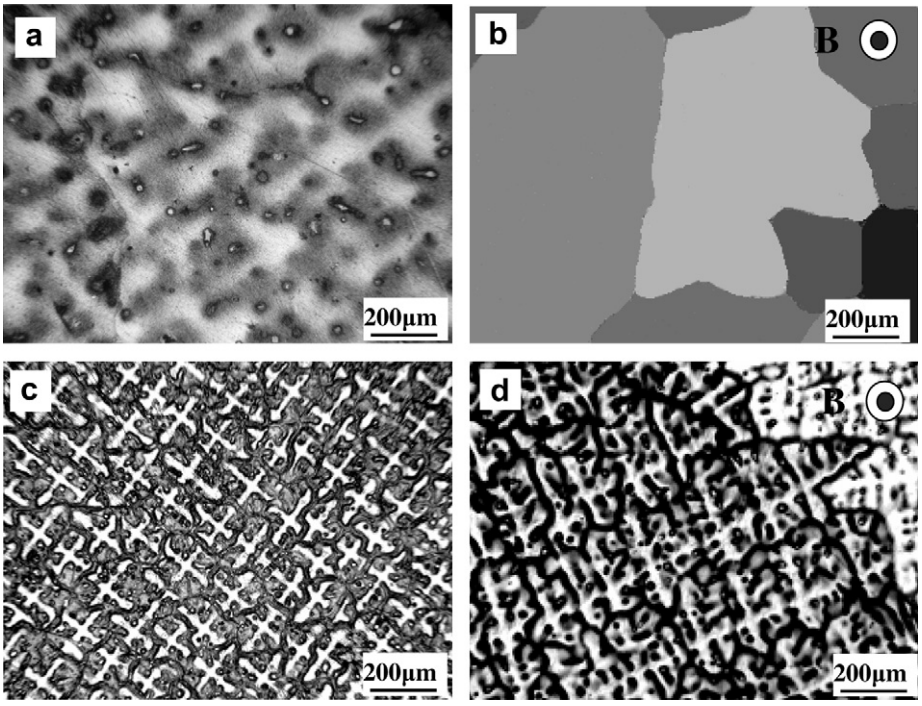

Fig. 7. Transverse microstructures below the eutectic isotherm (perpendicular to the growth direction) of Al–4.5 wt.% Cu alloy solidified at a temperature gradient in liquid (G_L) of 38 K/cm for various growth speed. (a) $B = 0$ T, $R = 10$ μm/s; (b) $B = 10$ T, $R = 10$ μm/s; (c) $B = 0$ T, $R = 100$ μm/s; and (d) $B = 10$ T, $R = 100$ μm/s.

susceptibilities of A and B in the solid, respectively; V_L^A and V_L^B are the partial molar volumes of A and B in the liquid, respectively; V_S^A and V_S^B the partial molar volumes of A and B in the solid, respectively. Setting Eq. (12) equal to Eq. (13) at equilibrium, the following equation is obtained:

$$\frac{\Delta H^B(T_M^A - T_M^B)}{T_M^B} = RT_M^A \ln k' - \frac{\mu_0\left(\chi_S^B V_S^B - \chi_L^B V_L^B\right)}{2} H^2 \qquad (14)$$

where k' is the partition coefficient C_S^*/C_L^* in the case of the magnetic field. Substituting Eq. (8) reduces to Eq. (14) and approximating for $k \simeq k'$, we obtain

$$\frac{k'}{k} = 1 + \mu_0 \frac{\left(\chi_S^B V_S^B - \chi_L^B V_L^B\right)}{2RT_M^A} H^2 \qquad (15)$$

Now we can also set Eq. (10) equal to Eq. (11) and obtain, for dilute solutions at equilibrium:

$$\Delta S^A \Delta T^A + RT\left(C_L^* - C_S^*\right) - \frac{\mu_0\left(\chi_S^A V_S^A - V_L^A \chi_L^A\right)}{2} H^2 = 0 \qquad (16)$$

At the limit $C_L^* \to 0$, $\Delta T^A = \Delta T_H$, the undercooling of the phase with pure component A due to the application of the magnetic field H. The explanation of ΔT_H is given, according to Ref. [8], as:

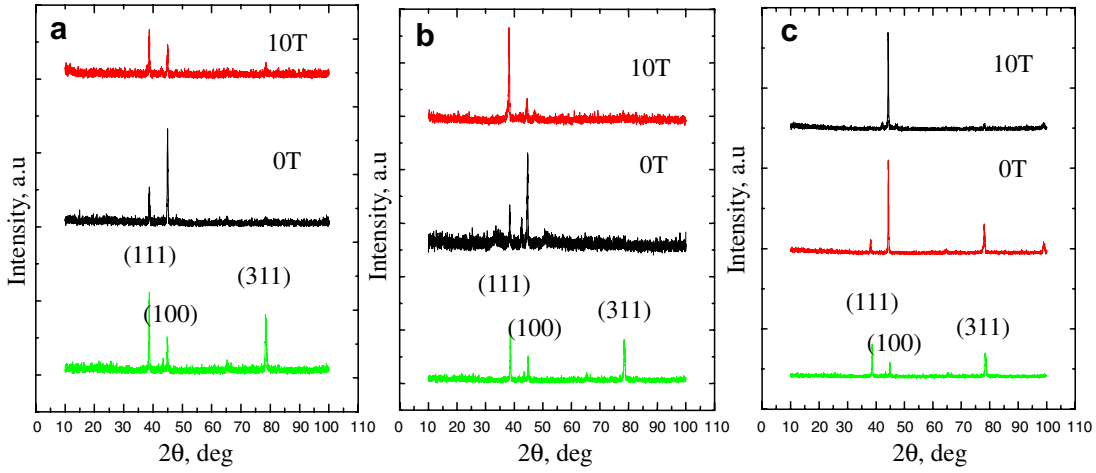

Fig. 8. X-ray diffraction patterns on the transverse plane of the samples ($G_L = 38$ K/cm). (a) $R = 5$ μm/s; (b) $R = 50$ μm/s; and (c) $R = 100$ μm/s.

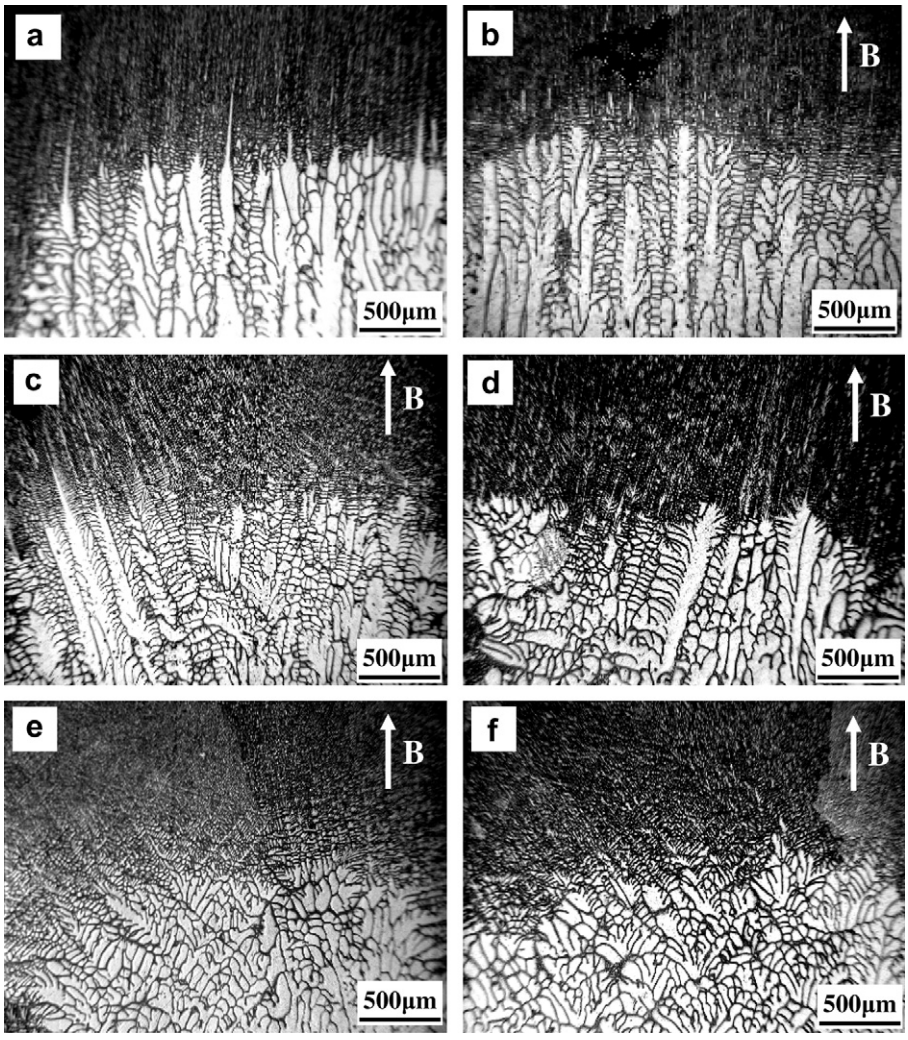

Fig. 9. Effect of the magnetic field intensity on the dendritic microstructure of Al–4.5 wt.% Cu alloy $G_L = 62.8$ K/cm and $R = 20$ μm/s. (a) 0 T; (b) 0.2 T; (c) 0.5 T; (d) 2 T; (e) 6 T; and (f) 10 T.

$$\Delta T_H = T_0^H - T_0 = \frac{\mu_0\, T_0(\chi_L V_L - \chi_S V_S)}{2\Delta H} H^2 \tag{17}$$

where ΔH is the change in solidification enthalpy at $H = 0$, and V_L and V_S are the molar volume of the liquid and solid, respectively. χ_L and χ_S are the molar magnetic susceptibility of the liquid and solid, respectively. Now, let us define $\Delta T'^A$ as

$$\Delta T'^A = \Delta T^A - \Delta T_H^A \tag{18}$$

where $\Delta T'^A$ is that of Eq. (16). This is the elevation of the liquidus temperature from that of pure A under a 0 T magnetic field to that of the alloy of liquid composition C_L and the application of the magnetic field H. Substituting Eq. (18) into Eq. (16) yields:

$$m'_L = -\frac{\Delta T'}{C_L} = \frac{RT_M^{A^2}(1-k')}{\Delta H^A} \tag{19}$$

where $m'_L = -\Delta T'/C_L$ is the slope of the liquidus of the binary alloy with the magnetic field H. For the equilibrium liquidus and solidus of α-Al in the Al–Cu phase diagram, A stands for Al and B stands for Cu. Thus the equilibrium partition coefficient k and the liquidus slope m_L are given as follows:

$$\frac{k'}{k} = 1 + \mu_0 \frac{\left(\chi_S^{Cu} V_S^{Cu} - \chi_L^{Cu} V_L^{Cu}\right)}{2RT_M^{Al}} H^2 \tag{20}$$

$$m'_L = -\frac{\Delta T'}{C_L} = \frac{RT_M^{Al^2}(1-k')}{\Delta H^{Al}} \tag{21}$$

The above relationships indicate that the magnetic field has affected the equilibrium partition coefficient k and the liquidus slope m_L, and thus changed the value of $\frac{G_L k D_L}{m_l C_0(1-k)}$. Accordingly, the field will affect the interface transformation. In the present work, the magnetic field causes a decrease in the stability threshold regarding the growth speed for the stability of the interface, which suggests that the magnetic field may cause a decrease in $\frac{G_L k D_L}{m_l C_0(1-k)}$. Thus it can be determined that the field may decrease the equilibrium partition coefficient k or increase the liquidus slope m_L.

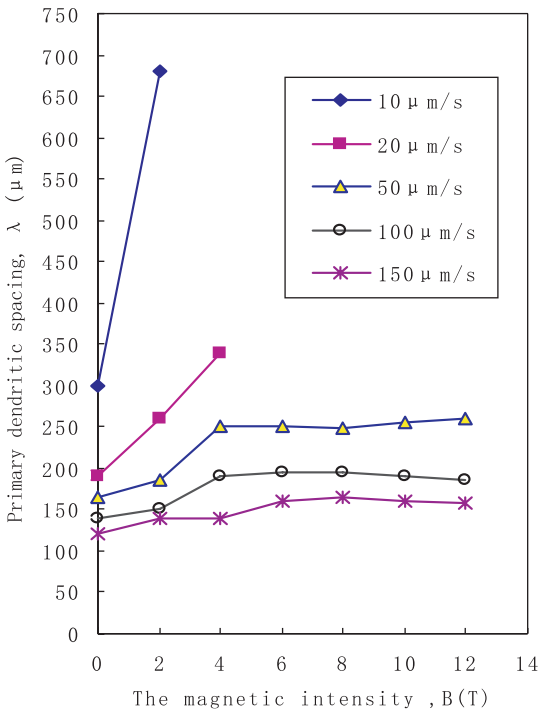

Fig. 10. Effect of the magnetic field intensity on the dendritic spacing ($G_L = 38$ K/cm).

4.2. Influence of the magnetic field on the cellular and dendritic array

The applied magnetic field also clearly causes severe distortion in the cellular and dendritic array, which can be attributed to the magnetic anisotropy of the crystal. For a crystal, the χ-values depend on the crystal directions. Therefore, from formula (9), the magnetizing entropy is varied correspondingly. For α-Al crystal, the ⟨1 1 1⟩-crystal direction is the easy magnetization direction because the (1 1 1)-plane is the closest-packed plane [9], so that $\chi_{\langle 1\,1\,1\rangle} > \chi_{\langle 1\,0\,0\rangle}$. Then the difference in the magnetizing entropy between the ⟨1 1 1⟩-crystal direction and ⟨1 0 0⟩ is

$$\Delta G_M^{\langle 1\,1\,1\rangle-\langle 1\,0\,0\rangle} = G_M^{\langle 1\,1\,1\rangle} - G_M^{\langle 1\,0\,0\rangle} < 0 \tag{22}$$

It is well known that the preferred crystallographic growth direction of α-Al is the ⟨1 0 0⟩-direction. In normal directional solidification, the crystal usually grows along the ⟨1 0 0⟩-direction, as shown in Fig. 11a. When the magnetic field is applied, it can be learnt from formula (22) that the magnetic energy along the ⟨1 1 1⟩-crystal direction is the lowest. Thus, when an axial magnetic field is applied during the directional solidification, the ⟨1 1 1⟩-crystal direction of α-Al tends to rotate and orientate along the magnetic field direction. As a consequence, the ⟨1 0 0⟩-direction will deviate from the solidification direction, as shown in Fig. 11b, and form the structure shown in Fig. 11c. The effect of the magnetic field on the microstructure takes place in the mushy zone mainly; so the longer the microstructure stays in the mushy zone, the more the field affects the microstructure. Consequently, at the lower growth speed, the effect of the field on the microstructure is more remarkable, whilst with an increase in the growth speed, the dendrites are hardly tilted because the time the microstructure stays in the mushy zone is reduced. So, the dendrites grown at 100 μm/s (Fig. 2d) are not apparently tilted. Moreover, because the magnetic energy is the lowest along the ⟨1 1 1⟩-crystal direction, the field enhances the growth of α-Al crystal along this direction. As a consequence, the field promotes the branching of the cell as well as the dendrite crystals.

4.3. Influence of the magnetic field on the interface shape and the crystal boundary

The experimental results of the undulating and bumpy liquid–solid interface in Figs. 2–4 show that the application of the magnetic field also had a considerable effect on the

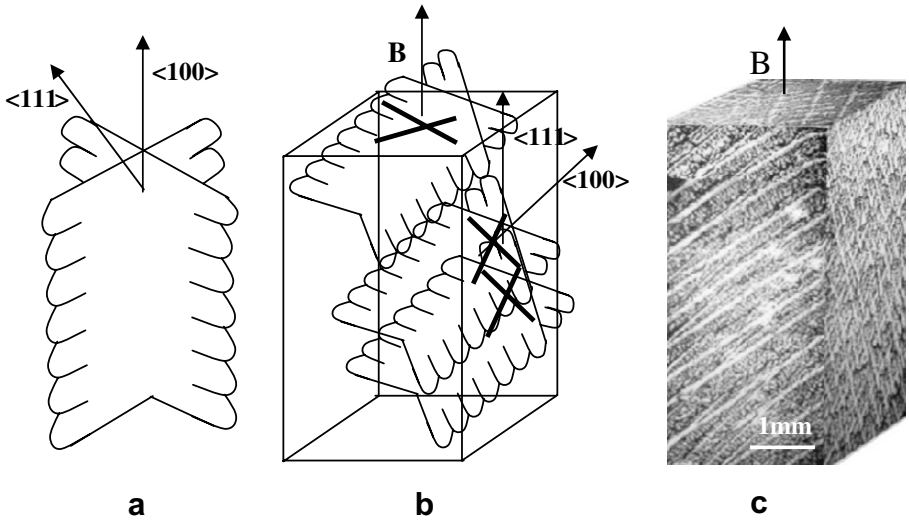

Fig. 11. A three-dimensional schematic illustration of the dendrite orientation during directional solidification of Al–4.5 wt.% Cu alloy. (a) 0 T; (b) 10 T; and (c) the three-dimensional diagram of the microstructure below the eutectic isotherm ($R = 50$ μm/s).

interface shape. It is well known that in any material temperature G produces a Seebeck electromotive force SG where S is the thermoelectric power of the material. If the gradients of S and T are not parallel, then a thermoelectric current (TE) is generated in the system. The application of the magnetic field to such a system produces a thermoelectromagnetic body force which generates a meridional flow. Generally, for vertical Bridgman crystal growth of Al–Cu alloys with the melt above the crystal, the heavier species Cu migrates down to the protruding liquid–solid interface due to the gravitation force. Since the solidification temperature decreases as the local concentration of the heavier species Cu increases, the solidification temperature for a Cu-rich melt at the ampoule wall is lower than that for the Al-rich melt at the centerline, leading to a crystal–melt interface which is far more protruding than the local isothermal surfaces. Moreover, for the Al–Cu hypoeutectic alloy, the value of S for the crystal is different from that for the melt. In this situation, thermoelectric currents arise from two closely related sources. The axial high magnetic field retards the descent of the Cu species toward the bottom of the protruding interface, so that the protruding surface is reduced (as shown in Fig. 3a). However, the magnetic field can only retard the motion of the Cu species and cannot completely prevent it. Accordingly, some thermoelectric currents still occur from both sources and can drive a TEMC circulation. This meridional flow interacts with the prevailing buoyancy-driven flows to modify the interface shape as well as the bulk liquid composition.

The TEMC effects consist of two types of Lorentz force; one is generated by the internal electric current at the interface due to TE effects, $J_{\mathrm{TE}} \times B$, and the other is generated by the induced electric current caused by the motion $-\sigma(u \times B) \times B$. The former plays a role in the motion as a driving force proportional to the first order of B and the latter as a braking force proportional to the second order of B. A complete numerical treatment of the TEMC effects with magnetic field damping was performed by Khine and Walker [6]. Their results showed that, as the magnetic field strength was increased from zero, the magnitude of the meridional circulation first increased from zero to a maximum at a Hartmann number Ha of approximately 10 and then decreased toward zero as the magnetic damping increased faster than the thermoelectric effects. In our experiment, when $Ha = 10$, for the crucible scale, the magnetic field intensity is approximately 0.4 T. However, our experimental results indicate that the effect of the field is still significant when the magnetic field intensity is of order of 10 T. In Fig. 4, for example, the liquid vortex was found near the ampoule wall. It is possible that the TEMC effects originate from near the ampoule wall, because an instability involving a strong azimuthal velocity near the ampoule wall in the Bridgman growth process would not be submitted to a strong magnetic damping, for the electrically insulating ampoule would block the local radial electric current needed for the damping. Croll et al. [10] also found that rotational striations were concentrated near the periphery of a crystal under a 5 T magnetic field. Moreover, it is possible that other new effects of the magnetic field influence the crystal growth.

At the same time, segregation occurs over distances of the order of the cell and dendrite spacing during the directional growth [11], which leads to the difference in the thermoelectric power (S) over these distances. Therefore, the Seebeck effect works in cells and dendrites (including the crystal boundary) and an electron flow is produced. The interaction between the electron flow and the magnetic field produces a meridional electron flow in the solid phase, which may promote solid diffusion and cause the crystal boundary to disappear.

5. Conclusions

1. The magnetic field has a destabilizing effect on the planar interface and enhances planar–cellular and cellular–dendritic transformation. This is attributed to the change in the equilibrium partition k and the liquidus slope m_{L} caused by the field.
2. The magnetic field causes severe distortion in the cellular and dendritic arrays, and breaks and orientation the dendrites in the $\langle 1\,1\,1 \rangle$-direction along the solidification direction instead of the $\langle 1\,0\,0 \rangle$-direction. This is attributed to the magnetic anisotropy of α-Al crystal.
3. The field causes the liquid–solid interface to become bumpy and irregular; moreover, the field decreases the crystal boundary and promotes solid diffusion in the solid phase. This may be attributed to the TEMC effects created by the interaction between the thermoelectric current and the magnetic field.

Acknowledgements

This work is supported by Natural Science Foundation of China (Nos. 50234020, 50225416 and 59871026). L.X. is also grateful for an Egide/Eiffel Doctorate Scholarship.

References

[1] Youdelis WV, Dorward RC. Can J Phys 1966;44:139.
[2] Tewari SN, Shah R, Song H. Met Trans A 1994;25A:1535.
[3] Alboussière T, Moreau R, Camel D. Acad Sci Paris 1991;313:749.
[4] Lakar O, Ph.D. Thesis, INPG, France; 1994.
[5] Yesilyurt S, Vujisic L, Motalkef S, Szofran FR, Volz MP. J Crystal Growth 1999;207:278.
[6] Khine YY, Walker JS. J Crystal Growth 1998;183:150.
[7] Martin JW, Doherty RD, Cantor B. Stability of microstructure in metallic systems. 2nd ed. Cambridge: Cambridge University Press; 1997. p. 391.
[8] Valko L, Valko M. IEEE Trans MAG 1994;30:1122.
[9] Zhong QC. Metallography and heat treatment. China Machine Press; 1994. p. 10.
[10] Croll A, Szofran FR, Dold P, Benz KW, Lehoczky SL. J Crystal Growth 1998;183:47.
[11] Bower TF, Brody HD, Flemings MC. Trans Aime 1966;236:624.

[A2] Xi Li, Yves Fautrelle, Zhongming Ren

Influence of thermoelectric effects on the solid-liquid interface shape and cellular morphology in the mushy zone during the directional solidification of Al-Cu alloys under the magnetic field,

Acta Materialia 55 (2007) 3803-3813.

Available online at www.sciencedirect.com
ScienceDirect
Acta Materialia 55 (2007) 3803–3813
Acta MATERIALIA
www.elsevier.com/locate/actamat

Influence of thermoelectric effects on the solid–liquid interface shape and cellular morphology in the mushy zone during the directional solidification of Al–Cu alloys under a magnetic field

Xi Li [a,b,*], Yves Fautrelle [b], Zhongming Ren [a]

[a] Department of Material Science and Engineering, Shanghai University, Shanghai 200072, China
[b] EPM-Madylam/CNRS, ENSHMG BP 38402 St Martin d'Heres Cedex, France

Received 11 December 2006; received in revised form 20 February 2007; accepted 20 February 2007
Available online 19 April 2007

Abstract

In this work thermoelectromagnetic convection (TEMC) is evaluated at different scales and the result shows that the effect of TEMC is different for different scales. To validate this analysis, Al–Cu hypoeutectic alloys were solidified directionally under a magnetic field, and both the interface shape and cellular morphology in the mushy zone investigated. The experimental results show that a weak magnetic field ($B \leqslant 0.5$ T) has a significant affect on the cellular liquid–solid interface and the cellular morphology. This is attributed to the TEMC caused by the interaction between the field and the thermoelectric (TE) current, which is consistent with the analysis. Under a higher magnetic field, the field causes the cells to break and makes the liquid–solid interface uneven; these effects are attributed to the magnetic force and the TE torque.

Keywords: Magnetic field; Thermoelectric (TE) effects; Al–Cu hypoeutectic alloys; Directional solidification

1. Introduction

It has been determined that the application of a magnetic field during the directional solidification of materials can significantly reduce the thermosolutal buoyant flow [1–3]. However, no influence on microstructure or longitudinal macrosegregation has been detected upon application of either a transverse or an axial field (0.1 T) during the directional solidification of the near eutectic Pb–57 wt.% Sn alloy, which contained only a small volume fraction of primary dendrites [4]. To investigate this further, Tewari et al. [5] studied the effect of a stronger transverse magnetic field (0.45 T) on cellular microstructures in directionally solidified Pb–17.7 wt.% Sn alloy and showed experimentally that no influence on macrosegregation could be detected. However, at very low pulling rates (less than 1 μm s^{-1}), the cellular array was found to be severely distorted. This was due to the damping braking of one of the components of the natural thermosolutal convection by the field. Alboussiere and Moreau [6] and Laskar [7] investigated the effect of a magnetic field on Bi–60 wt.% Sn and Cu–45 wt.% Ag alloys, solidified vertically under solutally and thermally stabilizing conditions with a 0.6 T transverse or a 1.5 T axial magnetic field, and found that large freckles appeared, showing that a new movement had been created. Alboussiere et al. [6] suggested that this new flow was induced by the interaction between the magnetic field and thermoelectric (TE) effects, and subsequently, Lehmann [8] offered some experimental evidence for thermoelectromagnetic convection (TEMC). Recently, Yesilyurt et al. [9] presented numerical solutions for buoyant convection and TEMC in an actual (single) crystal growth process with an axial magnetic field. Their results indicated that TE currents at the growth interface during

* Corresponding author.
E-mail address: xi@hmg.inpg.fr (X. Li).

1359-6454/$30.00
doi:10.1016/j.actamat.2007.02.031

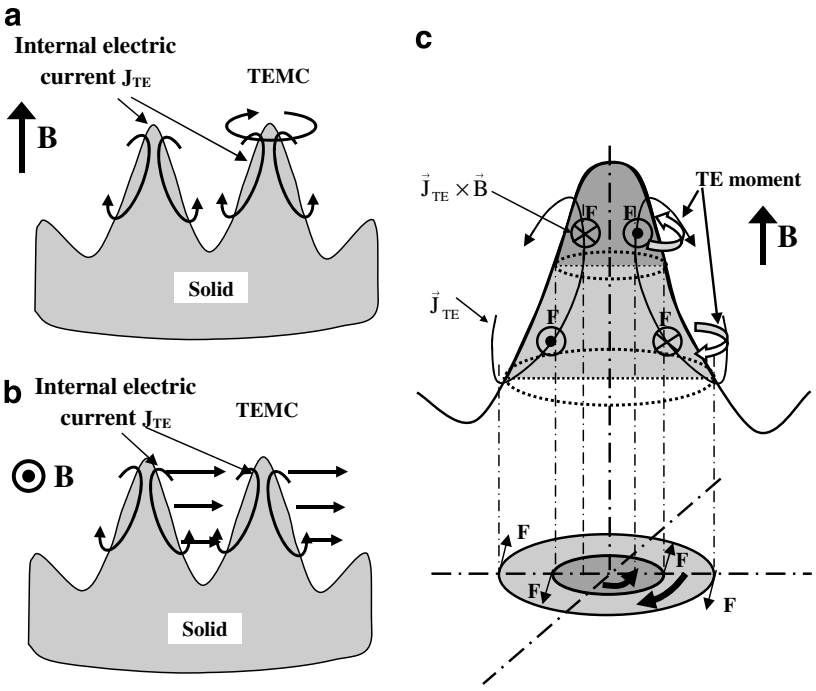

Fig. 1. Schematic views of the TE effects under a magnetic field: (a) TEMC under a magnetic field parallel to the solidified direction; (b) TEMC under a magnetic field perpendicular to the solidified direction; (c) TE moment applied on the cell/dendrite under a magnetic field parallel to the solidified direction.

Bridgman growth promoted convection when a low-intensity axial magnetic field was applied. For high magnetic field strengths, meridional flow typically slows down due to the Lorentz force. According to Khine and Walker [10], the magnitude of the TEMC is maximum when the Hartmann number, *Ha*, is about 10. Nevertheless, little work has been done to evaluate TEMC for various scales, i.e. the pool width, the primary dendrite and the high-order dendrite arm scales, during dendrite/cell growth. Moreover, there is insufficient experimental evidence to prove the existence of TEMC. This paper presents an analysis of TEMC for different scales, and then offers experimental evidence to support this. Furthermore, the force moment caused by the interaction between the TE current on the dendrite/cell and the magnetic field is examined for the first time. The cellular microstructure of Al–Cu hypoeutectic alloys is investigated to prove this new effect.

2. Experimental

The Al–0.85 wt.% Cu and Al–4.5 wt.% Cu alloys used in this study were prepared with high-purity Al (99.99%) and Cu (99.99%) in an induction furnace. The alloy was placed in a high-purity graphite crucible (10 cm diameter), heated to 900 °C, magnetically stirred for half an hour and poured into a graphite mold to cast samples with a diameter of 3 mm and a length of 200 mm. The cast sample was enveloped in a high-purity corundum tube with an inner diameter of 3 mm and a length of 200 mm. The samples were directionally solidified in a Bridgman apparatus at various speeds. The experimental apparatus and many experimental details can be found in Ref. [11]. The temperature gradient and the growth speed were adjusted to form plane and cellular regions. Microstructures were examined in the etched condition by optical microscopy.

2.1. Evaluation of the thermoelectric effects

It is well known that in any material a temperature gradient $\vec{\nabla}T$ produces a Seebeck electromotive force $S\vec{\nabla}T$, where S is the TE power of the material [4–6]. If the gradients of S and T are not parallel, then a TE current is generated in the system. Thus, the interaction between TE current and the magnetic field will produce a thermoelectromagnetic force and a convection (TEMC) will develop

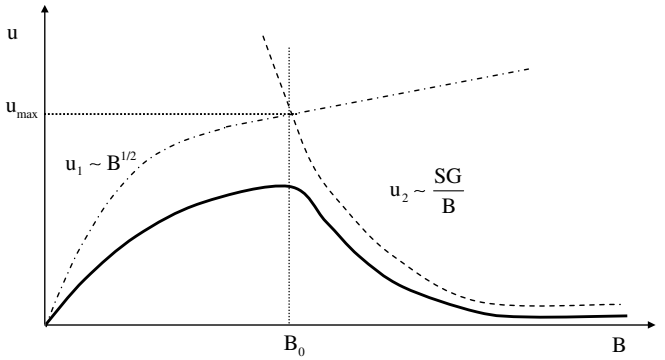

Fig. 2. Schematic illustration of TEMC amplitude (u) as a function of the external magnetic field (B).

Table 1
Physical properties of the Al–Cu alloy used in the evaluation [7,8]

Properties	Magnitude
Thermoelectric power (S, V K^{-1})	2×10^{3}
Electrical conductivity (σ, Ω^{-1} m^{-1})	3.8×10^{6}
Density (ρ, kg m^{-3})	2.4×10^{3}
Kinematic viscosity (v, m^2 s^{-1})	2.6×10^{-9}
Diffusion coefficient (D, m^2 s^{-1})	4×10^{-9}

near the interface on the microscopic scale. Fig. 1a and b describes the influence of the TEMC in the two cases of an external magnetic field parallel and perpendicular to the growth direction, respectively. If the magnetic field is parallel to the growth direction, the TEMC causes rotatory flow around the tip of the primary arm of the dendrite. If the magnetic field is perpendicular to the growth direction, the interaction between the internal electric current and the external magnetic field causes a uniform flow within the mush, just like "interdendritic forced convection".

In order to provide a qualitative analysis of the TEMC effects, let us recall the basic equations that govern the overall phenomenon. Firstly, Ohm's law relates the electric current density $\vec{j}$ to the electric field $\sigma\vec{E}$, the TE electromotive force $\sigma S\vec{\nabla}T$ and the current generated by the liquid motion across the magnetic field lines $\sigma\vec{u}\times\vec{B}$ in the following way (see e.g. Ref. [10]):

$$\vec{j}=\sigma\vec{E}+\sigma S\vec{\nabla}T+\sigma\vec{u}\times\vec{B}, \tag{1}$$

where σ, S, $\vec{u}$ and $\vec{B}$, respectively, denote the electrical conductivity, the absolute TE power of the conducting medium, the liquid velocity field and the vertical applied magnetic field. It should be noted that the value of S also depends on the alloy concentration. The above equation holds in the liquid zone. A second similar equation must be written for the solid with different physical properties as well as matching boundary conditions for the electric current density. Eq. (1) shows that the electric current density is generated by two main mechanisms, namely the TE effect in the presence of a temperature gradient and the induced electric current generated by the liquid motion itself. Note that the electric field in the present case does not generate directly an electric current density. It only insures that the electric current density is divergence-free. Concerning the liquid motion, let us assume that the fluid is incompressible. Furthermore, we do not take into account the buoyancy forces (which will be discussed later). Thus the fluid flow is governed by the Navier–Stokes equations:

$$\rho\frac{\partial\vec{u}}{\partial t}+\rho(\vec{u}\cdot\vec{\nabla})\vec{u}=-\vec{\nabla}p+\vec{j}\times\vec{B}+\rho v\nabla^2\vec{u}=-\vec{\nabla}p+\sigma\vec{E}\times\vec{B}+\sigma S\vec{\nabla}T\times\vec{B}+\sigma(\vec{u}\times\vec{B})\times\vec{B}+\rho v\nabla^2\vec{u}, \tag{2}$$

together with the continuity equation:

$$\vec{\nabla}\cdot\vec{u}=0,$$

where, ρ, v, p are the density, the kinematic viscosity and the pressure, respectively. Note that the TE force is zero if the temperature gradient is exactly parallel to the magnetic field. Thus no flow can be expected in this case. The electric field balances the TE term in Eq. (2). Moreover, Eq. (2) shows that the TEMC involves two types of Lorentz forces. One is generated by the internal electric current at the interface due to TE effects $\sigma S\vec{\nabla}T\times\vec{B}$, whilst the other is generated by the induced electric current via the liquid motion $\sigma(\vec{u}\times\vec{B})\times\vec{B}$. The former plays a role in the motion field as an accelerating force proportional to the first order of B, and the latter acts usually as a braking force proportional

Table 2
Values of the parameters deduced from the order of magnitude analysis

	$\lambda=R=1500$ μm	$\lambda=100$ μm	$\lambda=1$ μm
$B_{\max}=\left(\frac{\rho SG}{\lambda\sigma}\right)^{1/3}$	0.17 T	0.43T	–
$u_{\max}=\left(\frac{\lambda\sigma}{\rho}(SG)^2\right)^{1/3}$	72,000 μm s^{-1}	29,000 μm s^{-1}	–
$B'_{\max}=\frac{1}{\lambda}\left(\frac{\rho V}{\sigma}\right)^{1/2}$	–	–	25 T
$u'_{\max}=SG\lambda\left(\frac{\sigma}{\rho V}\right)^{1/2}$	–	–	500 μm s^{-1}
$Re=\frac{\lambda u_{\max}}{V}$	108	2.9	5×10^{-4}
$Ha_{\max}=\lambda B_{\max}\left(\frac{\sigma}{\rho V}\right)^{1/2}$	10.1	1.71	1
$Pe=\frac{u\lambda}{D}$	–	2900	0.5

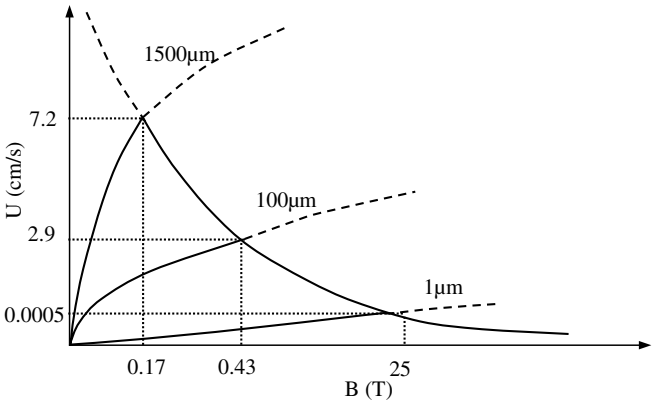

Fig. 3. Schematic illustration of the evolution of the TEMC amplitude (U) with respect to the external magnetic field (B) for different length scales: $\lambda = 1500$, 100 and 1 μm representing, respectively, the scale of the pool, the primary dendrite spacing and the smallest scales as the grain boundary thickness.

to the square of B. The above driving forces are balanced either by the viscous friction or inertia. Let us introduce the following orders of magnitude, namely the typical fluid velocity u, the temperature gradient G and a typical length scale λ. It must be emphasized that in the present case there are at least three different main length scales: the pool radius $R = 1.5$ mm, and the primary and the secondary dendrite arm spacing $\lambda_1 \approx 100$ μm and $\lambda_2 \approx 1$ μm, respectively. Let us estimate a typical velocity u_1 from the balance between the TE force and inertia in Eq. (2):

$$\rho \frac{u_1^2}{\lambda} \approx \sigma SGB. \tag{3}$$

We thus obtain the following velocity scale:

$$u_1 \approx \left(\frac{\sigma SGB\lambda}{\rho}\right)^{1/2}. \tag{4}$$

The latter estimate holds when the magnetic field is weak or moderate. Its damping effect occurs as soon as the induced electric current generated by the flow is comparable to the TE electric current, so that:

$$\sigma SGB \approx \sigma u_2 B^2. \tag{5}$$

We then obtain a second velocity estimate u_2 valid for large magnetic field amplitudes:

$$u_2 = \frac{SG}{B}. \tag{6}$$

In the large magnetic field limit viscous friction is restricted to the so-called Hartmann wall layer located along the liquid boundaries perpendicular to the magnetic field. Their thickness δ is estimated by:

$$\delta = \frac{1}{B}\left(\frac{\rho\nu}{\sigma}\right)^{1/2}. \tag{7}$$

Note that the estimate of u_2 given by (6) may also be obtained by balancing the TE forces with the viscous friction in the Hartmann layer as follows:

$$\rho\nu \frac{u_2}{\delta^2} \approx \sigma SGB. \tag{8}$$

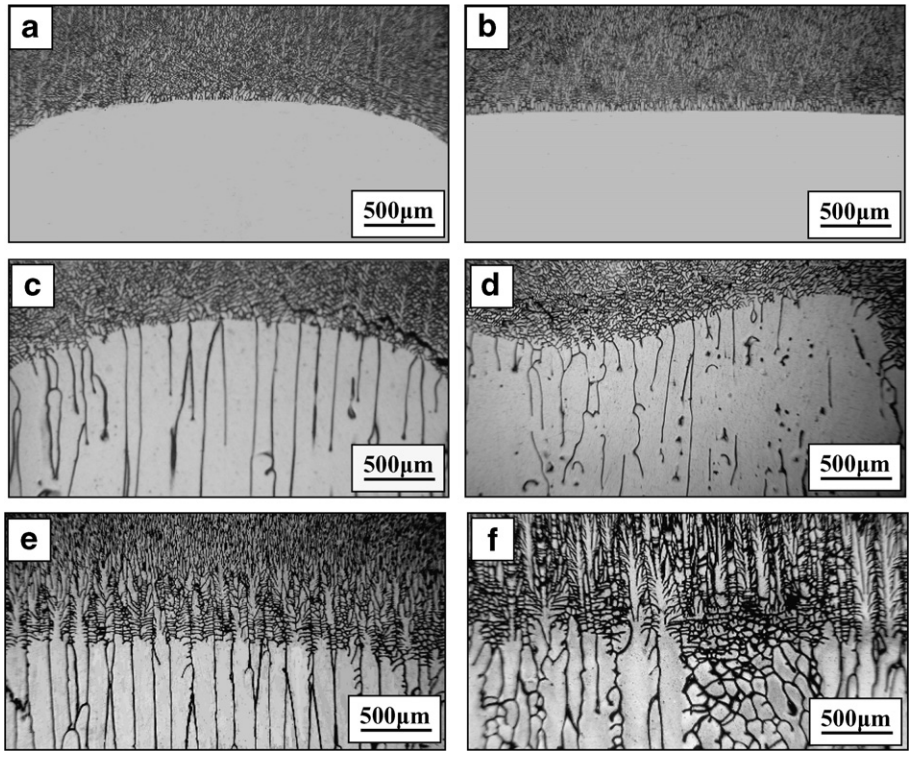

Fig. 4. Longitudinal structures of an Al–0.85 wt.%Cu alloy and the quenched liquid–solid interface for various growing velocities: (a) 0 T, 0.5 μm s^{-1}; (b) 10 T, 0.5 μm s^{-1}; (c) 0 T, 2.5 μm s^{-1}; (d) 10 T, 2.5 μm s^{-1}; (e) 0 T, 20 μm s^{-1}; (f) 10 T, 20 μm s^{-1}.

This means that the estimate u_2 corresponds to the case where the damping is involved directly in Eq. (5), for example, or indirectly through the viscous friction in the Hartmann layers in Eq. (8).

It must emphasized that u_1 increases as $B^{1/2}$ for weak magnetic field values whilst u_2 decreases as B^{-1} for large magnetic field amplitudes. The evolution of the typical velocity with respect to the magnetic field is illustrated qualitatively in Fig. 2. Firstly, it is clear that the motion may be suppressed if the magnetic field is strong enough. Secondly, there exists a maximum value which corresponds to the intersection between the two curves. The magnetic field $B_{\max}$, which corresponds to the maximum, is obtained by setting $u_1(B_{\max}) = u_2(B_{\max})$ and replacing u_1 and u_2 by their expressions (4) and (6). Its expression is:

$$B_{\max} = \left(\frac{\rho SG}{\lambda\sigma}\right)^{1/3}. \tag{9}$$

The corresponding velocity $u_{\max}$ is:

$$u_{\max} = \left(\frac{\lambda\sigma}{\rho}(SG)^2\right)^{1/3}. \tag{10}$$

The magnetic field required to damp the TE flow must be larger than $B_{\max}$. From Eq. (9) we note that the finer the

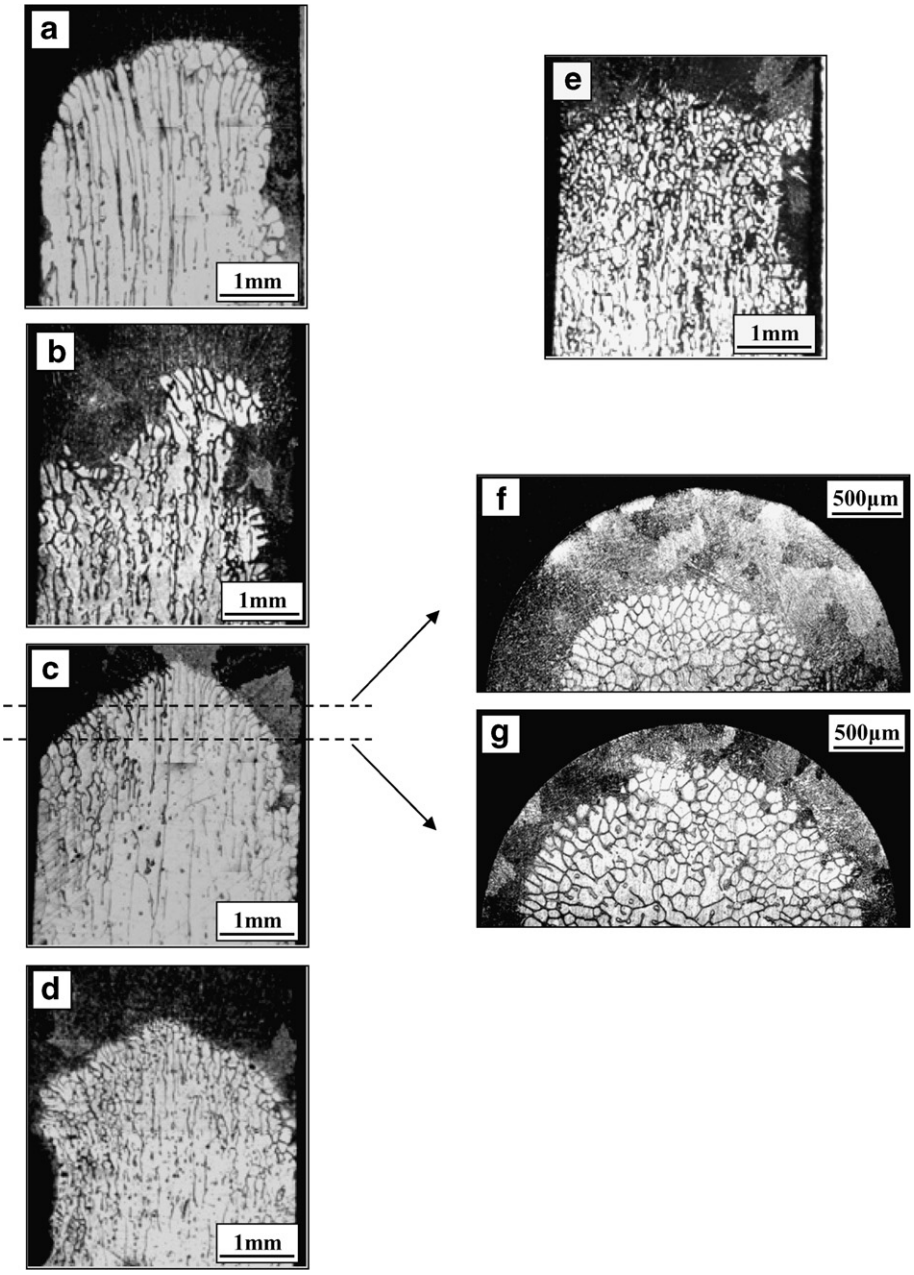

Fig. 5. Structures of an Al–4.5 wt.%Cu alloy solidified at 2 μm s^{-1} under various magnetic field intensities ($G = 62.8$ K cm^{-1}). Longitudinal structures at the liquid–solid interface: (a) 0 T; (b) 0.1 T; (c) 0.3 T; (d) 0.5 T; (e) 10 T. Transverse structures at various positions from the tips in the quenched mushy zone for the sample solidified under a 0.3 T-magnetic field: (f) 0.5 mm; (g) 1 mm.

length scale the larger the magnetic field amplitude required to suppress the TE motion. It is of interest to evaluate the Hartmann number based on B_{max}:

$$Ha_{max} = \lambda B_{max}\left(\frac{\sigma}{\rho v}\right)^{1/2}.$$

Note that the above estimates hold only if the flow Reynolds number is large enough to justify that inertia is dominant as compared with viscous friction:

$$Re = \frac{\lambda u_{max}}{v} \gg 1. \tag{11}$$

We notice from Eqs. (4) or (9) that for the smallest length scales (secondary arm spacing or grain boundary thickness) the Reynolds number is small and another estimate must be derived by using a balance between the TE forces and viscous friction. With the same procedure as in Eq. (3), the latter balance may be written as:

$$\rho v \frac{u_3}{\lambda^2} \approx \sigma SGB. \tag{12}$$

The corresponding velocity estimate valid for weak magnetic field amplitudes is:

$$u_3 \approx \frac{\sigma SGB\lambda^2}{\rho v}. \tag{13}$$

For large magnetic field amplitude the trend given by Eq. (6) still holds, and, as in the previous case, there exists a maximum velocity u'_{max} obtained by setting $u_3(B'_{max}) = u_2(B'_{max})$. The expressions of B'_{max} and u'_{max} are:

$$B'_{max} = \frac{1}{\lambda}\left(\frac{\rho v}{\sigma}\right)^{1/2} \quad \text{and} \quad u'_{max} = SG\lambda\left(\frac{\sigma}{\rho v}\right)^{1/2}. \tag{14}$$

Note that in the latter case the Hartmann number corresponding to the value of B'_{max} is unity.

Let us apply the above estimate to the present experimental situation by considering the three length scales quoted previously. Table 1 shows the physical properties of the Al–Cu alloy used in the evaluation. The results are gathered in Table 2 and illustrated in Fig. 3. From Table 2, we observe that the effect of the magnetic field is different for different scales. The smaller the structure, the larger the

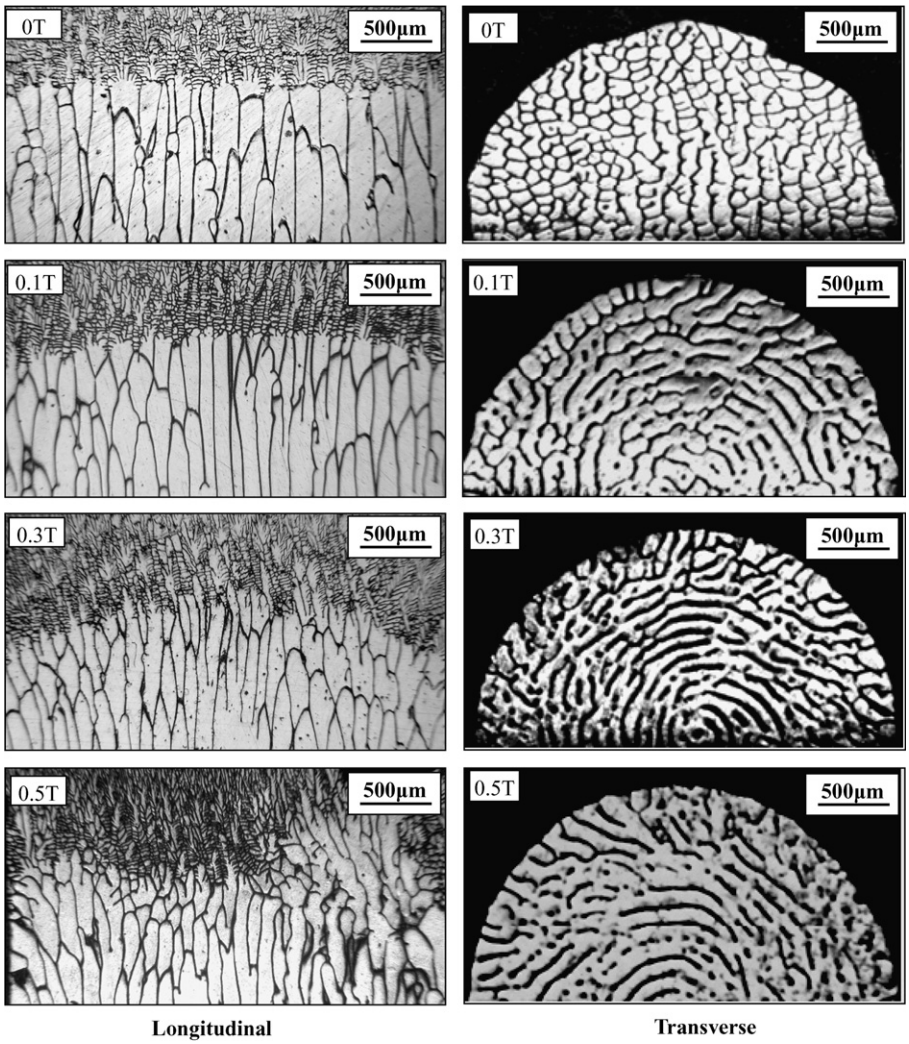

Fig. 6. Longitudinal structures of an Al–0.85 wt.%Cu alloy at the liquid–solid interface and the corresponding transverse structures at 3 mm in the mushy zone from the liquid–solid interface with a lower magnetic field ($G = 62.8$ K cm^{-1} and $V = 10\mu$m s^{-1}).

magnetic field needed to modify the structure by the TE effect. At the macroscale of the sample ($\lambda = R =$ 1500 μm) a moderate magnetic field is sufficient both to create and damp the TE flow. A higher field will produce a significant flow field at the scale of the dendrites ($\lambda = 100$ μm). However, a very high magnetic field is required to damp the flow motion at the smallest length scale of the phenomenon, i.e. $\lambda = 1$ μm. The above results are illustrated in Fig. 3.

On the other hand, a torque on the cell/dendrite will be produced by the interaction between the TE current on the cell/dendrites and the applied magnetic field as shown in Fig. 1c. From this figure, it can be seen that the moment at the tip of the cell is clockwise and the one on the bottom is anticlockwise, and thus a tangential stress will be produced at the middle of the cell. Unlike the TEMC effect, this torque increases with increasing the magnetic field. The stress may cause the cell or the dendrite to break.

3. Influence of the magnetic field on the solid–liquid interface shape and cell morphology

The liquid–solid interface shape and the cellular morphology in the mushy zone directly reflect the solidification behavior. Therefore, in order to validate the above analysis, the influences of the magnetic field on the interface shape and on the cellular morphology in the mushy zone have been investigated. Fig. 4 shows the liquid–solid interface of directionally solidified Al–0.85 wt.% Cu alloy with a temperature gradient in the liquid of $G_L =$ 62.8 K cm^{-1}. Fig. 4a and b shows the interface solidified at 0.5 μm s^{-1} both without and with a 10 T magnetic field, respectively. It can be observed that the interface shape without the magnetic field is convex. The curvature of the interface is attributed to the natural convection intrinsic to the system itself. The thermal conductivity of the crystal is larger than that of the melt and quartz,

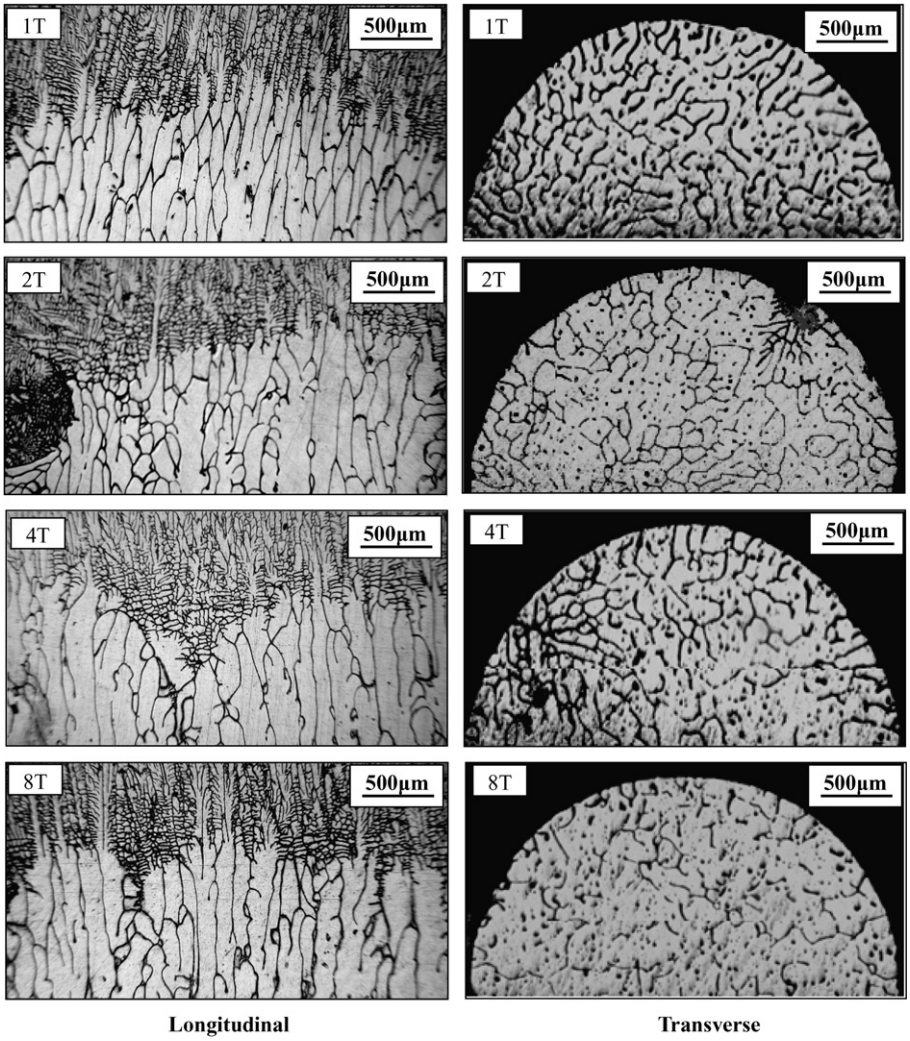

Fig. 7. Longitudinal structures of an Al–0.85 wt.%Cu alloy at the liquid–solid interface and the corresponding transverse structures in mushy zone at 3 mm from the liquid–solid interface with a higher magnetic field ($G = 62.8$ K cm^{-1} and $V = 10$ μm s^{-1}).

and therefore the axial heat flux flows mainly from the center of the melt to the crystal, leading to protruding isothermal surfaces and forming the convex interface. Generally, for an axial Bridgman experiment with melt above the crystal, the heavier species (in this case Cu) flows down to the bottom of protruding surfaces. Since the solidification temperature decreases as the local concentration of the heavier species Cu increases, the solidification temperature for a Cu-rich melt at the ampoule wall is lower than that for the Al-rich melt at the centerline, leading to a liquid–solid interface that is far more protruding than the local isothermal surfaces. Nevertheless, after the application of a 10 T magnetic field, the convex interface disappears and becomes flat. Fig. 4c and d shows the interface at 2.5 μm s^{-1} both without and with a 10 T magnetic field, respectively. The interface shape in the case of no field is regularly convex and the reason is similar to the case of solidification at 0.5 μm s^{-1}. However, after the application of a 10 T magnetic field, the regular convex interface disappears and becomes uneven, and it can be observed that the cells in the concave zone of the interface are more developed than in the convex zone and the cellular spacing in the concave zone of the interface is smaller than in the convex zone. According to the constitutional supercooling theory [12], it can be deduced that the constitutional supercooling in the concave zone is larger than that in the convex zone. This implies that the solute Cu in the concave zone of the interface is richer than that in the convex zone and segregation occurs at the interface. Fig. 4e and f shows the microstructures at the interface directionally solidified at 20 μm s^{-1} both without and with a 10 T magnetic field, respectively. It can be observed that the microstructure without the magnetic field is near the cell-to-dendrite transition. After the application of a 10 T magnetic field, the microstructure transforms into developed dendrites and grains. This indicates that the field has enhanced the interface transformation from cells to dendrites and led to the breakdown of the cells.

Here, it is necessary to mention the effect of a higher magnetic field (2–10 T) on the planar interface directionally solidified at 1.5 μm s^{-1} reported in Ref. [11], where the results showed that the field caused an uneven plane crystal interface. Nevertheless, the results in Fig. 4b and that in Ref. [11] are not contradictory. It was proved in Ref. [11] that the field can break the interface and promote the transformation of the interface. This was attributed to the effect of the magnetic field on the equilibrium partition coefficient k. Thus, for an interface near the planar–cellular transformation (e.g. the interface solidified at 1.5 μm s^{-1}), the field first breaks the planar interface and then causes the cellular interface to become uneven via the same mechanism shown in Fig. 4d. However, for an interface far from the planar–cellular transformation (e.g. the interface solidified at 0.5 μm s^{-1}), a 10 T magnetic field is not strong enough to break the planar interface, so the effect of the field on the interface solidified at 0.5 μm s^{-1} (Fig. 4b) only

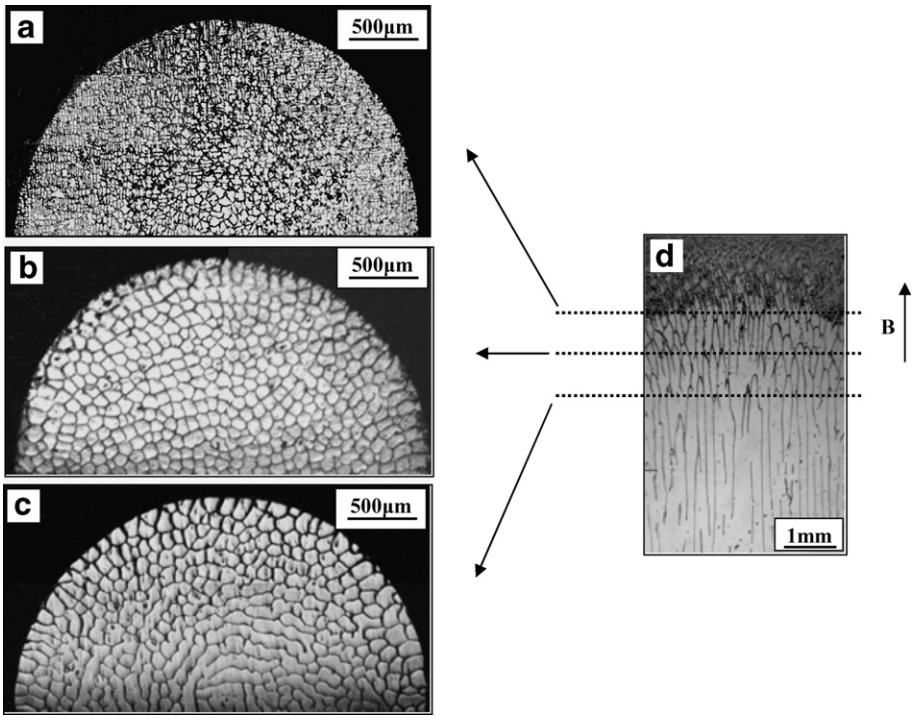

Fig. 8. Structures directionally solidified Al–0.85 wt.%Cu alloy at 10 μm s^{-1} under a 0.3 T-magnetic field. Transverse structures at various positions from the tips in the quenched mushy zone: (a) 0.1 mm; (b) 1 mm; (c) 2 mm; longitudinal structure near the quenched tips (d).

involves the effect of the magnetic field on the plane interface.

Fig. 5 shows the liquid–solid interface of directionally solidified Al–4.5 wt.% Cu alloy at 2 μm s^{-1} under various magnetic field intensities at the same temperature gradient as in the previous case, $G_L = 62.8$ K cm^{-1}. Fig. 5a–d shows the interface under a lower magnetic field ($B \leqslant 0.5$ T). Compared with the interface shape in the case of no field (Fig. 5a), the application of a 0.1 T magnetic field causes a more irregular interface shape (Fig. 5b). This indicates that the application of a 0.1 T magnetic field produces a strong flow in the mushy zone. For a 0.3 T magnetic field, the interface becomes regular convex (Fig. 5c, e and f), which implies that the flow in the sample scale may become small and regular. When a 10 T magnetic field is imposed, the directional structure disappears and forms grains, whilst the interface shape is similar to the one without the field. This means that the flow at the scale of sample is retarded. However, the magnetic field still affects the microscale structure.

Fig. 6 shows the longitudinal and transverse microstructures of Al–0.85 wt.% Cu alloy directionally solidified at 10 μm s^{-1} under a moderate magnetic field ($B \leqslant 0.5$ T). From the longitudinal microstructures, it can be observed that the cellular spacing decreases and the liquid–solid interface becomes protuberant as the magnetic field intensity increases (0.1–0.5 T). The transverse microstructures in the mushy zone at 3 mm from the solid–liquid interface have also been investigated and the results show that under a 0.1 T magnetic field, the morphology of the cell changes greatly and forms a ring-like structure. Under a 0.3 or 0.5 T magnetic field, the ring-like structure becomes more regular. Nevertheless, from Fig. 7 it can be observed that a higher magnetic field ($B \geqslant 1$ T) causes cells to become irregular and broken.

In order to study the formation mechanism of the ring-like structure on the transverse section under a moderate magnetic field, a sample under a 0.3 T magnetic field is chosen, and the microstructures in the mushy zone at different positions from the solid/liquid interface have been investigated. Fig. 8 shows transverse microstructures at various positions in the mushy zone and the corresponding longitudinal microstructure at the interface. The microstructure at 0.1 mm from the cell tip (Fig. 8a) shows that the microstructure in the center of the sample is cellular with small dendrites appearing at the periphery, which is consistent with the convex interface. The microstructure at 1 mm shows regular cells (Fig. 8b). However, the microstructure at 2 mm (Fig. 8c) shows that the cells in the center of the sample tend to form the ring-like structure. Comparison of the transverse microstructures at various positions from the cell tips (Figs. 6 and 8) shows that the formation mechanism of the ring-like structure should be attributed to the merging of cells along the azimuthal direction caused by the field. Thus, the cells at the same radius will merge together and form the ring-like structure. Moreover, it is interesting to note that, along with the amalgamation of the cells at the same radius along the azimuthal direction, the liquid thickness in the crystal boundaries of the cells at different radii increases.

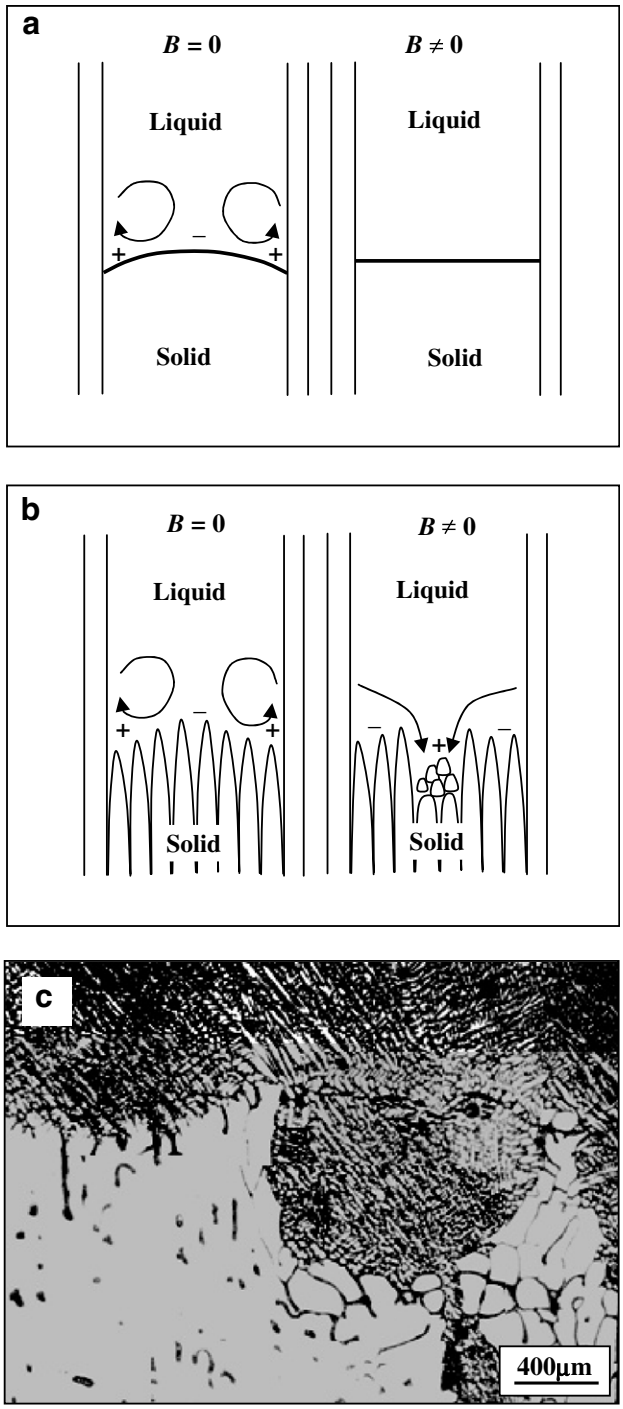

Fig. 9. Schematic illustration of the effect of a high magnetic field on the convective flow at the liquid/solid interface and on the interface shape, and an example of channel segregation: (a) effect of a high magnetic field on the boundary layer mode of a planar interface; (b) effect of a high magnetic field on the boundary layer mode of a cellular interface (symbols + and – indicate excess and deficiency of Cu solute); (c) microstructure of the interface of a Al–0.85 wt.%Cu alloy solidified at 1.5 μm s^{-1} in a 11 T-magnetic field, revealing the strong channel segregation caused by the break of the cell.

4. Discussion

According to the above analysis of TEMC, a 10 T magnetic field is strong enough to damp the flow at the macroscale (the scale of the sample) and microscale (the scale of the cells and primary dendrites). Therefore, it is reasonable to attribute the interface transformation of the plane crystal from convex to flat to the damping effect of the magnetic field as shown in Fig. 9a. However, we cannot explain the unevenness of the interface shape of the cellular crystal under a 10 T magnetic field by the damping effect. The above experimental results, as in Ref. [11], show that a higher magnetic field is capable of breaking the cells/dendrites. This may be attributed to the magnetic force and the stress caused by the TE torque. Thus, as shown in Fig. 9b, the cell breakage the can cause irregularities in the liquid–solid interface. The heavier species Cu will then flow down to the concave zone of the surfaces and cause the spot and channel segregation (Fig. 9c), thereby rendering the interface even more irregular. The unevenness of the cellular crystal interface under a higher magnetic field should thus be attributed to the fragmentation of the cell caused by the magnetic field and the subsequent segregation. Note that the TEMC seems to be more pronounced in the case of the Al–4.5 wt.% Cu, which can be attributed to the fact that the TE constant is probably larger in the case of the more concentrated alloy.

The TEMC also affects the microstructures in the mushy zone. Experimental results indicate that under a moderate magnetic field ($B \leqslant 0.5$ T), the field causes a decrease in the cellular spacing and the formation of the ring-like solidification structure. It is well known that flow may enhance cell branching and reduce the cellular spacing. Hence the decrease in the cellular spacing could be attributed to the TEMC effect. The formation of the ring-like solidification structure is attributed to the TEMC caused by the interaction between the magnetic field and the radial temperature gradient. Owing to the protruding isothermal surfaces, there is an unavoidable radial temperature gradient. Thus, the TE current will be generated along the radial direction as shown in Fig. 10a. Under the magnetic field, an azimuthal Lorentz force perpendicular to both the radial and axial direction forms. This force causes the liquid between cellular crystals generally to flow along the azimuthal direction. Thus, the liquid between cellular crystal boundaries in the radial direction will flow towards the

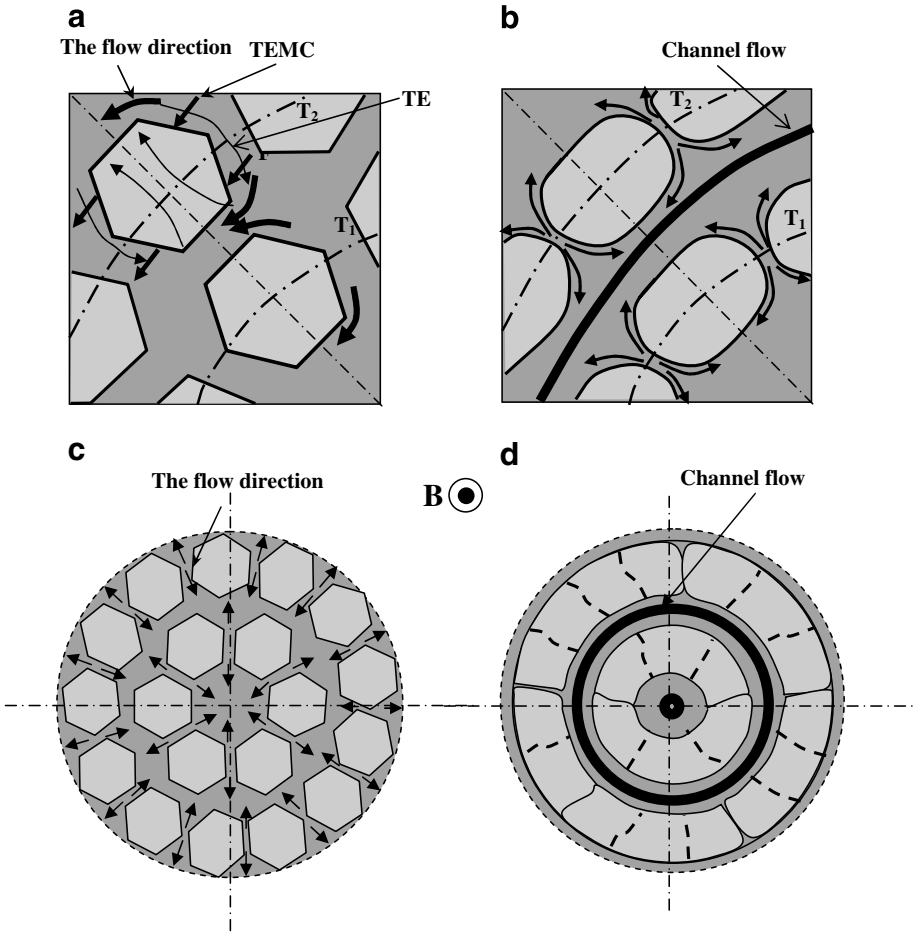

Fig. 10. Schematic views of the ring-like channel flow occurrence: (a) TEMC effects along the radius direction; (b) the amalgamation of neighboring cells and the formation of channel flow; (c) the channel flow caused by THMC effects; (d) the formation of ring-like structure and ring-like channel flow.

cellular boundaries perpendicular to the radial direction (Fig. 10a and c) and increase the amount of liquid here. As a result, the ring-like channel flow shown in Fig. 10d will be produced. This channel flow encourages the cells to merge along the radial direction on the one hand and increases the liquid between the cell boundaries along the azimuthal direction on the other. Consequently, the ring-like structure forms.

5. Conclusions

1. The TEMC has been evaluated for different scales, and the results show that the effect of the magnetic field is different for different scales. The smaller the structure, the larger the magnetic field needed to modify the structure by the TE effect. Moreover, the TE torque on the cell is proposed as another new factor, in addition to the magnetic force, that causes breakage of the dendrite/cell.
2. The effect of a 10 T magnetic field on the interface shape has been investigated, and the results indicate that this field results in a flattened interface shape. This is attributed to the flow being retarded by the field. However, the magnetic field gives an uneven cellular interface shape, which is attributed to the spot and channel segregation caused by the fragmentation of the cell under a higher magnetic field.
3. The effect of the magnetic field on the cell array has been investigated and the results show that the field changes the structure greatly. A lower magnetic field ($B \leqslant 0.5$ T) causes a decrease in the cellular spacing and the formation of a ring-like structure in the mushy zone, which is attributed to TEMC. However, a higher magnetic field ($B \geqslant 1$ T) causes the cell to break, and this is attributed to the stress caused by the torque and the magnetic force.

Acknowledgements

This work is supported by the European Space Agency through the IMPRESS project and the Natural Science Foundation of China (Nos. 50234020, 50225416 and 59871026). One of the authors (L.X.) is also grateful for an Egide/Eiffel Doctorate Scholarship. The authors are indebted to Professor R. Moreau and Professor T. Duffar, CNRS, Grenoble, for helpful and fruitful discussions.

References

[1] Carruthers JR. In: Wilcox WR, Lefever RA, editors. Preparation and properties of solid state materials, vol. 3. New York: Marcel Dekker; 1997. p. 1.
[2] Matheson DH, Wargo MS, Motakef D, Carlson J, Nakos A. J Cryst Growth 1987;85:557.
[3] Robertson GD, O'Connor D. J Cryst Growth 1986;76:100.
[4] Boettinger WJ, Biancaniello F, Coriell S. Met Trans A 1981;12A:321.
[5] Tewari SN, Shah R, Song H. Met Mater Trans A 1994;25A:1535.
[6] Alboussiere T, Moreau R, Compte D. Rendu de l'Acad Sci 1991;313:749.
[7] Laskar O. Thesis, INPG, France; 1994.
[8] Lehmann P, Moreau R, Camel D, Bolcato R. Acta Mater 1998;46:4067.
[9] Yesilyurt S, Vujisic L, Motalkef S, Szofran FR, Volz MP. J Cryst Growth 1999;207:278.
[10] Khine YY, Walker JS. J Cryst Growth 1998;183:150.
[11] Li X, Fautrelle Y, Ren ZM. Acta Mater 2006.
[12] Flemings MC. Solidification processing. New York: McGraw-Hill; 1974. p. 117.

[A3] Xi Li, Yves Fautrelle, Zhongming Ren

Influence of a high magnetic field on the columnar dendrite growth during the directional solidification,

Acta Materialia 55(2007) 5333-5347.

Available online at www.sciencedirect.com
ScienceDirect
Acta Materialia 55 (2007) 5333–5347
Acta MATERIALIA
www.elsevier.com/locate/actamat

Influence of a high magnetic field on columnar dendrite growth during directional solidification

Xi Li [a,b,*], Yves Fautrelle [b], Zhongming Ren [a]

[a] Department of Material Science and Engineering, Shanghai University, Shanghai 200072, China
[b] EPM-Madylam/CNRS, ENSHMG BP 38402, St. Martin d'Heres Cedex, France

Received 27 February 2007; received in revised form 21 May 2007; accepted 28 May 2007

Abstract

The influence of a high magnetic field on the growth of MnBi, α-Al and Al_3Ni dendrites in directionally solidified Bi–Mn, Al–Cu and Al–Ni alloys have been investigated. Results indicate that the magnetic field changes the dendrite growth significantly. Indeed, the magnetic field aligns the primary dendrite arm and the effect is different for different dendrites. For the MnBi dendrite, an axial high magnetic field enhanced the growth of the primary dendrite arm along the solidification direction; however, for the α-Al and Al_3Ni dendrites, the magnetic field caused the primary dendrite arm to deviate from the solidification direction. At a lower growth speed, a high magnetic field is capable of causing the occurrence of the columnar-to-equiaxed transition (CET). Moreover, it has also been observed that a high magnetic field affects the growth of the high-order (i.e., secondary and tertiary) dendrite arms of the α-Al dendrite at a higher growth speed; as a consequence, the field enhances the branching of the dendrite and the formation of the (1 1 1)-twin planes. The above results may be attributed to the alignment of the primary dendrite arm under a high magnetic field and the effect of a high magnetic field on crystalline anisotropy during directional solidification.

Keywords: High magnetic field; Columnar dendrite; Directional solidification; Crystalline anisotropy; Columnar-to-equiaxed transition (CET)

1. Introduction

The effect of a steady-state magnetic field applied during the solidification of a metallic alloy is not always well understood. Apart from the convection damping effect in the liquid bulk during the solidification process, which is well investigated, some unexpected results have recently been observed in the presence of a high magnetic field. Youdelis et al. [1] applied a 3.4 T transverse magnetic field to a directionally solidifying Al–Cu alloy, with the result that the effective partition coefficient of the solute decreased with the application of the field. Alboussière et al. [2] and Laskar [3] have found that "freckles" appeared in Sn–40 wt.%Bi and Cu–45 wt.%Ag alloys solidified vertically with 0.6 T horizontal or 1.5 T vertical magnetic fields. They attributed the results to the occurrence of so-called thermoelectromagnetic convection (TEMC). Moreover, the control of aligned or textured structure during solidification by application of a magnetic field has been also investigated widely. Asai [4] found that the primary phase in Al–Si–Fe alloy was aligned with a longer axis perpendicular to the magnetic field direction during solidification. Yasuda et al. [5] and the present authors [6] have studied the alignment behavior of primary phase MnBi in Bi–Mn alloys under a magnetic field in detail and have found that the *c*-axis of the MnBi crystal (i.e., the easy magnetic axis) was aligned along the magnetic field direction. Textured crystal growth of Bi-2201[7] and Bi (Pb) 2212 [8] has been obtained in a high magnetic field.

All these works have shown that a high static magnetic field exerts a strong influence on solidification and further work is needed to explore this effect. Dendrite growth, as a

* Corresponding author. Address: Department of Material Science and Engineering, Shanghai University, Shanghai 200072, China.
E-mail address: xi@hmg.inpg.fr (X. Li).

1359-6454/$30.00
doi:10.1016/j.actamat.2007.05.036

natural phenomena and one fundamental to the processing materials, is an interesting and important topic for research. However, up to now, little work has been done on the influence of a high static magnetic field on dendrite growth. It is expected that dendrite growth may change its behavior under a high magnetic field and that the field may present new effects on solidification. In our previous work [9], the influence of a high magnetic field on the α-Al primary dendrite arm has been mentioned. The present paper extends this work and investigates experimentally the growth of MnBi, α-Al and Al_3Ni dendrites in directionally solidified Bi–Mn, Al–Cu and Al–Ni alloys under an axial high magnetic field. It was found that the growth behaviors of dendrites under a high magnetic field changed significantly. Indeed, it was observed that the magnetic field was capable of aligning the primary dendrite arm; and for different dendrites, the alignment behaviors under a high magnetic field were different. The solidification behavior of the α-Al dendrite under a magnetic field was investigated in detail. It was found that the columnar-to-equiaxed transition (CET) occurred at a lower growth speed and that the CET was related to the magnetic field intensity and the growth speed. At a moderate growth speed, the field led to deflecting of the growth of the dendrite. At a higher growth speed, the field ($B \leqslant 10$ T) increased the spacing of the α-Al primary dendrite arm, although it was not capable of aligning the primary dendrite arm. Moreover, it was also found that the field enhanced the growth of the high-order dendrite arms and the formation of the (1 1 1)-twin plane.

2. Experimental set-up

The Al–4.5 wt.%Cu, Al–12 wt.%Ni and Bi–0.85 wt.%Mn alloys used in this study were prepared with pure substances (4 N) in an induction furnace. The alloys were placed in a high-purity graphite crucible (10 cm diameter), heated to 900°, magnetically stirred for half an hour and poured into a graphite mold to cast samples of diameter 3 mm and length 200 mm. The cast sample was enveloped in a high-purity corundum tube with an inner diameter of 3 mm and a length of 200 mm. The samples were directionally solidified in a Bridgman apparatus at various growth speeds. The experimental apparatus and many experimental details can be

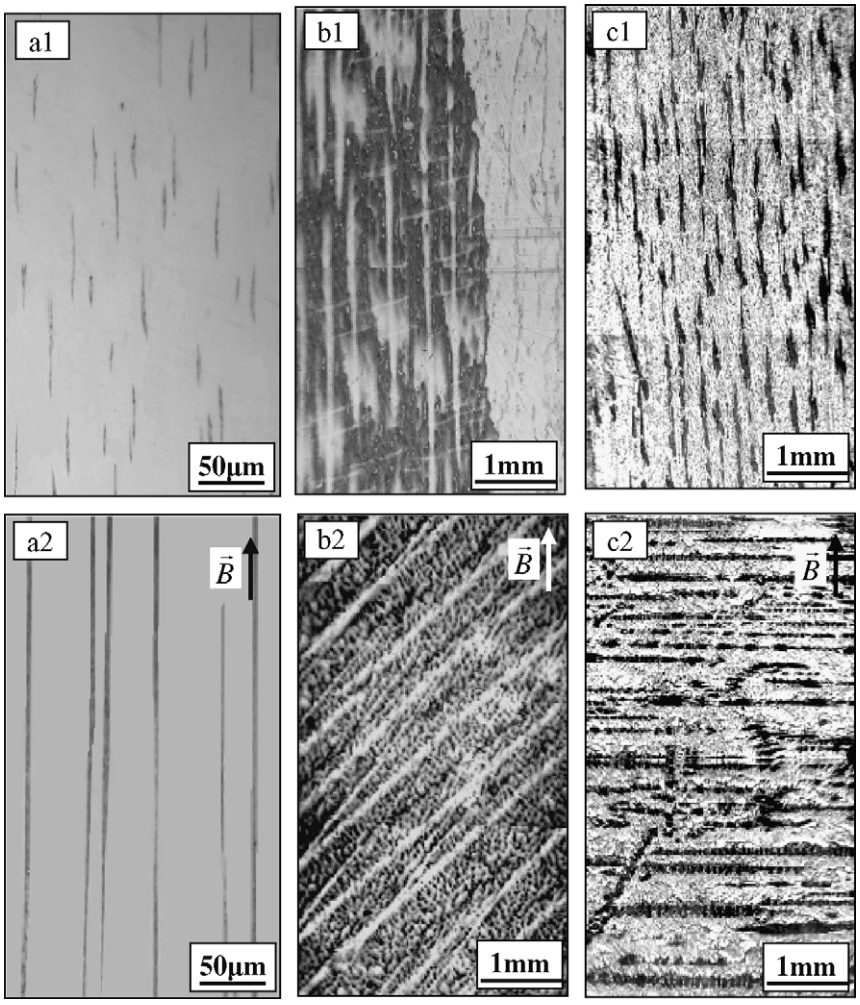

Fig. 1. Influences of a 10 T-magnetic field on the primary dendrite arm during the directional solidification: (a) Bi–0.85 wt.%Mn alloy, (b) Al–4.5 wt.%Cu alloy and (c) Al–12 wt.%Ni alloy. The primary phases in above alloys are MnBi, α-Al and Al3Ni ones, respectively.

found in Ref. [9]. The temperature gradient and the growth speed were adjusted to form dendritic regions. In order to study the magnetic anisotropy of MnBi and Al_3Ni crystals, Bi–3 wt.%Mn and Al–12 wt.%Ni alloys were solidified from the melted state both without and with a high magnetic field. The microstructures of the sample were characterized by optical microscopy, scanning electron microscopy (SEM) and X-ray diffraction (XRD).

3. Results

3.1. Influence of a high magnetic field on the growth of the primary dendrite arm

Fig. 1 shows the microstructures on the section parallel to the solidification direction (i.e., the magnetic field direction) in directionally solidified Bi–0.85 wt.%Mn hypereutectic,

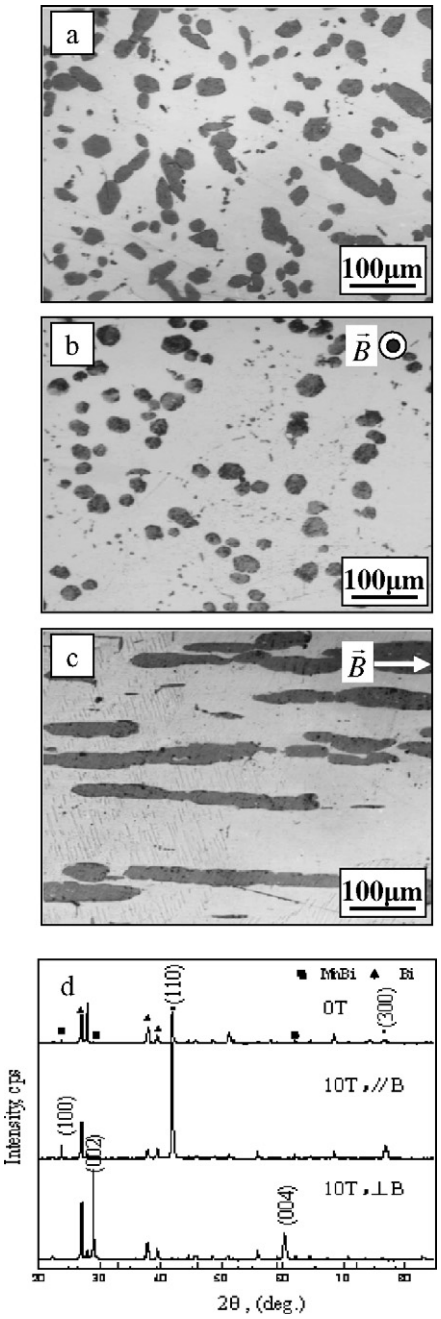

Fig. 2. Microstructures of the Bi–3 wt.%Mn alloy solidified from 300 °C at a cooling rate of 0.3 °C min: (a) without the magnetic field, (b) transverse microstructure under a 10 T-magnetic field, (c) longitudinal microstructure under a 10 T-magnetic field and (d) the corresponding XRD of (a), (b) and (c).

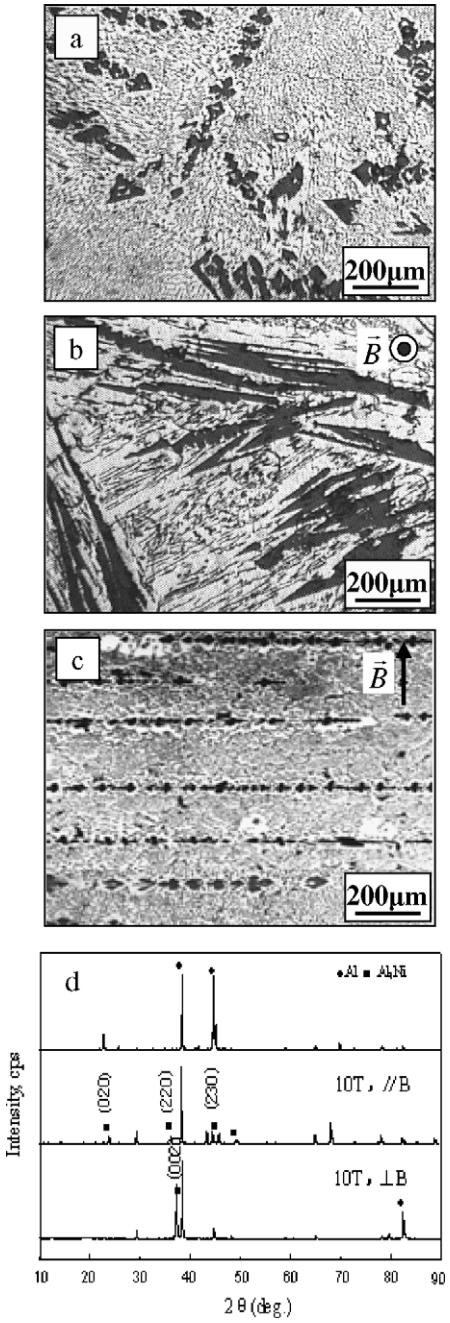

Fig. 3. Microstructures of the Al–12 wt.%Ni alloy solidified from 750 °C by a cooling rate of 8 °C min: (a) without the magnetic field, (b) transverse microstructure under a 10 T-magnetic field, (c) longitudinal microstructure under a 10 T-magnetic field and (d) the corresponding XRD of (a), (b) and (c).

Al–4.5 wt.%Cu hypoeutectic and Al–12 wt.%Ni hypereutectic alloys with and without a 10 T magnetic field. The primary phases in these alloys are MnBi, α-Al and Al_3Ni, respectively. Comparison of the microstructures with and without the magnetic field shows that the field has significantly influenced the growth of the primary dendrite arm. As a consequence, for the Bi–0.85 wt.%Mn alloy directionally solidified at a growth speed of 5 μm/s and a temperature gradient of 50°C/cm (Fig. 1a), the field increased the ratio of length to diameter and made the alignment of the MnBi dendrite more regular. This means that the field has enhanced the growth of the MnBi dendrite along the solidification direction. However, for the Al–4.5 wt.%Cu alloy directionally solidified at a growth speed of 50 μm/s and a temperature gradient of 38°C/cm under the field, the primary dendrite arm was deflected from the solidification direction and aligned at ~45° to the solidification direction (Fig. 1b). For the Al–12 wt.%Ni alloy directionally solidified at a growth speed of 100 μm/s and a temperature gradient of 68°C/cm, the field caused the primary dendrite arm to align perpendicular to the solidification direction (Fig. 1c). The above results indicate that for different dendrites; the influences of the magnetic field on the primary dendrite arm are different.

To study the alignment mechanism of the primary dendrite arm during directional solidification under a high magnetic field, the magnetic anisotropy of the MnBi and Al_3Ni crystals was investigated. For this, the Bi–3 wt.%Mn and Al–12 wt.%Ni hypereutectic alloys were solidified from the melted state under a 10 T magnetic field. Figs. 2 and 3 show the microstructures of the Bi–Mn and Al–Ni alloys and the corresponding XRD patterns, respectively. The black phases in the Bi–3 wt.%Mn and Al–12 wt.%Ni alloys are MnBi and Al_3Ni, respectively. It can be observed from Fig. 2 that the MnBi phase is aligned with a longer axis along the magnetic field direction and further XRD indicates that the ⟨0 0 1⟩-crystal direction of the MnBi crystal orients along the magnetic field direction. Fig. 3 indicates that planes of the Al_3Ni phase are aligned perpendicular to the magnetic field direction and that the ⟨0 0 1⟩-crystal direction orients along the magnetic field direction. These results indicate that the Al_3Ni and MnBi crystals own remarkable magnetic anisotropy. Further, it can be seen that for the MnBi crystal, the easy magnetic axis and the preferred growth direction are same and that for the Al_3Ni crystal, they are different. As the easy magnetic axis and preferred growth direction of a crystal are normally different, we chose to investigate the Al_3Ni and α-Al dendrites in order to elucidate the solidification behavior of dendrites during directional solidification under a magnetic field.

Fig. 4 shows the microstructures of directionally solidified Al–12 wt.%Ni alloy at a growth speed of 100 μm/s under various magnetic field intensities. It can be seen that the microstructure without the magnetic field has the usual

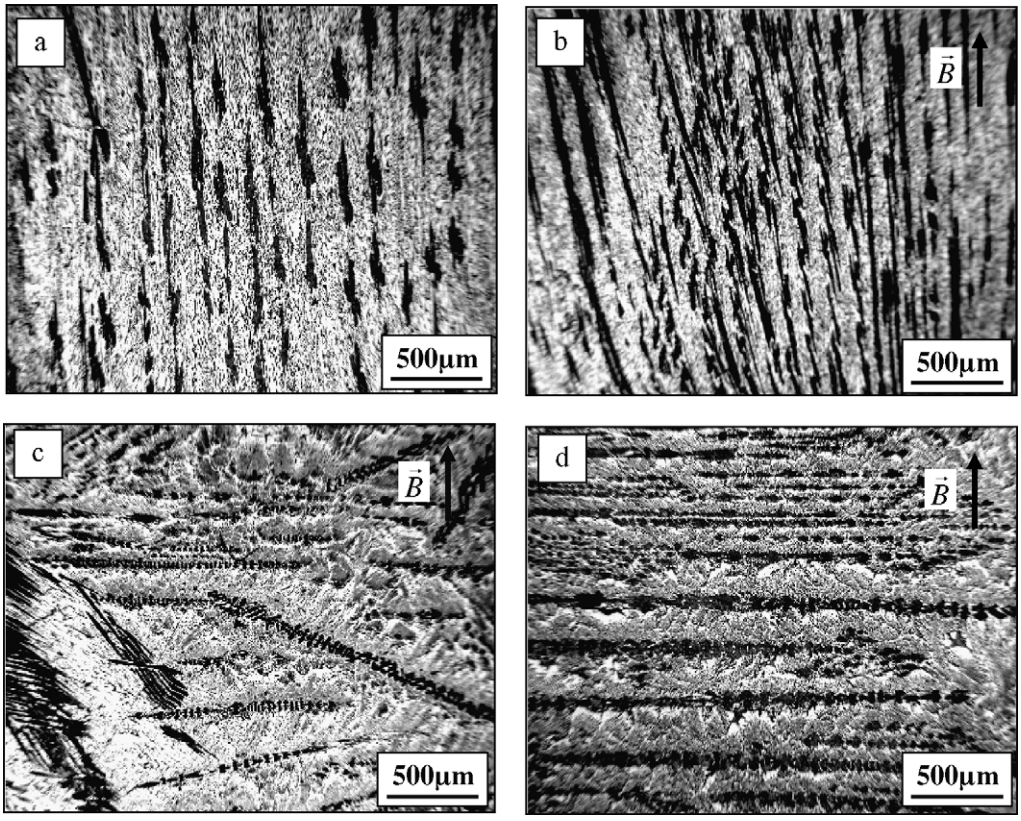

Fig. 4. Microstructures in directionally solidified the Al–12 wt.%Ni alloy at a growth speed of 100 μm/s and a temperature gradient of 68 °C/cm under various magnetic field intensities: (a) 0 T, (b) 2 T, (c) 6 T and (d) 12 T.

regular alignment along the solidification direction. However, with application of the magnetic field, observations of the microstructures indicate that with increase of the magnetic field intensity, the primary dendrite arm gradually deviates from the solidification direction. When the magnetic field intensity increases to 12 T, the primary dendrite arm forms planes perpendicular to the solidification direction (i.e., the magnetic field direction). Moreover, it can be seen that the alignment behavior of the Al_3Ni dendrite during directional solidification under a magnetic field is similar to that in the case of the volume solidification. Therefore, the alignment mechanism should be attributed to the difference between the easy magnetic axis and the preferred direction.

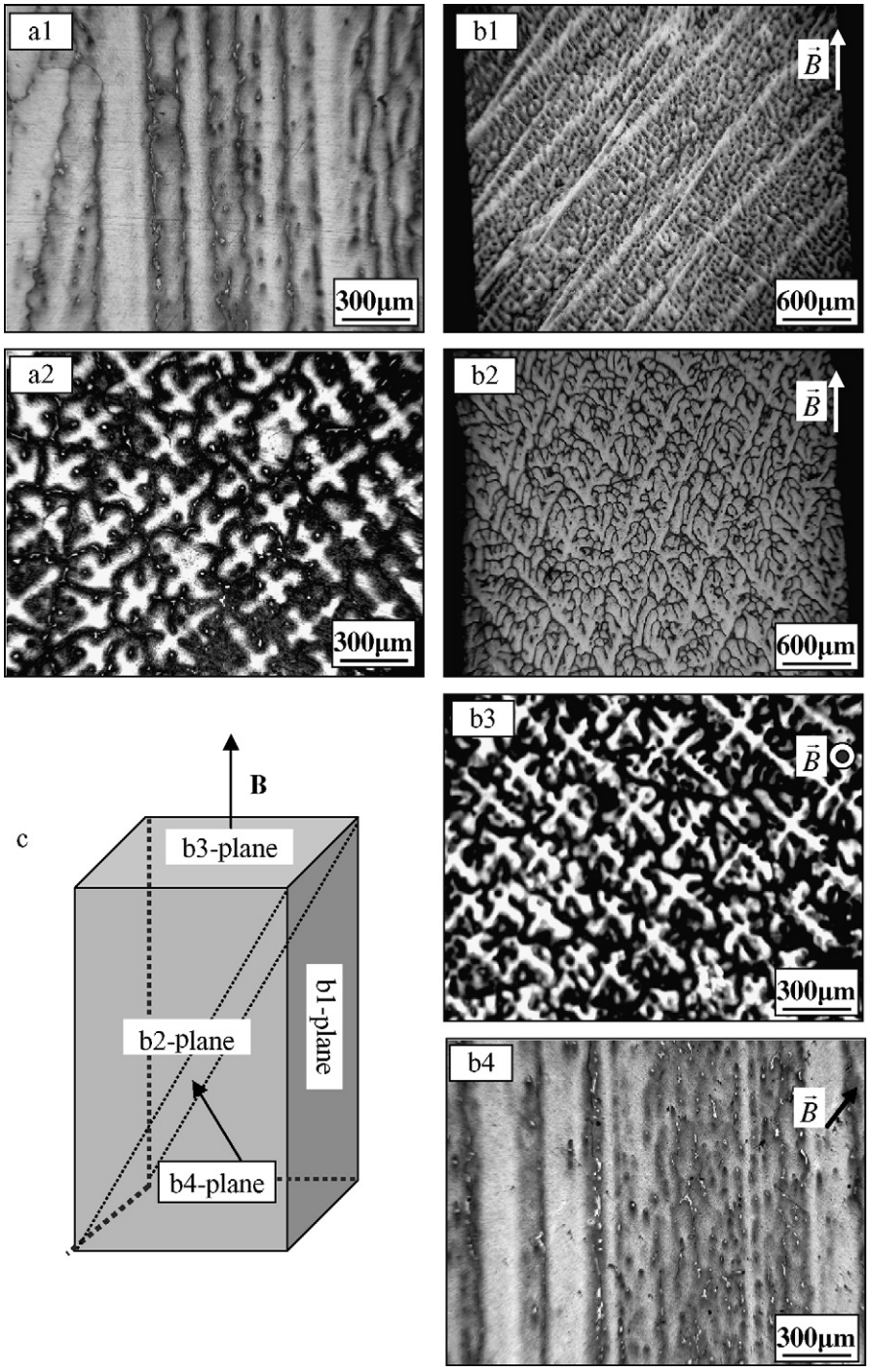

Fig. 5. Microstructures in directionally solidified the Al–4.5 wt.%Cu alloy at a growth speed of 50 μm/s and a temperature gradient of 38 °C/cm (a) without and (b) with a 10 T-magnetic field: (a1) Longitudinal microstructure; (a2) transverse microstructure; (b1) longitudinal microstructure; (b2) longitudinal microstructure; (b3) transverse microstructure; (b4) microstructure along the direction angled 45° with the solidification direction and (c) schematic view of incising sample.

To investigate in detail the alignment mechanism of the α-Al dendrite during directional solidification under a magnetic field, the sample in Fig. 1b was observed three-dimensionally by cutting the sample as shown in Fig. 5c. First of all, the deflecting structure (Fig. 5b1) was found successfully on a longitudinal section parallel to the magnetic field direction (b1 plane in Fig. 5c). Then, on another longitudinal section perpendicular to the previous one (b2 plane in Fig. 5c), a gridding structure (Fig. 5b2) appears; and a regular aligned structure (Fig. 5b4) was found on the section along a 45° angle to the solidification direction (b4 plane in Fig. 5c). Further, the magnified structure in Fig. 5 was observed and its microstructure is shown in Fig. 6. From Figs. 5 and 6, it can be deduced that the gridding structure appearing on the longitudinal section should consist of the secondary and tertiary dendrite arms. Therefore, the dendrite should align as shown in Fig. 6d. Moreover, comparison of the microstructures with and without the magnetic field (Fig. 6b and a) indicates that the magnetic field has enhanced the growth of the secondary and tertiary dendrite arms. Further, the microstructures close to the liquid–solid interface on the two inter-perpendicular longitudinal sections of the above sample (Fig. 7a and b) were investigated and this revealed that the gridding and deflecting structures grow regularly and stably. This implies that the dendrite may grow as shown in Fig. 7c; i.e., at the beginning of the solidification, the dendrite is aligned with the easy magnetic axis along the magnetic field direction (i.e., the solidification direction; Fig. 7c2) and subsequently the dendrites grow along the preferred growth direction (Fig. 7c3).

3.2. The CET under a high magnetic field

Figs. 8 and 9 show the microstructures close to the solid–liquid interface and below the eutectic isotherm in directionally solidified Al–4.5 wt.%Cu alloy with a temperature gradient of 62.8°C/cm at lower growth speeds of 5 and 10 μm/s, respectively. It can be seen that the field has caused the occurrence of the CET. To investigate the mechanism of formation of the CET, a 1 T magnetic field was applied for a certain time during the directional solidification process when the sample had grown 60 mm at a growth speed of 5 μm/s and a temperature gradient of 62.8°C/cm with no applied magnetic field. Fig. 10a–c show the quenched interface after the application of the magnetic field for 3, 6 and 9 min, respectively. It can be seen that with increasing time of application of the magnetic field, the columnar dendrites gradually tilt and become equiaxed grains. Further, the influence of the magnetic field on the remaining interface was also investigated. Fig. 11a and b show the structure close to the remaining interface, respectively with and without a 10 T magnetic field applied for 30 min after the sample had grown 60 mm in the case of no field at a growth speed of 10 μm/s and a temperature gradient of 62.8°C/cm. It can be seen that the remaining interface in the case of no magnetic field is merged. Never-

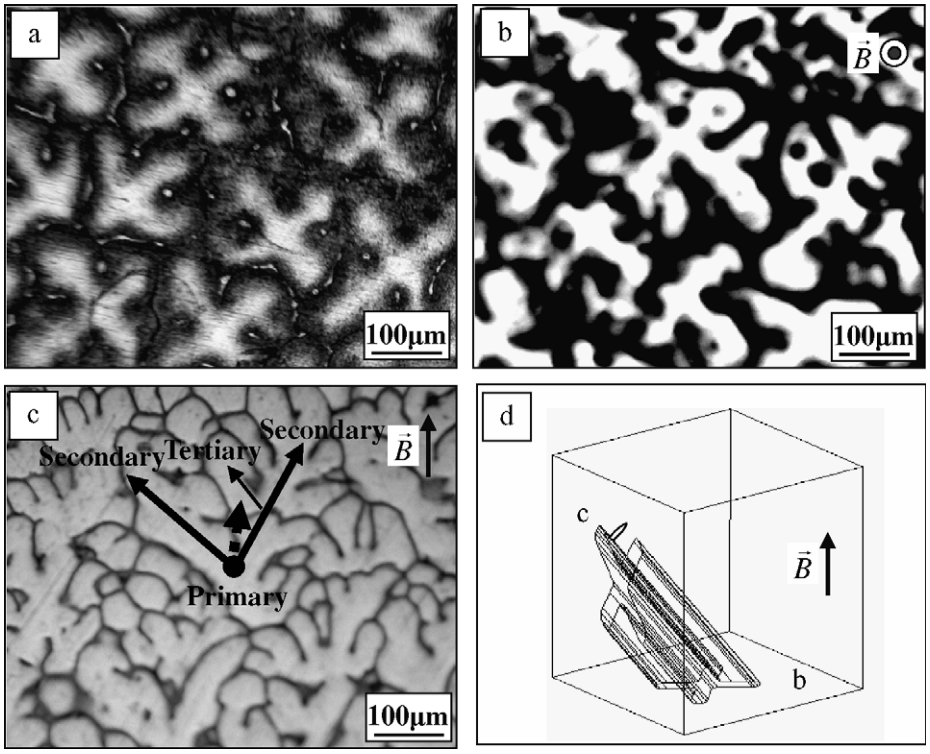

Fig. 6. The magnified microstructure in Fig. 5 and schematic illustration of the α-Al dendrite alignment under the magnetic field: (a) transverse microstructure without the magnetic field, (b) transverse microstructure with a 10 T-magnetic field, (c) longitudinal microstructure with a 10 T-magnetic field and (d) schematic illustration of the dendrite alignment *e* under the magnetic field.

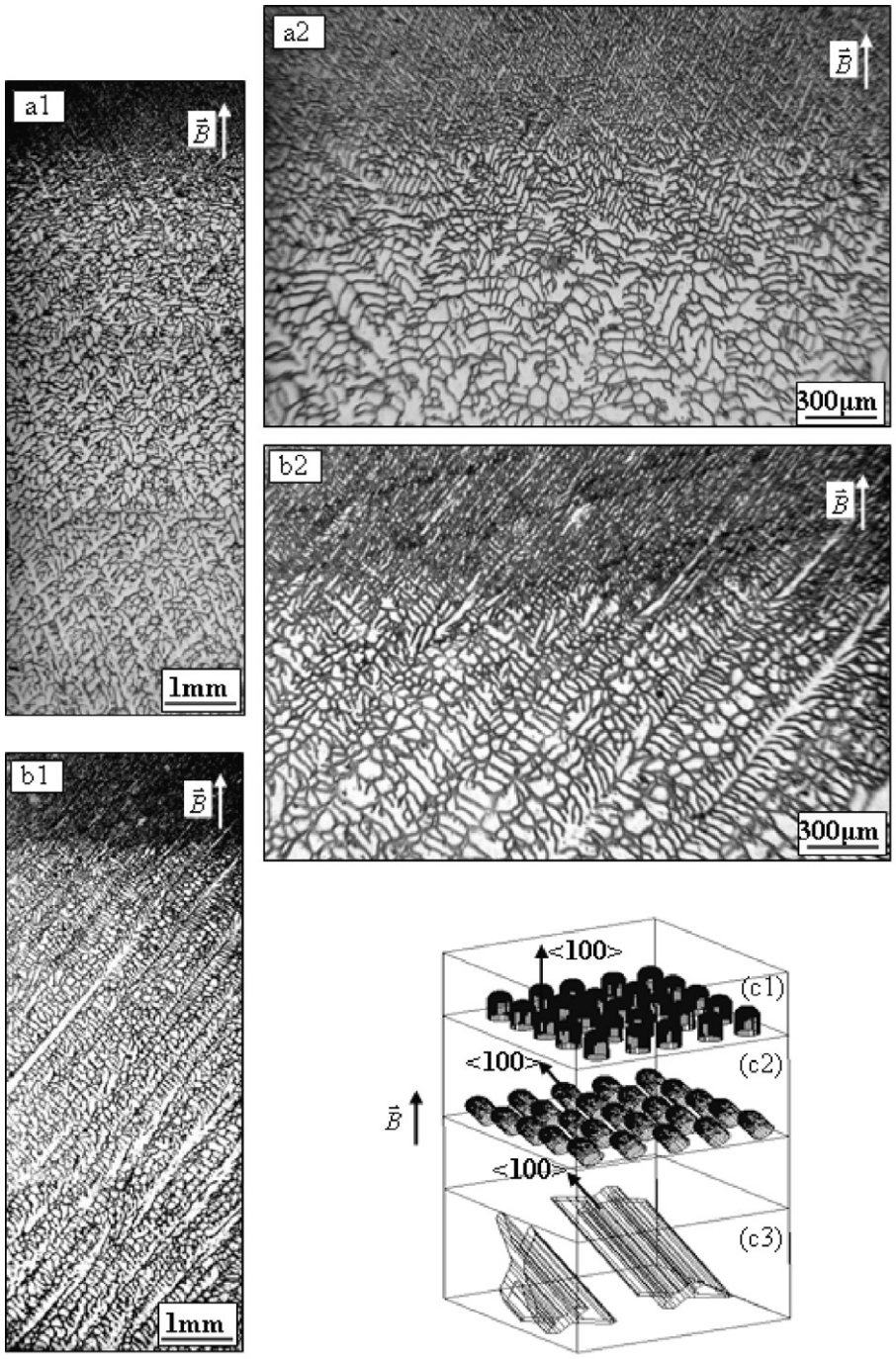

Fig. 7. The liquid/solid interface and schematic illustration in directionally solidified the Al–4.5 wt.%Cu alloy: (a) the liquid/solid interface of the gridding structure in Fig. 5, (b) the liquid/solid interface of the deflecting structure in Fig. 5 and (c) schematic illustration of the α-Al dendrites growth under the magnetic field.

theless, the remaining interface under the magnetic field is not merged or broken. The amalgamation of the interface remaining in the case of no field should be attributed to natural convection. Since a 10 T magnetic field is enough to damp the flow [10], the amalgamation of the interface remaining under the field does not occur. However, note that a 10 T magnetic field can not break or deflect the dendrite. This means that the CET under a magnetic field should occur during the growth process. To investigate this further, we studied the magnified microstructure close to the solid–liquid interface in Fig. 10. Our observation shows that the microstructures close to the solid–liquid interface (Fig. 12a) without the magnetic field are small dendrites in front of the cell. However, with the application of a 1 T magnetic field for 3 min during the growth process, some small dendrites in front of the cell disappear and are replaced by the equiaxed grains (Fig. 12b). As the applied time of the magnetic field increases, equiaxed

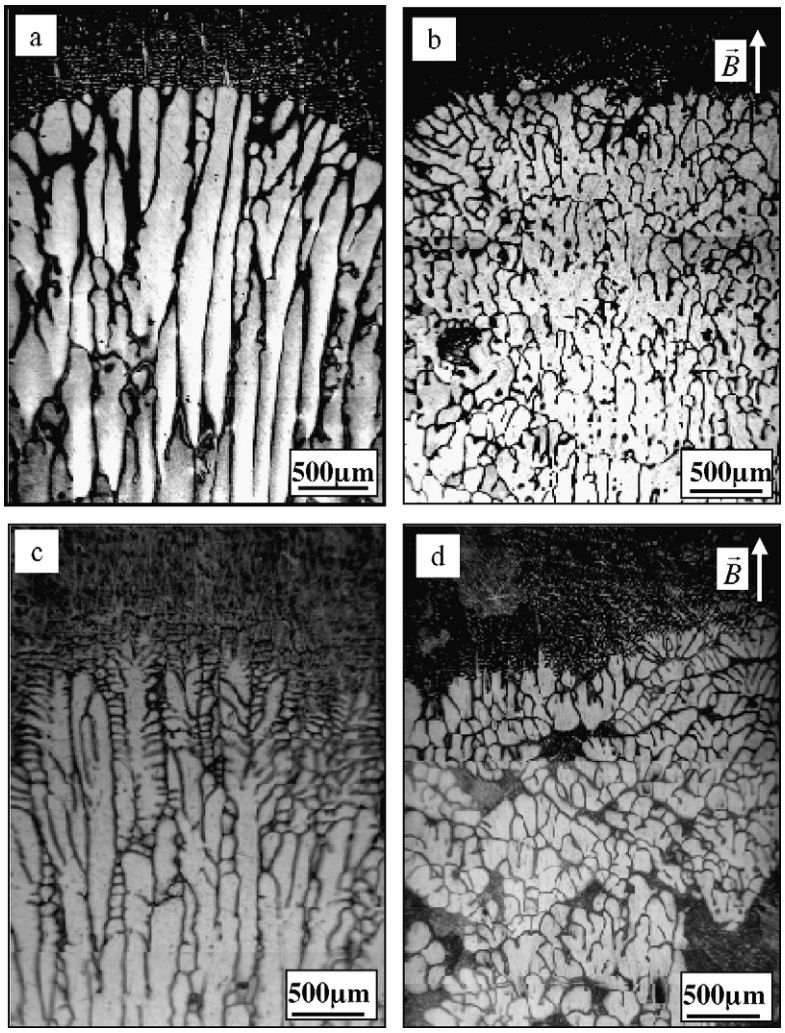

Fig. 8. The columnar-to-equiaxed transition (CET) close to the liquid/solid interface in directionally solidified the Al–4.5 wt.%Cu alloy at a temperature gradient of 62.8°C/cm and a lower growth speed: (a) 5 μm/s, 0 T, (b) 5 μm/s, 10 T, (c) 10 μm/s, 0 T and (d)10 μm/s, 10 T.

grains grow up and increase and then the CET occurs. These experimental results indicate that the occurrence of the CET under the magnetic field should be attributed to the enhancement of equiaxed grains at the interface during the growth process.

The influence of magnetic field intensity and growth speed on the CET of the α-Al dendrite was investigated. Fig. 13 shows the macrostructures on the transverse section of the samples directionally solidified at various growth speeds under a 6 T magnetic field. It can be seen that at 20 μm/s the dendrites disappear on the entire sample. Nevertheless, at 30 μm/s dendrites exist on some regions of the sample. When the growth speed increases to 50 μm/s, the dendrites with larger dendrite spacing exist on the entire sample. Fig. 14 indicates the macrostructure directionally solidified at 20 μm/s under various magnetic field intensities. It can be seen that with the increase of the magnetic field intensity, the dendrites gradually disappear on the entire sample. The above results indicate that the CET during directional solidification under a magnetic field is related to the magnetic field intensity and the growth speed, and that with an increase of magnetic field intensity and a decrease of the growth speed, the CET will occur. The CET solidified at a 62.8°C/cm temperature gradient as a function of the magnetic field intensity and the growth speed was investigated; the result is shown in Fig. 15.

3.3. Influence of a high magnetic field on the growth of the high-order dendrite arm

The microstructure solidified at 50 μm/s in above experiment indicates that the magnetic field has enhanced the growth of the secondary and tertiary dendrite arms. Nevertheless, owing to the deflection of the primary dendrite arm from the solidification direction, the temperature gradient may affect the growth of the high-order dendrite arms. In Ref. [9], it was mentioned that with increasing growth speed, the influence of the magnetic field on the alignment of the primary dendrite arm becomes weak and that when the growth speed exceeds 100 μm/s, a 10 T magnetic field

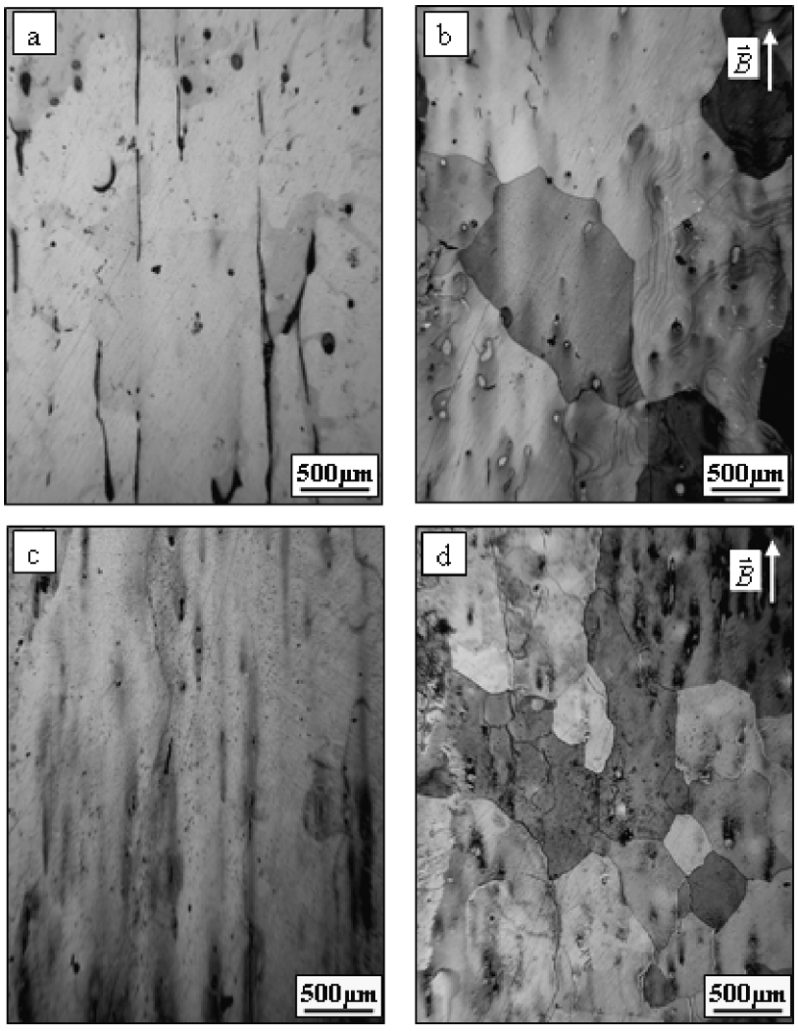

Fig. 9. The columnar-to-equiaxed transition (CET) below the eutectic isotherm of the same sample in Fig. 8: (a) 5 μm/s, 0 T, (b) 5 μm/s, 10 T, (c) 10 μm/s, 0 T and (d) 10 μm/s, 10 T.

hardly affects the alignment of the primary dendrite arm. Therefore, to investigate the influence of the magnetic field on the growth of high-order dendrite arms, the microstructures solidified at a higher growth speed (150, 200 and 500 μm/s) were chosen. Fig. 16 shows the microstructures of the Al–4.5 wt.%Cu alloy solidified at a growth speed of 150 μm/s and a temperature gradient of 62.8°C/cm under various magnetic field intensities. Compared with the microstructure without the magnetic field (Fig. 16a), it can be seen that the application of a 2 T magnetic field has coarsened the primary dendrite arms and enhanced the growth of the secondary and tertiary dendrite arms. Under a 6 T magnetic field, the secondary and tertiary dendrite arms become broken. Further increasing the magnetic field to 10 T, causes the amalgamation of the dendrite. Fig. 17 indicates the microstructures solidified at 200 μm/s without and with a 10 T magnetic field. Comparison of the microstructures without and with the magnetic field shows that the application of a 10 T magnetic field has enhanced the formation of the (1 1 1)-twin planes, besides coarsening the primary arm and enhancing the growth of the high-order dendrite arms. Fig. 18 shows the microstructures solidified at 500 μm/s and reveals that similar phenomena to those at 200 μm/s have occurred. The above experimental results indicate that a high magnetic field influences the growth of the high-order dendrite arms.

4. Discussion

4.1. Influence of a high magnetic field on the growth of the primary dendrite arm

The above experimental results indicate that a high magnetic field aligns the primary dendrite arm. This should be analyzed in terms of the magnetic and growth anisotropy of a crystal. In general, when a magnetic anisotropic grain with a volume V is placed in a magnetic field H, it will be rotated by the magnetic field to its lowest energy state. The

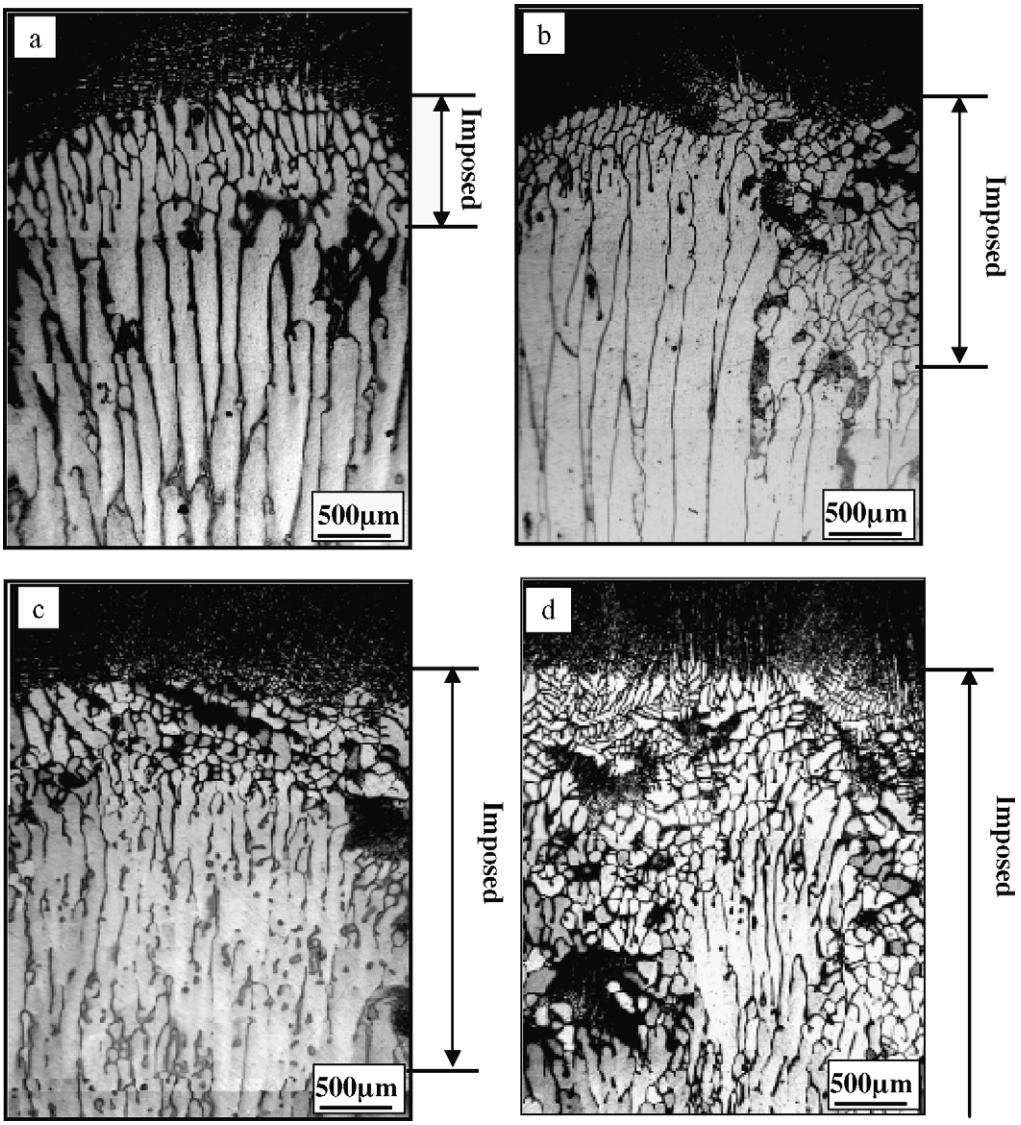

Fig. 10. The developing process of the columnar-to-equiaxed transition (CET) in directionally solidified the Al–4.5 wt.%Cu alloy at a growth speed of 5 μm/s and a temperature gradient of 62.8 °C/cm: (a) application of a 1.0 T-magnetic field for 3 min after growing to 60 mm without the magnetic field, (b) application of a 1.0 T-magnetic field for 6 min after growing to 60 mm without the magnetic field, (c) application of a 1.0 T-magnetic field for 9 min after growing to 60 mm without the magnetic field and (d) application of a 1.0 T-magnetic field during the entire solidification process.

driving force is the anisotropic magnetic energy of the grains. The magnetic energy of a grain can be written as [11]

$$E_{\mathrm{m}}(\theta, H) = -(x_{ab} + \Delta x \cos^2\theta) V H^2/2 \quad (1)$$

where θ is the angle between the magnetic field and the c-axis of the grain, $\Delta x = x_c - x_{ab}$ is the difference in the volume susceptibilities of the grains between the c- and ab-axes. Hence, when $\theta = 0$, we have

$$E_{\mathrm{m}}(0, H) = -V x_c H^2/2 \quad (2)$$

whereas, when $\theta = \pi/2$, we have

$$E_{\mathrm{m}}(\pi/2, H) = -V x_{ab} H^2/2 \quad (3)$$

For a paramagnetic crystal, in the case where $x_c > x_{ab}$, then $E_{\mathrm{m}}(0, H) < E_{\mathrm{m}}(\pi/2, H)$. This means that the magnetic field tends to rotate the grains to $\theta = 0$ (i.e., the c-axis direction), a lower energy state. On the other hand, when $x_c < x_{ab}$ and $E_{\mathrm{m}}(0, H) > E_{\mathrm{m}}(\pi/2, H)$, the magnetic field tends to rotate the grains to $\theta = \pi/2$ (i.e., the ab-axes direction). This indicates that for a paramagnetic crystal, the easy magnetic axis tends to rotate to the magnetic field direction. During the directional growth of a crystal under a magnetic field, a crystalline anisotropic dendrite will grow along the preferred growth direction on the one hand (Fig. 7c1), and the magnetic field tends to rotate the easy magnetic axis to the magnetic field direction on the other hand (Fig. 7c2). Thus, if the easy magnetic axis of a crystal is the same as its preferred growth direction, the field does not deflect the primary dendrite arm from the solidification direction during directional growth in an axial magnetic field. However, if there is an angle between the easy

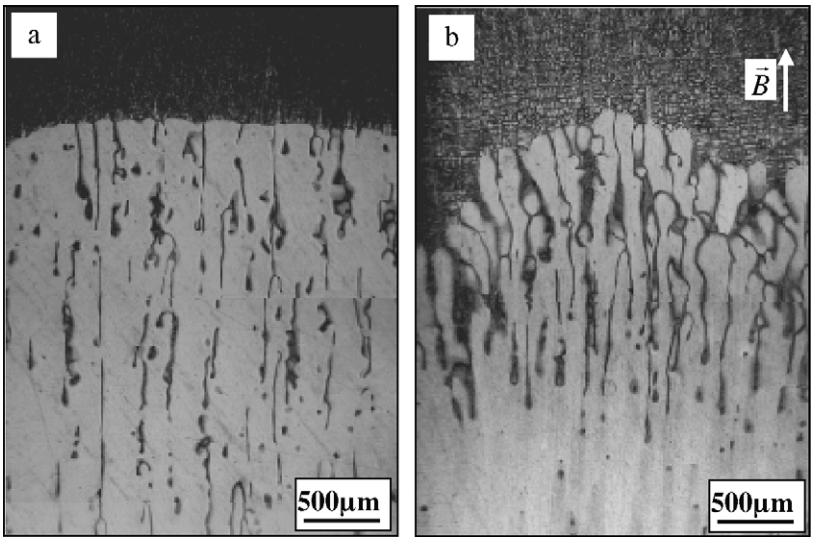

Fig. 11. Effect of a high magnetic field on the staying liquid/solid interface: (a) the quenched liquid/solid interface staying for 30 min after growing 60 mm at 10 μm/s, (b) the quenched liquid/solid interface staying for 30 min in a 10 T-magnetic field after growing 60 mm at 10 μm/s without the magnetic field.

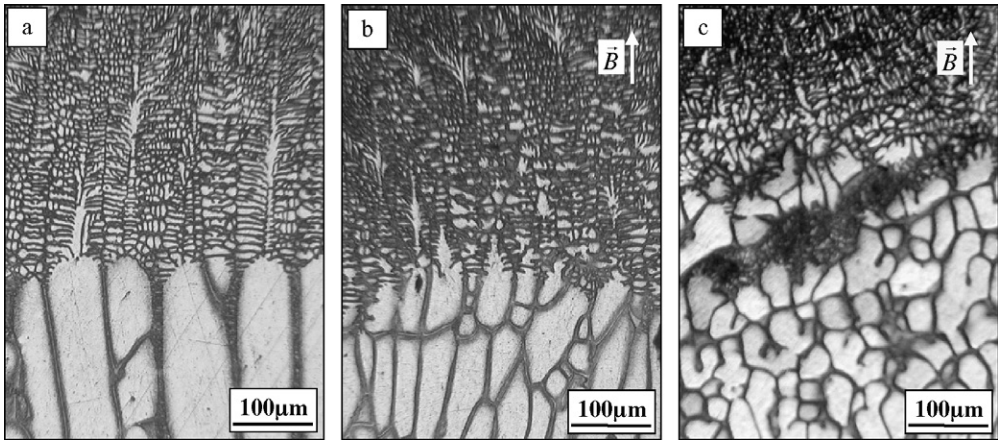

Fig. 12. The magnified microstructures close to the liquid/solid interface in Fig. 8a and 10a and c: (a) microstructure directionally solidified in the case of no field, (b) application of a 1.0 T-magnetic field for 3 min after growing 60 mm without magnetic field and (c) application of a 1.0 T-magnetic field for 9 min after growing 60 mm without magnetic field.

magnetization axis and the preferred growth direction of a crystal, the axial magnetic field tends to rotate the easy magnetization axis to the magnetic field direction; as a consequence, the preferred growth direction will deviate from the solidification direction. In particular, if the easy magnetization axis of a crystal is perpendicular to its preferred growth direction, the axial magnetic field will tend to turn the preferred growth direction to the plane perpendicular to the solidification direction.

For the MnBi crystal, as its ⟨0 0 1⟩-crystal direction is not only an easy magnetization axis but also a preferred growth direction, an axial magnetic field does not deflect the preferred growth direction (i.e., the primary dendrite arm) from the solidification direction during directional solidification. However, for the Al crystal, as its ⟨0 0 1⟩- and ⟨1 1 1⟩-crystal directions are the preferred growth direction and the easy magnetization axis, respectively; the α-Al dendrites will orientate with the ⟨1 1 1⟩-crystal direction along the magnetic field direction (i.e., the solidification direction). As a consequence, the primary dendrite arm will be deflected from the solidification direction. The orientation of the Al_3Ni dendrite in this experiment is because the preferred growth direction is perpendicular to the easy magnetic axis. Thus, the magnetic field will align the Al_3Ni dendrite with the preferred growth direction (i.e., the primary dendrite arm) perpendicular to the magnetic field and form the planes. Therefore, it may be concluded that the alignment behavior of the primary dendrite arm during directional solidification under a magnetic field depends on the crystal intrinsic property (i.e., the relation between the growth and magnetic anisotropy of the dendrite) and the extrinsic condition (i.e., the relation between the solidification direction and the applied magnetic field direction). This means that application of a magnetic field may control

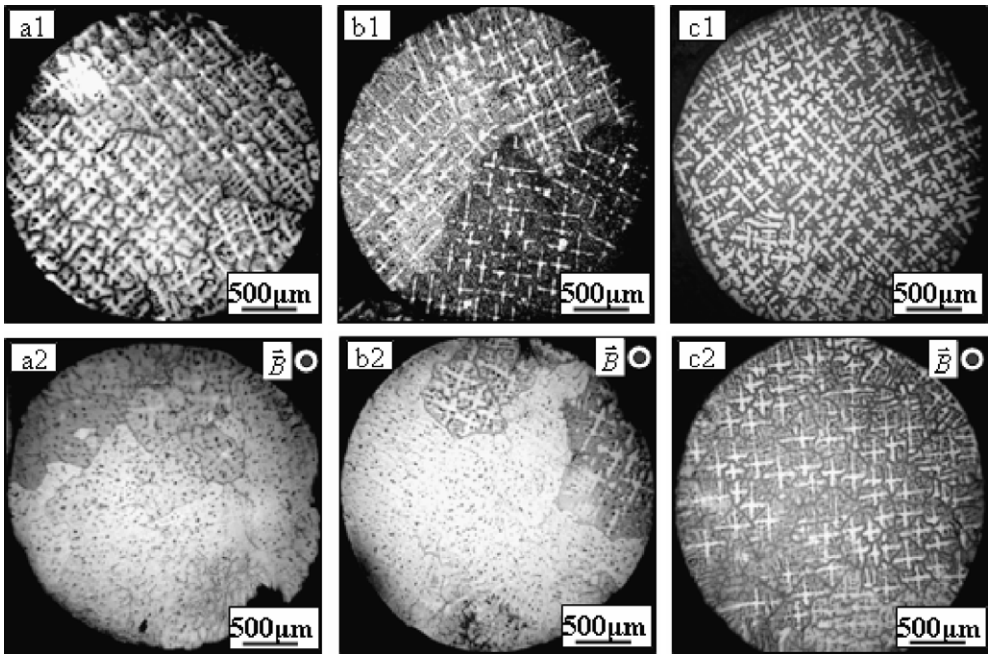

Fig. 13. Effect of a 6 T-magnetic field on dendrites for various growth speeds in directionally solidified the Al–4.5 wt.%Cu alloy at a temperature gradient of 62.8°C/cm and a lower growth speed: (a) 20 μm/s, (b) 30 μm/s and (c) 50 μm/s.

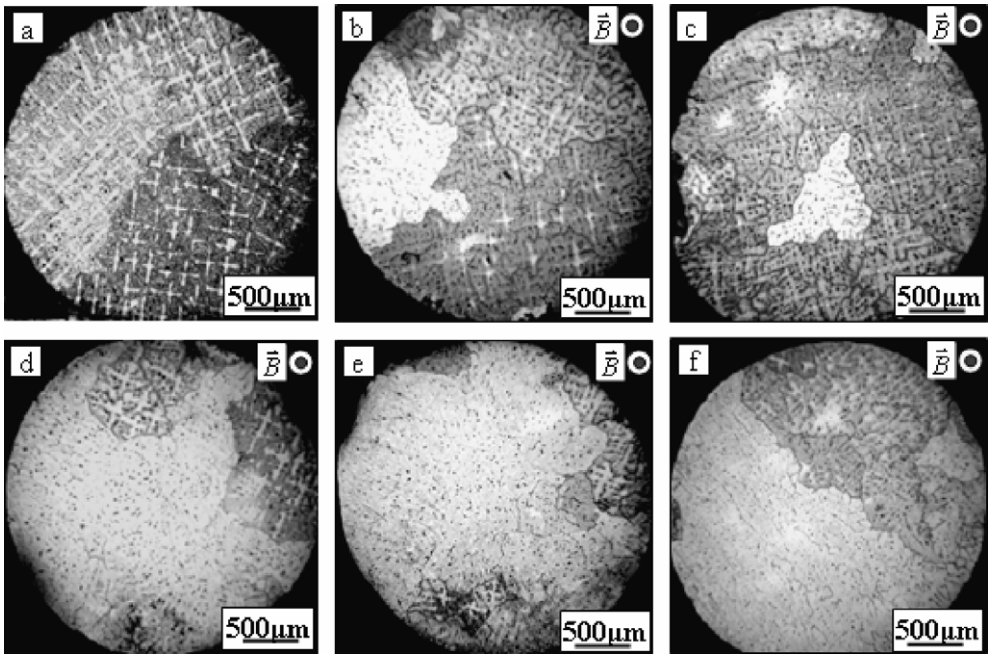

Fig. 14. The columnar-to-equiaxed transition as a function of the magnetic field intensity in directionally solidified the Al–4.5 wt.%Cu alloy at a growth speed of 20 μm/s and a temperature gradient of 62.8°C/cm: (a) 0 T, (b) 2 T, (c) 4 T, (d) 6 T, (e) 8 T and (f) 10 T.

the direction of the primary dendrite arm and tailor a special alignment structure during directional solidification.

Moreover, Ref. [9] mentions that a high magnetic field enlarges the average primary dendrite arm spacing of the α-Al dendrite at a higher growth speed. The enlargement of the primary dendrite arm spacing is attributable to the effect of the magnetic field on competitive growth during the selecting crystal process. Since the field is capable of causing the α-Al dendrites to deviate from the solidification direction, some small dendrites may not survive during competitive growth; as a consequence, the average primary dendrite arm spacing increases. The effect of crystallographic orientation on primary dendrite arm spacing was investigated through simulations in Ref. [12] and it was found that for columnar dendrites with slight misalignment, the average primary dendrite arm spacing increases.

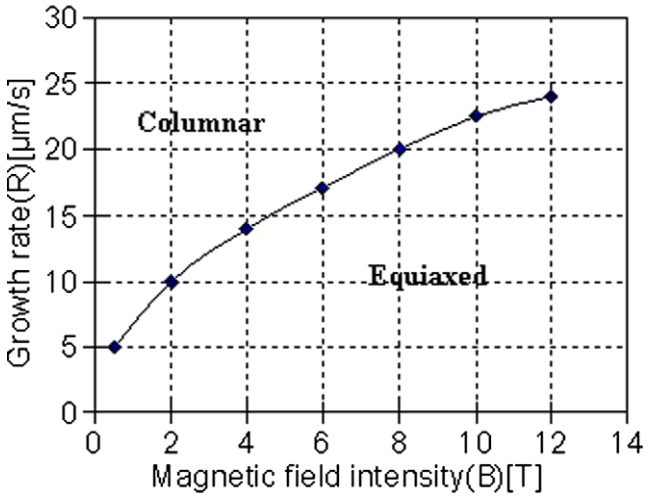

Fig. 15. The columnar-to-equiaxed transition (CET) of the Al–4.5 wt.%Cu alloy directionally solidified at a temperature gradient of 62.8°C/cm as a function of the magnetic field intensity and the growth speed.

Further, due to the larger average spacing, undercooling in the grooves between these primaries increases, causing more misoriented "islands" to form and this will further increase the primary dendrite arm spacing. Therefore, it is reasonable to attribute the enlargement of the primary dendrite arm spacing to the misalignment caused by the magnetic field.

4.2. CET under a magnetic field

The above experimental result shows that the CET occurs during directional solidification at a low growth speed under a high magnetic field. The CET has been investigated for many years and numerous mechanisms have been proposed. However, little research has been done on the CET caused by a high magnetic field during directional solidification. In early 1984, Hunt [13] developed the first analytical model to predict the CET, based on the potential for equiaxed grains to nucleate in the constitutionally undercooled region ahead of the columnar front. He assumed that if the volume fraction of equiaxed grains exceeded 0.49, then the columnar dendrites will be blocked and the CET will occur. Although the model was updated by later work [14–17], it is still reasonable to suppose that the increase of the equiaxed grains blocks the growth of the columnar dendrites. The above experimental results have shown that equiaxed grains increase at the solid–liquid interface. Thus the growth of some dendrites is blocked and the equiaxed grains germinate. With increasing applied time of the magnetic field, the volume fraction of equiaxed grains increases at the solid–liquid interface. According to the Hunt model, when the volume fraction of equiaxed grains exceeds a certain value, the columnar dendrites will be blocked and then the CET occurs. Moreover, it is easy to understand that at a lower growth speed and higher magnetic field intensity, the operating time of the magnetic

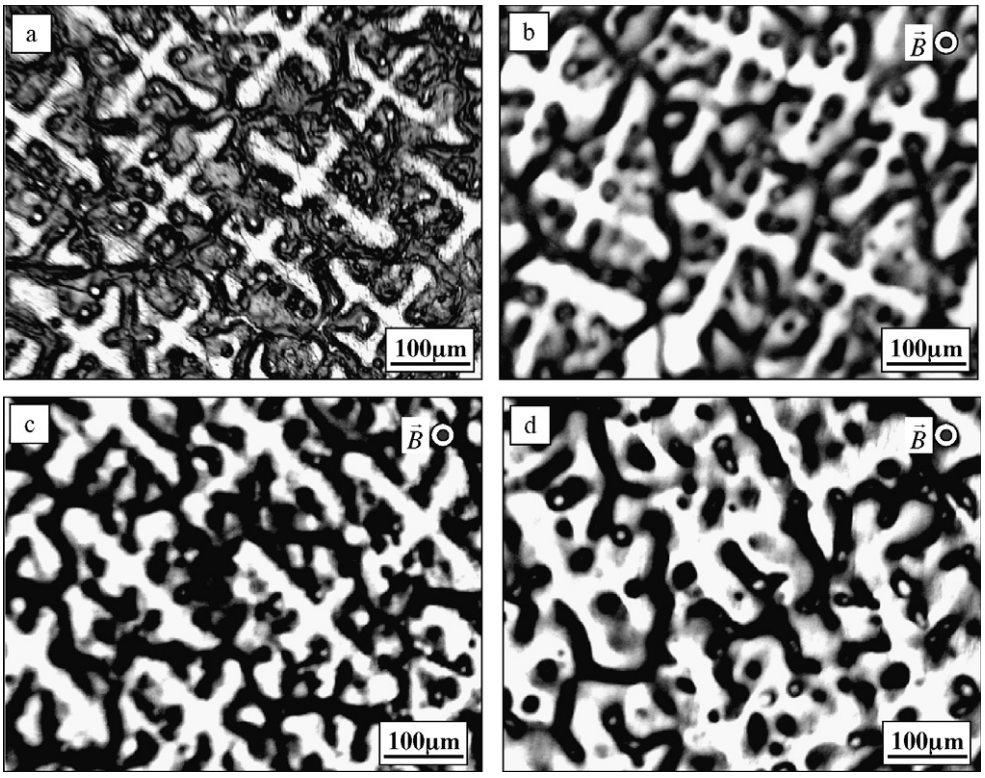

Fig. 16. Microstructures of the Al–4.5 wt.%Cu alloy directionally solidified at 150 μm/s and a temperature gradient of 62.8°C/cm under various magnetic field intensities: (a) 0 T, (b) 2 T, (c) 6 T and (d) 10 T.

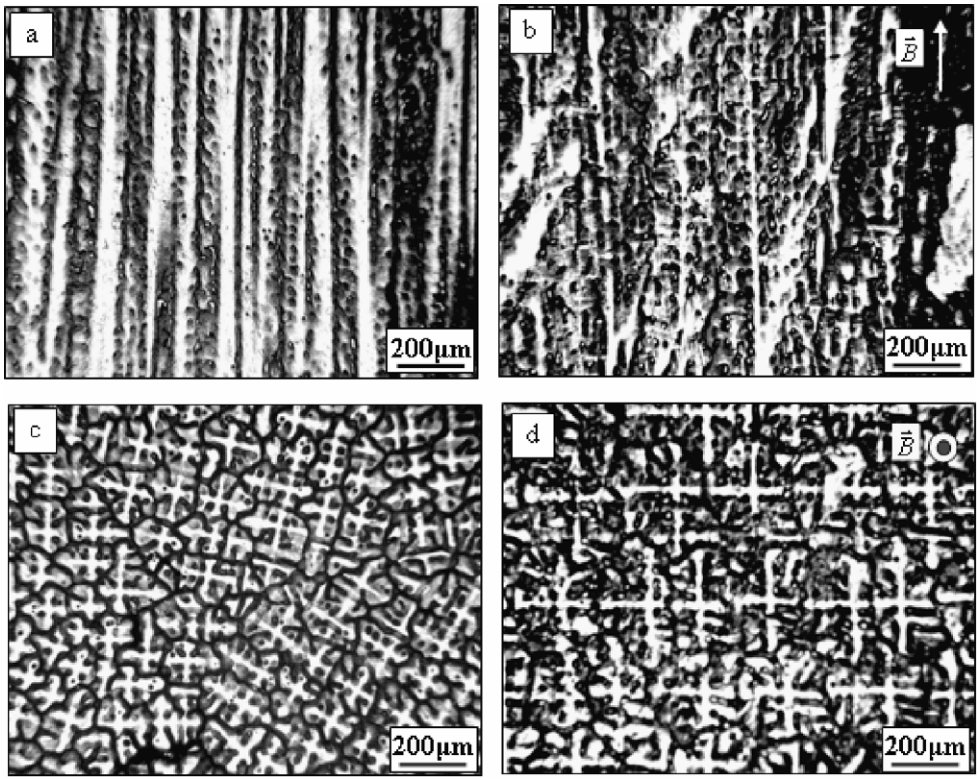

Fig. 17. Microstructures of the Al–4.5 wt.%Cu alloy directionally solidified at a growth speed of 200 μm/s and a temperature gradient of 62.8°C/cm with and without a 10 T-magnetic field: (a) longitudinal microstructure, (b) longitudinal microstructure, (c) transverse microstructure and (d) transverse microstructure.

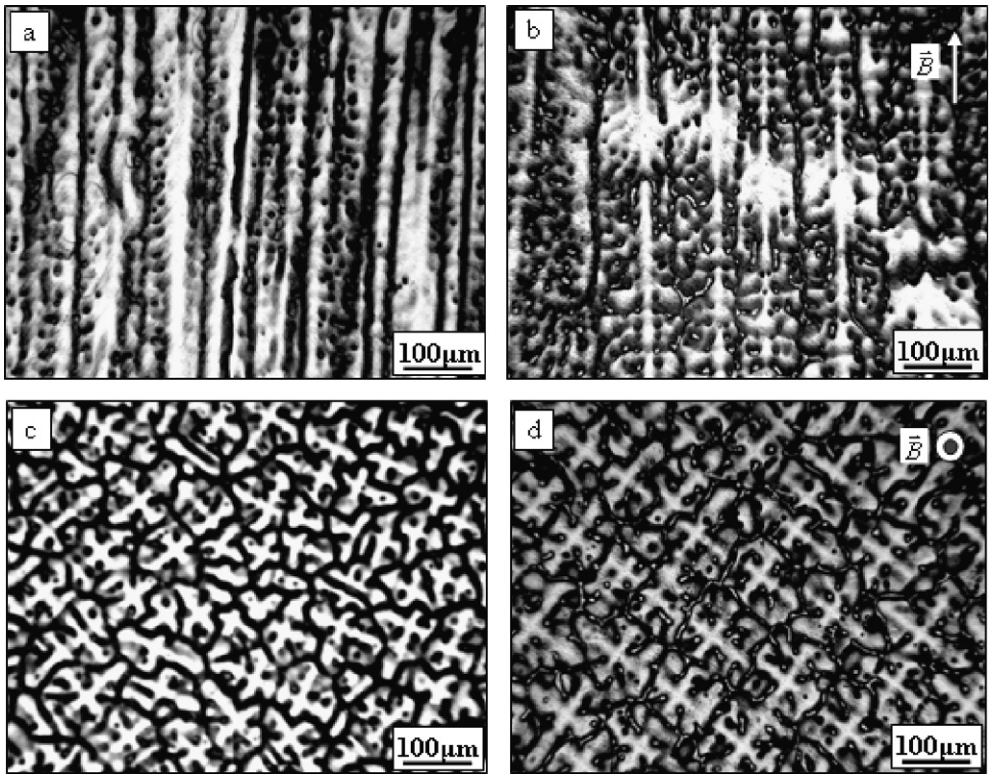

Fig. 18. Microstructures of the Al–4.5 wt.%Cu alloy directionally solidified at a growth speed of 500 μm/s and a temperature gradient of 62.8°C/cm with and without a 10 T-magnetic field: (a) longitudinal microstructure, (b) longitudinal microstructure, (c) transverse microstructure and (d) transverse microstructure.

field on the mushy zone and the operating intensity increase. Therefore, with increase of the magnetic field, the CET occurs even though the growth speed decreases.

4.3. Influence of the magnetic field on the growth of the high-order dendrite arm

The above experimental results show that the magnetic field has affected the growth of high-order dendrite arms. This should be attributed to the change of the crystalline anisotropy under a high magnetic field. During growth of a crystal under a high magnetic field, the magnetic field will magnetize the crystal and lead to a decrease of the crystal plane energy. Owing to the magnetic anisotropy of a crystal, the decrease of crystal plane free energy on various crystal planes is different. It is well known that the crystal plane free energy on closely packed planes is least and the preferred growth direction is generally the axis of the pyramid whose sides are most the closely packed planes with which a pyramid can be formed [18]. If the decrease of the energy on the most closely packed planes caused by the magnetic energy is the largest, the magnetic field will enlarge the growth anisotropy and enhance the growth of the most closely packed planes; thus the growth of dendrites along the preferred growth direction will be enhanced. However, if the decrease of the energy on the most closely packed planes caused by the magnetic energy is not the largest, the magnetic field will reduce the growth anisotropy. Thus the growth of the crystal along other crystal directions will be enhanced; as a consequence, the magnetic field will lead to the branching of the dendrite. Therefore, the enhancement of MnBi dendrite growth along the growth direction should be attributed to the increase of the growth anisotropy under a high magnetic field. The branch of the α-Al dendrite and the (1 1 1)-twin plane growth may be attributed to the decrease of the growth anisotropy under a high magnetic field.

5. Conclusions

The present results may be summarized as follows:

1. A high magnetic field is capable of changing the direction of the primary dendrite arm during directional solidification and the alignment behaviors of the primary dendrite arm are different for different dendrites. This may be attributed to the alignment of the dendrite caused by the magnetic field owing to the crystalline anisotropy.
2. For the dendrite whose easy magnetic axis is different from its preferred growth direction, the field will cause the occurrence of the CET at a lower growth speed during directional solidification under an axial magnetic field. The CET of the α-Al dendrite as a function of magnetic field intensity and growth speed was investigated and it was found that with increasing the magnetic field intensity, the CET occurs even though the growth speed decreases. This may be attributed to enhancement of the formation of equiaxed grains at the interface under the magnetic field.
3. A high magnetic field affects the growth of the dendrite significantly; as a consequence, the field enhances the MnBi primary dendrite arm along the solidification direction, the growth of the high-order dendrite arm and the formation of the twin planes of the α-Al dendrite. This may be attributed to the effect of the magnetic field on the crystalline anisotropy of the Al crystal.

Acknowledgements

This work is supported partly by the European Space Agency through the IMPRESS project and the Natural Science Foundation of China (Grant Nos. 50234020, 50225416 and 59871026). One of the authors (Xi Li) is also grateful for an Egide/Eiffel Doctorate Scholarship. The authors are indebted to Professors R. Moreau and T. Duffar at EPM/CNRS, Grenoble, for helpful and fruitful discussions.

References

[1] Youdelis WV, Dorward RC. Can J Phys 1966;44:139.
[2] Alboussiere T, Moreau R, Camel D. Acad Sci Paris 1991;313:749.
[3] Laskar O, Ph.D. thesis, INPG, France; 1994.
[4] Asai S. Sci. Tech Adv Mater 2000;1:199.
[5] Yasuda H, Ohnala I, Yamamoto Y. Mater Trans JIM 2003;44:2550.
[6] Li X, Ren ZM, Fautrelle Y. Intermetallics 2007;15:845.
[7] Nagata A, Watanabe K, Nojima T, Sugawara K, Kamada S, Lu XY. Phys C: Superconduct Appl 2002;382:27.
[8] Chen W P, Maeda H, Kakimoto K, Zhang XP, Watanabe K, Motokawa M, et al. J Cryst Growth 1999;204:69.
[9] Li X, Fautrelle Y, Ren ZM. Acta Mater 2007;55:1377.
[10] Li X, Fautrelle Y, Ren ZM. Acta Mater 2007;55:3803.
[11] Ferreira PJ, Liu HB, Vander JB. J Mater Res 1999;14:275.
[12] Dong HB, Lee PD. Acta Mater 2005;53:659.
[13] Hunt JD. Mater Sci Eng 1984;65:75.
[14] Gaumann M, Trivedi R, Kurz W. Mater Sci Eng A 1997;226:763.
[15] Spittle JA, Brown SGR. J Mater Sci 1995;30:823.
[16] Nastac L. Acta Mater 1999;47:4253.
[17] Martorano MA, Beckermann C, Gandin ChA. Metall Meter Trans A 2003;34A:1657.
[18] Flemings MC. Solidification processing. New York: McGraw Hill; 1974.

[A4] Xi Li, Zhongming Ren,Yves Fautrelle

Effect of a high axial magnetic field on the microstructure in a directionally solidified Al–Al_2Cu eutectic alloy,

Acta Materialia 54 (2006) 5349–5360.

Available online at www.sciencedirect.com
ScienceDirect
Acta Materialia 54 (2006) 5349–5360
Acta MATERIALIA
www.actamat-journals.com

Effect of a high axial magnetic field on the microstructure in a directionally solidified Al–Al_2Cu eutectic alloy

Xi Li [a,b,*], Zhongming Ren [a], Yves Fautrelle [b]

[a] *Department of Material Science and Engineering, Shanghai University, Shanghai 200072, PR China*
[b] *EPM-Madylam/CNRS, ENSHMG, BP 38402, St Martin d'Heres Cedex, France*

Received 26 January 2006; received in revised form 26 June 2006; accepted 27 June 2006
Available online 18 October 2006

Abstract

The effect of a high axial magnetic field (up to 12 T) on the microstructure in a directionally solidified Al–Al_2Cu eutectic alloy has been investigated experimentally. The results show that a high magnetic field decreases the eutectic spacing and degenerates the lamellar structure into a wavy one at a low growth speed. X-ray diffraction, selected-area electron diffraction and high-resolution electron microscopy analyses indicate that the field changes the preferred orientation. The Al_2Cu crystal is oriented with the $\langle 0\,0\,1\rangle$-crystal direction along the solidification direction (i.e., the magnetic field direction). At a pulling velocity of 0.5 μm/s, the magnetic field ($B \geqslant 4$T) is responsible for the segregation; which consists of Al striations on the longitudinal section and Al-rich zones on the transverse section. The effects of the field may be attributed to the orientation of the Al_2Cu and the Al crystals and the decrease of the diffusion coefficient caused by the magnetic field.

Keywords: High axial magnetic field; Directional solidification; Al–Al_2Cu eutectic alloy

1. Introduction

The application of a high magnetic field has attracted much attention in the area of electromagnetic processing of metallic materials. Owing to the magnetic anisotropy of the phase and crystal, phase alignment and crystal orientation by the application of a magnetic field lad to very interesting phenomena. The experimental research works have demonstrated that a high magnetic field has a significant influence on the solidification of materials. Mikelson and Karklin [1] obtained aligned solidification structure in Al–Ni and Cd–Zn alloys in a 1.5 T magnetic field. Savitisky et al. [2] found that during the solidification of a Bi–Mn alloy in a magnetic field, the MnBi phase in the alloy aligned along the direction of the magnetic field. De Rango [3] extended investigations to the solidification of paramagnetic $YBa_2Cu_3O_7$ material and obtained textured crystal structure in a magnetic field. Katsuki et al. [4] reported that diamagnetic benzophenone crystallized from *n*-hexane, and KCl and $BaCl_2$ crystallized from a solution aligned in a 10 T magnetic field. This alignment behavior of the primary phase in hypo- and hyper-eutectic alloys has been much investigated by several researchers [5–7]. However, little attention has been paid to the effect of a high magnetic field on the modification of eutectic structure.

In the work reported in the present study, we chose the Al–Al_2Cu eutectic alloy with typical lamellar structure to investigate the effect of a high magnetic field on the eutectic alloy in the directional solidification process. It was the intention to obtain basic and valuable information leading to an extension of the magnetic field application to exert microstructure and property control on metallic materials. The results indicate that the field modifies the eutectic structure and changes the preferred crystallographic orientation relationship. The experimental phenomena mentioned above are interpreted as an effect on the orientation of the Al_2Cu and the Al crystals on the one hand and the decrease

* Corresponding author.
E-mail address: xi@hmg.inpg.fr (X. Li).

1359-6454/$30.00
doi:10.1016/j.actamat.2006.06.051

of the diffusion coefficient caused by the magnetic field on the other hand.

2. Experimental

The Al–Al_2Cu eutectic, Al–4.5 wt.% Cu hypoeutectic and Al–35 wt.% Cu hypereutectic alloys used in this study were prepared with high-purity Al (99.99 wt.%) and Cu (99.99 wt.%) in an induction furnace. The alloys, placed in a high-purity graphite crucible (length 200 mm, diameter 100 mm), were heated to 900 °C, magnetically stirred for half an hour, and then Al–Al_2Cu eutectic and Al–4.5 wt.% Cu hypoeutectic alloys were poured into a graphite mold to cast samples with a diameter of 3 mm and length of 200 mm. Then the cast samples were enveloped in tubes of high-purity corundum with an inner diameter of 3 mm and length of 200 mm for the directional solidification. To investigate the alignment of the primary Al_2Cu phase in Al–Cu alloys under the magnetic field, the Al–35 wt.% Cu hypereutectic alloy was poured into a graphite mold to cast samples with a diameter of 10 mm and length of 30 mm for the solidification.

A schematic of the directional solidification apparatus in a high magnetic field is shown in Fig. 1. It is comprised of a static superconductor magnet, a Bridgman–Stockbarger-type furnace, and a growth velocity and temperature controller. The superconductor magnet can produce an axial static magnetic field with an adjustable intensity up to 14 T. The furnace, consisting of nonmagnetic material, has negligible effect on field uniformity. The temperature in the furnace can reach 1600 °C, and was controlled with a precision of ±0.1 K. A water-cooled cylinder containing liquid Ga–In–Sn metal (LMC) was used to cool the sample. The temperature gradient in the sample was controlled by adjusting the temperature of the furnace hot zone, which is insulated from the LMC by a refractory disc. In order to perform the directional solidification, the apparatus is designed in such way that the sample moves downward while the furnace remains fixed. During the experiment the samples in the corundum crucibles were melted and directionally solidified in the Bridgman apparatus by pulling the crucible assembly at various velocities into the LMC cylinder.

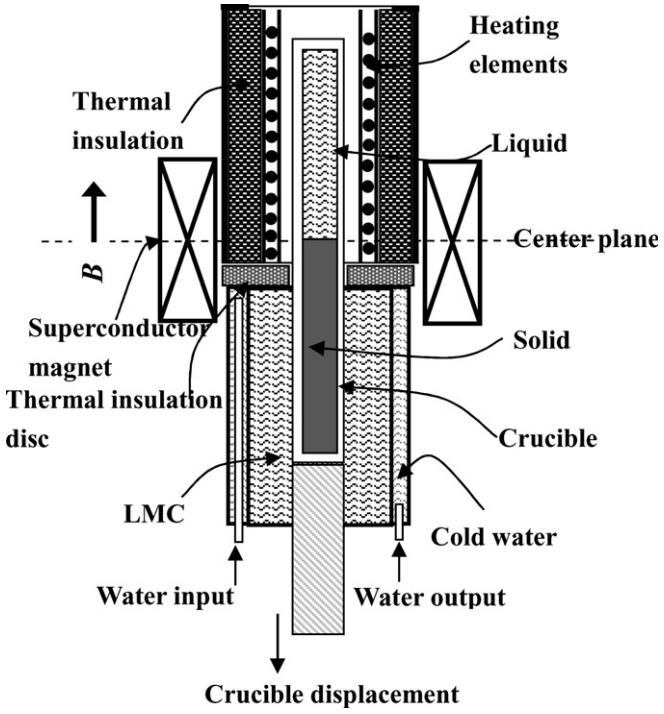

Fig. 1. The schematic illustration of the Bridgman solidification apparatus in a superconducting magnet.

The samples were made under various magnetic field intensities and growth velocities in order to study the effect of the field on the microstructures at various growth velocities. To investigate the transition in the microstructures in more detail, two other experiments were carried out made while increasing the magnetic field from 0 to 12 T and decreasing from 12 to 0 T, respectively. The samples obtained in the experiments were sectioned and mechanically polished both parallel and perpendicular to the solidification direction. The microstructures on both sections of samples were characterized using optical microscopy and scanning electron microscopy (SEM). The crystal orientation was examined by means of X-ray differential (XRD) with Cu Kα radiation. The crystallographic orientation relation between the Al and the Al_2Cu phase was determined using selected-area electron diffraction (SAD) and high-resolution electron microscopy (HREM) with thin sections of the samples. The lamellar spacing measurements were made using a Vernier eyepiece in conjunction with a standard scale and a Cambridge Quantimet 500 Image Processing and Analysis System. The error was around 5–10%.

3. Results

The transverse microstructures directionally solidified at 1.0 μm/s and a temperature gradient in the liquid G_L of 66.8 K/cm without and with 2–10 T magnetic fields are shown in Fig. 2. The microstructure without the magnetic field (Fig. 2a) has the usual regular lamellar nature. Under the influence of the imposed magnetic field, the observations of the microstructures indicate that with the increase of the magnetic field intensity, the lamella eutectic degenerates gradually. When the magnetic field intensity B exceeds 6 T, the lamellar eutectic becomes irregular leading to a wavy semi-degenerated structure. The transverse sections of the samples obtained with and without a 10 T magnetic field were examined using XRD analysis, and the results are illustrated in Fig. 3. Considering the Al_2Cu crystal it is found that the application of a 10 T magnetic field causes an increase of the peaks corresponding to the (004) plane as well as a decrease of the peaks corresponding to (222) and (112) planes. Concerning the α-Al, the peak corresponding to the (111) plane increases. Thus, it can be stated that the application of the magnetic field causes the ⟨001⟩ crystal direction of the Al_2Cu crystal as well as

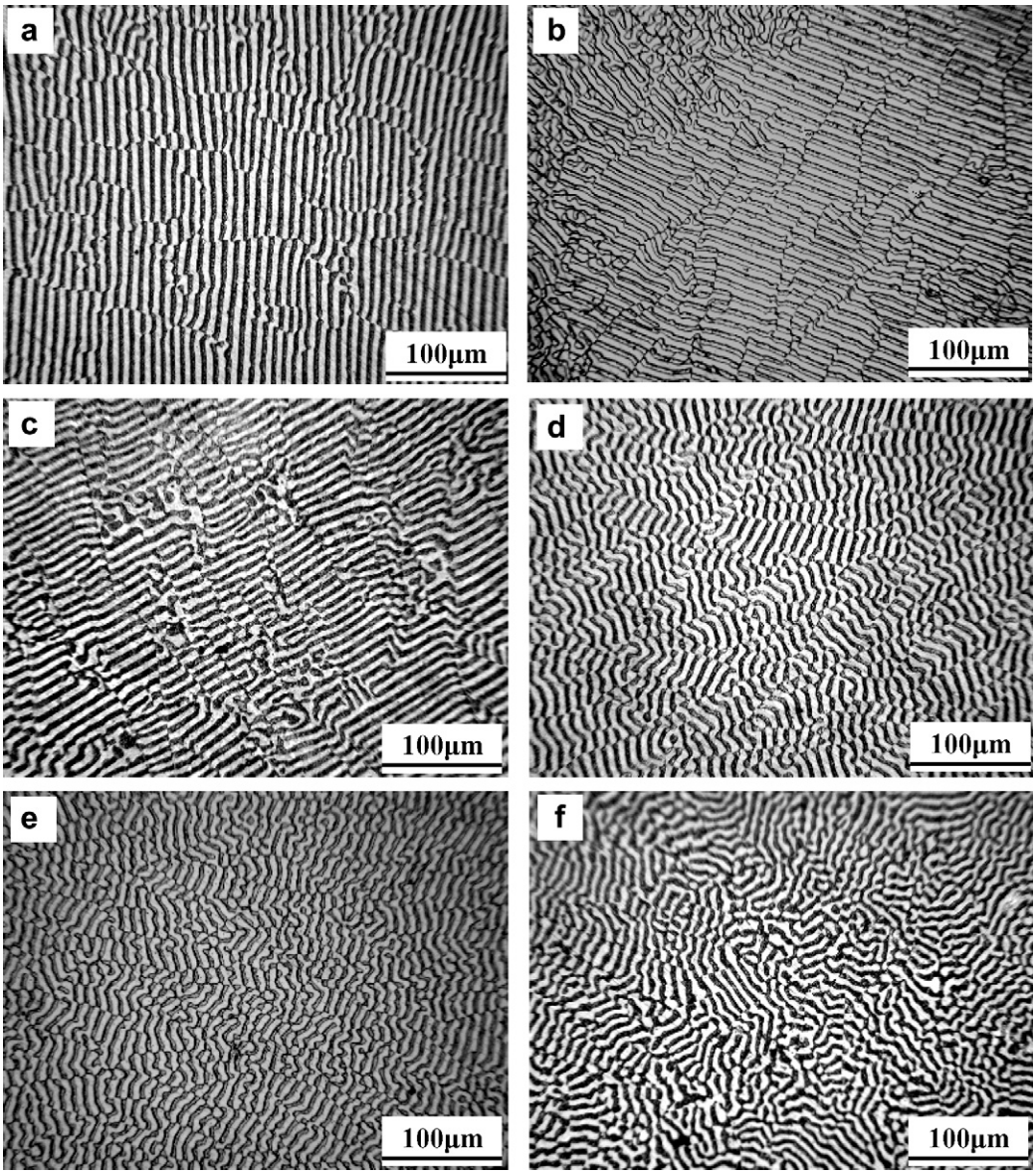

Fig. 2. Transverse microstructures of the samples solidified at 1 μm/s and the temperature gradient in the liquid of GL = 66.8 K/cm. (a) 0 T, (b) 2 T, (c) 4 T, (d) 6 T, (e) 8 T and (f) 10 T.

the ⟨1 1 1⟩ crystal direction of the Al crystal to tend be oriented along the solidification direction (i.e., the magnetic field direction). A large number of "eutectic grains" were observed using SAD and HREM from thin sections of the same samples as seen in Fig. 3. Fig. 4 shows the SAD patterns taken on the transverse section. The SAD pattern taken across the Al–Al_2Cu interface (Fig. 4a) may specify the crystallographic orientation relation between the Al and the Al_2Cu phase as "lamellar $//(3, 1, 0)_{Al_2Cu}//(0,2,0)_{Al}$". The SAD pattern obtained from the Al_2Cu (Fig. 4b) shows that the ⟨0 0 1⟩ crystal direction is parallel to the solidification direction. Fig. 4c shows the SAD pattern of the Al crystal on the plane rotated with an angle of 7° from the solidification direction. From Fig. 4c, we can observe that the ⟨0 0 1⟩ crystal direction of the Al crystal deviates from the solidification direction by about 7°. Fig. 5 shows a HREM image, which indicates that the Al and the Al_2Cu mate well. It can be observed that the ⟨0 0 1⟩ crystal direction of the Al_2Cu is parallel to the solidification direction and the ⟨0 0 1⟩ crystal direction of the Al deviates slightly from the solidification direction. The HREM result is consistent with the one obtained from the SAD analysis. Thus, we can say that there exists an approximately constant crystallographic orientation such that the solid–solid interphase boundary is parallel to $(3, 1, 0)_{Al_2Cu}$ and $(0,2,0)_{Al}$ and the ⟨0 0 1⟩ crystal direction of the Al_2Cu orientates along the solidification direction (i.e., the magnetic field direction). In the case with no magnetic field, the crystallographic orientation of the Al–Al_2Cu eutectic had been investigated and specified as "lamellar $//(2, 1, 1)_{Al_2Cu}//(1,1,1)_{Al}$". There were no crystal directions for the Al_2Cu and the Al parallel to the growth direction

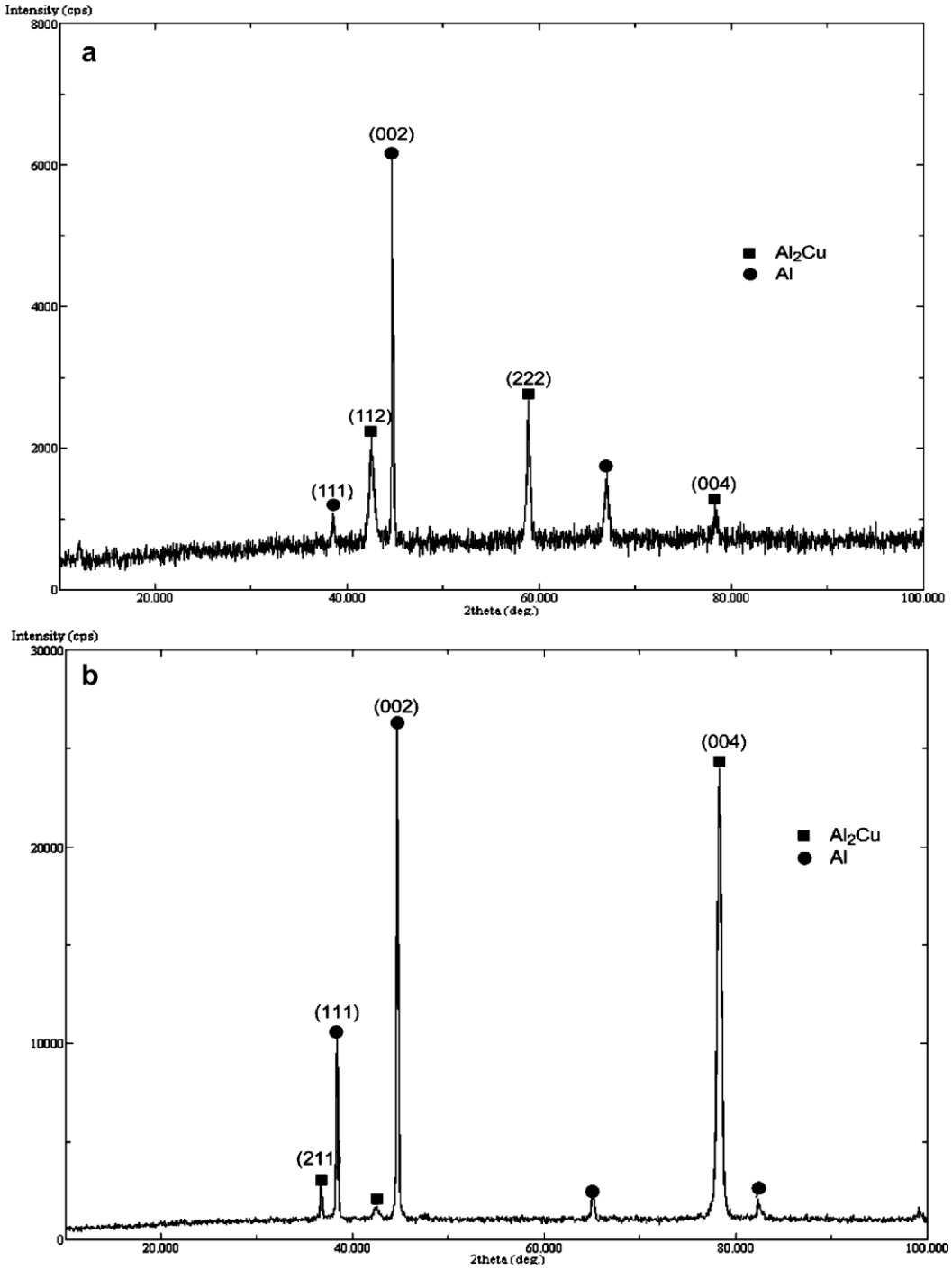

Fig. 3. X-ray diffraction patterns on the transverse sections of the samples directionally solidified without and with 10 T magnetic field ($V = 1$ μm/s, $G_L = 66.8$ K/cm). (a) 0 T and (b) 10 T.

[8–13]. Hence the application of the magnetic field has affected the crystallographic orientation of the Al–Al_2Cu eutectic.

The microstructures directionally solidified at 0.5 μm/s without and with a 12 T magnetic field are shown in Fig. 6. Comparison of the microstructures without and with the field indicates that the application of the magnetic field results in the decrease of the lamellar spacing besides the structure degeneration and the appearance of the α-Al single-phase striations. The microstructures solidified at 0.5 μm/s under various magnetic field intensities (Fig. 7) indicate that the lamellar spacing begins to reduce when a 4 T field is imposed, and under a 10 T field the eutectic spacing reaches a minimum value. The values of the lamellar spacing at different magnetic field intensities are shown in Fig. 8a. Lamellar spacing at various growth velocities in a 10 T field (Fig. 8b) shows that the effect of the field on the lamellar spacing is different at various growth velocities. At

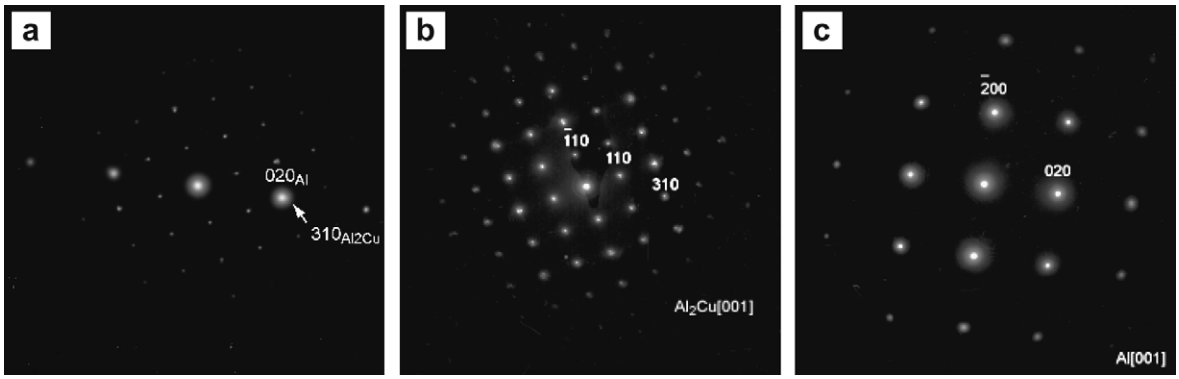

Fig. 4. Selected area diffraction (SAD) pattern for Al–Al_2Cu eutectic crystal taken from the transverse section of the sample grown at 1 μm/s under 10 T magnetic field. (a) Across the Al–Al_2Cu interface; (b) the Al_2Cu lamellae; and (c) the α-Al lamellae rotated 7° from the magnetic field direction.

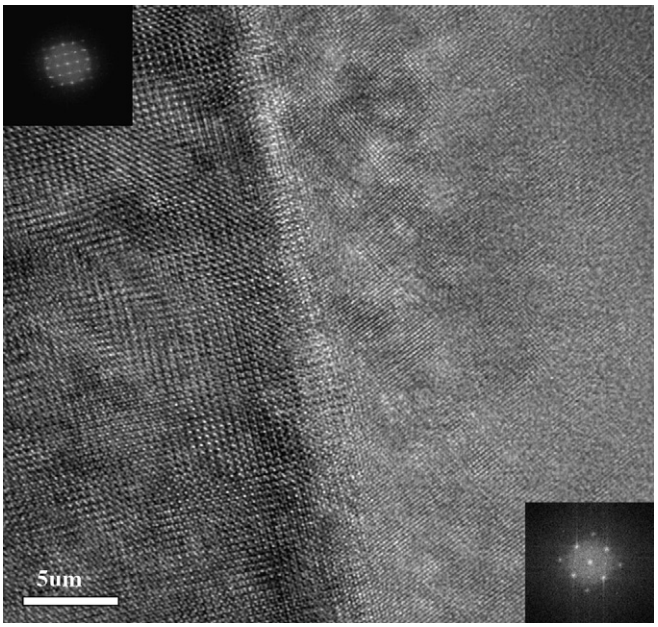

Fig. 5. High resolution electron microscopy (HREM) image across the Al–Al_2Cu interface on the transverse section of the sample solidified at 1 μm/s under 10 T magnetic field.

a growth velocity $V > 1$ μm, there are no apparent effects of the field on the lamellar spacing. However, when the growth velocity is such that $V < 1$ μm, the effect becomes stronger and stronger as the growth velocity decreases. Fig. 9 shows the macrostructures directionally solidified at 0.5 μm/s with various magnetic fields. It can be noticed that when the magnetic field $B \geqslant 4$ T, Al striations appear on the longitudinal section and segregation takes place on the transverse section. An example of the macro- and micro-structure of the sample solidified in a 10 T field is shown in Fig. 10. It can be seen that the segregation zone is enriched in Al. The above experimental results indicate that the modification of eutectic structure caused by the field becomes significant when the magnetic field intensity exceeds a certain limit value (3–4 T).

Fig. 11 shows the microstructures when the magnetic field increases from 0 to 12 T. It is evident that the lamellar spacing begins to decrease when the field reaches a certain value (about 3.3 T), as can be seen in Fig. 11d. For a certain value (about 10 T) the lamellar begins to deviate from the solidification direction distinctly and becomes wavy. Moreover, the lamellar spacing decreases further, as shown in Fig. 11e. This is consistent with the foregoing results and proves that the field has modified the eutectic microstructure more. Fig. 12 shows the microstructure when the magnetic field decreases from 12 to 0 T. There appears a wider single-phase Al striation before the Al striation vanishes at a certain field (about 3.2 T). It can also be noticed that the magnetic field intensity at which the Al striation vanishes during the field decrease agrees with the result in Fig. 9.

In order to study the magnetic anisotropy of the Al and the Al_2Cu crystals, the orientation behaviors of the Al and the Al_2Cu crystals in the hypo- and hyper-eutectic alloy under the magnetic field were investigated. Fig. 13 shows the microstructures and the XRD patterns of the Al–35 wt.% Cu sample solidified from 750 °C at cooling speed of 18 K/min in the cases with and without a 1 T field. The microstructures (Fig. 13a–c) indicate that the field has aligned the Al_2Cu phases with their longest axes along the magnetic field direction. The XRD patterns of these samples show that the application of a 1 T field has caused the peaks which indicate the (0 0 4) planes to increase on the plane perpendicular to the magnetic field direction and decrease on the parallel plane. Thus it can be deduced that the ⟨0 0 1⟩ crystal direction of the Al_2Cu crystal orientates along the magnetic field direction. The orientation behavior of the Al crystal has been studied in solidified Al–4.5 wt.% Cu alloy under a high magnetic field. It is found that the field has an effect on the orientation only in directional solidification processes. Fig. 14 shows the microstructures and the XRD patterns of the Al–4.5 wt.% Cu samples directionally solidified at 50 μm/s and a temperature gradient in the liquid (G_L) of 62.8 K/cm. The microstructures (Fig. 14a and b) indicate that a 10 T field causes the α-Al dendrites to deviate from the solidification direction. The XRD patterns of the samples mentioned above (Fig. 14c) show that the field orients the Al crystal with the ⟨1 1 1⟩ crystal direction of α-Al crystal along the solidification direction instead of the ⟨1 0 0⟩ direction. Consequently, a high magnetic field is able to

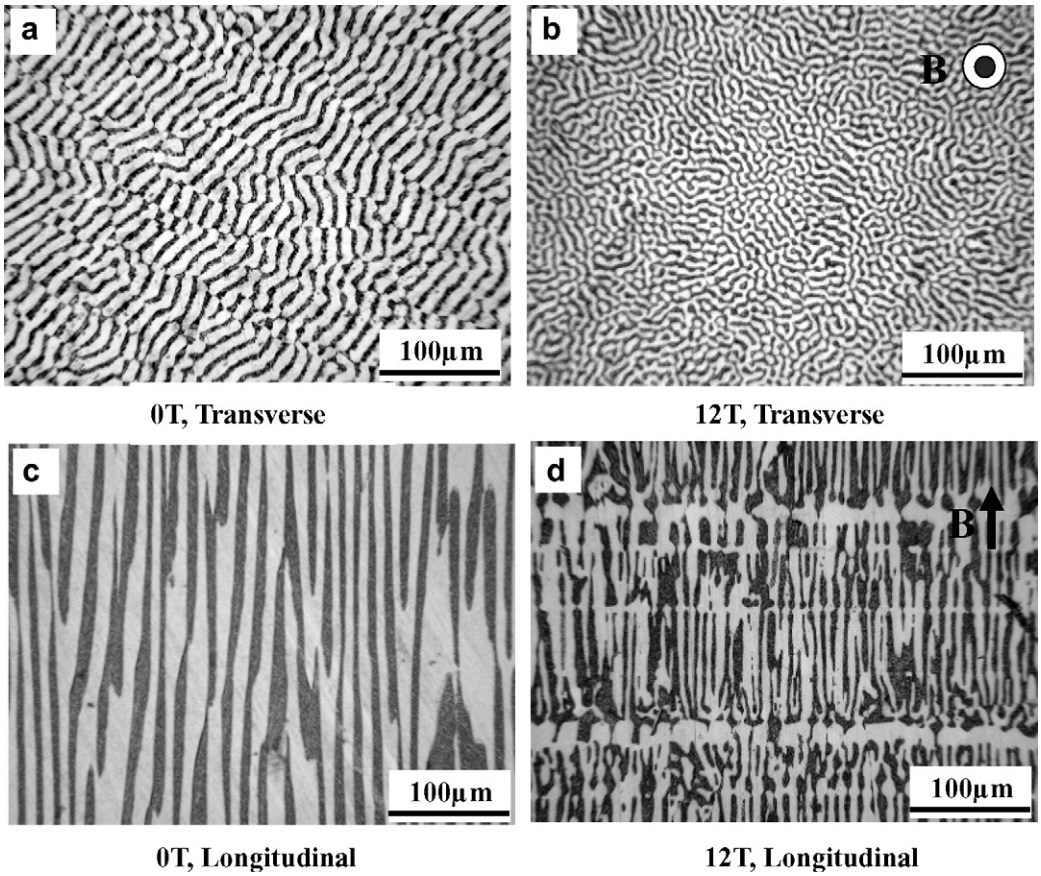

Fig. 6. Microstructures directionally solidified with and without magnetic field ($G_L = 66.8$ K/cm, $V = 0.5$ μm/s).

affect the orientation of α-Al and Al_2Cu crystals and it can be deduced that the ⟨0 0 1⟩ crystal direction of the Al_2Cu crystal and the ⟨1 1 1⟩ crystal direction of the α-Al crystal could be the easy magnetization axes.

4. Discussion

4.1. Effect of a high magnetic field on the preferred orientation between Al and Al_2Cu

The above experimental results indicate that the application of a magnetic field has changed the preferred orientations between the Al and the Al_2Cu and modified the eutectic microstructure significantly. Preferred orientation is developed in eutectics in various ways. The change of the crystallographic direction of phases during growth or encroachment of favorably oriented eutectic grains of other grains greatly affects the eutectic growth. Hopkins and Kraft [14] studied the growth of an Sn–Pb eutectic alloy using an Sn single crystal to nucleate a single eutectic grain. In their seeding experiments, they found that when the Sn seed crystal was grown according to its preferred orientation, the lamellar structure developed immediately in its equilibrium orientation. However, if the $(0\bar{1}1)$ plane of the Sn single crystal was not parallel to the growth direction, the lamellar structure did not form immediately. Instead, a wavy semi-degenerate structure was obtained. Consequently, it can be stated that the preferred orientation is vital for the formation of regular lamellar microstructure. So the wavy semi-degenerate structure obtained with the magnetic field should be attributed to the deviation of the preferred orientation from the solidification direction caused by the field.

From the results shown in Figs. 13 and 14, it can be stated that the application of the magnetic field has a considerable effect on the orientation of the Al and Al_2Cu crystals and turns the ⟨0 0 1⟩ direction of the Al_2Cu crystal and the ⟨1 1 1⟩ direction of the α-Al crystal along the magnetic field direction. So in directionally solidified Al–Al_2Cu eutectic under a high magnetic field, the field will tend to rotate the ⟨0 0 1⟩ direction of the Al_2Cu crystal and the ⟨1 1 1⟩ direction of the α-Al crystal along the magnetic field direction. However, the crystal orientation in eutectic solidification is more difficult than that in hypo- and hyper-eutectic alloys, and the Al crystal orientation is more difficult than that of the Al_2Cu crystal. Accordingly, only the ⟨0 0 1⟩ crystal direction of the Al_2Cu crystal orientates along the magnetic field direction and the ⟨1 1 1⟩ crystal direction of the α-Al crystal does not. However, the XRD result (Fig. 3) indicates that the field causes a decrease of the angle between the ⟨1 1 1⟩ crystal direction and the solidification direction. Thus the preferred crystallographic directions can deviate from the solidification direction on application of the field. Consequently, as in the mechanism mentioned

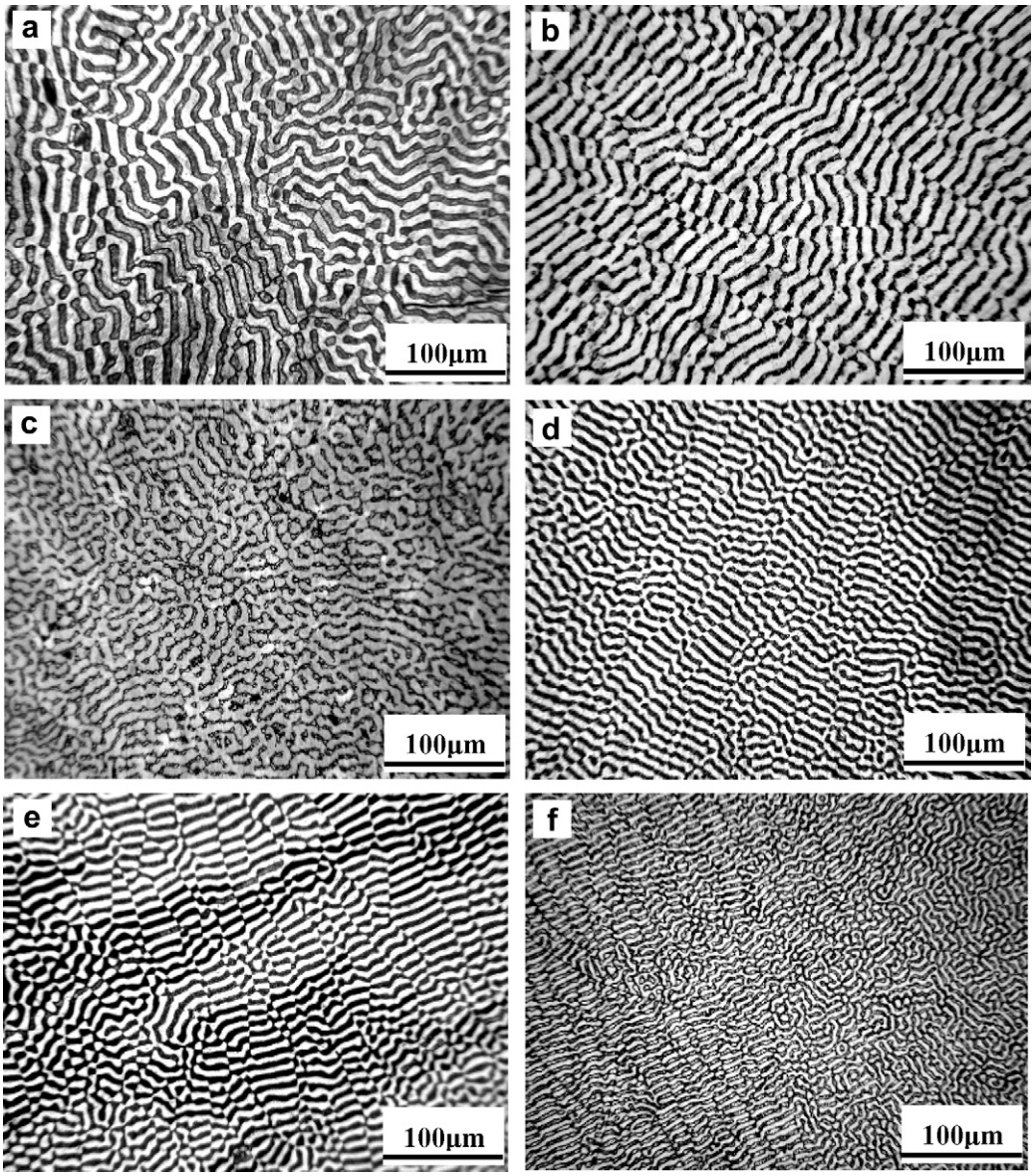

Fig. 7. Transverse microstructures of the samples directionally solidified at 0.5 μm/s in various magnetic field intensities. (a) $B = 2$ T, (b) $B = 3$ T, (c) $B = 4$ T, (d) $B = 6$ T, (e) $B = 8$ T and (f) $B = 10$ T.

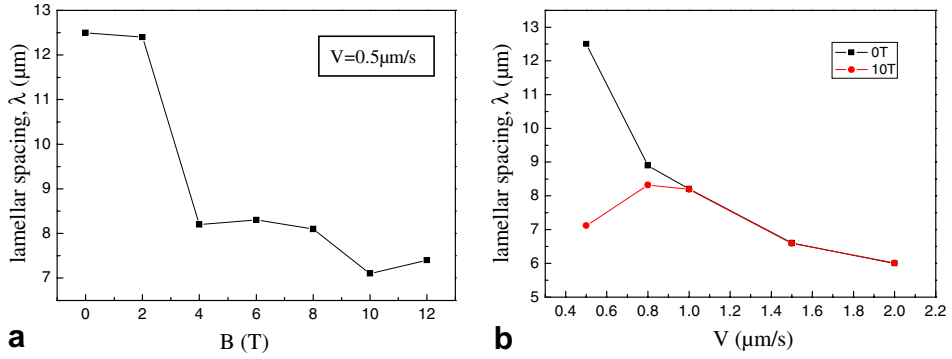

Fig. 8. Effect of high magnetic field on lamellar spacing. (a) Lamellar spacing of the samples solidified at 0.5 μm/s at different magnetic field intensity. (b) Lamellar spacing of the samples solidified at various velocities without and with 10 T field.

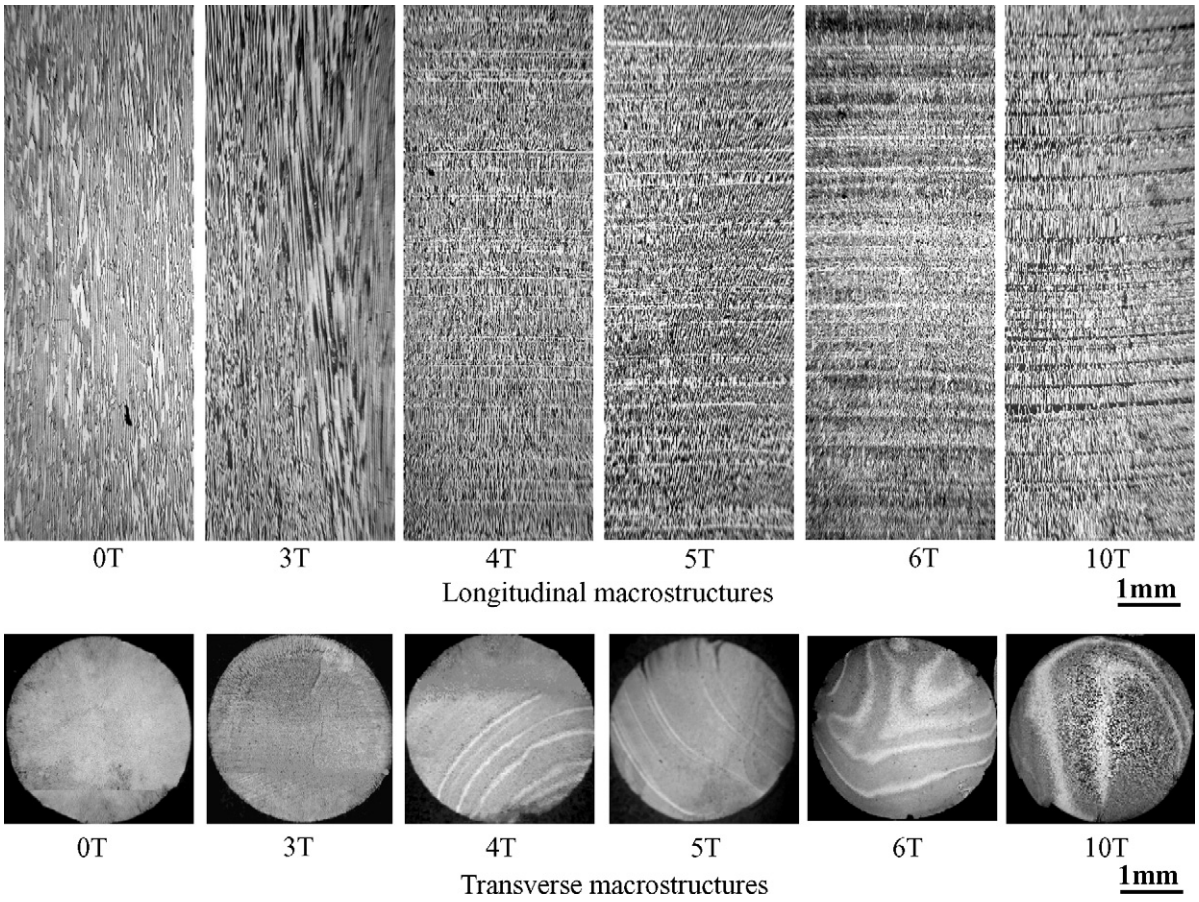

Fig. 9. Effect of the magnetic field intensity on the macrostructure of Al–Al_2Cu eutectic alloy ($V = 0.5$ μm/s, $G_L = 66.8$ K/cm).

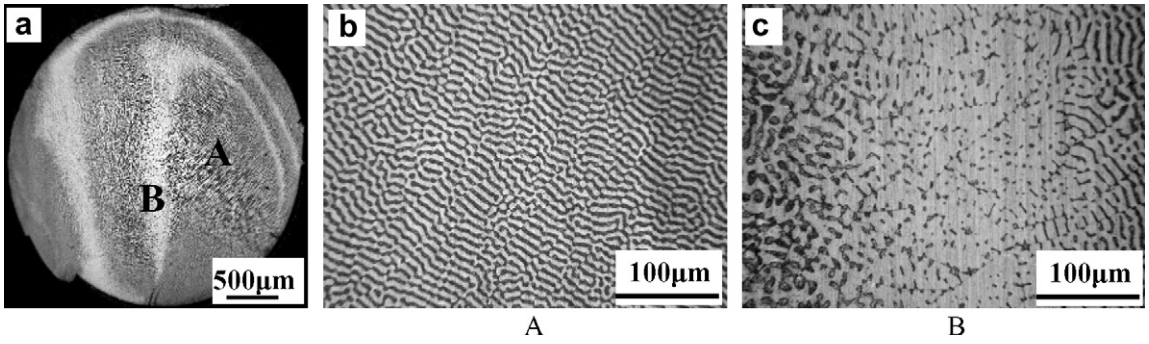

Fig. 10. Micrograph and microstructure of Al–Cu eutectic alloy solidified under 10 T magnetic field ($V = 0.5$ μm/s, $G_L = 66.8$ K/cm). (a) Macro structure, (b) microstructure at A position of (a) and (c) microstructure at B position of (a).

by Hopkins and Kraft, the lamella eutectic becomes a wavy semi-degenerate structure.

4.2. Effect of a high magnetic field on diffusion

The above experimental results also indicate that the magnetic field has decreased the eutectic spacing and caused segregation. It is well known that the growth speed in eutectic growth depends on diffusion in the liquid–solid interface. The diffusion controls the lamellar spacing as well, and affects the segregation greatly. So it is reasonable to attribute the change of the eutectic spacing and the segregation under the magnetic field to the effect of the magnetic field on the diffusion. The effect of the magnetic field on the diffusion coefficients has been investigated and the apparent diffusion coefficient decreased as B^{-2} [15]. The latter effect was attributed to the braking effect of the magnetic field on the thermo-solutal convection. However, the convection is weak in the eutectic directional solidification. So a new mechanism is proposed to illustrate the effect of a high magnetic field on the diffusion coefficient in the eutectic directional solidification.

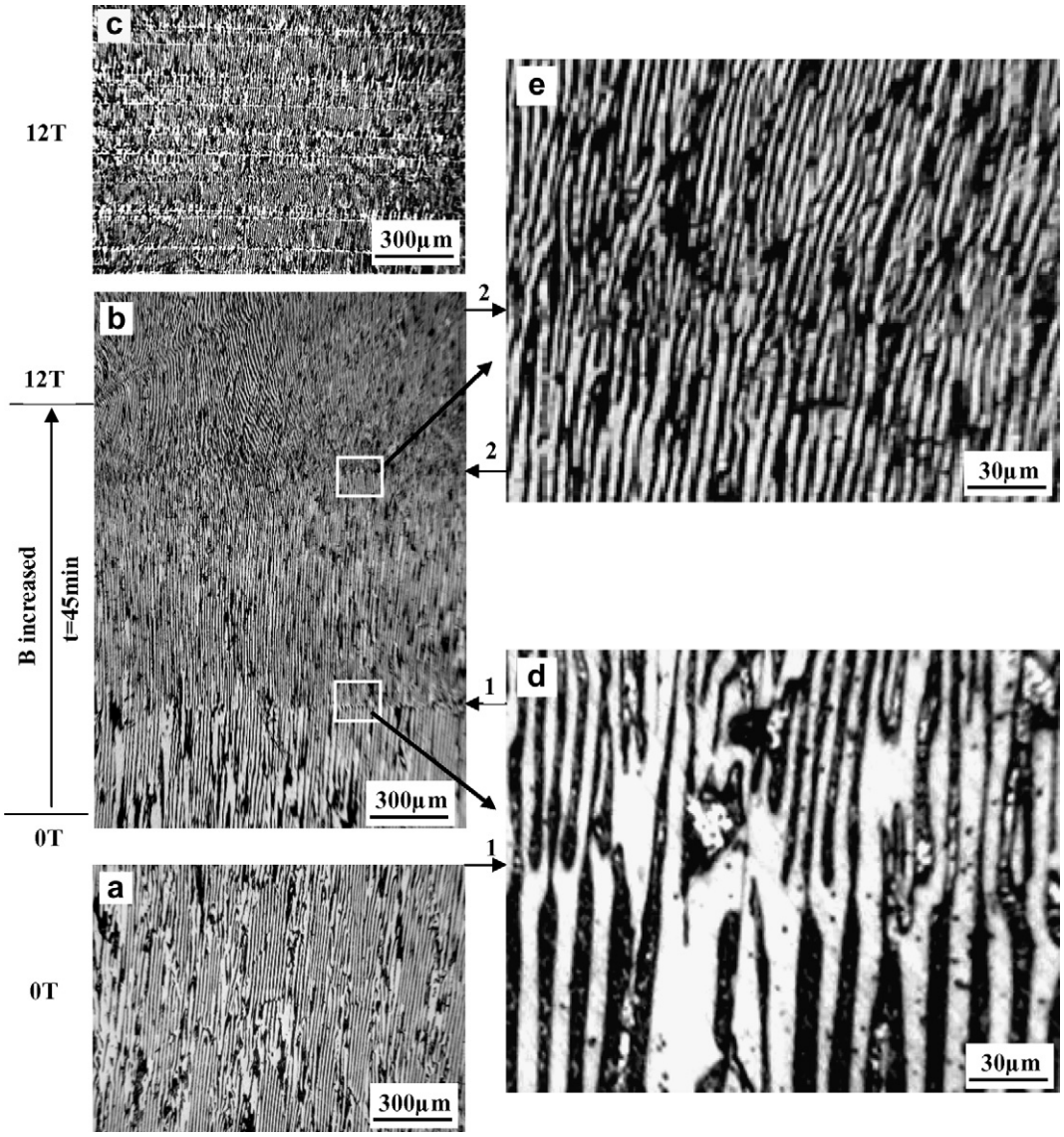

Fig. 11. Composition and structure changes during increase in magnetic filed intensity form 0 T to 12 T ($V = 0.5$ μm/s, $G_L = 66.8$ K/cm). (a) The microstructure before imposed of the magnetic field. (b) The microstructure during imposed of the magnetic field form 0 to 12 T; it can be seen that eutectic spacing decreases at arrowhead 1 and the lamellar deviates the solidification direction at arrowhead 2; 9d and 9e are the amplified microstructure at the transition, respectively. (c) The microstructure under 12 T magnetic field.

It is well known that for lamellar eutectic growth, the lamellar structure consists of the α phase and the β phase. For the Al–Al_2Cu eutectic alloy, the lamellar structure consists of the α-Al phase and the β-Al_2Cu phase. As the Al_2Cu phase grows, it rejects Al atoms into the liquid; similarly, the growing α-Al phase rejects Cu atoms. Thus, there is a buildup of Al atoms in front of the Al_2Cu lamellae and depletion in front of the α-Al lamellae. Since Cu is diamagnetic and Al is paramagnetic, the magnetic field in the enriched layers of Cu atoms decreases and the magnetic field in the buildup of Al atoms increases. As a result, a magnetic field gradient will be produced in the enhanced layers as shown in Fig. 15b. The gradient fields will restrain the diffusion of Cu and Al atoms. Consequently, the applied magnetic field will slow the atom diffusion and decrease the diffusion coefficient (D_L). Thus, some results of the present work can be illustrated easily. The eutectic spacing is given by [16]

$$\lambda^2 V = \frac{D_L \Gamma \left(\frac{1}{m_b} - \frac{1}{m_a}\right)}{C_E(1-k)} \tag{1}$$

where $k = \frac{C_S^*}{C_L^*}$, $\Gamma = \frac{\sigma_{SL}}{\Delta S}$ and λ is the lamellar spacing, D_L the liquid–solid diffusion coefficient, C_E the eutectic composition, k an equilibrium partition, σ_{SL} the liquid–solid surface energy, m_a and m_b the slopes of the α and β phases in the eutectic, respectively, and ΔS is the change in enthalpy. According to Eq. (1), it can be deduced that the field will decrease the lamellar spacing owing to the decrease of diffusion coefficient (D_L), and will result in the buildup

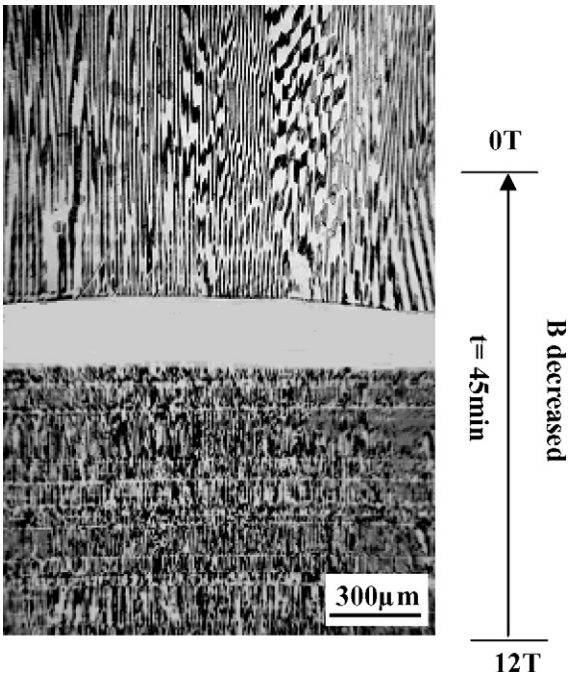

Fig. 12. Composition and structure changes during decrease in magnetic filed intensity form 12 T to 0 T ($V = 0.5$ μm/s).

of Al and Cu atoms in front of the interface (Fig. 15a). Thus, with the buildup of Al and Cu atoms, the gradient fields in the enhanced layers in front of the α-Al phase and the β-Al_2Cu phase will increase even more. As a result, Al and Cu atoms are more enriched in the enhanced layers. Since the magnetic susceptibility of Al is greater than that of Cu, the accumulation speed of Al atoms in front of the Al_2Cu lamellae is quicker than that of Cu atoms in front of the Al lamellae. When the concentration of Al in front of the Al_2Cu lamellae is high enough that the concentration of Cu is below the maximum solubility of the α-Al phase, the growth of the Al_2Cu lamellae is stopped and the single-phase Al striation will form.

Moreover, there exists a boundary layer in front of the single-phase Al striation, which has width $\delta_c = 2D_L/V$, where, D_L is the diffusion coefficient and V is the growth velocity. According to our interpretation the diffusion coefficient will increase while the field decreases. Thus, a decrease of the magnetic field will result in an increase of the width of the boundary layer in front of the single-phase Al striation. Consequently, the average composition of the solid $\overline{C}_S$ in the Al striation will drop, and then the Al striation will widen (Fig. 10).

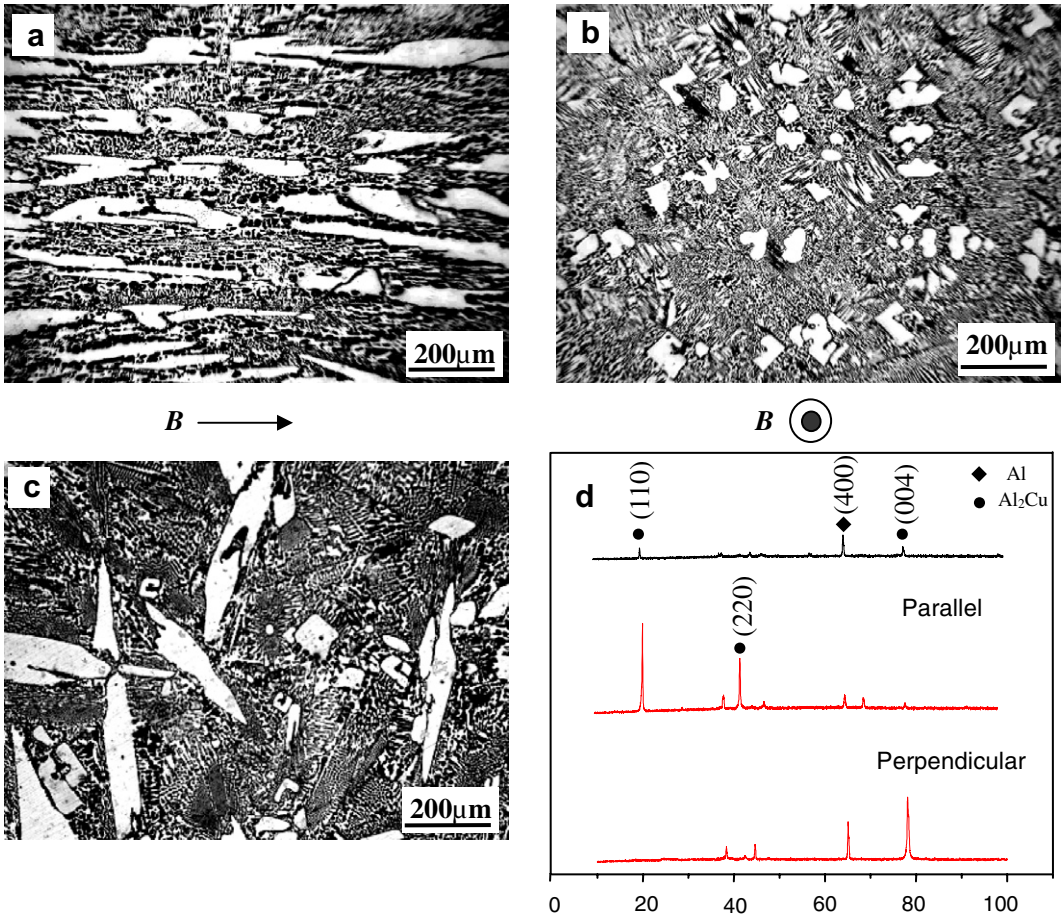

Fig. 13. Effect of high magnetic field on the microstructure of Al–35 wt.% Cu alloy cooled from 750 °C at cool speed of 18 K/min. (a) Without magnetic field; (b) longitudinal section, $B = 10$ T; (c) transverse section, $B = 10$ T; and (d) the XRD of Al–35 wt.% Cu alloy.

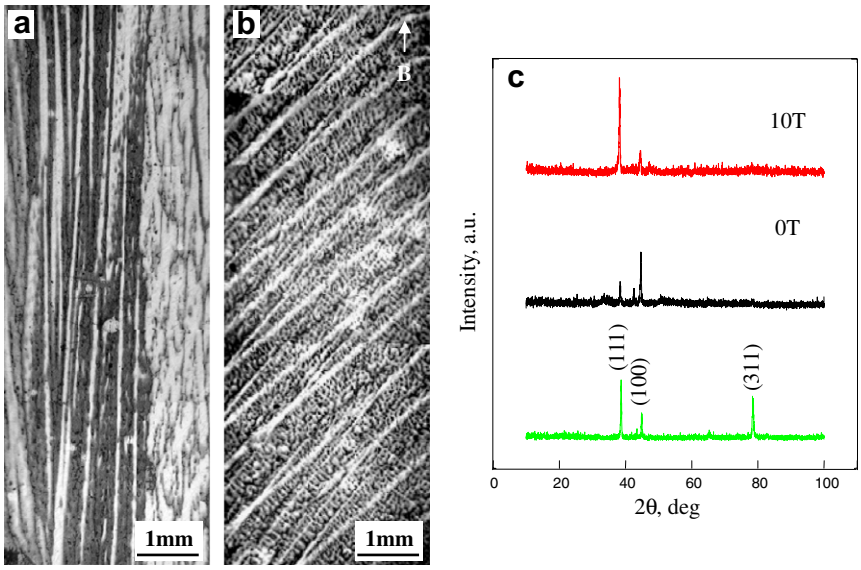

Fig. 14. Effect of high magnetic field on the alignment of α-Al in directionally solidified Al–4.5 wt.% Cu alloy ($G_L = 62.8$ K/cm and $V = 50$ μm/s). (a) The microstructure without magnetic field; (b) the microstructure with 10 T magnetic field; and (c) X-ray diffraction patterns of the alloy in the plane perpendicular to growth direction.

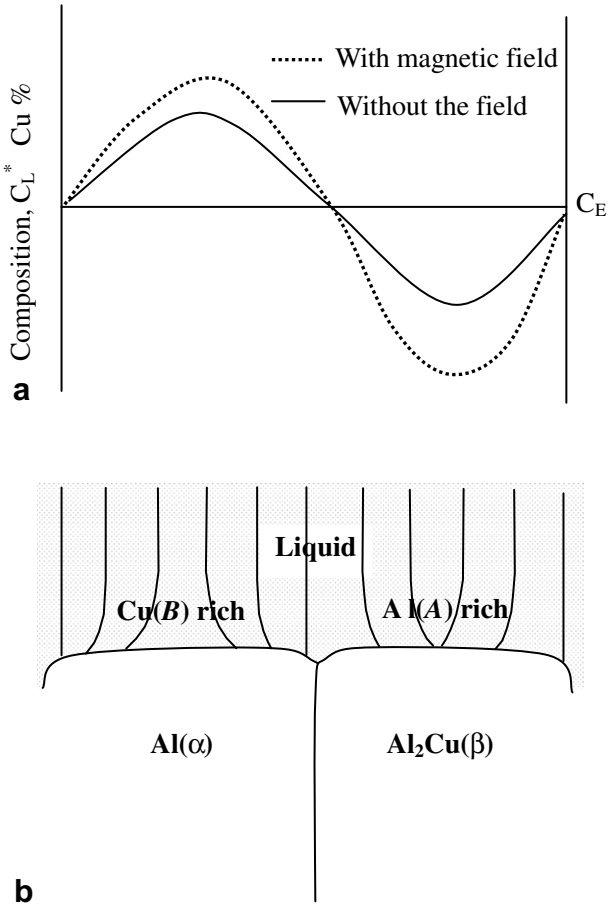

Fig. 15. Lamellar eutectic growth under a magnetic field. (a) Solute concentration in the liquid at the interface and (b) the distribution of magnetic field in the liquid at the interface.

5. Conclusions

The modifying effect of a high axial magnetic field (up to 12 T) on the eutectic microstructure has been investigated experimentally during the growth of an Al–Al_2Cu eutectic alloy in a Bridgman–Stockbarge-type furnace. The magnetic field decreases the eutectic spacing and degenerates the lamellar structure into a wavy one at lower growth speeds. From XRD, SAD and HREM analysis, it is found that the preferred orientation relation of the Al–Al_2Cu eutectic is modified by the field. As a result, the ⟨0 0 1⟩ crystal direction of the Al_2Cu orientates along the solidification direction (i.e., the magnetic field direction). Moreover, the magnetic field also causes segregations. Indeed, the Al striations on the longitudinal and rich-Al zone on the transverse sections are produced at lower growth speeds. The latter results may be attributed to the orientation of the Al_2Cu and the Al crystals as well as the decrease of the diffusion coefficient caused by the magnetic field.

Acknowledgements

This work was financially supported by the National Natural Science Foundation of China (Nos. 50234020, 50225416 and 59871026) and one of the authors (L.X.) is also grateful for an Egide/Eiffel Doctorate Scholarship.

References

[1] Mikelson AE, Karklin YK. J Cryst Growth 1981;52:524.
[2] Savitisky EM, Torchinova RS, Turanoy SA. J Cryst Growth 1981;52:519.

[3] De Rango PD, Lee M, Lejay P, Sulpice A, Tournier R, Ingold M, Germi P, Pernet M. Nature 1991;349:770.
[4] Katsuki A, Tokunaga R, Watanabe SI. Chem Lett 1996;8:607.
[5] Wang H, Ren ZM, Deng K. Acta Metall Sinica 2002;38:41.
[6] Yasuda H, Ohnala I, Yamamoto Y. Mater Trans JIM 2003;44:2550.
[7] Morikawa H, Sassa K, Asai S. Mater Trans JIM 1998;l39:814.
[8] Kraft RW. TMS-AIME 1961;221:704.
[9] Davies IG, Hellawell A. Philos Mag 1970;20:1255.
[10] Kraft RW, Albright SL. TMS-AIME 1962;224:1176.
[11] Double DD, Hellawell A. Philos Mag 1969;19:1299.
[12] Cantor B, Chadwick GA. J Cryst Growth 1974;23:12.
[13] Lawson WHS, Kerr HW. J Cryst Growth 1972;12:209.
[14] Hopkins RH, Kraft RW. Trans Met Soc AIME 1968;242: 1627.
[15] Botton V, Lehmann P, Bolcato R, Moreau R, Haettel R. Int J Heat Mass Transfer 2001;44:1639.
[16] Hu HQ. Metal solidification theory. Beijing: Chinese Mechanical Publishing; 2000. p. 187.

[A5] Xi Li, Zhongming Ren,Yves Fautrelle

The spiral growth of lamellar eutectics in a high magnetic field during the directional solidification process,

Scripta Materialia 56 (2007) 505–508.

Available online at www.sciencedirect.com
ScienceDirect
Scripta Materialia 56 (2007) 505–508
Scripta MATERIALIA
www.actamat-journals.com

The spiral growth of lamellar eutectics in a high magnetic field during the directional solidification process

Xi. Li,[a,b,*] Zhongming Ren[a] and Yves Fautrelle[b]

[a] *Department of Material Science and Engineering, Shanghai University, Shanghai 200072, China*
[b] *EPM-Madylam/CNRS, ENSHMG BP 38402 St Martin d'Heres Cedex, France*

Received 18 September 2006; revised 16 November 2006; accepted 23 November 2006
Available online 27 December 2006

The effect of a high magnetic field on lamellar eutectic growth was investigated in directionally solidified Al–Al_2Cu and Pb–Sn eutectic alloys. It was found that the magnetic field has degenerated the lamellar eutectics; as a consequence, the microstructures in the section perpendicular to the solidification direction (i.e. the magnetic field direction) became whorled and the ones in the section parallel to the growth direction deviated from the solidification direction. This may be attributed to the spiral growth of the lamellar eutectic caused by the magnetic field.

Keywords: High magnetic field; Lamellar eutectics; Spiral growth; Directional solidification

Numerous works have been performed on the effect of a magnetic field on crystal growth. These are mainly related to such topics as the crystal orientation [1–6] and micro- and macro-segregation [7]. However, little attention has been paid to the modification of eutectic structures under a magnetic field [8]. This is due, on the one hand, to the fact that eutectic orientation in a weak and moderated magnetic field is difficult; on the other hand, because of the formation of the "boundary layer", or stagnant layer, at the solid–liquid interface, the size of which is several tens of times larger than the dimension of the eutectic microstructures, it is hard to consider that the macroscopic flow would have any effect on the microstructure. However, it is possible that a high magnetic field could modify the eutectic. We found that a high magnetic field can modify the eutectic microstructure of Al–Al_2Cu and attributed this to the effect of a high magnetic field on the orientation relationship [8].

The purpose of this work is to study the growth mechanism of the lamellar eutectic under a high magnetic field. By investigating two typical lamellar eutectics of Al–Al_2Cu and Pb–Sn alloys during the directional solidification process, a growth model of the lamellar eutectic in a high magnetic field is proposed and the degeneration of the lamellar eutectic in a high magnetic field is attributed to the spiral growth caused by the magnetic field.

The Al–Al_2Cu and Pb–Sn eutectics used in this study were prepared with high-purity substances (5 N) in an induction furnace. The alloys, being put in a high-purity graphite crucible of 10 cm diameter, were heated to 900 and 600 °C, respectively, then magnetically stirred for half an hour and poured into a graphite mold to cast samples with the diameter of 3 mm and length of 200 mm. The cast sample was enveloped in the tube of high-purity corundum with the inner diameter of 3 mm and length of 200 mm. The experimental apparatus consists of a static superconductor magnet and a Bridgman–Stockbarge-type furnace equipped with a growth velocity and temperature controller as shown in Ref. [8]. The superconductor magnet can produce an axial static magnetic field with the intensity adjustable up to 14 T. The furnace, consisting of nonmagnetic material, has a negligible effect on field uniformity. A water-cooled cylinder containing liquid Ga–In–Sn metal (LMC) was used to cool down the sample. The temperature gradient in the sample was controlled by adjusting the temperature of the furnace hot zone, which was insulated from the LMC by a refractory disc. The apparatus was designed such that the sample moves downward while the furnace remains stationary. Growth velocities, R, lie in the range $0.5 \leqslant R \leqslant 5000$ μm s^{-1}.

* Corresponding author. Address: Department of Material Science and Engineering, Shanghai University, Shanghai 200072, China; e-mail: xi@hmg.inpg.fr

1359-6462/$ - see front matter © 2006 Acta Materialia Inc. Published by Elsevier Ltd. All rights reserved.
doi:10.1016/j.scriptamat.2006.11.019

During the experiment, the samples in the corundum crucibles were melted and directionally solidified in the Bridgman apparatus by drawing the crucible assembly at a certain speed into the LMC cylinder. The microstructures were examined in the etched condition by optical microscopy, scanning electron microscopy (SEM) and transmission electron microscopy (TEM). The dislocation was determined by the high-resolution electron microscopy (HREM) from thin sections of the samples.

Figure 1 shows the transverse microstructures of the Al–Al_2Cu eutectic solidified directionally at 1 μm s^{-1} with various magnetic field intensities. As can be seen, the microstructure without the magnetic field was a regular lamellar structure with a normal fault. However, the magnetic field applied had a considerable influence on the microstructures; as a result, under a 4 T magnetic field, it can be seen that the fault was extended. Under a 6 T magnetic field, the eutectic became short and twisty. The application of a 10 T magnetic field caused the eutectic to degenerate significantly and it seemed to grow in the spiral way. Figure 2 shows the transverse microstructures of the Pb–Sn eutectic solidified directionally at 1 μm s^{-1} with various magnetic field intensities. The same phenomena as those of the Al–Al_2Cu eutectic occurred: with increasing magnetic field intensity, the microstructures degenerated gradually, and under a 10 T magnetic field the eutectic became distorted significantly.

The corresponding longitudinal microstructures of Al–Al_2Cu and Pb–Sn eutectics in Figures 1 and 2 without and with a 10 T magnetic field were observed and the results are shown in Figure 3. It can be seen that the application of a 10 T magnetic field caused the eutectic lamellae to deviate from the solidification direction and grow in a wavy way. In order to investigate the effect of the magnetic field on the microstructures at various growth speeds, the longitudinal microstructures of the Pb–Sn eutectic at 1, 3, 5 and 10 μm s^{-1} in a 10 T

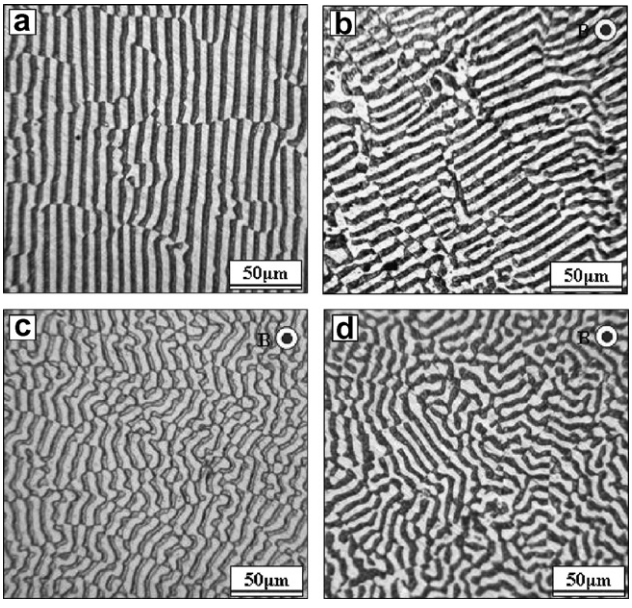

Figure 1. Transverse microstructures of the Al–Al_2Cu eutectic solidified at 1 μm/s and the temperature gradient in the liquid of $G_L = 66.8$ K/cm with various magnetic field intensities. The double ring denoting the direction of applied magnetic field. (a) 0 T; (b) 4 T; (c) 6 T; (d) 10 T.

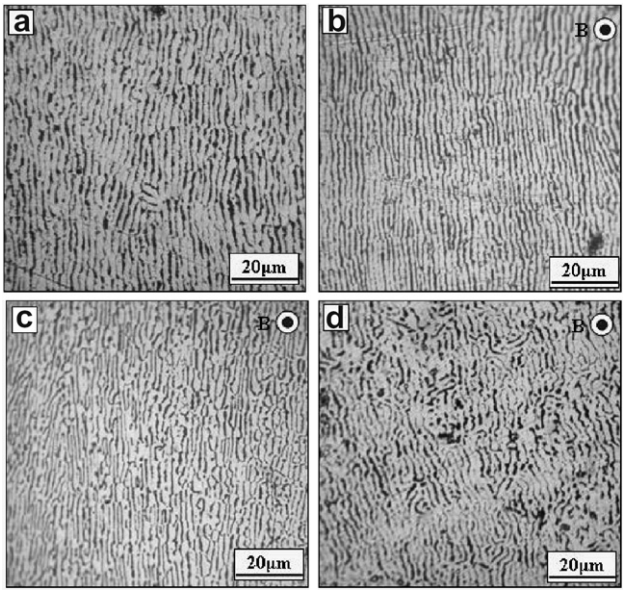

Figure 2. Transverse microstructures of the Pb–Sn eutectic solidified at 2 μm/s and the temperature gradient in the liquid of $G_L = 45$ K/cm with various magnetic field intensities. (a) 0 T; (b) 2 T; (c) 6 T; (d) 10 T.

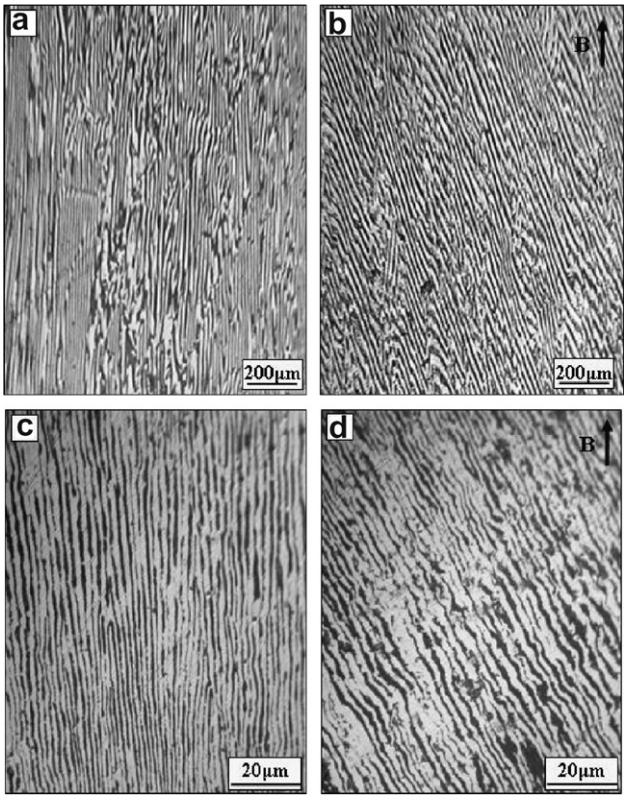

Figure 3. Longitudinal microstructures corresponding to the ones in Figures 1 and 2, respectively. Al–Al_2Cu eutectic: (a) 0 T; (b) 10 T. Pb–Sn eutectic: (c) 0 T; (d) 10 T.

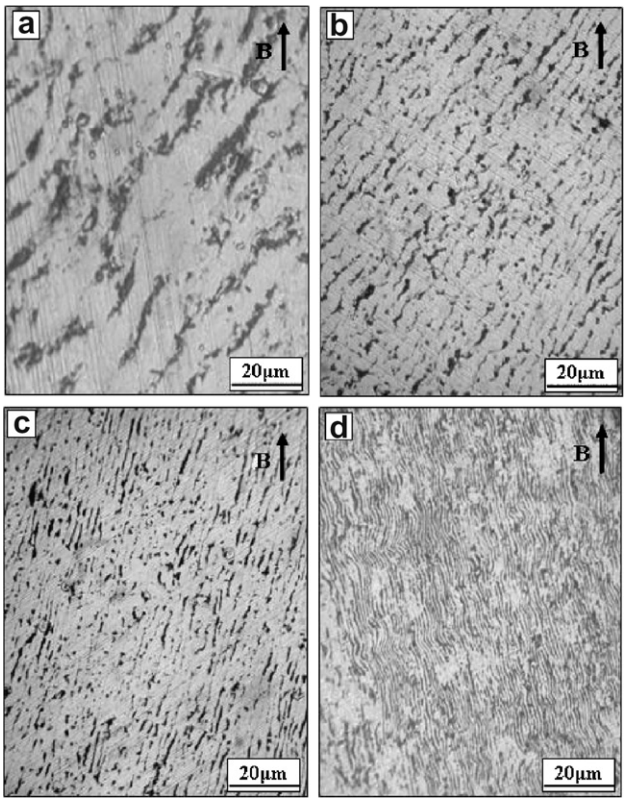

Figure 4. Longitudinal microstructures of the Pb–Sn eutectic under a 10 T magnetic field at various growth speeds. (a) 1.0 μm/s; (b) 3.0 μm/s; (c) 5.0 μm/s; (d) 10 μm/s.

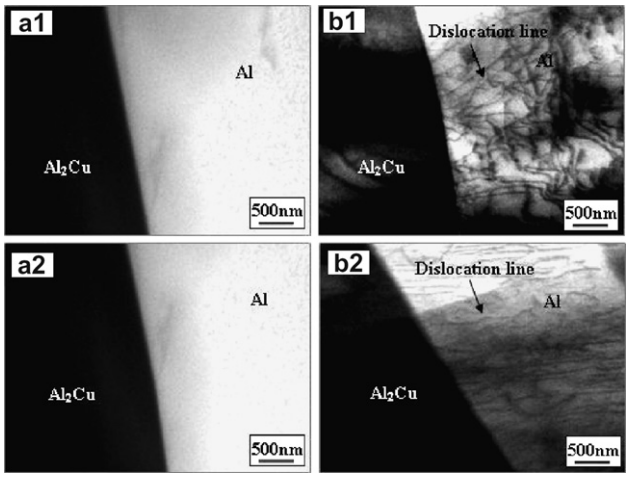

Figure 5. TEM bright-field micrographs of the samples directionally solidified at 1 μm/s and a temperature gradient of 66.8 K/cm: (a) without and (b) with a 10 T magnetic field.

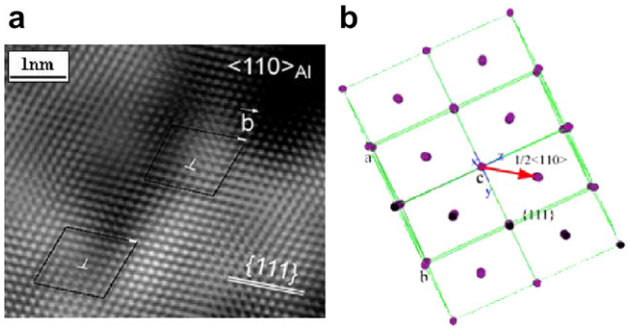

Figure 6. HREM image of the Al lamellar in Figure 5(b1) and the dislocation schematic map. (a) The HREM image on the {1 1 1}-crystal plane; (b) the schematic map of the dislocation analyses.

magnetic field (Fig. 4) were observed. It can be seen that with the increase of the growth speed, the angle between the growth direction of the lamellar and the solidification direction decreased. This indicates that with increasing growth speed, the effect of the magnetic field on the eutectic growth decreases.

Further, to study the effect of the magnetic field on the substructure of the eutectic, the microstructures of the Al–Al_2Cu eutectic solidified at 1 μm s^{-1} with and without a 10 T magnetic field were observed with TEM. The TEM observation shows that there were no clear dislocation tangles in the non-field-treated specimens (Fig. 5(a1) and (a2)); however, a large number of dislocation tangles or pile-ups and networks in the Al lamellar were found in the specimen treated with the magnetic field (Fig. 5(b1) and (b2)). This suggests that the application of a magnetic filed produced dislocation from the interface boundary.

A large number of "eutectic grains" were observed with HREM when we studied the dislocation type. The dislocation took place on the {1 1 1}-crystal plane of the Al phase. In the HREM image in Figure 6(a) the Burgers vector is shown as the arrowhead $\vec{b}$. According to the crystal structure of Al, the {1 1 1}-crystal plane is the close-packed plane of atoms and the ⟨1 1 0⟩-crystal direction on the {1 1 1}-crystal plane is the close-packed direction, as shown in Figure 6(b). This means that the atoms space along the ⟨1 1 0⟩-crystal direction is the least and equal to the $1/2\langle 1\,1\,0\rangle a_{Al}$, so the Burgers vector is identified as the $1/2\langle 1\,1\,0\rangle$ one. The above results show that, along with the change in the lamellar structure of the eutectic, the substructure is also affected.

The above experimental results show that the application of a magnetic field has degenerated the eutectics and resulted in the production of a dislocation. It had been found that, during the directional growth, spiral growth occurred in some regions in several lamellar eutectic systems, including Al–Al_2Cu and Pb–Sn eutectics [9,10], which was responsible for the degeneration and fault. According to the Attallah–Gruzeleski model [11], the driving force leading to the spiral growth of a lamellar eutectic was the deviation of the preferred growth direction of one, or even both, of the phases from the overall growth direction of the system. Owing to the magnetic anisotropy of the crystal, a high magnetic field may align one, or even both, of the phases in eutectic and cause the preferred growth direction to deviate from the solidification direction. Thus, according to the Attallah–Gruzeleski model, spiral growth will be produced. It had been assuredly proven in Ref. [8] that the field was capable of changing the orientation relationship in the Al–Al_2Cu eutectic and caused the preferred growth direction to deviate from the solidification direction.

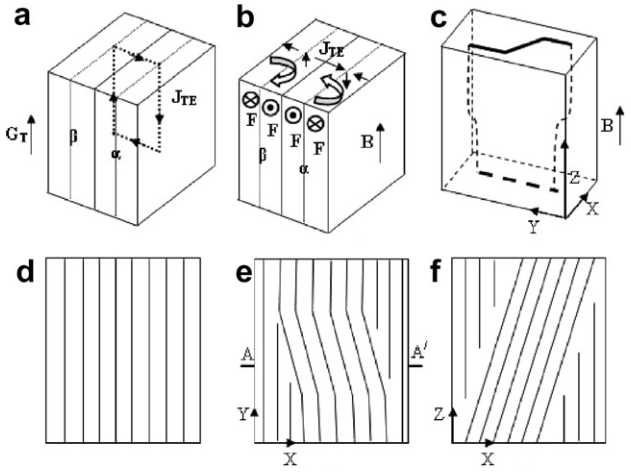

Figure 7. Schematic diagram of the spiral growth of the lamellar eutectic under a high magnetic field during directional solidification process. (a) Elementary short-circuited thermocouple at the interface of the eutectic, (b) the force caused by the interaction between the magnetic field and the electric current, (c) the three-dimensional schematic map of the spiral lamellar eutectic, (d) the regular lamellar eutectic in the case of no magnetic field, (e) the structure in the Y–X section perpendicular to the magnetic field, a broken line indicates the orientation of lattice, (f) the structure in the X–Z section parallel to the magnetic field at A–A'.

A second possible mechanism that can induce spiral growth in a lamellar eutectic may be attributed to the thermoelectro effect (TE). It is well known that in any material a temperature gradient, ΔT, produces a Seebeck electromotive force S, where S is the thermoelectric power of the materials. Consider now an elementary part of the eutectic in a given temperature gradient. Provided that two phases in a eutectic show a difference in the thermoelectric power, this elementary part can be looked upon as the same thermocouple as shown in Figure 7(a); however, this thermocouple is now short-circuited. So, the previously measured tension now generates a current and each portion of the interphase interface behaves as an elementary current generator. Consequently, the interaction between the magnetic field and the current will produce a force moment on the two phases in the eutectic, respectively, as shown in Figure 7(b). Owing to the difference of the content and the thermoelectric power of the two phases in the eutectic, a rotating force moment will form, which will cause the eutectic to rotate during the directional growth process. Thus, the eutectic will grow in a spiral way and the regular lamellar structure will degenerate. A possible example of the idea is proposed in Figure 7(c), which shows the morphology of the lamellar eutectic on the sections parallel and perpendicular to the solidification direction (Fig. 7(e) and (f)). At the same time, the spiral growth will produce stress in the crystal; consequently, a dislocation is produced. According to the above two mechanisms for inducing spiral growth in the lamellar eutectic, it can be deduced that the spiral growth is related to the growth speed and the magnetic field intensity. Thus, with decreasing growth speed and increasing magnetic field, the degeneration of the eutectic is enhanced; as a consequence, the distortion on the transverse section and the gradient of the lamellar on the longitudinal increases (Figs. 1, 2 and 4).

In conclusion, the effect of a high magnetic field on Al–Al_2Cu and Pb–Sn lamellar eutectic growth has been investigated during the directional solidification process. It is found that the magnetic field causes the lamellar eutectics to degenerate; as a result, the microstructures perpendicular to the growth direction (i.e. the magnetic field direction) become distorted and whoerled, and those parallel to the growth direction deviate from the solidification direction. Along with the degeneration of the lamellar structure, the substructure is also changed significantly. As an example, the effect of the magnetic field on the dislocation of the Al lamellae in the Al–Al_2Cu eutectic was investigated. It was found that the magnetic field caused a large number of dislocation tangles or pile-ups and networks on the Al lamellar. The above experimental phenomena are attributed to the spiral growth of the eutectic caused by the magnetic field.

This work was supported by Natural Science Foundation of China (Nos. 50234020, 50225416 and 59871026). L. X. is also grateful for an Egide/Eiffel Doctorate Scholarship. The authors are indebted to Prof. R. Moreau and Prof. T. Duffar in CNRS, Grenoble, for helpful and fruitful discussions.

[1] A.E. Mikelson, Y.K. Karklin, J. Cryst. Growth 52 (1981) 524.
[2] E.M. Savitisky, R.S. Torchinova, S.A. Turanoy, J. Cryst. Growth 52 (1981) 519.
[3] P.D. De Rango, M. Lee, P. Lejay, A. Sulpice, R. Tournier, M. Ingold, P. Germi, M. Pernet, Nature 349 (1991) 770.
[4] A. Katsuki, R. Tokunaga, S.I. Watanabe, Chem. Lett. 8 (1996) 607.
[5] H. Yasuda, I. Ohnala, Y. Yamamoto, Mater. Trans. JIM 44 (2003) 2550.
[6] H. Morikawa, K. Sassa, S. Asai, Mater. Trans. JIM 139 (1998) 814.
[7] J.Z. Jin, K.F. Kobayashi, P.H. Shingu, Metall. Mater. Trans. A 15 (1984) 307.
[8] X. Li, Z.M. Ren, Y. Fautrelle, Acta Mater. 54 (2006) 5349.
[9] D.P. Mourer, J.D. Verhoeven, J. Cryst. Growth 37 (1977) 197.
[10] D.D. Double, P. Truelove, A. Hellawell, J. Cryst. Growth 2 (1968) 191.
[11] T. Attallah, J.E. Gruzleski, J. Cryst. Growth 34 (1976) 164.

[A6] Xi Li, Zhongming Ren,Yves Fautrelle

Effect of high magnetic fields on the microstructure in directionally solidified Bi–Mn eutectic alloy,

Journal of Crystal Growth 299 (2007) 41–47.

Available online at www.sciencedirect.com
ScienceDirect
Journal of Crystal Growth 299 (2007) 41–47
JOURNAL OF CRYSTAL GROWTH
www.elsevier.com/locate/jcrysgro

Effect of high magnetic fields on the microstructure in directionally solidified Bi–Mn eutectic alloy

Xi Li[a,b,*], Zhongming Ren[a], Yves Fautrelle[b]

[a]Department of Material Science and Engineering, Shanghai University, Shanghai 200072, PR China
[b]Institut National Polytechnique de Grenoble, ENSHMG, B.P. 95 38402 Saint Martin d' Heres Cedex, Grenoble, France

Received 28 February 2006; received in revised form 28 September 2006; accepted 23 October 2006
Communicated by M.E. Glicksman
Available online 12 January 2007

Abstract

The eutectic Bi/MnBi alloy has been directionally solidified in the presence of an axial magnetic field to investigate the influence of high magnetic fields on the growth of eutectic Bi/MnBi. The morphology and magnetic properties of the specimens indicate that a high magnetic field promotes the formation of MnBi fiber and makes the directional solidification structure of the eutectic more regular. The MnBi inter-rod spacing and rod diameters gradually increase with the magnetic field intensity. Furthermore, the magnetic field enhances the faceted growth of MnBi phase and the magnetic coercivities of the alloy. This may be attributed to the magnetic anisotropy and the shift of the eutectic point by the magnetic field.

Keywords: A1. Directional solidification; A1. High magnetic field; B1. MnBi/Bi eutectic

1. Introduction

Many investigations have focused on controlled directional solidification of binary eutectics and the relationship between their microstructures and solidification conditions [1–3]. In addition to the influence of solidification rate, composition, convection and gravity, the effect of magnetic fields on unidirectional solidification has also been studied. The microstructure of directionally solidified eutectic Bi/MnBi can be characterized by an aligned rod eutectic morphology with a faceted–nonfaceted phase interface. Thus, rod diameter, inter-rod spacing and solidification temperature can be used to monitor solidification process effects. Research on the directional solidification of Bi–Mn compounds has indicated significant gravity and transverse magnetic field related effects [4–6]. It has been shown that growth in a low-gravity environment results in a decrease in MnBi rod diameter and inter-rod spacing due to the elimination of convection in the melt. The directional solidification of Bi/MnBi eutectic has also been investigated in transverse uniform magnetic fields, and results similar to those in low gravity were obtained owing to the damping effect on the gravity-driven convection. Up to now, however, few studies have been devoted to the effect of longitudinal magnetic fields, especially those with high intensities, on the morphology and magnetic properties of Bi/MnBi. This paper reports on an experimental investigation of the influence of a longitudinal high magnetic field on eutectic growth of Bi/MnBi. The results will be discussed in terms of the thermodynamics of the eutectic growth related to the magnetization.

2. Experimental procedure

The Bi-0.72 wt%Mn eutectic alloy was prepared by melting pure Mn(99.9%) and Bi(99.9%) together in a vacuum induction furnace. The alloy was heated to about 500 °C, maintained at this temperature for a certain time with sufficient stirring, and then poured into a cold graphite mould to freeze the melt quickly into a specimen without segregation. The specimens used for the

*Corresponding author. Institut National Polytechnique de Grenoble, ENSHMG, B.P. 95 38402 Saint Martin d' Heres Cedex, Grenoble, France, Tel./fax: +(33)4 76 82 52 62.
E-mail address: xi@hmg.inpg.fr (X. Li).

0022-0248/$ - see front matter © 2006 Elsevier B.V. All rights reserved.
doi:10.1016/j.jcrysgro.2006.10.249

experiments were 8 mm in diameter and 100 mm long. The experimental apparatus is shown in Fig. 1. It consists of a static superconducting magnet and a Bridgman–Stockbarge type furnace equipped with growth velocity and temperature controllers. The superconducting magnet can produce a static axial magnetic field with an adjustable intensity of up to 14 T. The furnace, consisting of a nonmagnetic material, has a negligible effect on field uniformity. The temperature in the furnace can reach 1600 K and is controlled within ± 0.1 K. A water-cooled cylinder containing liquid Ga–In–Sn metal (LMC) is used to cool down the specimen. The temperature gradient in the specimen is controlled by adjusting the temperature of the furnace hot zone, which is insulated from the LMC by a refractory disc. In this work, the temperature gradient in front of the solid/liquid interface was maintained at 50 K/cm at a furnace temperature of 650 °C. The apparatus is designed so that the specimen moves downward while the furnace remains stationary. Growth velocities, V, lie in the range $0.5\,\mu m/s \leqslant V \leqslant 5000\,\mu m/s$. In order to observe the morphology of the liquid/solid interface during the growth of the crystal, quenching experiments were carried out by quickly drawing the specimen into the LMC cylinder to cool the specimen immediately to room temperature.

The specimens obtained from experiments were cut with the edges parallel and perpendicular to the solidification direction, polished and etched. Next, the structure of the samples was characterized by optical microscopy and scanning electron microscopy (SEM). The diameter and inter-fiber spacing of the eutectic MnBi fibers were measured by a computer-aided WT-MiVnt analyzer system. The magnetization characteristics of the specimens were measured using a physical property measurement system.

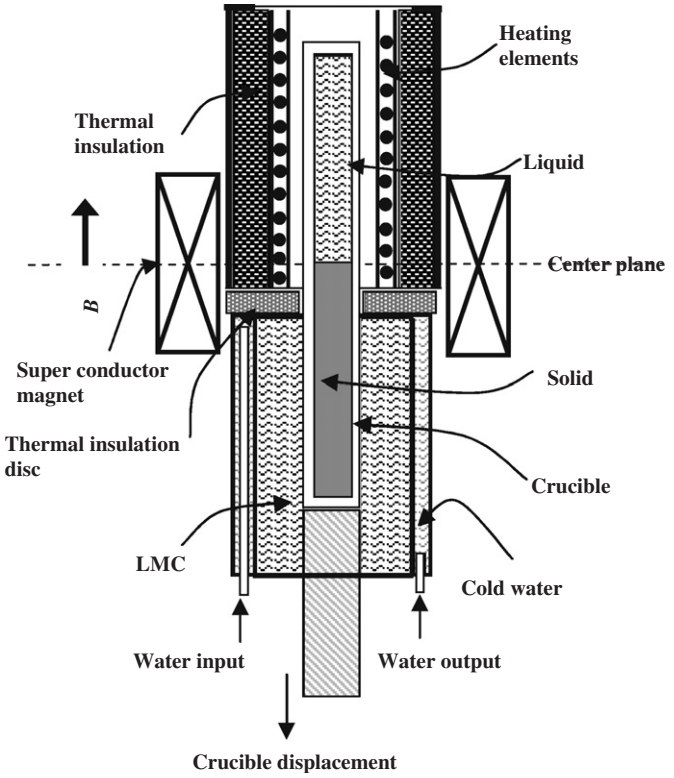

Fig. 1. Schematic illustration of the Bridgman solidification apparatus in a superconducting magnet.

3. Results

Fig. 2 shows the microstructure of the eutectic MnBi/Bi solidified at 1 μm/s. Note that the microstructure of MnBi in the case of no field shows flake and is disordered as mentioned in previous papers [8]. However, with an application of a 2 T magnetic field, the MnBi phase grows in the form of fibers aligned with the solidification direction. On the solid/liquid interface, the MnBi fibers protrude into the liquid, exhibiting a typical characteristic of facet growth. This indicates that the magnetic field has enhanced the directional growth of the MnBi crystal and promoted the formation of regular eutectic. At 2 μm/s, the microstructure without the field (Fig. 3a) exhibits the fiber eutectic form as mentioned in previous papers [8]. Comparison of the microstructures with and without the field indicates that the application of a 10 T magnetic field enhances the alignment of MnBi phase and some aligned flake phases appear at the solid–liquid interface with solidification behavior similar to that of hypereutectic under a magnetic field [7]. At 5 μm/s, the application of the field coarsens MnBi fibers and significantly enhances their growth in the solidification direction (Fig. 4d). The "V" shape MnBi appears on the transverse section (Fig. 4b) suggesting that the field enhances the growth of MnBi phase in the faceted form.

Fig. 5 shows the microstructures of the eutectic MnBi/Bi solidified at 10 μm/s with different magnetic field intensities. With increasing magnetic field intensity, the MnBi fibers become more faceted and the length and diameter of the fibers clearly increases. Fig. 6 shows the diameter (d) and inter-fiber spacing (λ) of the MnBi fibers at 10 μm/s as a function of the external magnetic field.

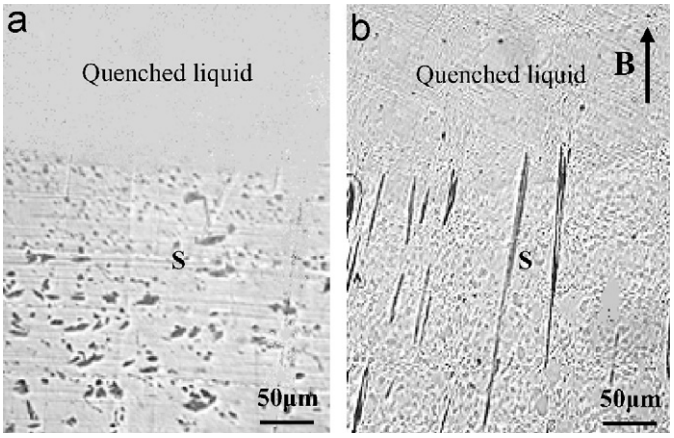

Fig. 2. The microstructure at the solid/liquid interface solidified at 1 μm/s (parallel to the solidification direction)without the magnetic field(a) and with a 2 T magnetic field(b); the black materialis MnBi phase.

Fig. 7 shows the values of diameter and inter-fiber spacing with and without the field. Note that the fiber diameter and inter-fiber spacing decrease with increasing growth rate and the influence of the magnetic field on MnBi growth weakens.

Fig. 8 shows the magnetization hysteresis loops for the same specimens as in Fig. 4. The specimen grown in a magnetic field has a higher coercivity and magnetic anisotropy than the one grown without the magnetic field. This can be attributed to the better orientation of the MnBi fibers and more regular growth produced by the field.

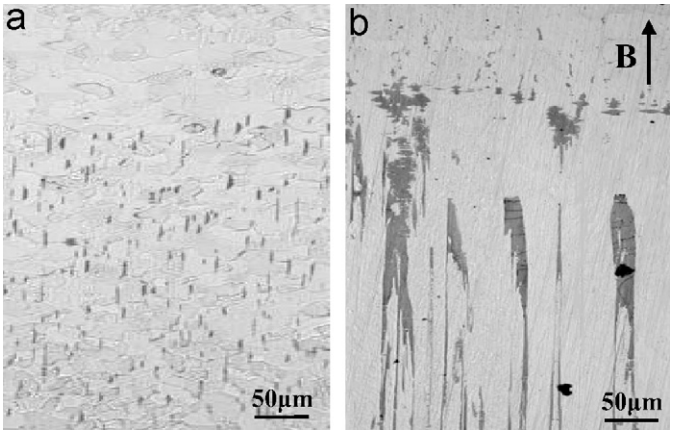

Fig. 3. The microstructure at the solid/liquid interface solidified at 2 μm/s without the field (a) and with a 10 T field (b).

4. Discussion

4.1. The influence of the magnetic field on the growth anisotropy of MnBi crystals

The above results indicate that the magnetic field affects the orientation of MnBi crystals. The crystal aligning and orientating effect of high magnetic fields has been investigated extensively. Research has shown that the magnetizing force rotates the crystals so that their easily magnetized axis aligns with the magnetic field direction [9]. In this experiment, the MnBi crystal in the eutectic alloy could not be rotated by the field. The experiment results show that the fibers grown under a magnetic field were much longer than those without the magnetic field, suggesting that the magnetic field promoted the continuous growth of the MnBi crystal. Therefore, the magnetic field clearly influenced the growth of the eutectic. From a thermodynamic viewpoint, the magnetizing of a crystal is a process involving an input of magnetization energy to the system. The magnetic energy can be expressed as

$$G_{\mathrm{M}} = -\int_0^{H_{\mathrm{ex}}} \mu_0 M \, \mathrm{d}H_{\mathrm{ex}}. \tag{1}$$

For a non-ferromagnetic substance

$$M = \chi H_{\mathrm{ex}}. \tag{2}$$

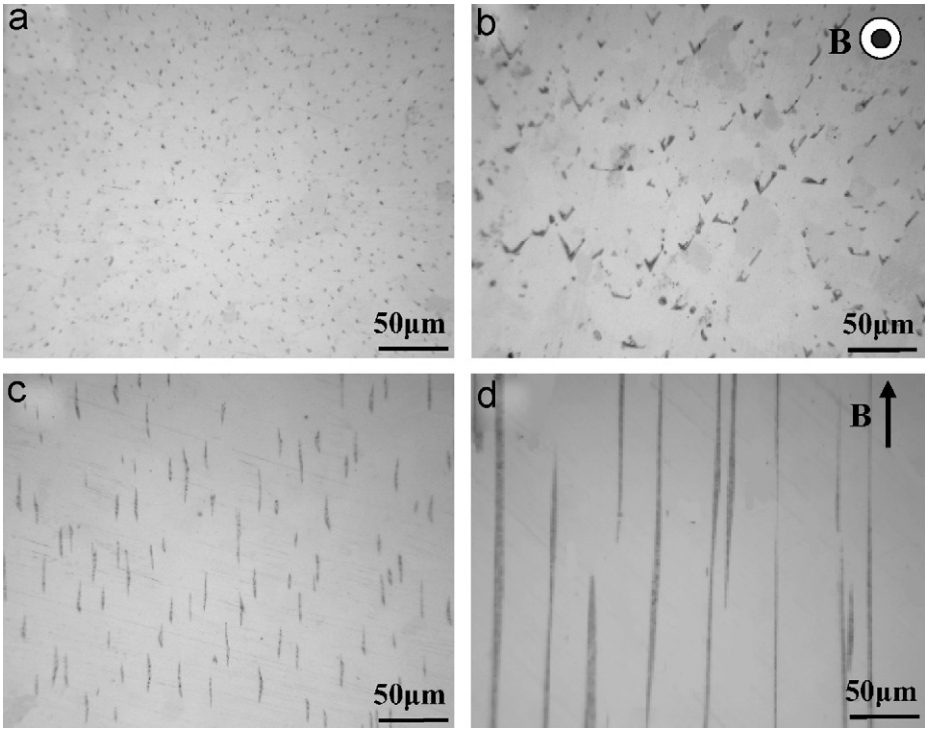

Fig. 4. Microstructure of MnBi/Bi eutectic solidified at 5 μm/s without and with the magnetic field (a) 0 T, transverse section; (b) 10 T, transverse section; (c) 0 T, longitudinal section; (d) 10 T, longitudinal section.

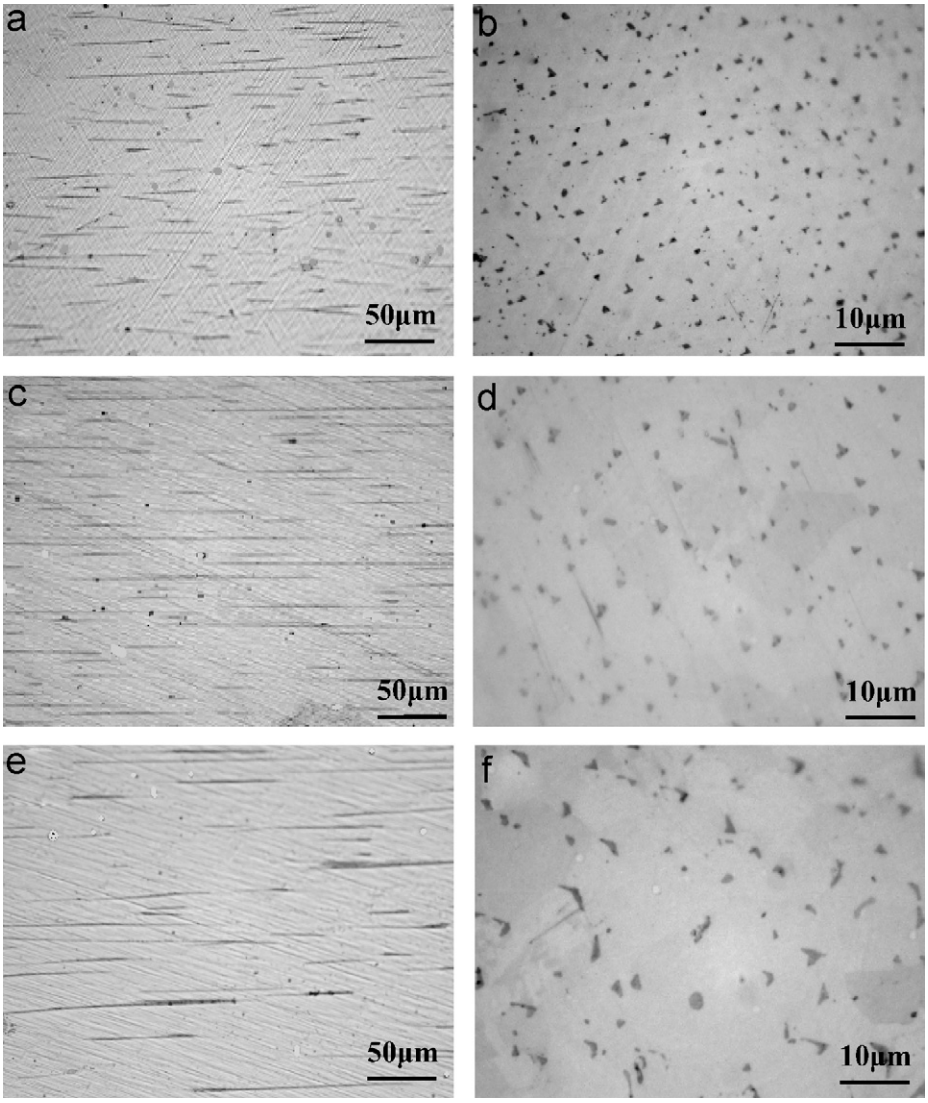

Fig. 5. The microstructures solidified at 10 μm/s under various magnetic field intensities (a) and (b) 0 T; (c) and (d) 5 T; (e) and (f) 10 T.

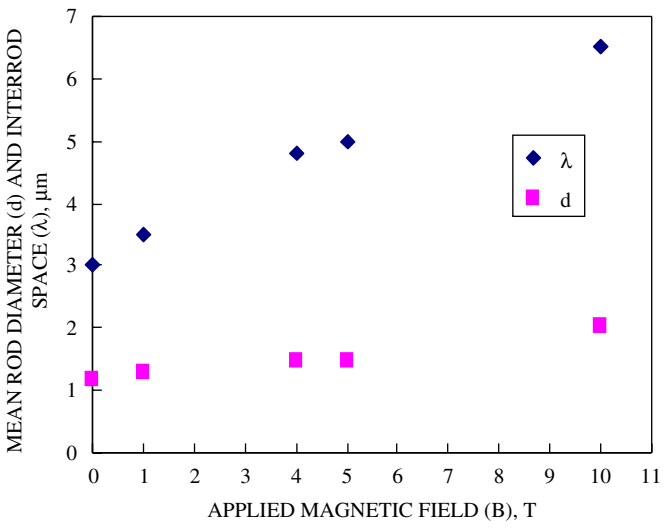

Fig. 6. Influence of high magnetic field on MnBi inter-rod spacing (λ) and rod diameter (d) of eutectic MnBi/Bi alloy solidified at 10 μm/s.

Inserting Eq. (2) into Eq. (1) gives

$$G_M = -\int_0^{H_{ex}} \mu_0 \chi H_{ex}\, dH_{ex} = -\frac{1}{2}\mu_0 \chi H_{ex}^2, \quad (3)$$

where G_M is the magnetization entropy, μ_0 the magnetic permeability, $4\pi \times 10^{-7}\, H\, m^{-1}$, H_{ex} the imposed magnetic field and χ the magnetic susceptibility. For a crystal, the χ-values are heterogeneous for different crystal directions. Therefore, from formula (3), the magnetizing entropy varies correspondingly. MnBi crystal has remarkable magnetic anisotropy and the easily magnetized axis is the *c*-axis [4], so it may be given that $\chi_c > \chi_{ab}$. Then the difference in the magnetizing entropy between crystal direction *c* and *ab* is

$$\Delta G_M^{c\text{-}ab} = G_M^c - G_M^{ab} < 0. \quad (4)$$

This means that the decrease of free energy in the *c*-axis direction is more than in the *ab*-axis direction. Therefore the magnetic field enhances the growth in the *c*-axis

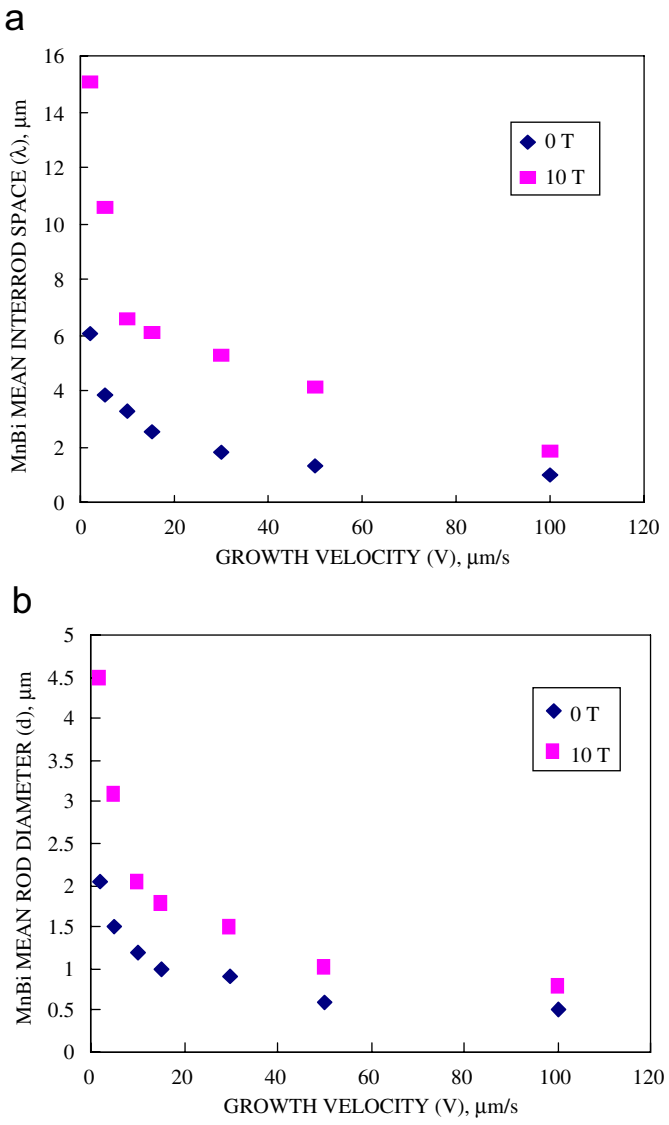

Fig. 7. The MnBi mean inter-rod spacing (λ) and rod diameter (d) of eutectic Bi/MnBi alloy.

direction. Given that the *c*-axis is also the preferred growth direction, the axial magnetic field enhances the growth of MnBi phase in the solidification direction. As a consequence, the facet characteristics of the MnBi crystal may be enhanced resulting in the "V" shape MnBi phase with a strong faceted form (Figs. 3 and 4). Furthermore, the magnetic field can prevent the MnBi from deviating from the solidification direction, also enhancing the growth of MnBi phase in the solidification direction. Owing to the enhancement of MnBi growth in the *c*-axis direction by the field, the coercivity and magnetic anisotropy are increased.

4.2. The influence of the magnetic field on the eutectic point of MnBi alloy

The above results show that the field has coarsened the MnBi fiber significantly. Coarsening of lamellar eutectic has also been observed when an alternating magnetic field was imposed during growth of the eutectic alloy [10]. This was attributed to convection in the melt, given that convection enhances the lateral diffusion of a component in front of the solid/liquid interface. However, in our investigation, the static magnetic field does not stir the melt and therefore damps convection in the melt. Therefore, other effects must be present to cause the coarsening of the MnBi fibers, such as the effect of high magnetic field on the phase diagram of Bi–Mn alloy. Fig. 9a shows the phase diagram near the Bi. Owing to the difference in saturation magnetization of the MnBi and $Mn_{1.08}Bi$ in the Bi–Mn phase diagram, the high magnetic field affects the phase transformation between the MnBi and $Mn_{1.08}Bi$ and raises the phase transformation temperature [11]. This can result in the elevation of the equilibrium liquidus. If the influence of the field on the melting point of Bi is ignored (because it is diamagnetic), the application of the magnetic field will raise the eutectic temperature and the eutectic composition shifts leftward as shown in Fig. 9b. Thus, when the field is applied, the eutectic alloy in the case of no the field will become the hypereutectic. Consequently, some solidification behavior of the hypereutectic alloy appears (Fig. 3b). Moreover, according to the theory concerning eutectic growth, the inter-fiber spacing in the eutectic is expressed as

$$\lambda^2 V = \frac{D\Gamma(1/m_b - 1/m_a)}{C_E(1-k)}, \tag{5}$$

where $k = C_S^*/C_L^*$, $\Gamma = \sigma_{SL}/\Delta S$, λ is the lamellar spacing, D the liquid–solid coefficient, C_E the eutectic composition, k an equilibrium partition, σ_{SL} the liquid–solid surface energy, C_E the eutectic composition and ΔS the change in enthalpy. According to Eq. (5), the field will increase the eutectic spacing owing to the decrease of the eutectic composition (C_E).

5. Conclusions

In directionally solidified Bi/MnBi eutectic, at 1 μm/s, the application of a 2 T axial magnetic field transforms the irregular flake MnBi phases in the case of no field to fibers aligned in the solidification direction. At a growth rate $R \geqslant 2$ μm/s, the magnetic field coarsens the MnBi fibers and increases the ratio of length to diameter. Furthermore, the morphology of MnBi rod crosssections in a high magnetic fields becomes more faceted. With the increase of the magnetic field intensity and the decrease of the growth rate, the influence of the magnetic field becomes strong. The above results may be attributed to the influence of a high magnetic field on the growth anisotropy of MnBi phase and the shift of the eutectic point in Bi–Mn alloy.

Acknowledgments

This work is supported by the Natural Science Foundation of China (no. 50234020, 50225416 and 59871026) and

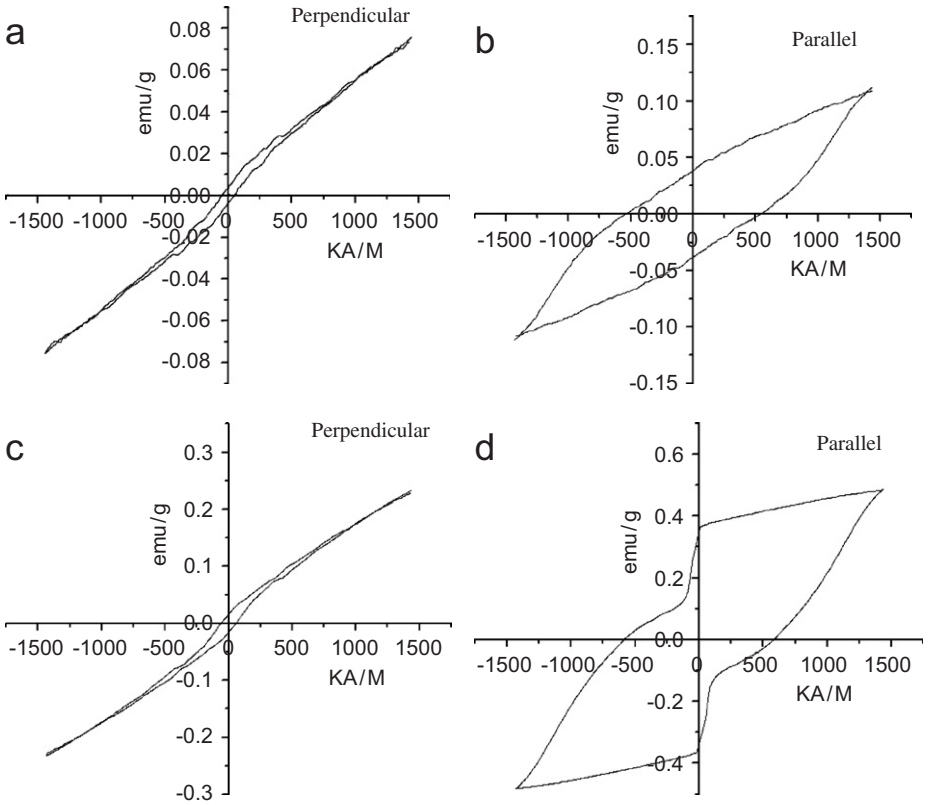

Fig. 8. Hysteresis loops for the sample at $R = 5\,\mu m/s$ with and without magnetic field; (a,b) without magnetic field, (c,d) with 4 T magnetic field. "Parallel and perpendicular" indicate the directions of the magnetic field imposed for the magnetization measurement with respect to the magnetic field imposed during the solidification.

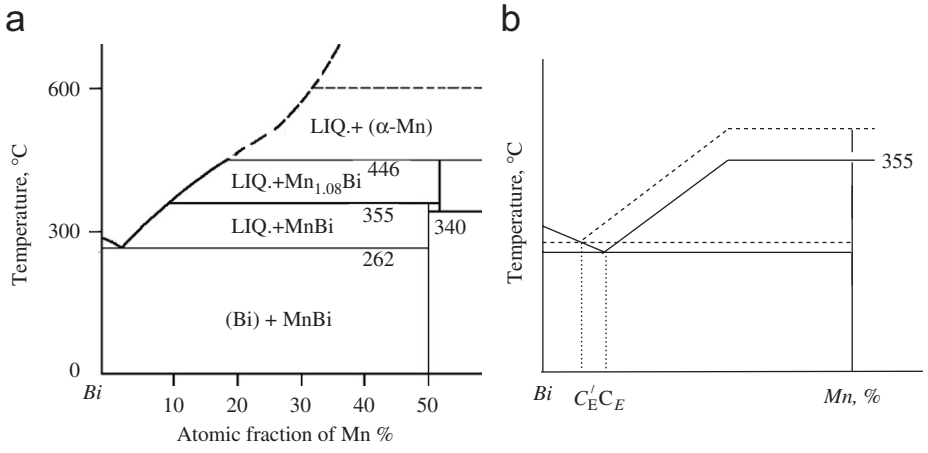

Fig. 9. The effect of a high magnetic field on the phase diagram of the Bi-Mn system. (a) The phase diagram of the Bi–Mn system near the Bi; (b) Schematic illustration of the phase diagram near Bi without and with a magnetic field. The magnetic field influences on the eutectic point by shifting the eutectic temperature upward and the eutectic composition to left.

the Science and Technology Committee of Shanghai (04ZD14002) and one of the authors (LX) is also grateful for an Egide/Eiffel Doctorate Scholarship.

References

[1] W.A. Tiller, Liquid Metals and Solidification, ASM, Metal Park, OH, 1958, p. 276.
[2] F.R. Mollard, M.C. Flemings, Trans. TMS-AIME 239 (1967) 1534.
[3] M. Tassa, W. Kurz, J. Crystal Growth 28 (1976) 38.
[4] R.G. Pirich, Mettall. Trans. 15A (1984) 2139.
[5] J.L. Decarlo, R.G. Pirich, Metall. Trans. A 15A (1984) 2155.
[6] R.G. Pirich, D.J. Larson, Materials Processing in the Reduced Gravity Environment of Space, Elsevier Science Publishing Co., New York, NY, 1982 523.

[7] X. Li, Z.M. Ren, K. Deng, Y.Q. Zhunag, K.D. Xu, Acta Matall. Sin. 41 (6) (2005) 40.
[8] G.F. Eisa, W.R. Nilocox, J. Crystal Growth 78 (1986) 159.
[9] H. Wang, Z.M. Ren, K. Deng, Acta Matall. Sin. 38 (1) (2002) 41.
[10] J.Z. Jin, K.F. Kobayashi, P.H. Shingu, Transactions A 15A (1984) 307.
[11] X. Li, Z.M. Ren, Y. Gao, K. Deng, Y.Q. Zhuang, K.D. Xu, Chin. J. Nonferr. Met. 15 (3) (2005) 397.

[A7] Xi Li, Zhongming Ren,Yves Fautrelle

Effect of a high magnetic field on the phase transformation, morphology and magnetic properties of the MnBi and $Mn_{1.08}Bi$ compounds.

Effect of a high magnetic field on the phase transformation, morphology and magnetic properties of the MnBi and $Mn_{1.08}Bi$ compounds

Xi Li[a, b], Zhongming Ren[a], Yves Fautrelle[b]

[a] *Department of Material Science and Engineering, Shanghai University, Shanghai, 200072, P. R. China*

[b] *EPM-Madylam, ENSHMG BP 38402 St Martin d'Heres Cedex, France*

Abstract

Owing to the change in the magnetic susceptibility while the phase transformation occurs, a new method is suggested to determine the phase transformation temperature by measuring the temperature at which the magnetic force changes abruptly in a gradient magnetic field. The MnBi/$Mn_{1.08}$Bi phase transformation temperature under a high magnetic field is measured by this method and the result indicates that the magnetic field has increased the phase transformation temperature; as a result, a 10T-magnetic field has raised the phase transformation temperature about 20℃. The morphology and magnetic properties of the MnBi phase are also investigated and it is found that the field has cracked the MnBi crystal along the (001)-crystal plane and the split MnBi crystals align and aggregate along the magnetic field direction. Along with the change of the MnBi phase morphology, the magnetic property changes greatly; as a consequence, the saturation magnetization M_s and the magnetic susceptibility χ increase and the coercive field H_c and the remnant magnetization M_r decrease. This implies that the field causes the magnetic property of the MnBi phase to transform towards soft magnetism. The above results may be attributed to the magnetic energy and the force caused by the magnetic field.

Keywords: High magnetic field; Phase transformation; Bi-Mn alloys; Magnetization; Magnetic force

1. Introduction

Recently, owing to the development in the superconducting magnets, a high magnetic field up to 12T has been widely used to improve material properties during material processing such as the solidification, the electro-deposition and the phase transformation [1]. The application of a high magnetic field to the phase transformation has been the object of great attention in the area of electromagnetic processing of metallic materials. Usually, since the saturation magnetization of the parent and product phases is different, the application of an external magnetic field can modify the Gibbs free energy of phases and then affect the phase equilibrium and transformation speed. Some works have been performed on the influence of the magnetic field on the solid phase transformation. Martin *et al.* [2] reviewed this topic and demonstrated that the magnetic field raised the martensite starting temperature by a few degrees. Recently, the influence of a high magnetic field on the phase transformation in Fe-C system becomes the focus of the research and the results indicate that the phase diagram was shifted upward as the magnetic field was applied [3, 4]. The austenite-to-pearlite [5], the austenite-to-ferrite [6-8], the austenite-to-baintenite transformations [9] and the recovery as well as recrystalization[10] have also been investigated experimentally. All works have proved that the magnetic field had affected the phase

transformation. However, there are few reports about the influence of a high magnetic field on the phase transformation during the solidification process. As the saturation magnetization of the $Mn_{1.08}Bi$ and MnBi phases is widely different, the application of an external magnetic field will

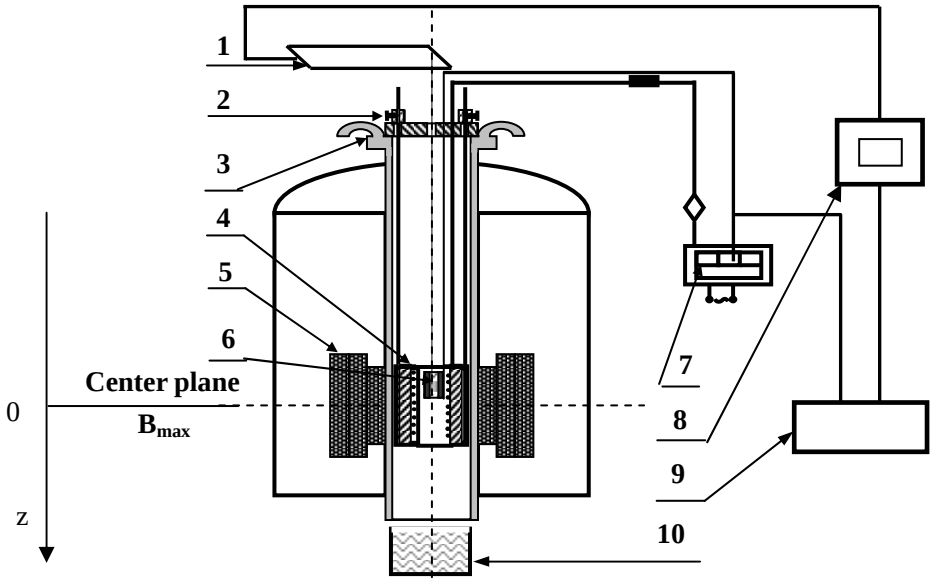

Fig. 1. Schematic diagram of the experimental device to fabricate samples and measure the phase transformation. 1, Force sensor; 2, furnace frame; 3, water-cool cover; 4 heat furnace; 5, superconductor magnet; 6, sample; 7, controlling temperature system; 8, dynamic resistance strain meter; 9, *X*-*Y* recorder; 10, quenching tank.

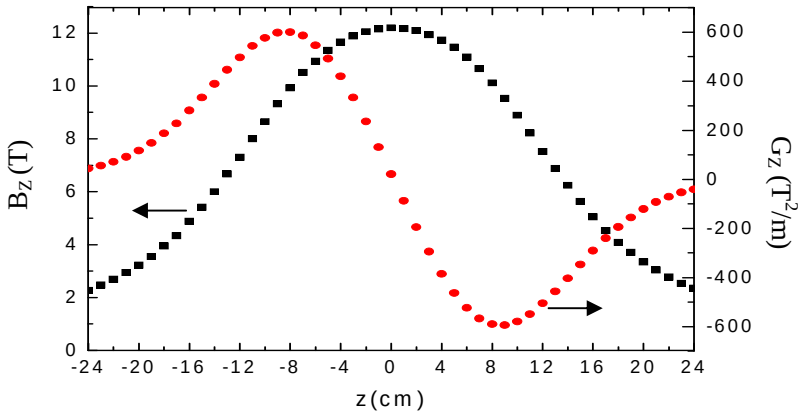

Fig. 2. Field profiles in the magnetic field operating at 12T. B_z is the vertical component of the field on the axis of the coil. G_z is the vertical component of grad ($B_z^2/2$) on the axis of the coil (i.e. $B_z dB_z/dz$), z is the distance above the coil.

modify the Gibbs free energy of the phases and then affect the $Mn_{1.08}Bi$/MnBi phase equilibrium. Moreover, the MnBi compound has unique magnetic and magneto-optical properties and characteristics in solidification [11-14]. Therefore, to investigate the effect of the magnetic field on

the phase transformation during the solidification process, the $Mn_{1.08}Bi$/MnBi phase transformation is chosen. This paper has investigated on the effect of a high magnetic field on the phase transformation, morphology and magnetic properties of the compounds. Change in the morphology and magnetic properties of the compounds around the phase transformation temperature under a high magnetic field are investigated in detail. The micro-zone x-ray diffraction (XRD) is applied to identify the phases with two different morphologies (cubic and ellipsoidal). The effect of the magnetic field on the phase transformation is proved more by XRD and investigating on the change in the morphology and magnetic property. In the light of the thermodynamics and magnetics, the above experimental results are analyzed and discussed.

2. Description of the experiments

Bi-Mn alloys with composition (wt.%) of 6%Mn and 21%Mn were prepared using bismuth (99.999% purity) and electrolytic manganese (99.5%). Raw materials were melted in an induction

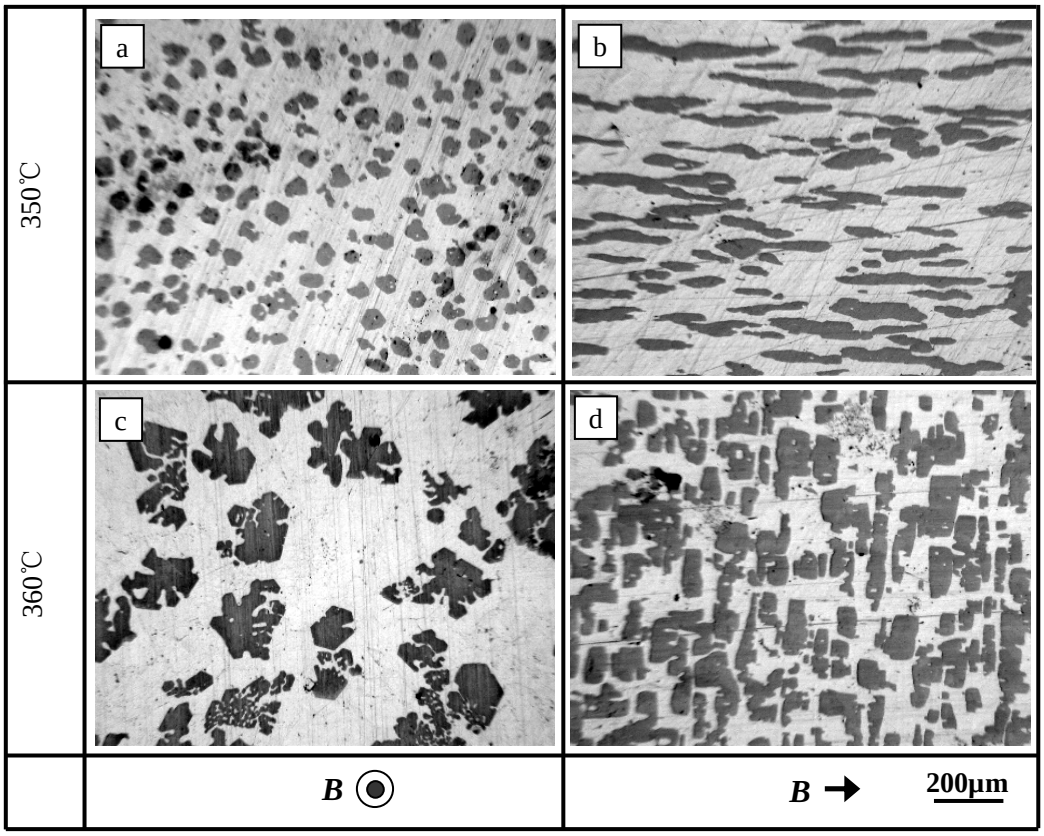

Fig. 3. Microstructures solidified from a certain temperature at a rate of 10K/min after holding temperature for 60 min at this temperature under a 10T-magnetic field.

furnace and cast to a graphite mold under argon at a pressure of 50.6 kPa. The samples with 9.5 mm in diameter and 25 mm in length were sealed in a graphite tube and inserted into a resistance furnace placed into the magnet. The intensity of the magnetic field (up to 14T) could be adjusted and the temperature in the furnace chamber could be controlled automatically during the experiment as shown in Fig. 1. The typical field and force profiles of the magnetic field are shown

in Fig. 2. The temperature in the furnace could reach 1000℃, and was measured with the precision of ± 1K by a NiCr-NiSi thermocouple which was in direct contact with the sample.

A method was applied to determine the phase transformation by measuring the change in the magnetic force. Under a gradient magnetic field, the vertical magnetic force F_z is:

$$F_z = (\chi/\mu_0) B_z \, \mathrm{d}B_z/\mathrm{d}z \qquad (1)$$

where χ is the susceptibility of the substance, μ_0 the permeability of free space, B_z the magnetic field induction or magnetic flux density on vertical direction. In S.I. unites, F is in N/kg,

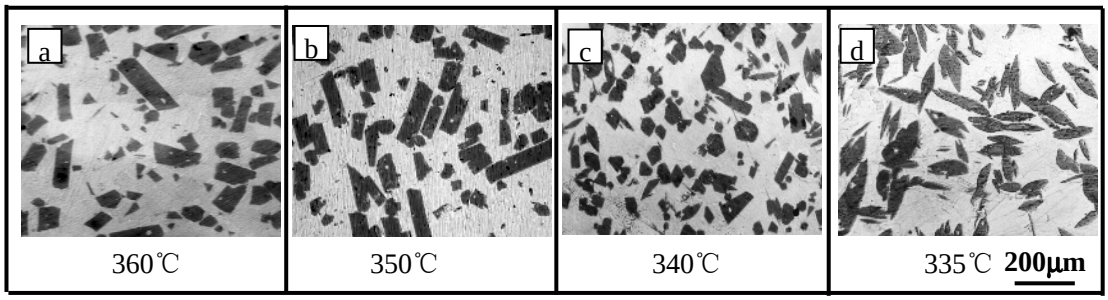

Fig. 4. Microstructures solidified from 380℃ at a rate of 10K/min to a certain temperature, and then quenched.

Primary phase (dark) have different morphologies at different temperatures.

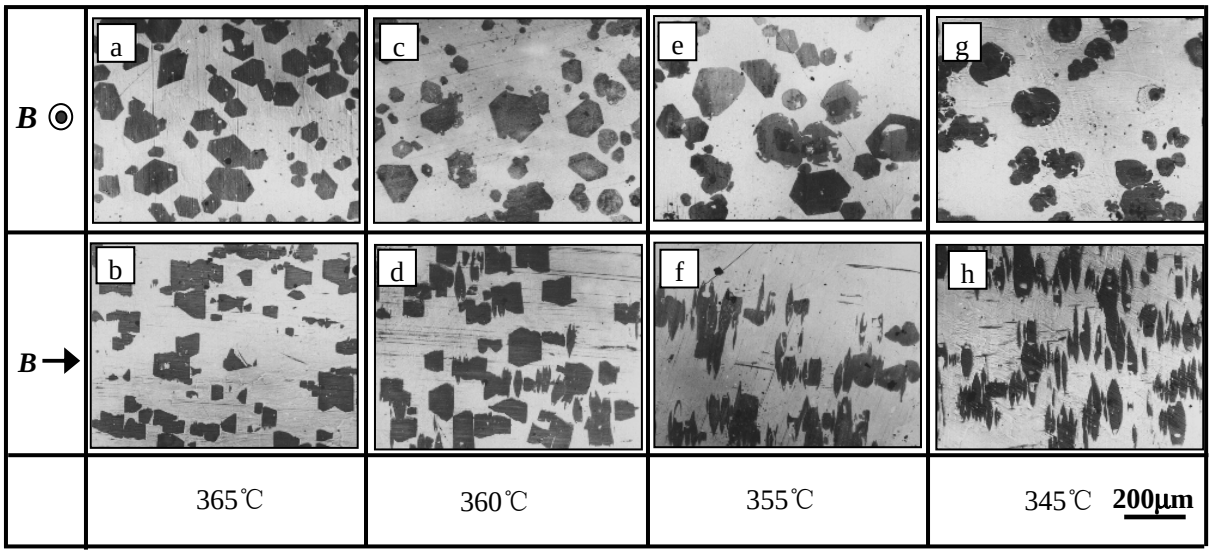

Fig. 5. Microstructures quenched at various temperatures upon cooling from 400℃ at a rate of 10K/min under a 10T-magnetic field.

and χ in m^3/kg. The value of μ_0 is $4\pi \times 10^{-7}$ H/m. Usually, the phase transformation can lead to the change in the magnetic susceptibility. From formula (1), it can be learned that the magnetic force will change during the phase transformation. According to the phase diagram of Bi-Mn system [16], the $Mn_{1.08}Bi$ compound is formed by the peritectic reaction of Mn + Bi-rich liquid solution at 446℃; and the ferro-to-paramagnetic transition upon heating to 355℃ and

para-to-ferromagnetic transition upon cooling to 340℃ correspond respectively to the phase decomposition of $MnBi \rightarrow Mn_{1.08}Bi + Bi$ and $Mn_{1.08}Bi \rightarrow MnBi + Mn$. Since the $Mn_{1.08}Bi$ and MnBi are paramagnetic and ferromagnetic, respectively, during the $Mn_{1.08}Bi$/MnBi phase transformation, the magnetic force changes obviously. Therefore, the phase transformation temperature can be determined by measuring the temperature at which the magnetic force changes abruptly in a gradient magnetic field. The experimental procedure is the follow: an alumina crucible containing the Bi-21wt%Mn sample was hung by a copper wire in a gradient magnetic field and the copper wire was connected to a self-designed magnetometer with a force sensor. The samples were heated to 380℃ by a rate of 0.25K/min, and then cooled to below 330℃ by a rate of 0.5K/min, meanwhile the force and temperature values were measured simultaneously. A sharp increase (decrease) of the force indicated the occurrence of paramagnetic (ferromagnetic) to ferromagnetic (paramagnetic) transition during cooling (heating) at $\boldsymbol{T_c}$ .Thus, $\boldsymbol{T_c}$ can be detected by the sharp change in the force. The error is around 5%.

The Bi-6wt%Mn alloy was prepared to investigate on effects of the magnetic field on the morphology and magnetic properties of the MnBi compounds. For this, the Bi-6wt%Mn samples were solidified under various solidification conditions and the magnetic field was imposed in a certain stage during the solidification process. Experimental details will be introduced later in the experimental result part. The samples obtained in the above experiment were sectioned along the

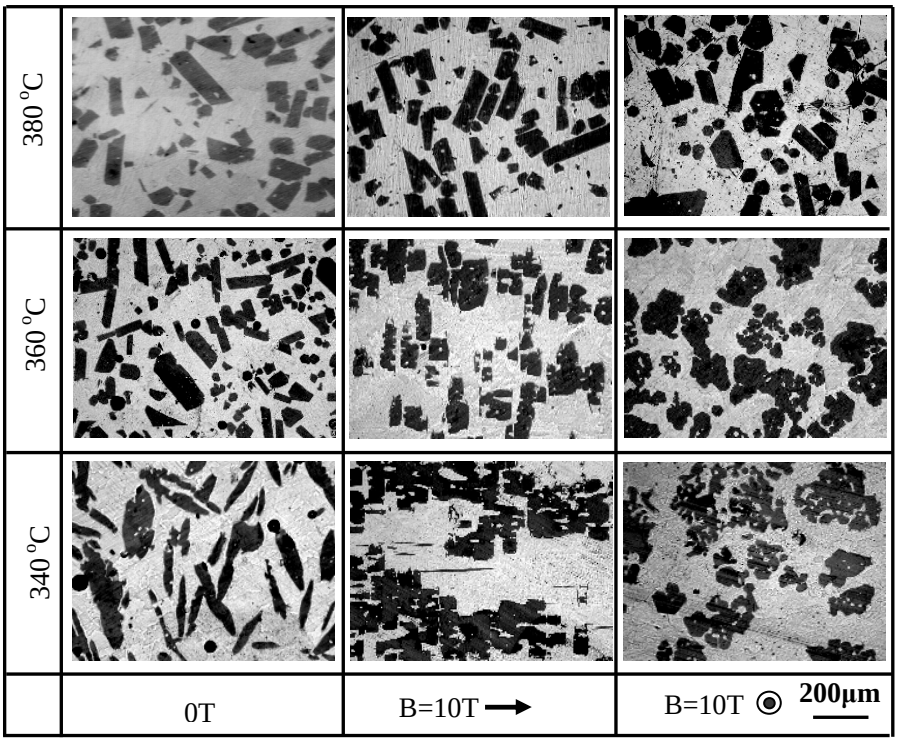

Fig. 6. Microstructures solidified from 400℃ at a rate of 10K/min to a certain temperature and held for 30min without or with a 10T-magnetic field, and then quenched.

direction parallel and perpendicular to the applied magnetic field $\boldsymbol{H_s}$ during the solidification. The microstructures on both longitudinal and transverse sections of the samples were polished mechanically and characterized by the optical microscopy, the scanning electron microscopy (SEM), and the x-ray diffraction (XRD) with Cu-K_α radiation, respectively. Magnetic

measurements were conducted under the applied magnetic field $\boldsymbol{H_m}$ up to 50 kOe by a physical properties measurement system (PPMS/Quantum Design). Samples were cut in the shape of cubes (to avoid demagnetization factor consideration) with the edges parallel and perpendicular to the $\boldsymbol{H_s}$ direction.

3. Results

3.1. Influence of a high magnetic field on the microstructures

Fig. 3 shows the microstructures of the samples solidified from a certain temperature by a rate of 10K/min to 262℃ (eutectic point temperature) under a 10T-magnetic field. The microstructures of the sample solidified from 350℃ (below 355℃) [Figs. 3(a) and 3(b)] show that the elongated MnBi crystals (dark gray) are oriented with a longer axis along the magnetic field direction in the Bi matrix (white). The hexagonal profile of the crystals only appears in the section perpendicular to the field. Furthermore, the XRD patterns show that the <001>-crystal direction (i.e., the easy

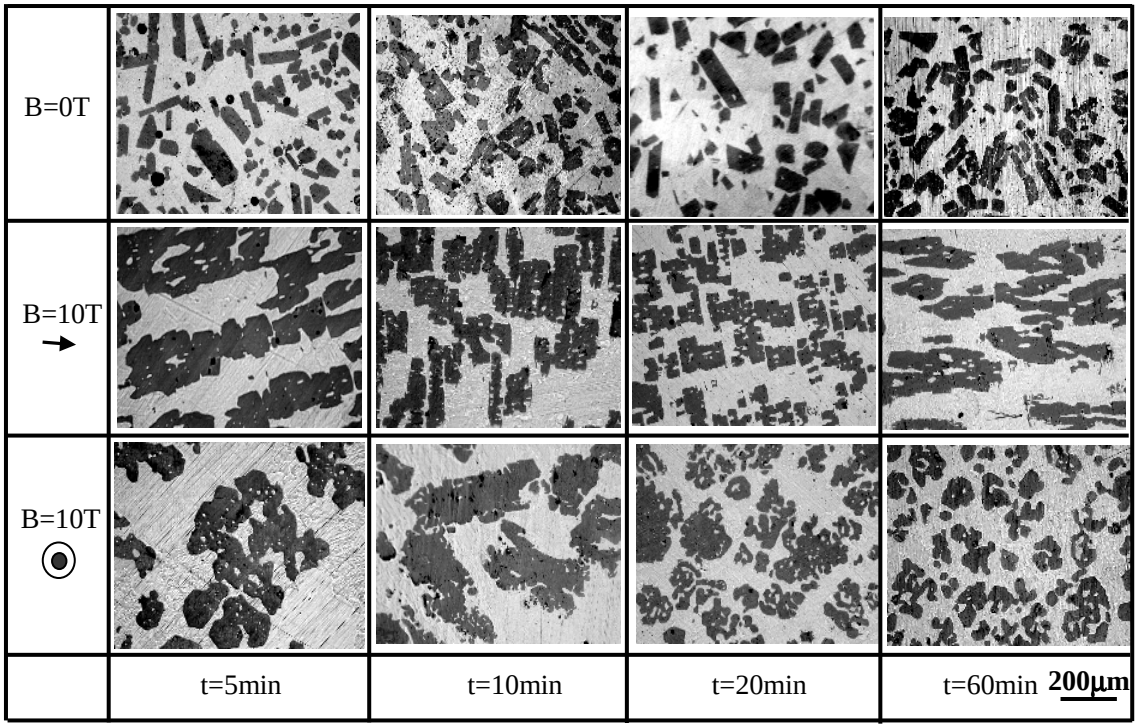

Fig. 7. Microstructures cooled from 400℃ at a rate of 10K/min to 360℃ and held for a certain time under a 10T-magnetic field, and then quenched.

magnetization axis) of hexagonal MnBi crystal is aligned along the magnetic field direction. Figs. 3(c) and 3(d) show the microstructures of the sample solidified from 360℃ (above 355℃). Compared with that of the sample solidified from 350℃, it can be observed that the morphology of the MnBi crystal is changed significantly. As a consequence, MnBi crystals are cracked along the (001)-crystal plane and oriented with a shorter axis along the $\boldsymbol{H_S}$ direction.

To study the morphological change of the compounds in detail, the samples were quenched in water to keep the morphology at different solidification stages. Fig. 4 shows the microstructures of the samples cooled from 380℃ by a rate of 10K/min to a certain temperature and quenched. It

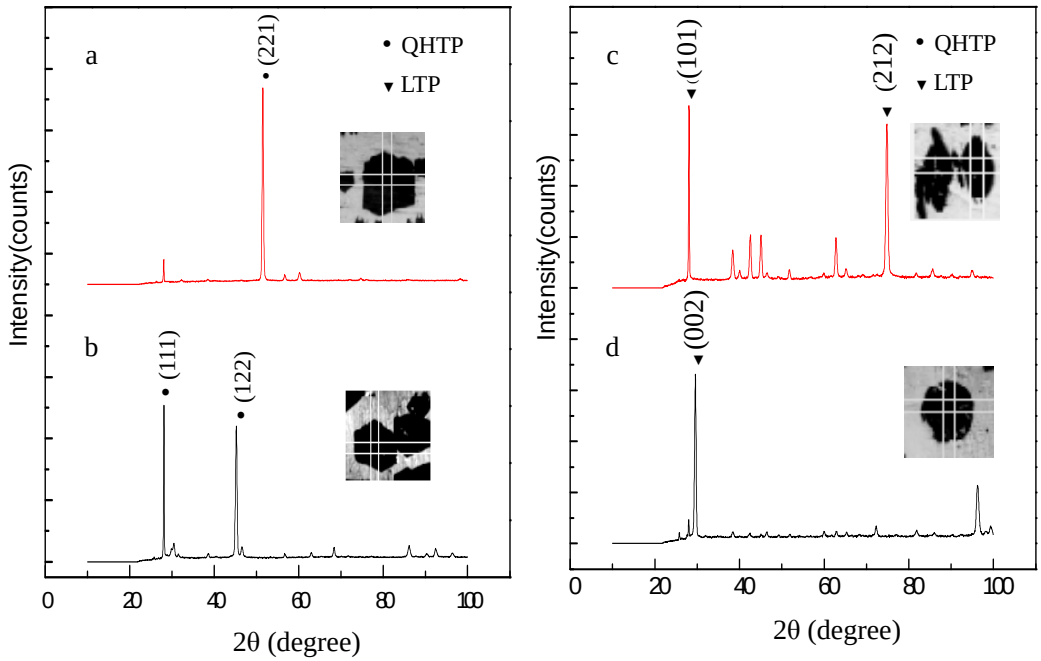

Fig. 8. Micro area x-ray diffraction (XRD) patterns of the cubic phase [(a), (b)] and the ellipsoidal phase [(c), (d)].

can be observed that the morphology of the compounds changes greatly near 340℃, and the morphology transforms from cubic to ellipsoidal. The above result implies that during the $Mn_{1.08}Bi$-to-MnBi phase transformation, the morphology of the primary phase changes from cubic to ellipsoidal. Moreover, it is suggested that the phase transformation may be studied by investigating the change in the phase morphology. For this, the microstructures under a 10T-magnetic field are investigated and the results are shown in Fig. 5. The solidification condition for these samples is otherwise identical to that in Fig. 4. It can be observed that under a 10T-magnetic field, new morphology phase (ellipsoidal) emerges on the edge of the cubic phase at 360℃, which suggests that the $Mn_{1.08}Bi$-to-MnBi phase transformation takes place near 360℃. To confirm the above results more, the samples were cooled from 400℃ by a rate of 10K/min to a certain temperature, and then hold for 30min and quenched. Fig. 6 shows the microstructures of the samples quenched at 380℃, 360℃ and 340℃, respectively. It can be observed that when the samples is quenched at 380℃, there are no clear influences of the field on the morphology of the primary phase; however, at 360℃ and 340℃, the field has oriented and cracked the primary phase. Since a 10T-magnetic field has few influences on the paramagnetic $Mn_{1.08}Bi$ phase; however, the alignment of the ferromagnetic MnBi phase under the magnetic field is very easy and a 10T-magnetic field is strong enough to align it well [17]. Therefore it can be deduced that the primary phase when quenched at 380℃ is the $Mn_{1.08}Bi$ phase and is the MnBi phase. when 360℃ and 340℃.The above results indicate that a 10T-magnetic field has induced the $Mn_{1.08}Bi$-to-MnBi phase transformation at the temperature ranging between 360℃ and 380℃. Furthermore, it is found that the field has cracked the MnBi phase. In order to investigate the phase cracking mechanism under the magnetic field, the samples were cooled from 400℃ to 360℃ and held for different time under a 10T-magnetic field, and then quenched. Fig. 7 shows the microstructures with various holding temperature time before quenching. It can be observed that

with the increase of the holding temperature time under the magnetic field, the phase is cracked gradually along the plane perpendicular to the magnetic field, and the split phase is aligned and aggregated along the magnetic field direction.

Further, the micro-area x-ray diffraction (XRD) was applied to identify the cubic and ellipsoidal phases. Fig. 8 shows the micro-area XRD patterns for different morphology phases in Fig. 5. Fig. 8(a) and Fig. 8(b) show the micro-area XRD patterns on the two different crystal planes of the cubic phase, respectively. From the peaks, it can be determined that the cubic phase is the quenched high temperature phase (QHTP) (HTP in the quenched state is named QHTP). This

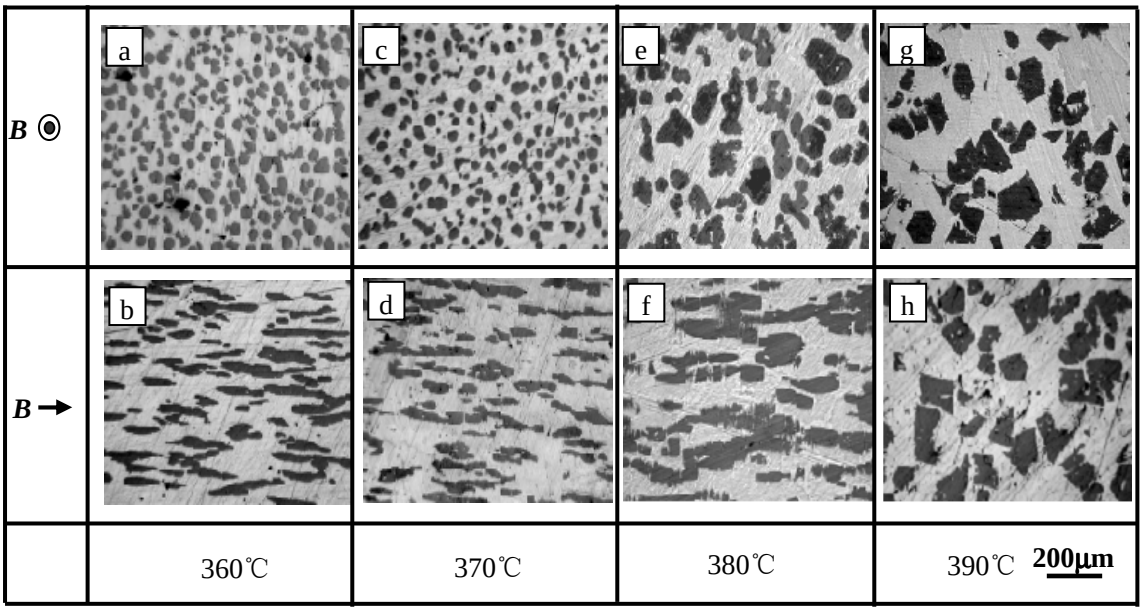

Fig. 9. Microstructures quenched at a certain temperatures upon heating at a rate of 1K/min under a 10T-magnetic field.

means that before quenched, the cubic phase is the high temperature $Mn_{1.08}Bi$ phase (HTP). Fig. 8(c) and Fig. 8(d) show the micro-area XRD patterns on the two different crystal planes of the ellipsoidal phase, respectively. From the peaks, it can be determined that the ellipsoidal phase is the low temperature MnBi phase (LTP). The above results show that the change in the morphology is brought by the change in the structure of primary phase during the phase transformation process. Therefore, it is reasonable that the phase transformation is estimated Fby investigating the morphological change of the primary phase.

To investigate the effect of the magnetic field on the MnBi-to-$Mn_{1.08}Bi$ phase transformation, the morphology of the primary phase upon heating under a 10T-magnetic field is observed. Fig. 9 shows the microstructures quenched at various temperatures upon heating by the rate of 1K/min under a 10T-magnetic field. It can be observed that the primary phases of the samples quenched at 360℃ and 370℃ align well and their alignment behaviors are similar to that of the ferromagnetic MnBi phase [17]. Thus, it can be deduced that the phases when quenched at 360℃ and 370℃ are MnBi phase. However, the alignment of the phases at both 380℃ and 390℃ is disordered and the cubic phase appears. Since a 10T-magnetic field is strong enough to promote the alingment, it can be deduced that the phases at 380℃ and 390℃ are the paramagnetic $Mn_{1.08}Bi$ phase. The above results show that the MnBi-to-$Mn_{1.08}Bi$ phase transformation under a 10T-magnetic field takes place at the temperature ranging between 370℃ and 380℃.

3.2. Measurement of the $Mn_{1.08}Bi$/MnBi phase transformation temperature

To study quantitatively the change in the $Mn_{1.08}Bi$/MnBi phase transformation temperature under the magnetic field, the magnetic force on the sample has been measured by using the method mentioned in experiment part. Fig. 10 shows the typical force and temperature curves in the gradient magnetic field of B=10T and $B_z dB_z / dz = 400 T^2/m$. From this figure, it can be observed that upon heating, the force decreases gradually at first, and at 375℃, the force drops abruptly to its minimum. This indicates that the MnBi-to-$Mn_{1.08}Bi$ phase transformation occurs at this temperature. Afterwards, further increasing temperature up to 380℃ does not cause the apparent change in the force. During cooling from 380℃, the force increases abruptly at 362℃, indicating the occurrence of the $Mn_{1.08}Bi$-to-MnBi phase transformation at this temperature. The above result shows that this method is very sensitive and feasible to detect the occurrence of the phase transformation. Fig. 11 shows the phase transformation temperature as a function of the magnetic field intensity upon heating and cooling, respectively. From this figure, it can be learned

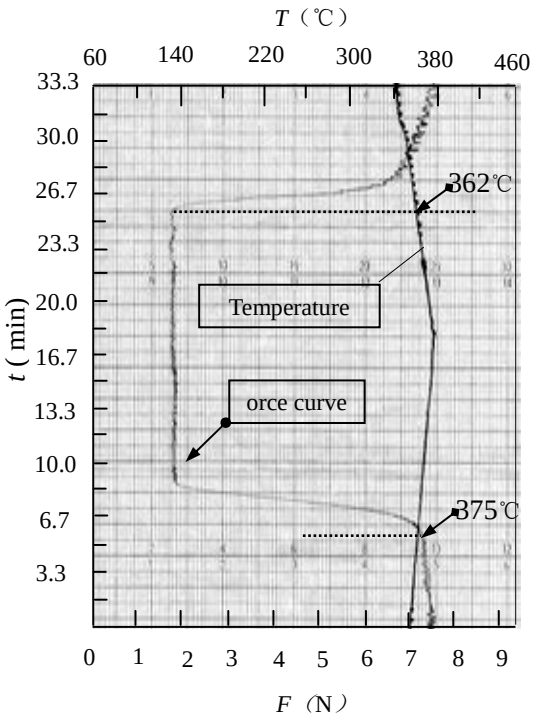

Fig. 10. Typical measurement curves of the force and temperature upon heating and cooling Bi-21wt%Mn alloy under a 10T-magnetic field.

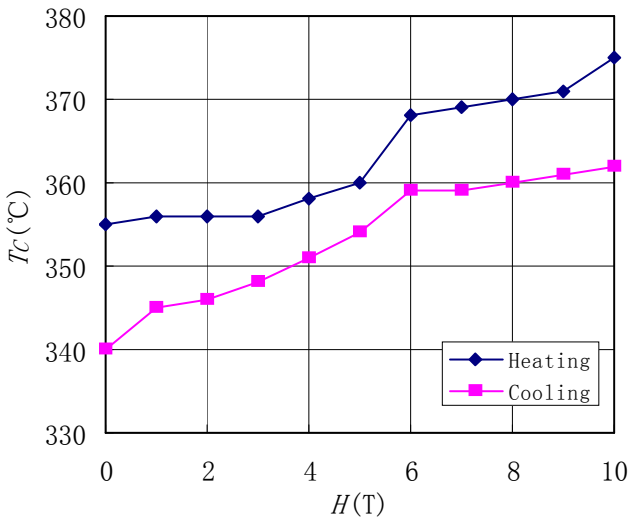

Fig. 11.The $Mn_{1.08}Bi$/MnBi phase transformation temperature T_C as a function of the external magnetic field H during heating and cooling, respectively.

that the field has raised the phase transformation temperature. On the whole, the phase transformation temperature increases with the increase of the magnetic field intensity.

3.3. Influence of a high magnetic field on the magnetic properties

During the phase transformation, the magnetic property of the compounds will change. Therefore, the phase transformation can be detected more by investigating the effect of the magnetic field on magnetic properties of the alloy. Moreover, since the magnetic property is an important physical one concerning the MnBi compound; by studying it, other effects of the

magnetic field may be discovered. To study the magnetic property, the magnetization and

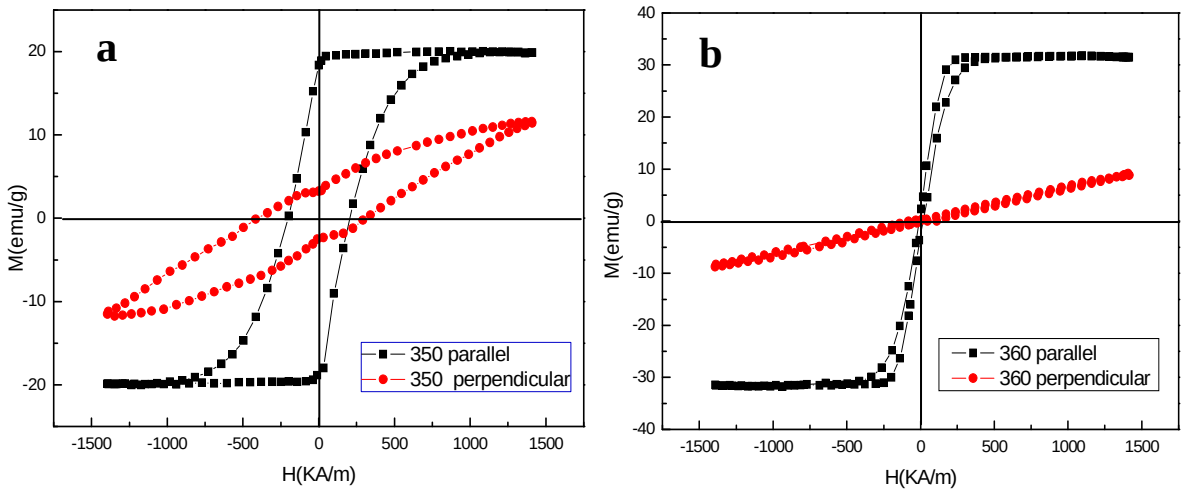

Fig. 12. Hysteresis loops of the same samples as shown in Fig. 3.

(a) 350℃; (b) 360℃.

"parallel and perpendicular" indicate directions of the magnetic field imposed for the magnetization measurement (H_m) with respect to the magnetic field imposed during the solidification (H_s).

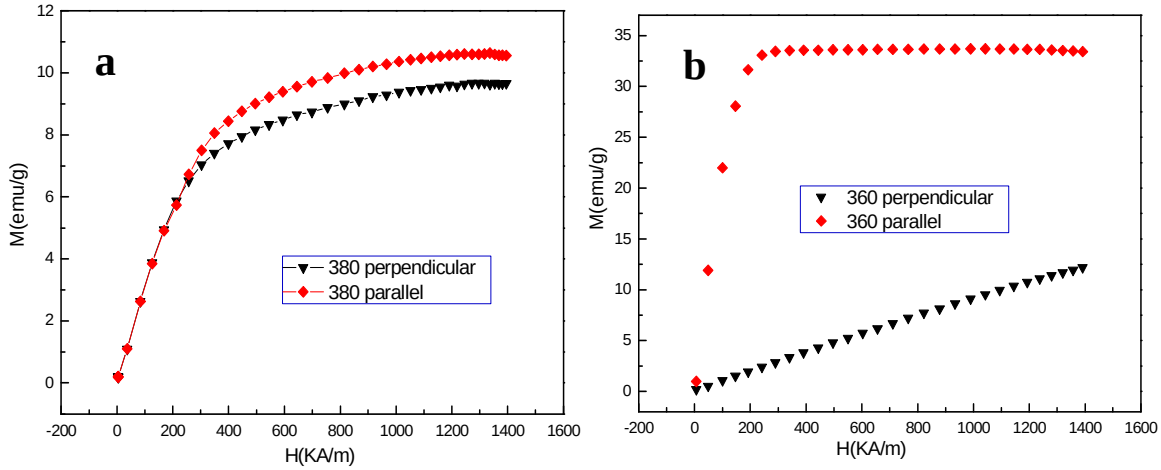

Fig. 13. Magnetizations curves of the same samples as shown in Fig. 6.

(a) 380℃; (b) 360℃.

"parallel and perpendicular " indicate directions of the magnetic field imposed for the magnetization measurement (H_m) with respect to the magnetic field imposed during the solidification (H_s).

hysteresis loops of the alloy are measured. Because Bi is diamagnetic, its effect has been ignored and only the MnBi compounds have been considered in the magnetization measurement.

Fig. 12 shows the hysteresis loops parallel and perpendicular to the H_s direction for the samples

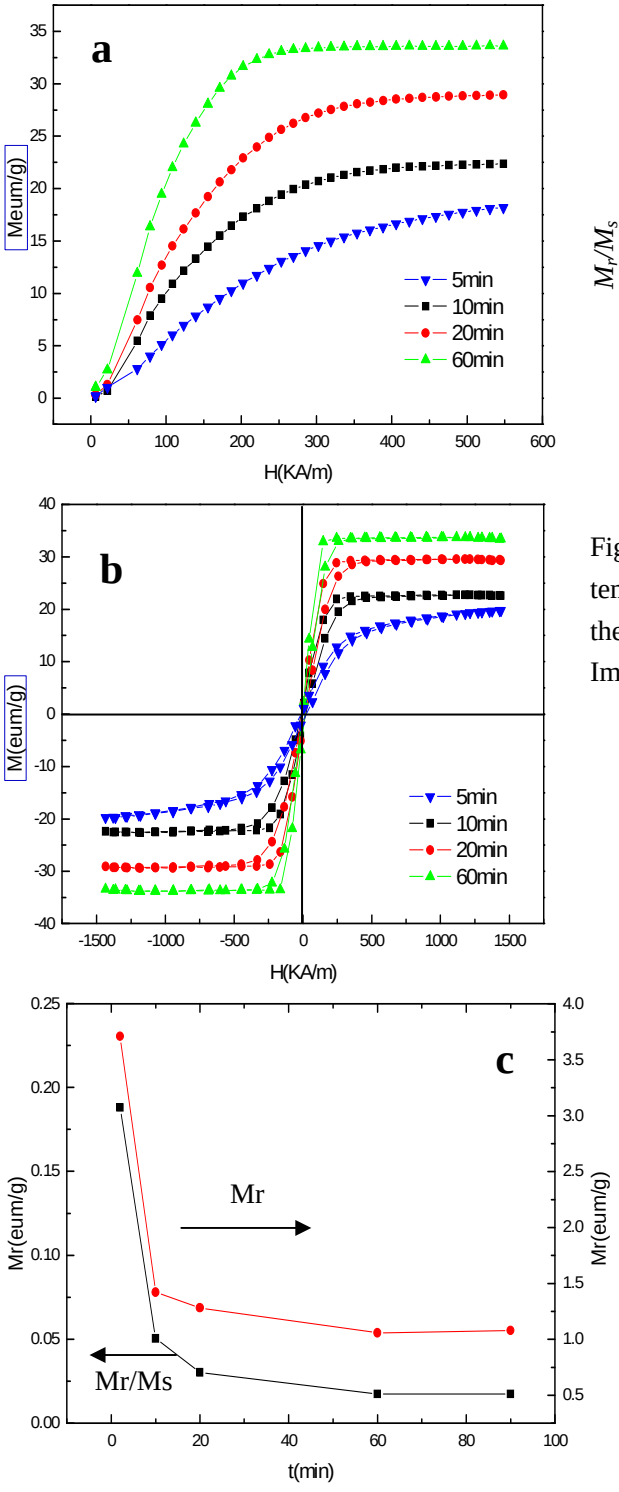

Fig. 14. The magnetic properties of the same sample as shown in Fig. 7.

(a) Magnetizations; (b) Hysteresis loops; (c) The remnant magnetization M_r and the M_r/M_s.

The directions of the magnetic field imposed for the magnetization measurement is parallel to the magnetic field imposed during the solidification.

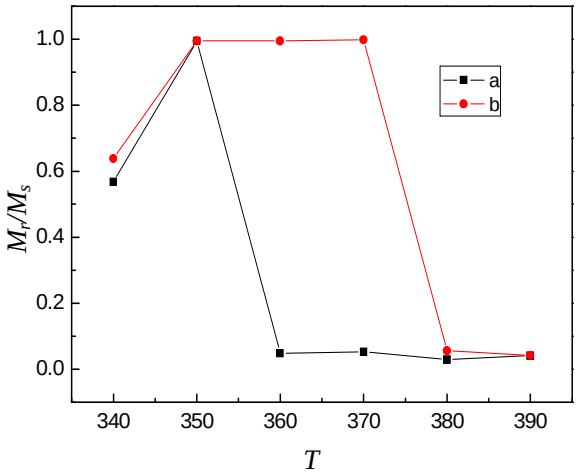

Fig. 15. The M_r/M_s as a function of the solidification temperature under a 10T-magnetic field. (a) Imposed the field during holding and cooling process; (b) Imposed the field during entire experiment process.

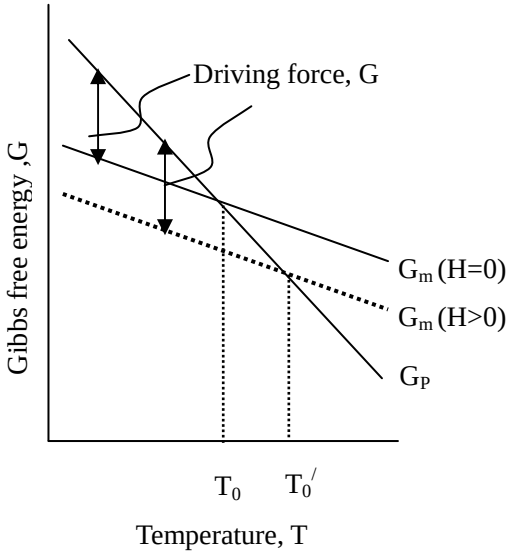

Fig. 16. Schematic illustration of free energy as the function of temperature with and without the magnetic field.

referred in Fig. 3. From this figure, it can be observed that the coercive field H_c and the remnant

magnetization M_r of the sample solidified from 360℃ are much lower than that of the sample solidified from 350℃. However; the saturation magnetization M_s is larger. This shows that when the MnBi phase has gone through the $Mn_{1.08}Bi$-to-MnBi phase transformation under the magnetic field, the magnetic properties are changed greatly. Fig. 13 presents the magnetizations parallel and perpendicular to the H_s direction for samples in Fig. 6. Mmagnetization for the sample quenched at 380℃ [Fig. 13 (a)] indicates that there is not obvious anisotropy in magnetic properties. However, for the sample quenched at 360℃ [Fig. 13 (b)], the magnetization shows a remarkable magnetic anisotropy; indeed, the magnetization saturates more easy with the case H_m along the H_s direction than that with the case H_m perpendicular to the H_s direction. This is consistent with the alignment behaviours of the $Mn_{1.08}Bi$ and MnBi phases under the magnetic field (Fig. 6). Fig. 14 shows the magnetizations [Fig. 14 (a)] and hysteresis loops [Fig. 14(b)] for the samples as referred in Fig. 7. It can be observed that with the increase of the holding temperature time under the magnetic field, the saturation magnetization M_s and the magnetic susceptibility χ increase. The remnant magnetization M_r and the ratio of M_r/M_s [Fig. 14 (c)] decrease. The above results indicate that the field has affected the magnetic properties (M_r and M_r/M_s) significantly during the $Mn_{1.08}Bi$-to-MnBi phase transformation process. Thus, the effect of the magnetic field on the $Mn_{1.08}Bi$/MnBi phase transformation can be determined by measuring the value of M_r and the ratio of M_r/M_s. To that purpose, the following experiments were designed: the samples were heated to a certain temperature in the range of 340℃-390℃ by a rate of 10K/min and held for 30min at this temperature. Then cooled below 262℃ at a rate of 8K/min. The magnetic field was applied at different stages. The ratios of M_r/M_s along the H_s direction for the above samples were measured, and the results are shown in Fig. 15. The black line stands for the value of M_r/M_s for the samples when a 10T-magnetic field is imposed during both holding temperature and cooling, and the red line stands for the value of M_r/M_s of the samples when a 10T-magnetic field is imposed during entire experiment process (including heating process). It can be observed that the M_r/M_s for the samples solidified from a certain temperature decreases abruptly. Comparison of two lines indicates that the application of the field during the heating process has raised the temperature at which the M_r/M_s decreased abruptly from 350℃−360℃ to 370℃-380℃. This indicates that the application of a 10T-magnetic field during heating has raised the MnBi-to-$Mn_{1.08}Bi$ phase transformation temperature to 370℃-380℃. The later result is consistent with the measurement showing that a 10T-magnetic field raises the MnBi-to-$Mn_{1.08}Bi$ transformation temperature from 355℃ to 375℃ and the microstructure change (Fig. 9).

By investigating the magnetic properties, it can be seen that the field has changed the magnetic property of the MnBi phase significantly; moreover, it is proved that the field has raised the $Mn_{1.08}Bi$/MnBi phase transformation temperature.

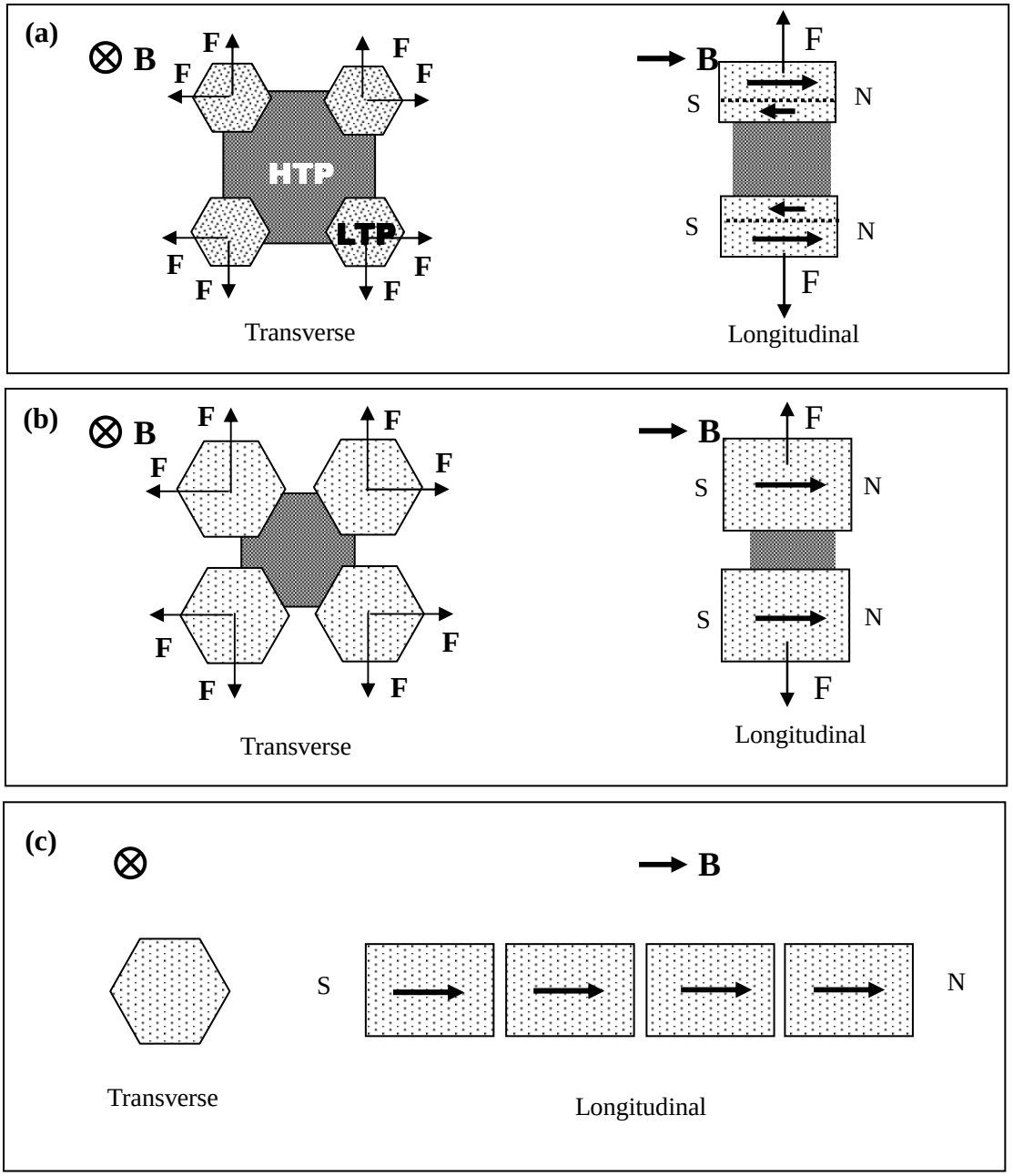

Fig. 17. Schematic illustration of the $Mn_{1.08}Bi$-to-MnBi phase transformation process in the magnetic field.
(a) Generation of magnetizing forces between the ferromagnetic MnBi phase (LTP) in the magnetic field; (b) The increase of the magnetizing forces along with the growth of the MnBi phase and the crack of the MnBi phase; (c) Aggregation of the spit phase.

4. Discussion

The above results show that the magnetic field has affected the $Mn_{1.08}Bi$/MnBi phase transformation process greatly. Indeed, the field has raised the phase transformation temperature. The morphology and the magnetic property of the MnBi phase are also changed greatly during the phase transformation process under the magnetic field. The above results will be interpreted below in terms of the magnetic energy and force.

4.1. Influence of the magnetic field on the Mn1.08Bi/MnBi phase transformation

As the saturation magnetization of the parent (MnBi) and the product ($Mn_{1.08}Bi$ and Bi) phases is different and the phase transformation temperature is determined by the Gibbs energy. Thus, when a high magnetic field is applied, the phase equilibrium will change due to magnetic Gibbs energy contribution. Consequently, the phase transformation temperature and the pressure may be changed. Fig. 16 shows the schematic illustration for the effect of the magnetic field on Gibbs free energy, where *G* is function of temperature, *T*. T_0 stands for the temperature at which parent (MnBi) and product phase ($Mn_{1.08}Bi$ and Bi) have the same free energy in the absence of an applied field. If the magnetic field is applied, the free energy of the ferromagnetic MnBi phase is decreased as shown by the dotted line. The free energies of the $Mn_{1.08}Bi$ and Bi phases are also changed, but it is neglected because they are non-ferromagnetic. Therefore the temperature at which parent and product phase has the same energy shifts to $T_0^{/}$. This means that the field raises the $Mn_{1.08}Bi$/MnBi phase transformation temperature. Further thermodynamic analysis is performed as follow.

The amount of energy per unit volume reduced by the magnetization can be expressed as [16]:

$$U_m = -\int_0^H \mu_0 \mathrm{M} d\mathrm{H} \tag{2}$$

where H is the imposed magnetic field.

For non-ferromagnetic substance

$$M = \chi V H \tag{3}$$

where χ is molar magnetic susceptibility.

Assuming that molar magnetic susceptibility χ is independence on the field, combining Eq. (2) to (3) yields

$$U_m = -\frac{\mu_0 V \chi}{2} \mathrm{H}^2 \tag{4}$$

Thus, for the paramagnetic $Mn_{1.08}Bi$ phase, the equation can be obtained

$$U_m^{\alpha} = -\frac{\mu_0 V \chi_{\alpha}}{2} \mathrm{H}^2 \tag{5}$$

For the diamagnetic liquid Bi, similar equation can be obtained

$$U_m^{L} = -\frac{\mu_0 V \chi_{L}}{2} \mathrm{H}^2 \tag{6}$$

For the ferromagnetic MnBi phase, the approximate expression of U_m can be obtained with the assumption that M is saturated at the magnetic intensity H_s as follow:

If $H < H_s$

$$U_m^{\beta} = -\int_0^H \mu_0 \mathrm{M} d\mathrm{H} = -\frac{\mu_0 V \chi_{\beta 1}}{2} \mathrm{H}^2 \tag{7}$$

If $H > H_s$

$$U_m^{\beta} = -\int_0^H \mu_0 \mathrm{M} d\mathrm{H}$$

$$= -\int_0^{H_s} \mu_0 V \chi_{\beta 1} \mathrm{H} d\mathrm{H} - \int_{H_s}^{\mathrm{H}} \mu_0 V \chi_{\beta 2} \mathrm{H} d\mathrm{H} \qquad (8)$$

$$= -\frac{\mu_0}{2} V[\chi_{\beta 1} \mathrm{H}_s^2 + \chi_{\beta 2} (\mathrm{H}_{ex} - \mathrm{H}_s)^2]$$

where χ_{β}^1 and χ_{β}^2 are the molar magnetic susceptibility of the MnBi phase before and after the saturated magnetization, respectively.

For the differential of Gibbs energy of the magnetic system we have [18]

$$dG = -SdT + VdP + \sum_{i=1} \mu_i dn_i - \mu_0 \mathrm{M} d\mathrm{H} \qquad (9)$$

The chemical potential μ_k

$$\mu_k(T, p, n, H) = \mu_k^0(T, p, n) + U_m$$

Here, we do not consider the effect of the field on the component. The chemical potential of the considered component, in the transition point, must be the same in each phase in which it exists, the molar entropy S_i and molar volumes V_i (i=$Mn_{1.08}$Bi, Bi, and MnBi) are not:

$$\mu_{MnBi}^0(T, P) = \mu_{Mn_{1.08}Bi}^0(T, P) + \mu_{L_{Bi}}^0(T, P) + \beta \qquad (10)$$

For $H < H_s$

where $\beta = (\frac{\mu_0 V_{MnBi} \chi_{MnBi}^1}{2} - \frac{\mu_0 V_{Mn_{1.08}Bi} \chi_{Mn_{1.08}Bi}}{2} - \frac{\mu_0 V_{Bi} \chi_{L_{Bi}}}{2})\mathrm{H}^2$ (11)

For $H > H_s$

where

$$\beta = \frac{\mu_0}{2} V_{MnBi}[\chi_{MnBi}^1 \mathrm{H}_s^2 + \chi_{MnBi}^2 (\mathrm{H} - \mathrm{H}_s)^2] - \frac{\mu_0 V_{Mn_{1.08}Bi} \chi_{Mn_{1.08}Bi}}{2} \mathrm{H}^2 - \frac{\mu_0 V_{L_{Bi}} \chi_{L_{Bi}}}{2} \mathrm{H}^2 \qquad (12)$$

Here, (*T*, P) are the temperature and pressure of solidification under the magnetic field. Both these parameters, or at least one from them should be different from the corresponding values of (T_0 and P_0) for H=0. After differentiation (10) with respect to H at the transition point $T=T_0$, and $P=P_0$, respectively, we have

$$\frac{dP}{d\mathrm{H}}=\frac{1}{\Delta V}\frac{d(\beta)}{d\mathrm{H}} \tag{13}$$

$$\frac{dP}{d\mathrm{H}}=\frac{T_0}{\Delta H_S^0}\frac{d(\beta)}{d\mathrm{H}} \tag{14}$$

where $\Delta V=V_{MnBi}-V_{Mn_{1.08}Bi}-V_{L_{Bi}}$, ΔH_S^0 is the change in enthalpy. After integration (13), the change of the solidification pressure, under the magnetic field is

$$P-P_0=\Delta P=\frac{\beta}{\Delta V} \tag{15}$$

Owing to β>0, we conclude that P-P_0>0, if ΔV>0, otherwise P-P_0<0, if ΔV<0.

After integration (14), the change of solidification temperature in the field is

$$T-T_0=\Delta T=\frac{T_0}{\Delta H_s^0}\beta \tag{16}$$

From the relation (16) follows that T-T_0>0, if ΔH_s^0>0, otherwise T-T_0<0, if ΔH_s^0<0. The above thermodynamic analysis indicates that an external magnetic field can influence the phase transformation temperature and the pressure during the $Mn_{1.08}$Bi/MnBi phase transformation process.

4.2. Influence of the magnetic field on the morphology and magnetic properties

During the $Mn_{1.08}$Bi-to-MnBi phase transformation process, the ferromagnetic MnBi phase (LTP) will nucleate on the surface of the paramagnetic $Mn_{1.08}$Bi phase (HTP). Along with the formation of the MnBi phase, the magnetic domains will produce. Under the magnetic field, during the magnetization of the LTP, the magnetic domains will rotate and the magnetic domain walls will move as shown in Fig. 17 (a). Thus, their same-name magnetic poles will align along the magnetic field direction [Fig. 17(b)] and then repulsive forces will produce among them. The repulsive force can be expressed as [19]:

$$\mathrm{F_M}=\frac{\mu_0(\chi+1)}{4\pi}\frac{\mathrm{Q_{m1}Q_{m2}}}{\mathrm{r}^2} \tag{17}$$

where Q_{m1}, Q_{m2} are the strength of two magnetic poles, r the distance between two magnetic poles. With the growth of the LTP phase, their volumes increase and the inter-grains distances decrease. Thus, according to formula (17), the repulsive forces increase significantly. Consequently, during the $Mn_{1.08}$Bi-to-MnBi phase transformation process, the force will separate the MnBi grains on the one hand, and crack the MnBi crystal on the other hand. At the same time, the split MnBi crystals will align and aggregate along the magnetic field direction as shown in Fig. 17(c).

From the physics of magnetism point of view, the magnetic domains in the substance rotate their easy magnetic axes towards the magnetic field direction by moving their magnetic domain walls during the magnetization. The grain boundary stress will retard the rotation and movement of the domains. Thus, the large coercive field H_C and the remnant magnetization M_r will form. It is well known that the LTP (MnBi) has the large coercive field H_C and the remnant magnetization M_r

as shown in Fig. 12(a). During the phase transformation under the field, the magnetic domain walls are destroyed owing to the crack of the MnBi crystal. Thus, the stresses in the grains are released and the magnetostriction is reduced; which will lead to the reduction of the coercive field

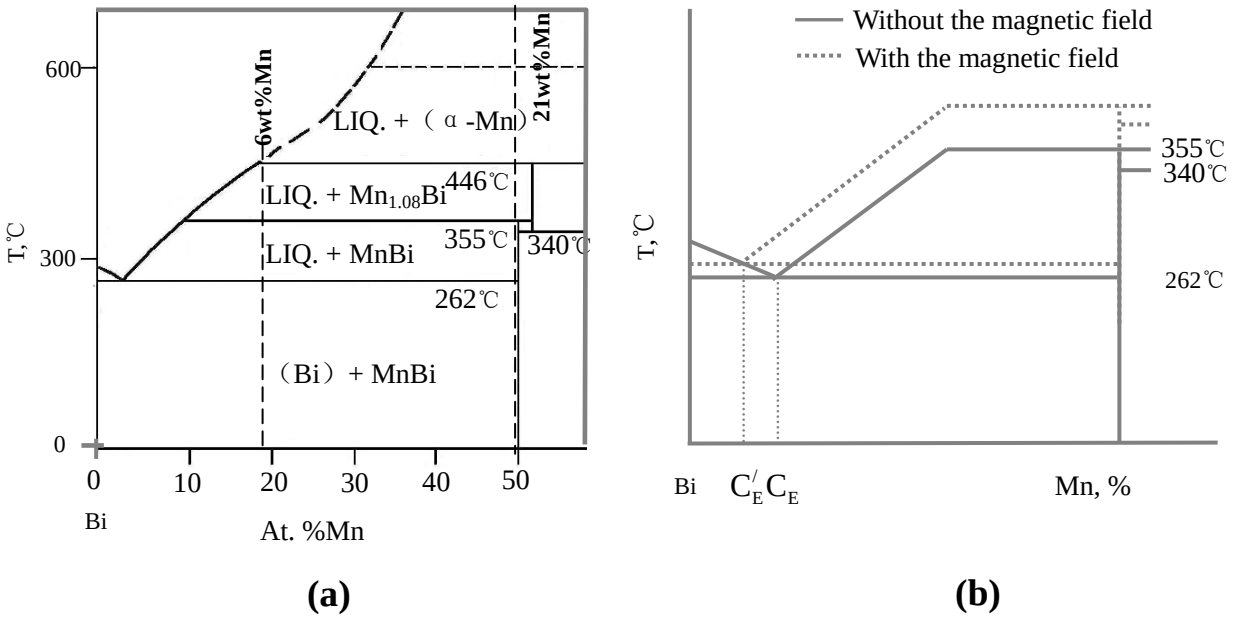

Fig. 18. Effect of the magnetic field on the equilibrium phase diagram of Mn-Bi system.
(a) Equilibrium phase diagram of Mn-Bi system near Bi;
(b) Schematic illustration of the modification of the phase diagram by the magnetic field.

H_C and the remnant magnetization M_r in the MnBi phase. Furthermore, the reduction of the magnetic domain walls and magnetostriction causes the motion of the magnetic domain easier. As a result, its magnetic susceptibility χ increases. It was reported that the cracks occurred frequently during the directional solidification of the TbDyFe alloy under a high magnetic field [20]. This may be attributed to the same mechanism presented here, because they both endure the peritectic transformation during the solidification process. From this mechanism, it may be concluded that the application of a high magnetic field during the peritectic phase transformation involving of a ferromagnetic phase have the same result as the MnBi and TbDyFe alloys.

The increase of the saturation magnetization M_s during the $Mn_{1.08}Bi$-to-MnBi phase transformation process in a high magnetic filed [Figs. 14 (a) and 14(b)] may be attributed to the increase of the MnBi phase in the alloy. There are several reasons, first of all, owing to the decrease of the MnBi free energy under the magnetic field, the $Mn_{1.08}Bi$-to-MnBi phase transformation course will be enhanced. Consequently, the content of the MnBi phase increases. Secondly, owing to the increase of the T_C under the magnetic field, the equilibrium liquidus near MnBi may be elevated. If ignoring the influence of the field on the melting point of Bi (because it is diamagnetic) and liquidus near it, the application of the magnetic field will cause an increase of eutectic temperature and a shift leftward of the eutectic composition as shown in Fig. 18(b). Thus, the content of the MnBi phase in the alloy will also increase. Moreover, the crack of the MnBi phase enhances the peritectic $Mn_{1.08}Bi$-to-MnBi phase transformation process under the magnetic field and leads to the increases of the MnBi phase.

5. Conclusions

1. Based on the difference of the magnetization force between the parent and product phases, the $Mn_{1.08}Bi$/MnBi peritectic phase transformation temperature under a high magnetic field was measured. It is found that the high magnetic field has raised the temperature significantly. As a result, the application of a 10T-magnetic field increases the temperature about 20℃.
2. The morphology of the MnBi phase was investigated and the results indicate that the field cracks the MnBi crystal along the (001)-plane during the $Mn_{1.08}Bi$/MnBi phase transformation process and the split MnBi crystals align and aggregate along the magnetic field direction.
3. The field has affected the magnetic properties of the MnBi phase greatly; as a result, the saturation magnetization M_s and the magnetic susceptibility χ increase and the coercive field H_c and the remnant magnetization M_r decrease. This implies that the field causes the magnetic property of the MnBi phase to transform towards soft magnetism during the phase transformation.

Acknowledgments

This work is supported by Natural Science Foundation of China (No. 50234020, 50225416 and 59871026) and one of the authors (LX) is also grateful for an Egide/Eiffel Doctorate Scholarship.

References

[1] Asai S. Sci Tech Adv. Mater 2000; 1:191.and its references.
[2] Martin JW, Doherty RD, Cantor B. Stability of microstructure in metallic systems. Cambridge University press;1997. p.391.
[3] Joo HD, Kim SU, Shin NS, Koo YM. Mater Lett 2000; 43:225.
[4] Joo HD, Choi JK, Kim SU, Shin NS, Koo YM. Metall Mater Trans A 2004; 35 A: 1663.
[5] Shimotomai M. Mater Trans JIM 2003; 44: 2524.
[6] Ghosh AK, Roy MN. Trans Indian Inst Met 1987; 40:329.
[7] Zhang YD, Esling C, Lecomte J S, He CS, Zhao X, Zuo L. Acta Mater 2005;53:5213.
[8] Peters CT, Miodowink AP. Scripta Mater 1973; 7:955.
[9] Hideyuki O. Curr Opin Solid St M 2004; 8: 279.
[10] Zhang YD, Gey N, He CS, Zhao X, Zuo L. Acta Mater 2004;52:3467.
[11] Saha S, Obermyer RT, Zande BJ, Chandhok VK, Sankar SG, Horton A. J Appl Phys 2002;91:8525.
[12] Chen T, Stutius W. IEEE Trans Magn 1974; 10:581.
[13] Harder KU, Menzel D, Widmer T, Schoenes J. J Appl Phys 1998; 84:3625.
[14] Yang JB, Kamaraju K, Yelon WB, James WJ. Appl Phys Lett 2001; 1846:79.
[15] Moffatt WG. The Handbook of Binary Phase Diagrams. USA: Genium, 1984.p.83.
[16] Morikawa H, Sassa K, Asai S. Mater Trans JIM, 1998; l39:814.
[17] Wang H. Ph.D. Thesis, Shanghai University, China, 2003.
[18] Valko L, Valko M. IEEE Trans Magn 1994; 30:1122.
[19] Hallen E. Electromagnetic theory. London: Chapman & Hall Ltd: 1962. p.185.
[20] Minagawa H, et al. J Magn and Magn Mater 2002; 248: 230.

[A8] Xi Li, Zhongming Ren,Yves Fautrelle

The alignment, aggregation and magnetization behaviours in MnBi/Bi composites solidified under a high magnetic field,

Intermetallics 15 (2007) 845-855.

Available online at www.sciencedirect.com
ScienceDirect
Intermetallics 15 (2007) 845–855
Intermetallics
www.elsevier.com/locate/intermet

The alignment, aggregation and magnetization behaviors in MnBi–Bi composites solidified under a high magnetic field

Xi Li [a,b,*], Zhongming Ren [a], Yves Fautrelle [b]

[a] Department of Material Science and Engineering, Shanghai University, Shanghai 200072, PR China
[b] EPM-Madylam, ENSHMG, BP, 38402 St Martin d'Heres Cedex, France

Received 5 April 2006; accepted 20 October 2006
Available online 1 February 2007

Abstract

Bi–6 wt% Mn alloy is solidified under a high magnetic field and its microstructures and magnetic properties have been investigated. Microstructure results show that three kinds of morphology of MnBi phase appear in different temperature zones. In all these cases, the grains are orientated with the ⟨001⟩-crystal direction along the magnetic field direction and aggregated. Magnetic measurement shows a pronounced anisotropy in magnetization in directions normal and parallel to the fabrication field, resulting from this alignment. The effect of the magnetic field on the $Mn_{1.08}Bi$/MnBi (paramagnetic/ferromagnetic) phase transformation has been studied and the result shows that the phase transformation temperature T_C increases with the increase of the external magnetic field and under a field of 10 T, a typical increase of T_C is 20 °C during heating and 22 °C during cooling. The change in the morphology and in the magnetic properties of MnBi phase is discussed from the phase transformation and the crystal structure change in magnetic field.

Keywords: High magnetic field; Alignment and aggregation; MnBi phase; B. Magnetic properties; B. Phase transformations

1. Introduction

For both improving the physical properties of materials and fundamental understanding, materials are often aligned in a specific crystallographic direction. The magnetic field is always used to achieve materials with high magnetic anisotropy. As a successful example, YBCO is aligned with the *c*-axis along a magnetic field-applied during the solidification process by Rango et al. [1]. Recently, many efforts have been focused on the high field-induced transformation [2–6]. For instance, the structure phase transformation induced by an external magnetic field has been reported [7]. Owing to unusual magnetic and magneto-optical properties, the physical properties of the binary compound MnBi have been investigated extensively [8–14]. It is a usual method to impose a magnetic field during the solidification process to align the MnBi phase. Savitisky et al. [15] and Asai et al. [16,17] found that MnBi phase aligned regularly along the magnetic field in Bi–0.9–10 wt% Mn alloy solidified in the 2.5–5 T magnetic field. Ren et al. [18,19] investigated the alignment behaviour of MnBi phase in detail and concluded that there existed critical values in the temperature and magnetic field intensity for influencing the alignment behaviour. Previous works on solidification behaviour of Bi–Mn alloys under a magnetic field have mainly focused on the alignment of MnBi phase. However, up to now, little work has been investigated on the effect of magnetic field on the structure of MnBi phase and its physical properties. Therefore, it is necessary to study the structure and physical property of solidified Bi–Mn alloys in a magnetic

* Corresponding author. EPM-Madylam, ENSHMG, BP, 38402 St Martin d'Heres Cedex, France.
E-mail address: xi@hmg.inpg.fr (X. Li).

0966-9795/$ - see front matter © 2006 Elsevier Ltd. All rights reserved.
doi:10.1016/j.intermet.2006.10.048

field. In this work, firstly we report the effect of the external magnetic field H on the temperature T_C of the $Mn_{1.08}Bi$/MnBi (paramagnetic/ferromagnetic) phase transformation (PFT) for MnBi; as a result, T_C increases with the increase of the external magnetic field. On the other hand, the microstructure and magnetic properties of magnetically aligned phase have been investigated. It is interesting to find that the phase morphology and the magnetic properties change greatly under a high magnetic field.

2. Experimental

The experimental apparatus is the same as that in Ref. [19]. The Bi–6 wt% Mn alloy was investigated in this research. The experimental procedure was as follows: samples sealed in a graphite tube with its longitudinal axis along the direction of the magnetic field were heated at a rate of about 10 °C/min to a certain temperature above the eutectic temperature (the eutectic temperature is 262 °C, the peritectic transformation temperature is 355 °C on heating and 340 °C on cooling [20]) and held at this temperature for a certain time, then cooled to below the eutectic temperature 262 °C at a rate of 0.18 °C/min. Quenching experiment was also carried out to investigate the evolution of solidification structure with various holding times at the solidification temperature. In this case, the sample held at the semisolid zone was dropped into water tank and cooled down quickly, so that the solidification structure before quenching was kept at room temperature. For characterizing the morphology of the MnBi phase, the samples obtained in the experiments were mechanically polished parallel and perpendicular to the magnetic field. The microstructure of the sample was characterized by optical microscopy, scanning electron microscopy, and X-ray diffraction (XRD) with Cu K_α radiation. To investigate the magnetic properties, magnetization measurements were performed under the applied magnetic field up to 50 kOe.

3. Results and discussion

3.1. Effect of magnetic field on $Mn_{1.08}Bi$/MnBi (paramagnetic/ferromagnetic) phase transformation

According to the phase diagram of Mn–Bi system [20], there are three different zones: (1) in the temperature range from T_C to 446 °C, mix of paramagnetic solid high-temperature phase (HTP) $Mn_{1.08}Bi$ and liquid Bi; (2) from 262 °C to T_C, mix of ferromagnetic solid low-temperature phase (LTP) MnBi and liquid Bi; (3) below 262 °C, composite of solid (LTP) MnBi and solid Bi. The effect of magnetic field on the T_C has been investigated and Fig. 1(a) shows the PFT as a function of the external magnetic field H_f during heating and cooling. It can be learned that on the whole, the T_C of PFT increases with the increase of the external magnetic field. Under the field of 10 T, T_C increases to 20 and 22 °C. The observed effect of a magnetic field on the T_C can be discussed from the point of view of magnetic free energy. In general, the magnetic free energy in ferromagnetic materials is given for unit volume by

$$U_f = -\mu_0\left(H - \frac{1}{2}NM_s\right)M_s \quad (1)$$

where M_s is the saturation magnetization, H the strength of a magnetic field, and N the demagnetizing factor. For paramagnetic materials, the magnetic free energy is given for unit volume by

$$U_p = -\frac{1}{2}\mu_0\chi(1-\chi N)H^2 \quad (2)$$

where χ is the susceptibility. Because the susceptibility of the paramagnetic $Mn_{1.08}Bi$ is extremely small ($\sim 10^{-5}$), the magnetic free energy may be much higher in the paramagnetic state than in the ferromagnetic state, that is $U_p \gg U_f$ in a high magnetic field. Consequently, the applied magnetic

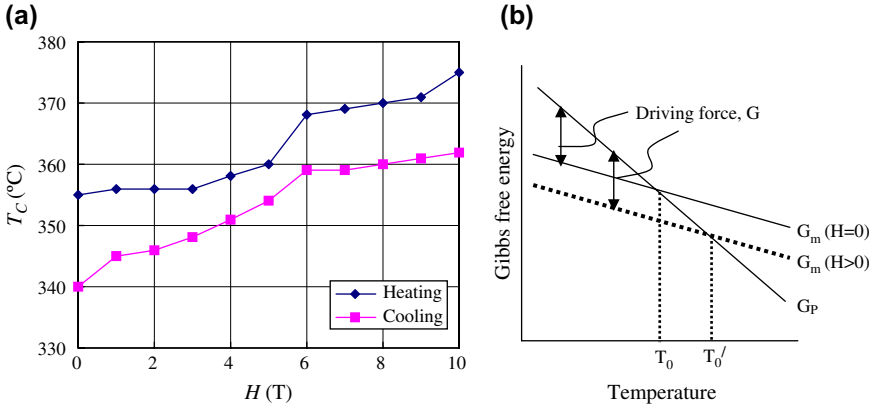

Fig. 1. (a) The $Mn_{1.08}Bi$/MnBi phase transformation temperature T_C as a function of the external magnetic field H_f during heating and cooling; (b) schematic illustration of free energy as a function of temperature with and without magnetic field.

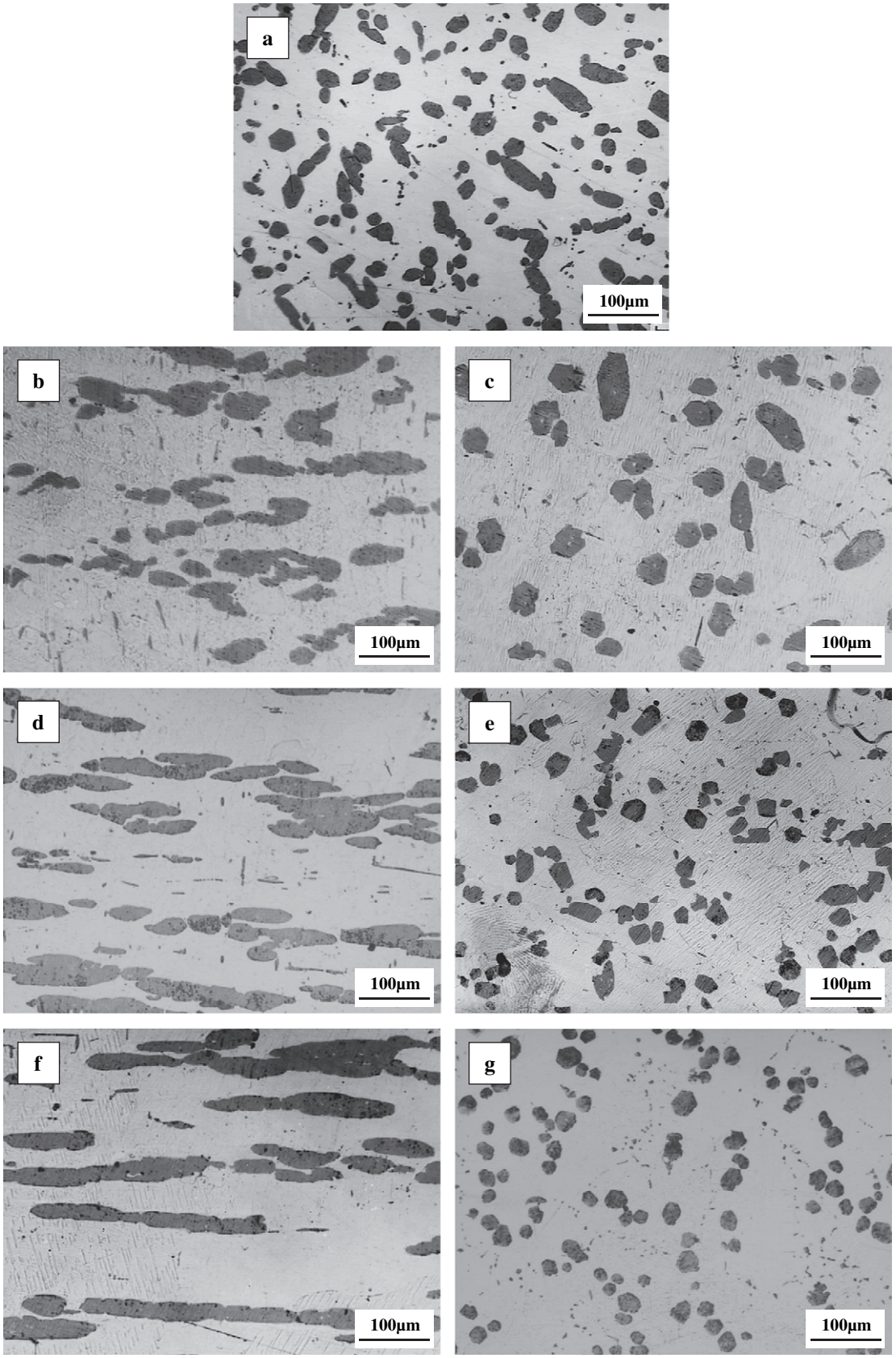

Fig. 2. Microstructures of Bi–6 wt% Mn alloy cooled from 300 °C at a cooling rate of 0.18 °C/min in different magnetic fields. The microstructure without the field (a). The microstructures in the section parallel to the magnetic field: (b) 0.3 T; (d) 0.5 T; (f) 1.0 T. The microstructures in the section perpendicular to the magnetic field: (c) 0.3 T; (e) 0.5 T; (g) 1.0 T.

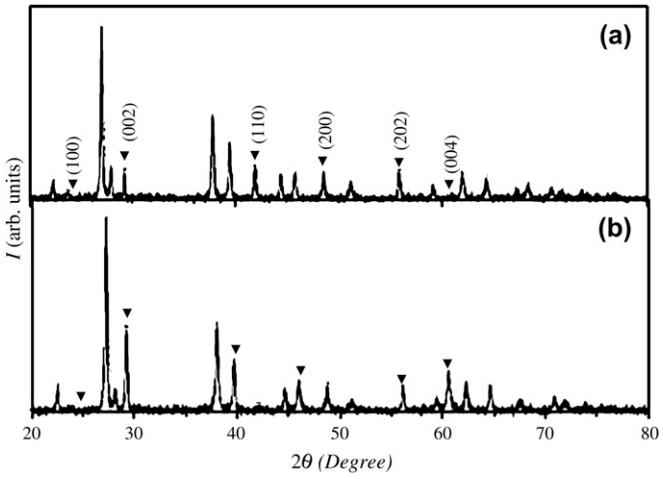

Fig. 3. XRD patterns of Bi–6 wt% Mn alloy solidified in a magnetic field of 0.5 T: (a) section parallel to H_f; (b) section perpendicular to H_f. Peaks labeled by (*hkl*) are for MnBi and others for Bi.

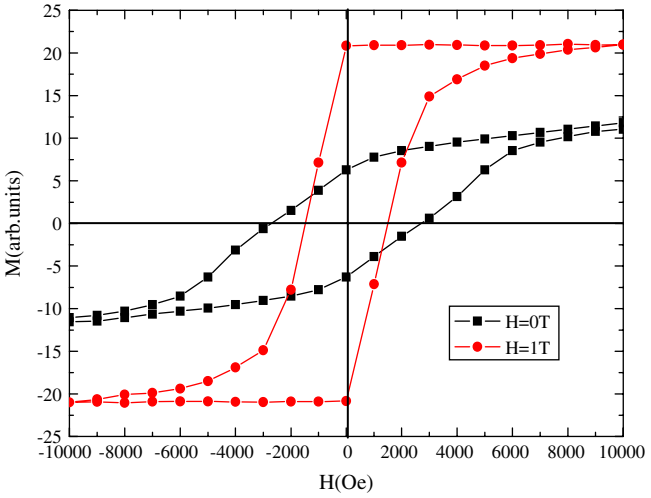

Fig. 5. Hysteresis loops of samples solidified at 0 T and 1 T which are measured along the fabrication field H_f.

field lowers the free energy of the system and heightens the T_C of PFT as shown in Fig. 1b.

3.2. Effect of magnetic field on the solidification behaviour of MnBi crystal solidified from below T_C

Fig. 2 shows the microstructures of the Bi–6 wt% Mn alloy solidified from 300 °C without and with a magnetic field. In the case without the field, the structure of the alloy had the usual disordered nature. In the case of imposed magnetic field, the MnBi grains were aligned with the longer axes along the magnetic field. With the increase of the magnetic field, the alignment becomes better and under 1 T magnetic field, the hexagonal sections of the crystals only appear in the section perpendicular to the field. Further, XRD patterns (Fig. 3) show that the *c*-axis of hexagonal MnBi crystal (an easy magnetization axis) is aligned along the field direction.

To study the magnetic anisotropy, the magnetization curves of the same samples as in Fig. 2 were measured along and perpendicular to the fabrication field. Fig. 4 presents the magnetizations parallel and perpendicular to the fabrication field for the sample solidified under 1 T magnetic field (a) and magnetization parallel to the fabrication field for various samples (b). It can be seen that magnetization saturates more easily with the field-applied parallel to the alignment direction than the one perpendicular to the alignment direction, which suggests that there is a very strong anisotropic nature of the sample. Comparison of the magnetization behaviours of the samples solidified under different fields indicates that the samples solidified in 0.5 and 1 T magnetic fields magnetized more easily than the ones solidified in 0 and 0.3 T, and they possess nearly the same magnetization behaviours. Fig. 5 shows the hysteresis loops measured along the H_f of the samples solidified under 0 and 1 T magnetic field. Comparison of the remnant magnetization M_r of the samples solidified in 0 and 1 T indicates a considerable increase for the 1 T sample and the coercive field H_C of 0 T sample is a little larger than the ones solidified in the field of 1 T. This may be attributed to

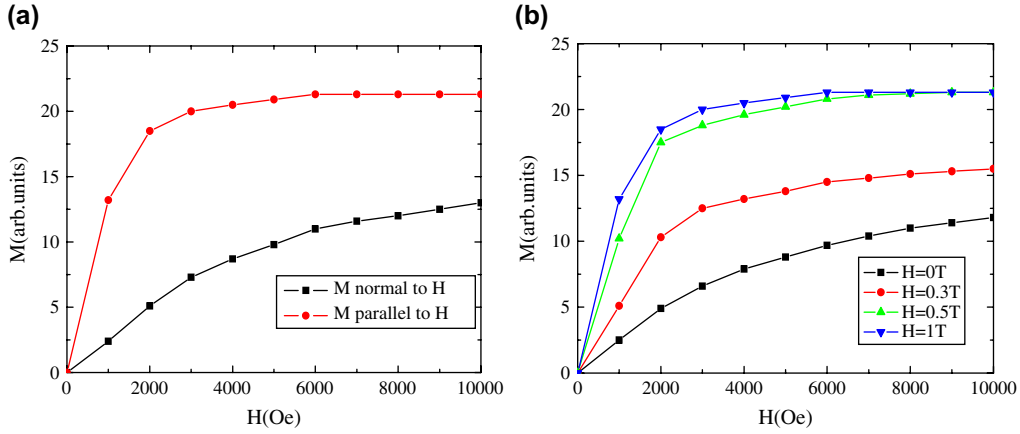

Fig. 4. (a) Magnetization parallel and perpendicular to the applied magnetic field during solidification for the samples solidified at 1.0 T; (b) magnetizations parallel to the fabrication field H_f for the samples that magnetically solidified at different H_fs.

the alignment of MnBi grains and to the improvement in crystal quality of MnBi.

The orienting effect of the homogenous magnetic field on an anisotropic crystal characterized by an anomaly of magnetic susceptibility $\Delta\chi$ along the two mutually perpendicular axes without taking into consideration the influence of the crystal shape can be obtained from the following equation [21].

$$K = \frac{\Delta\chi}{2\mu_0} B^2 V \sin 2a, \tag{3}$$

where α is the angle between B and the axis with the maximum $|\chi|$. From the above equation, it follows that the paramagnetic crystal in the homogenous magnetic field will align itself with easy magnetization axis along the magnetic field direction, while the diamagnetic crystal will position itself perpendicular to the magnetic field. In principle, the orienting action of the magnetic field must always affect a crystal with magnetic anisotropy; however, owing to the existence of viscous forces, convective flows in the melt and interaction of the crystals with each other and with the walls of the crucible, the alignment may not occur. MnBi crystal possessed a distinct magnetic anisotropy and c-axis is its easy magnetic axis, so it tends to be orientated with c-axis along the magnetic field.

In order to provide a quantitative analysis of the alignment, the degree of MnBi crystal alignment was evaluated by the alignment factor η. The alignment factor is defined by $\eta = M_r/M_s$ in Ref. [22] and it should have a value ranging from 0.5 (corresponding to a completely random distribution) to 1.0 (corresponding to a perfect alignment). Fig. 6 shows the alignment factor as a function of the fabrication field H_f for the samples solidified from various temperatures. It can be learned that when temperature is below a certain temperature, the field of 1 T cannot cause MnBi crystal to align and with the increase of the temperature and magnetic field, the alignment factor η increases. This is because with the decrease of the solidification temperature, the viscous forces increase; as a result, the alignment factor η reduces. When the temperature is very low so that the viscous forces are large enough to balance the magnetic force, thus, the alignment will not occur.

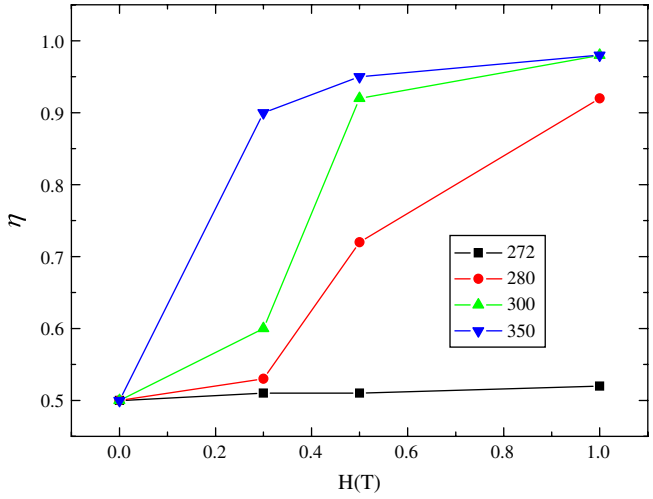

Fig. 6. The alignment factor $\eta = M_r/M_s$ as a function of the fabrication field for the samples solidified from various temperatures.

On the other hand, an attracting force F will be produced between the crystals with opposite poles, which will result in attraction of each other between neighbor phases and aggregation [23]

$$F = \frac{V_1 V_2}{4\pi\mu r^2} \chi_c^2 H_{ex}^2 \tag{4}$$

where μ is the magnetic permeability; r the interval distance between two neighboring MnBi particles; V_1 and V_2 the volumes of the two particles; χ_c the volume magnetic susceptibility along the c-axis and H applied field. This equation indicates that the increase of the field will cause a square increase in the force, and the volumes of the particles will affect the force linearly. Therefore, the length of the MnBi phase increases significantly with increasing magnetic field, because more particles may adhere together with stronger magnetic field. It is also easy to understand that with the increase of the length of the MnBi phase, the adhering rate of the particles will accelerate due to the enlargement of their volumes.

3.3. Effect of magnetic field on the solidification behaviour of MnBi crystal solidified from above T_C

Fig. 7 shows microstructures of Bi–6 wt% Mn alloy solidified from 400 °C. It can be learned that the morphology of MnBi phase is elliptical [Fig. 7(a)]. When imposed the magnetic field of 0.2 T, the part phases are aligned with its short axis along the field as shown in Fig. 7(b) and (c). Under 5 T, all phases are aligned. When the field increases to 10 T, it is interesting to find that the tips of elliptical phase disappear. This can be attributed to the expelling force between the neighbor crystals with the same magnetic poles in the same phase, the mechanism being discussed later.

To investigate the formation mechanism of the elliptical phase, the quenching experiment is designed. Fig. 8 shows the quenching microstructures of the samples quenched at various temperatures on cooling from 400 °C in a magnetic field of 10 T. It can be learned that the morphology of the sample quenched at 365 °C is block-like; however, at 360 °C, some elliptical phase appeared, with the decrease of the quenching temperature, the morphology of the primary phase transferred into the elliptical phase completely. The temperature at which the block-like phase begins to transfer into elliptical one (365–360 °C) agrees well with the phase transformation temperature from $Mn_{1.08}Bi$ to MnBi in the 10 T field (362 °C). This means that the phase morphology will change during the phase transformation process, which may be attributed to the crystal structure change during the

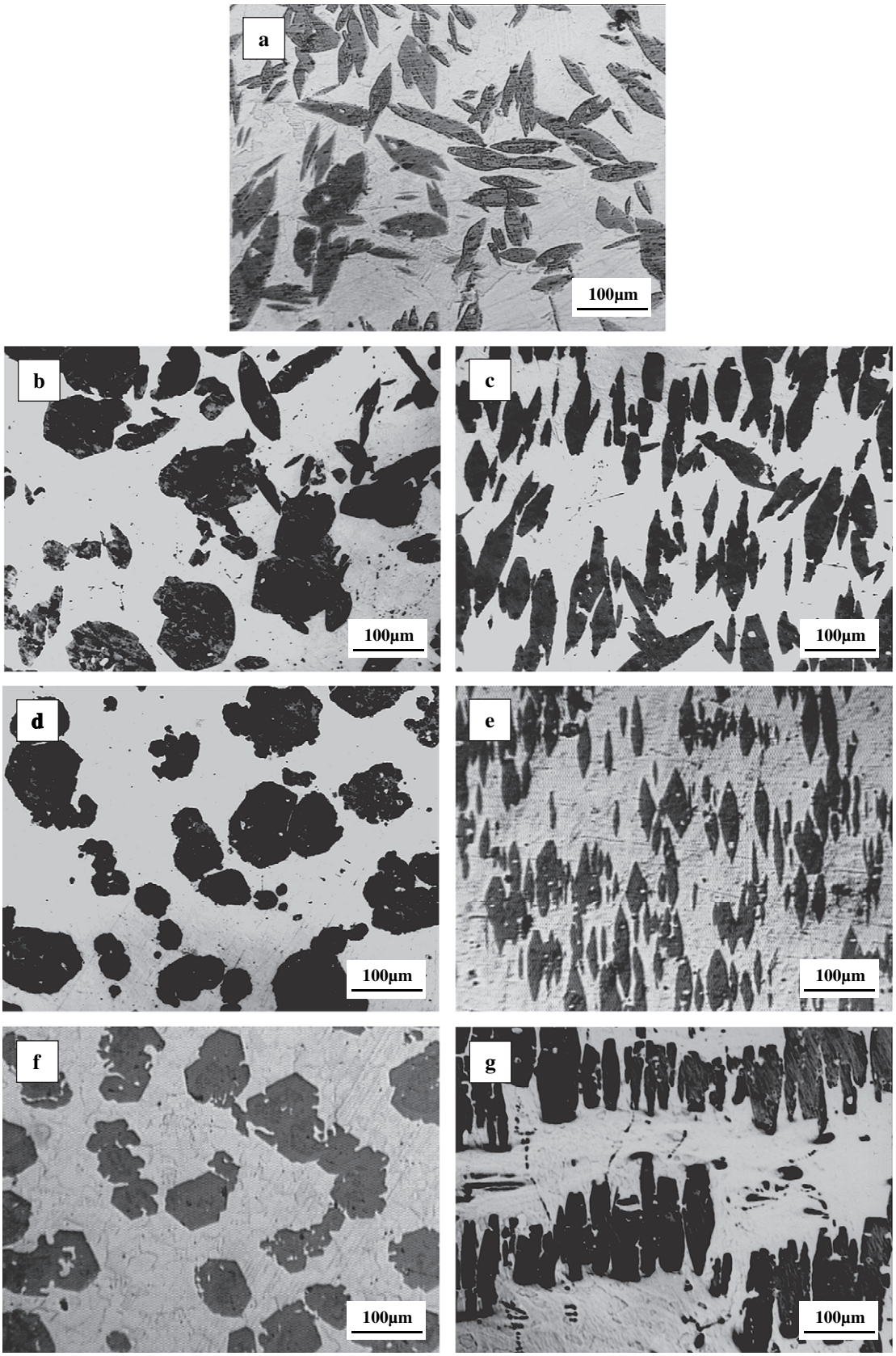

Fig. 7. Microstructures of the specimens of Bi–6 wt% Mn alloys solidified from 400 °C at a cooling rate of 0.18 °C/min under different magnetic fields. The microstructure without the field (a). The microstructures in the section perpendicular to the magnetic field: (b) 0.2 T; (d) 5 T; (f) 10 T. The microstructures in the section parallel to the magnetic field: (c) 0.2 T; (e) 5 T; (g) 10 T.

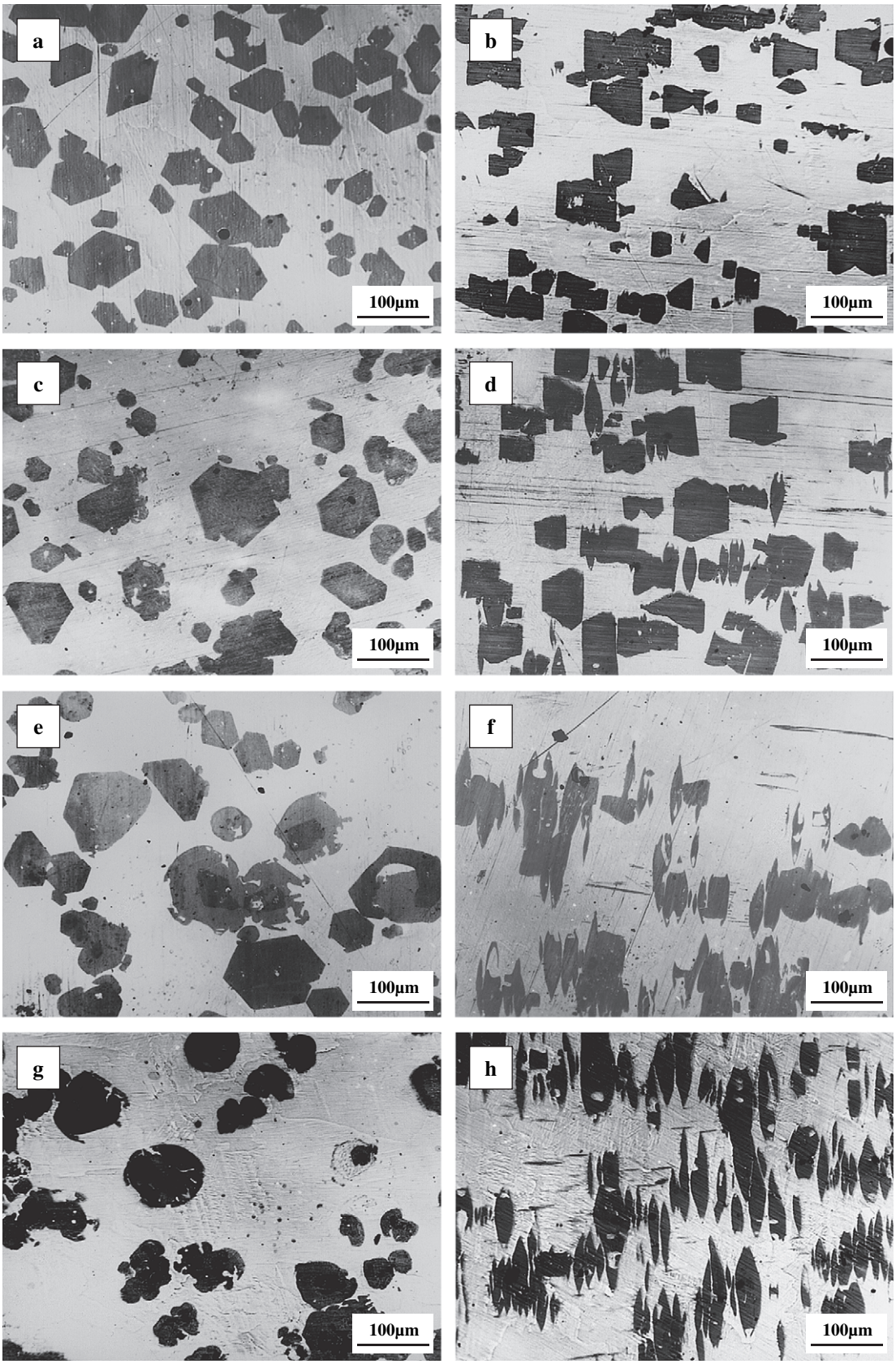

Fig. 8. Microstructures of Bi–6 wt% Mn alloys quenched at different temperatures on cooling from 400 °C in a 10 T magnetic field. Microstructure in the transverse section: (a) 365 °C; (c) 360 °C; (e) 355 °C; (g) 350 °C. Microstructure on the longitudinal section: (b) 365 °C; (d) 360 °C; (f) 355 °C; (h) 350 °C.

phase transformation. It is well known that MnBi (LTP) is hexagonal and $Mn_{1.08}Bi$ (HTP) is cubic, and during the peritectic phase transformation from $Mn_{1.08}Bi$ to MnBi, the *c*-axis is elongated 3% and the *a* and *b* axes are contracted; which can produce a stress and cause a single $Mn_{1.08}Bi$ crystal to split into many MnBi crystals so that the elliptical phase forms.

The magnetization and hysteresis loops of the same sample as in Fig. 8 were measured along the direction of the alignment. Comparison of the magnetizations for the samples quenched at different temperatures [Fig. 9(a)] shows that first with the decrease in quenching temperature of the samples, the magnetization becomes easier; and the samples quenched at 355 °C and 350 °C possess nearly the same magnetization behaviour which agrees with the microstructural change during the phase transformation. Quenched at 365 °C, the microstructure is in high-temperature quenching phase (HTQP), whose saturation magnetization is smaller than the one of LTP. For the sample quenched at 360 °C, the phase transformation takes place before quenching, some LTP forms; however, because there is no enough time to transform HTP into LTP completely; as a result, QHTP and LTP coexist in the quenching microstructure. Quenched at 355 °C, almost all phases are LTP. The hysteresis loops of the samples quenched at 350 °C and 365 °C [Fig. 9(b)] show that the coercive field H_C and the magnitude of remnant magnetization M_r are smaller than the one quenched at 365 °C and are nearly zero. This may result from the release of the stresses in crystals during phase transformation process.

The mechanism of the loss of the tips of leaf-like phase is studied by quenching samples cooled from 400 °C to 350 °C and held for certain time in 10 T magnetic field and then quenched. Microstructures (Fig. 10) indicate that with the increase of holding time in the magnetic field, the elliptical phase gradually splits into small blocks along the perpendicular direction of the field, and the distribution of the small blocks gets more uniform with their separation from each other. Besides, the small blocks aligned along the magnetic field direction and formed rod-like structure. It can be discussed from the mutually repulsive forces between the two neighbor MnBi crystal with same-name magnetic poles in the same phase in a high magnetic field. Thus a magnetized crystal will be repelled by the crystal with the same magnetic pole in same phase and is attracted by the crystal in other phase at the same time. As a result, crystals in the same phase are divided and realigned. The evolutive process of MnBi phase morphology is shown in Fig. 12. The magnetization of the same samples as in Fig. 10 along the direction of the alignment (Fig. 11) indicates that with the increase of the time imposed on the magnetic field before quenching, the magnetization saturates more easily and saturation magnetization increases. This can be attributed to the reorientation of MnBi and improvement of the orientation of MnBi crystals.

4. Summary and conclusions

In the present investigation, the structure, the temperature T_C of PFT and magnetization behaviours have been measured on MnBi–Bi as a function of temperature and magnetic field. The effect of the magnetic field on the $Mn_{1.08}Bi$/MnBi (paramagnetic/ferromagnetic) phase transformation shows that the phase temperature T_C increases with the increase of the external magnetic field and under the field of 10 T, a typical increase of T_C is 20 °C during heating and 22 °C during cooling. Microstructure results show that three kinds of morphology of MnBi phase appeared in different temperature zones. In all these cases, the grains were orientated with the ⟨001⟩-crystal direction along the field direction and aggregated. Magnetic measurement shows a pronounced anisotropy

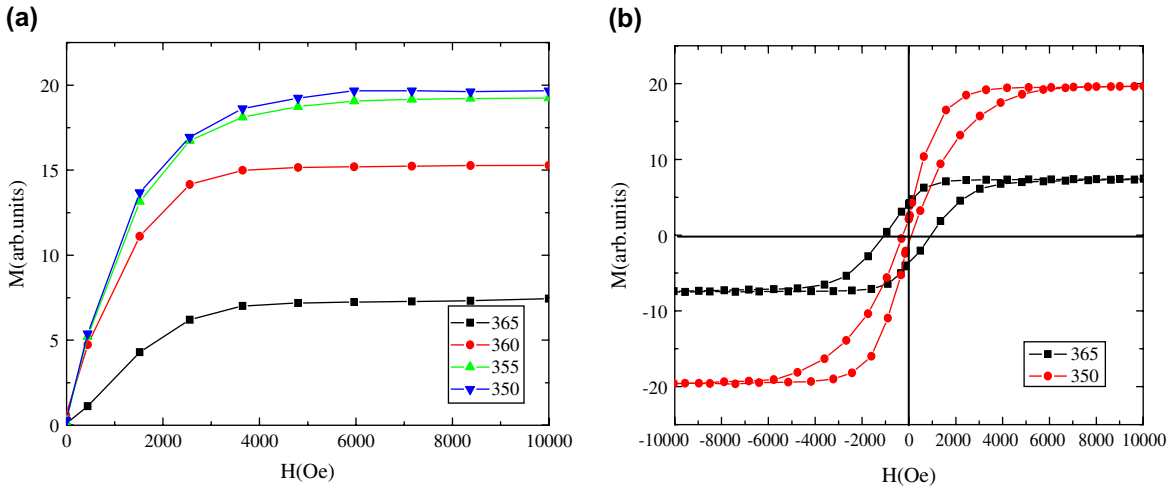

Fig. 9. (a) Magnetizations parallel to the fabrication field for the samples quenched at various temperatures under 10 T magnetic field; (b) hysteresis loops of samples quenched at 365 °C and 350 °C under 10 T magnetic field which are measured along the fabrication field H_f.

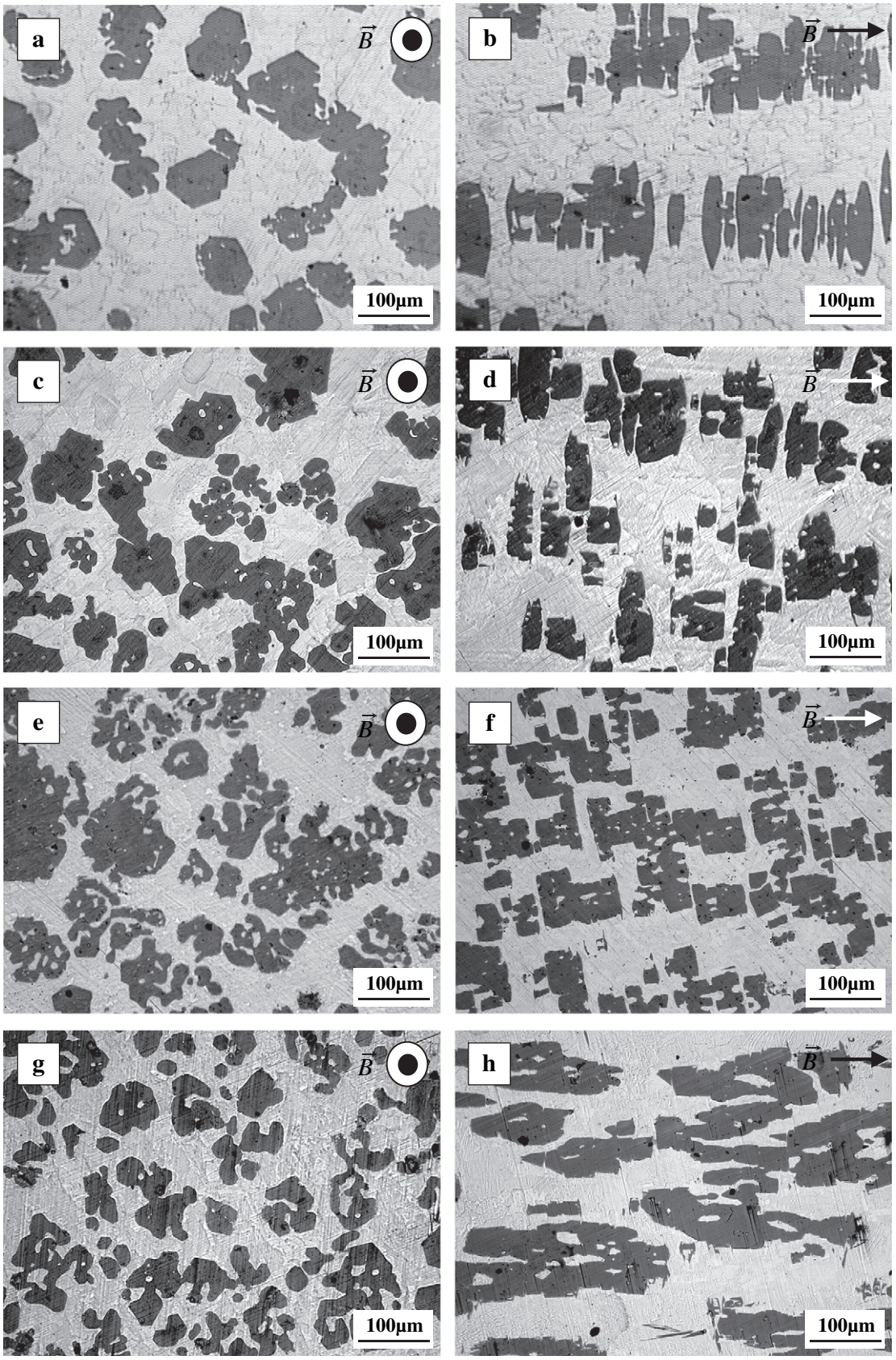

Fig. 10. Microstructures of Bi–6 wt% Mn alloys cooled from 400 °C to 350 °C and held for 5 min(a, b), 10 min(c, d), 30 min(e, f) and 60 min(g, h) and then quenched in a 10 T magnetic field.

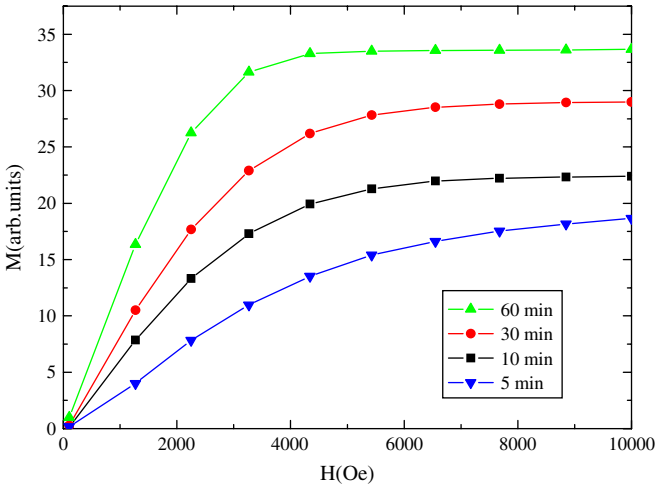

Fig. 11. Magnetizations parallel to the fabrication field H_f for the same samples as in Fig. 10.

in magnetization in directions perpendicular and parallel to the fabrication field, resulting from this alignment; and the remnant magnetization M_r and the coercive field H_C decrease with the phase morphology change from block-like phase to elliptical one. The change in the morphology and magnetic properties of MnBi phase is discussed from the phase transformation and the crystal structure change in a high magnetic field.

Acknowledgments

This work was financially supported by the Natural Science Foundation of China (nos. 50234020, 50225416 and 59871026) and the Science and Technology Committee of Shanghai and one of the authors (LX) is also grateful for an Egide/Eiffel Doctorate Scholarship.

References

[1] Rango PD, Lee M, Lejay P, Sulpice A, Tournier R, Ingold M, et al. Nature 1991;349:770.
[2] Joo HD, Kim SU, Shin NS, Koo YM. Mater Lett 2000;43:225.
[3] Zhang YD, He CS, Zhao X, Zhuo L, Esling C, He JC. J Magn Magn Mater 2005;294:267.
[4] Enomoto M, Guo H, Tazuker Y, Abe YR, Shimotomai M. Metall Mater Trans 2001;32A:445.
[5] Shimotomai M, Maruta K. Scripta Mater 2000;42:499.
[6] Chosh AK, Roy MN. Trans Indian Inst Met 1987;40:329.
[7] Asamitsu A, Moritomo Y, Tomioka Y, Arima T, Tokura Y. Nature 1995;373:407.
[8] Yang JB, Kamaraju K, Yelon WB, Jame W. J Appl Phys Lett 2001;79:1846.
[9] Xu YQ, Liu BC, Pettifor DG. Phys Rev B 2002;66:184435.
[10] Yang JB, Yelon WB, James WJ, Cai Q, Kornecki M, Roy S, et al. J Phy Condens Matter 2002;14:6509.
[11] Hihara T, Koi SY. J Phys Soc Jpn 1970;29:343.
[12] Chen T, Stutius W. IEEE Trans Magn 1974;10:581.
[13] Saha S, Obermyer RT, Zande BJ, Chandhok VK, Simizu S, Sankar SG, et al. J Appl Phys 2002;91:8525.
[14] Harder KU, Menzel D, Widmer T, Schoenes J. J Appl Phys 1998;84:3625.

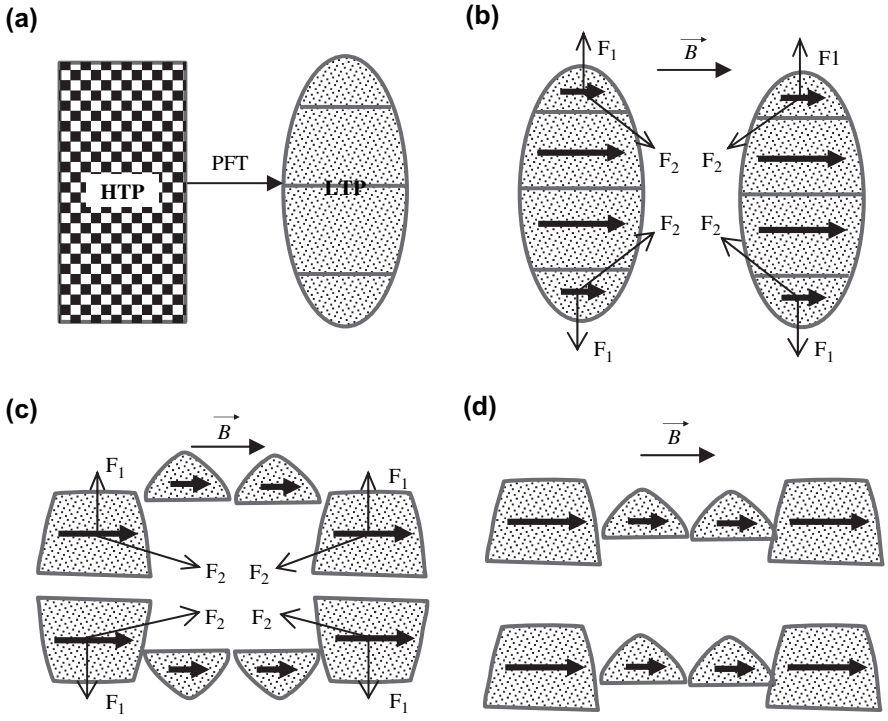

Fig. 12. Schematic diagram of the morphology changing process of MnBi crystal under a magnetic field. (a) The morphology change of MnBi phase during the phase transformation. (b) The magnetization and magnetic force of the crystal. (c) The tips of the crystal separating from the parent phase. (d) The reorientation of crystals and formation of the rod-like structure.

[15] Savitisky EM, Torchinova RS, Turanov SA. J Crystal Growth 1981;52:519.
[16] Sassa K, Yamao H, Asai S. In: Garnier M, editor. Proceedings of the international symposium on electromagnetic processing of materials, Paris; July 1997. p. 157.
[17] Morikawa H, Sassa K, Asai S. Mater Trans JIM 1998;39:814.
[18] Wang H, Ren ZM, Jiang GC. Mater Sci Eng 2001;19:119.
[19] Ren ZM, Li X, Wang H, Deng K, Xu KD. Mater Lett 2004;58:3405.
[20] Moffatt WG. The handbook of binary phase diagrams. USA: Genium; 1984.
[21] Kittel I. Introduction to solid-state physics. Moscow: GIFML Publ. House; 1963. p. 326.
[22] Liu S. J Appl Phys 1994;76:6757.
[23] Hallen E. Electromagnetic theory. London: Chapman & Hall Ltd; 1962. p. 233.

[A9] Xi Li, Zhongming Ren,Yves Fautrelle

Effects of the simultaneous imposition of electromagnetic and magnetic forces on the solidification structure of pure Al and Al-4.5wt.%Cu alloy,

Journal of Materials Processing Technology (In press).

ELSEVIER

Journal of Materials Processing Technology xxx (2007) xxx–xxx

Journal of Materials Processing Technology

www.elsevier.com/locate/jmatprotec

Effects of the simultaneous imposition of electromagnetic and magnetic forces on the solidification structure of pure Al and Al–4.5 wt.%Cu alloy

Xi Li [a,b,*], Zhongming Ren [a], Yves Fautrelle [b]

[a] *Department of Material Science and Engineering, Shanghai University, Shanghai 200072, PR China*
[b] *EPM-Madylam, ENSHMG BP 38402, St Martin d'Heres Cedex, France*

Received 14 September 2006; received in revised form 15 January 2007; accepted 19 April 2007

Abstract

Effects of the simultaneous imposition of an alternating current and a static magnetic field on the solidification structures of the pure Al and the Al–4.5 wt.%Cu alloy were investigated. The results show that the refined structure was gained by the application of the above complex fields. Owing to the fall of the refined nucleation during the electromagnetic vibration process (i.e. the formation of crystal rains), the refined structure was normally gained only at the bottom region of the sample. A method was proposed to restrain crystal rains by using an upward magnetic force and the results indicated that by using this method, the distribution of the refined grains was changed significantly. It was found that there existed a right magnetic force to make the whole sample refined; as a consequence, the uniformly refined structure was gained. In the case of the completely eliminating crystal rains, the effect of the electromagnetic force on the structure was investigated and result indicated that with the increase of the electromagnetic force density, the size of Al grains decreased and the depth of refinement zone increased. Moreover, the Al–4.5 wt.%Cu alloy was chosen to investigate the influence of the electromagnetic and magnetic forces on the growth of dendrite. It was observed that with the increase of the electromagnetic force density, the columnar dendritic structure changed into equiaxed ones that continued to disintegrate to isolated grains. Similar to the behavior of the pure Al, crystal rains formed during the electromagnetic vibration and could be restrained by using the magnetic force.

Keywords: Structure refinement; Electromagnetic force; Magnetic force; Distribution of the refined grains

1. Introduction

Many of the mechanical properties of metallic alloys depend on the size and distribution of grains in the structure. Therefore the structure refinement and the distribution of the refined grains have been the subject of numerous researches in the field of metallurgy. The structure is almost determined in the solidification process, so it is essential to control the solidification structure. Many different methods have been used for this purpose and the inoculation is a usual method. Though the inoculation can refine solidified structures, it is usually harmful for recycling of products because of added elements. The adoption of different combinations of electric and/or magnetic fields that are stationary and/or alternating has been investigated. Vives [1] studied the effect of electromagnetic vibrations induced by the interaction of alternating electric and static magnetic fields during the solidification of hypoeutectic Al–Si alloys and reported considerable microstructural refinement. Rajdai [2] investigated the effect of electromagnetic vibrations in hypereutectic Al–Si alloys and found that suspended silicon particles were crushed into small pieces by the cavitation phenomenon. Iwai and co-workers [3] studied the effect of the operating parameter on the solidified structure of the Sn–Pb alloy and concluded that the imposition of the electromagnetic force in the initial stage of the solidification was crucial to obtain the refined structure. Iwai and co-workers [4] and Wang [5] had researched the generation of compression and Alfvén waves by the simultaneously imposition of a static magnetic field and an alternating current and detected them in the liquid metal.

The purpose of the present work is to study the effect of the simultaneous imposition of electromagnetic and magnetic forces on the structure of pure metal and metallic alloy. For the pure Al and its Al–4.5 wt.%Cu alloy are useful and typical sub-

* Corresponding author at: EPM-Madylam, ENSHMG BP 38402, St Martin d'Heres Cedex, France.
E-mail address: xi@hmg.inpg.fr (X. Li).

0924-0136/$ – see front matter © 2007 Elsevier B.V. All rights reserved.
doi:10.1016/j.jmatprotec.2007.04.128

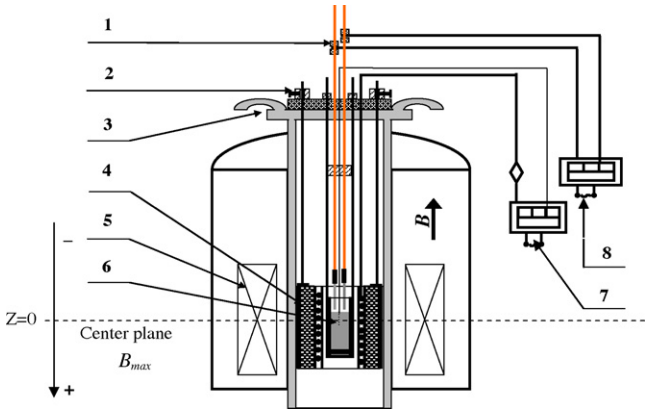

Fig. 1. Schematic diagram of the metal solidification experimental device in complex fields: (1) electric pole; (2) sample frame; (3) water-cool cover; (4) heat furnace; (5) superconductor magnet; (6) samples; (7) controlling temperature system; (8) ac electric source.

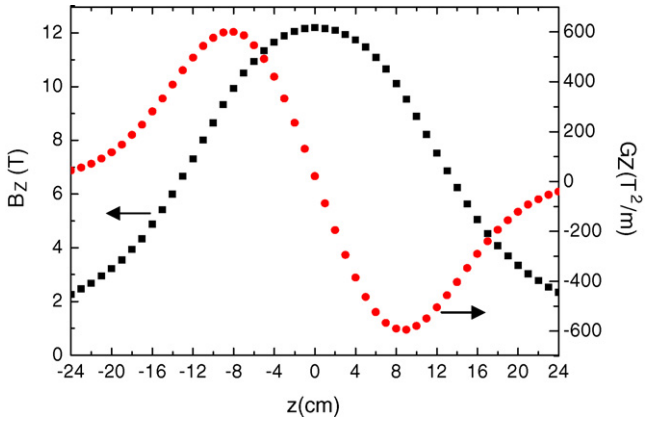

Fig. 2. Field profiles in the magnetic field operating at 12 T. B_z is the vertical (and only) component of the field on the axis of the coil. G_z is the vertical (and only) component of B_z dB_z/dz on the axis of the coil; z is the distance above the center of the coil.

stance, therefore they were chosen. Results show that the refined structures could be gained by the application of the electromagnetic force and the magnetic force was capable of restraining the formation of crystal rains and improving the distribution of the refining grains. Moreover, it was found that there existed a right magnetic force to make the entire sample refined; as a consequence, the uniformly refined structure was gained. The electromagnetic force has changed the original columnar dendritic structure in the Al–4.5 wt.%Cu alloy into one composed of large size equiaxed ones at lower intensity; and at the higher intensity changed the structure into the isolated grains.

2. Experimental device

The experimental apparatuses are shown in Fig. 1. A static magnetic field was imposed during all the experimental process by using a super-conducting magnet and the distribution of the field is shown in Fig. 2. Pure Al and Al–4.5 wt.%Cu alloy were prepared with high pure substance (4 N) in a vacuum induction furnace, and poured into a graphite mold to cast samples with

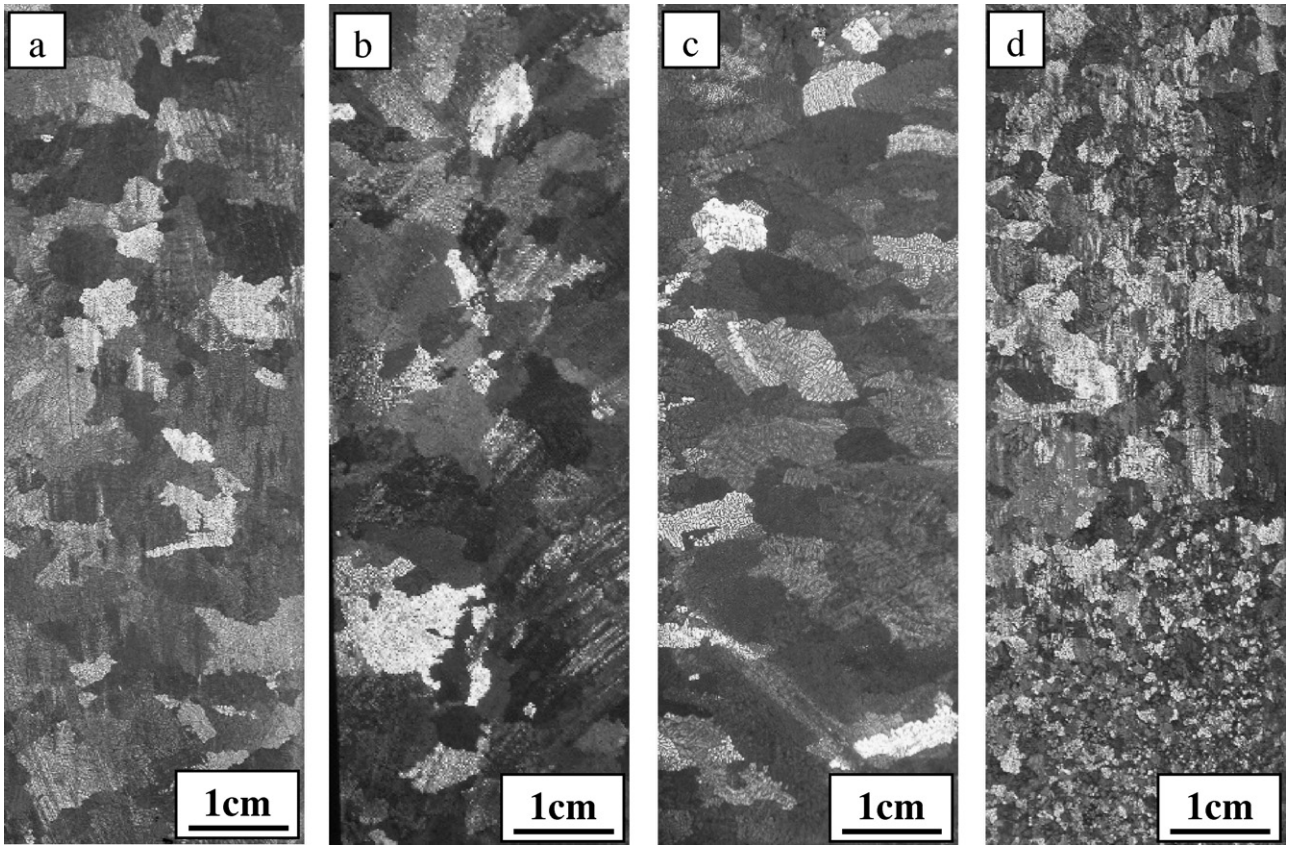

Fig. 3. Effects of a uniform magnetic field, alternating electric field with the frequency of 50 Hz and their complex fields on the structures of pure Al: (a) 0 T, 0 A; (b) 0 T, 10 A; (c) 10 T, 0 A; (d) 0.5 T, 10 A.

Please cite this article in press as: X. Li et al., Effects of the simultaneous imposition of electromagnetic and magnetic forces on the solidification structure of pure Al and Al–4.5 wt.%Cu alloy, J. Mater. Process. Tech. (2007), doi:10.1016/j.jmatprotec.2007.04.128

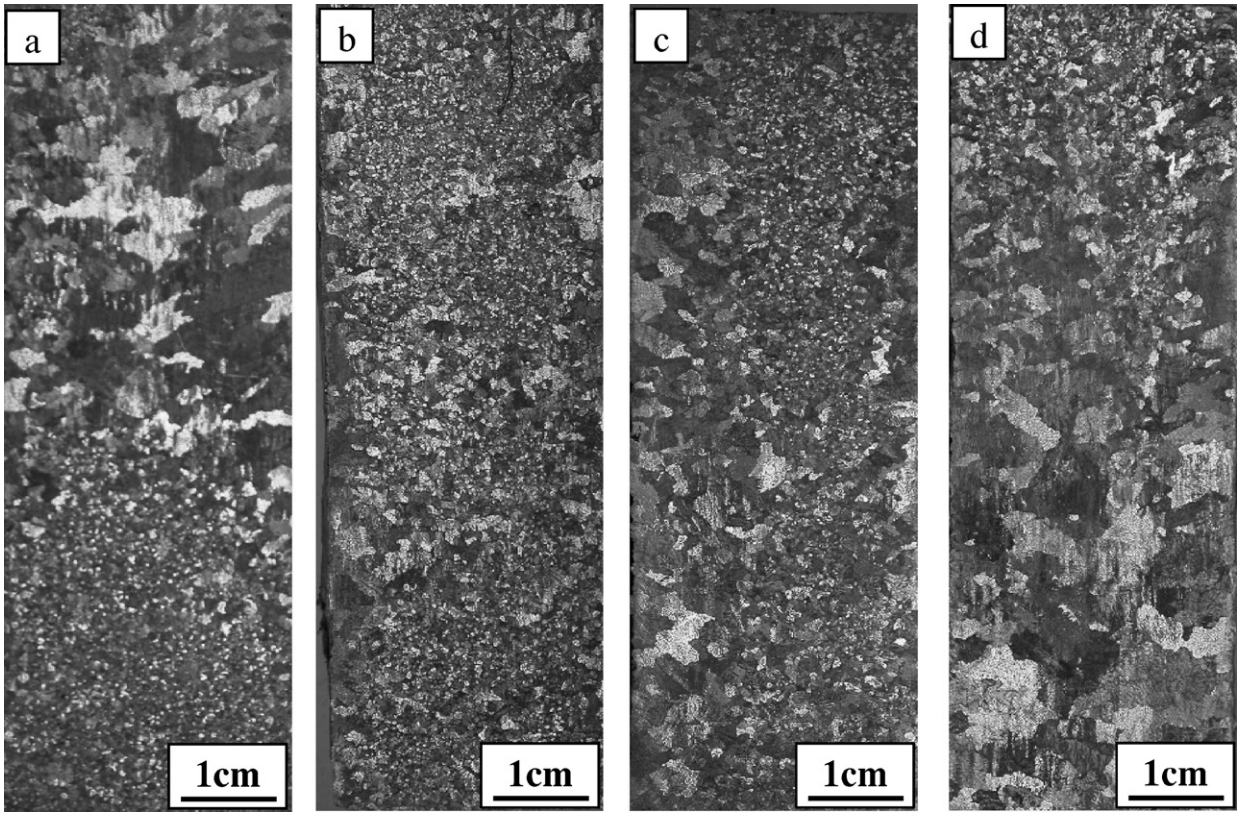

Fig. 4. Effects of a magnetic force on the structures of pure Al at the same electromagnetic force density: (a) $B = 0.5$ T and $B_z\,dB_z/dz = 0.95\ T^2/m$, $I = 20$ A; (b) $B = 1.5$ T and $B_z\,dB_z/dz = 8.5\ T^2/m$, $I = 6.5$ A; (c) $B = 2$ T and $B_z\,dB_z/dz = 16.2\ T^2/m$, $I = 5$ A; (d) $B = 6$ T and $B_z\,dB_z/dz = 150\ T^2/m$, $I = 1.6$ A.

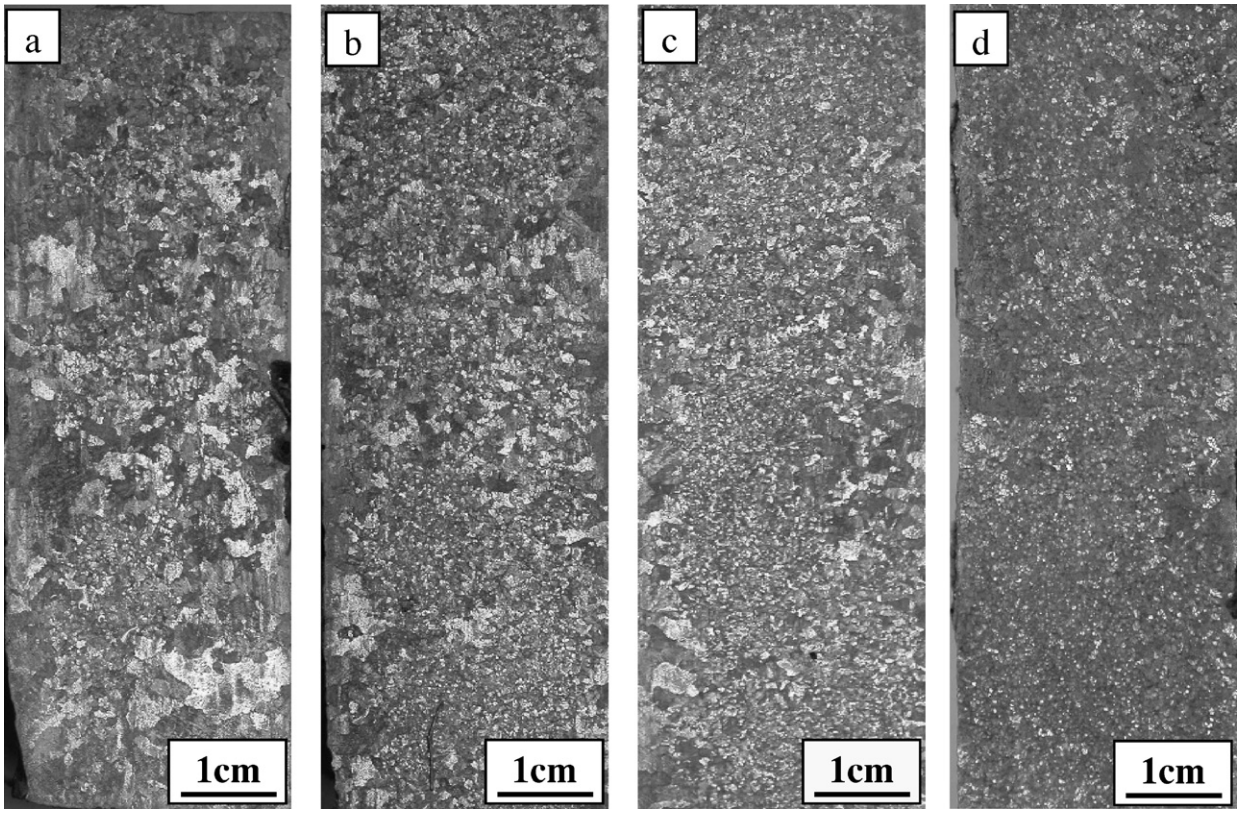

Fig. 5. Effect of the electromagnetic force on the structures of pure Al under the gradient magnetic field of $B = 1.5$ T, $B_z\,dB_z/dz = 8.5\ T^2/m$. (a) 1 A; (b) 4 A; (c) 7 A; (d) 10 A.

Please cite this article in press as: X. Li et al., Effects of the simultaneous imposition of electromagnetic and magnetic forces on the solidification structure of pure Al and Al–4.5 wt.%Cu alloy, J. Mater. Process. Tech. (2007), doi:10.1016/j.jmatprotec.2007.04.128

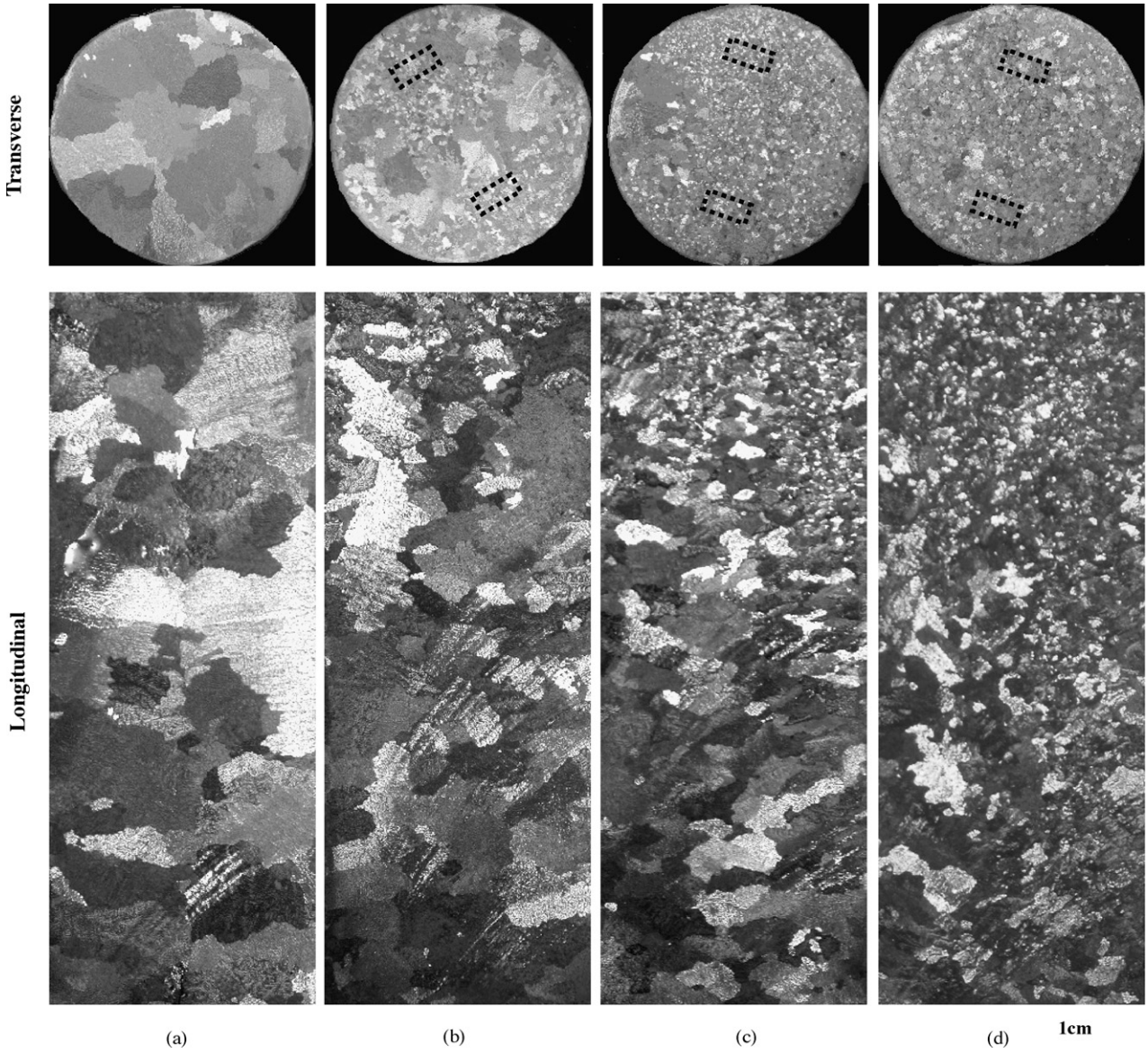

Fig. 6. Effect of the electromagnetic force on the structures under the gradient magnetic field of $B = 10\,T$, $B_z\,dB_z/dz = 400\,T^2/m$: (a) $I = 0\,A$; (b) $I = 1\,A$; (c) $I = 3\,A$; (d) $I = 10\,A$.

the diameter of 28 mm and length of 80 mm. Then, samples were placed in the alumina tube of almost the same inner diameter and set in a sample holding assembly; the assembly, being positioned at the different positions of the magnet. A removable resistance furnace was used to heat and melt the sample. In these experiments, samples were heated up to 750 °C and kept at this temperature for 30 min, which is enough to melt the sample completely; and then an alternating electrical current with the frequency of 50 Hz was supplied to the metal by inserting a couple of stainless steel electrodes at the top surface of the metal. The current was stopped until the sample was cooled to 600 °C. Temperature of the sample was measured by a K-type thermocouple that was put in direct contact with the sample and controlled by the controlling temperature equipment. The average cooling rate of sample was 20 °C/min.

Samples obtained from the experiment were cut at the position 2 mm from the electrode, and polished, etched and taken photos. Then, samples were cut along the electrode plane, polished, etched and taken photos. Samples of pure Al were etched with the solution composed of 90 ml HCL, 30 ml HNO_3, 30 ml HF and 50 ml H_2O and macrostructure photo was taken with a Leica. Samples of Al–4.5 wt.%Cu alloy were etched with the solution composed of 2.5 ml HNO_3, 1.5 ml HCL, 1 ml HF and 95 ml H_2O and microstructure was examined by using Leica optical microscope. The size of Al grains was evaluated by a computer-aided WT–MiVnt particle analyzer system.

3. Experimental results

3.1. Pure Al

Fig. 3 shows the structure in a static magnetic field, an alternating electric field with the frequency of 50 Hz and their complex fields. Fig. 3(b) and (c) shows the structure only imposed a single field. Comparison with the structure without any field (a) shows that the application of a single field (a 10 T magnetic field or a 10 A current with the frequency of 50 Hz) could not refine the structure. However, the simultaneous imposition of the magnetic field of 0.5 T and the alternating current of 10 A, the refined structure (d) was gained at the bottom region of the sample. This phenomenon should be attributed to the fall of the refined grains (i.e. crystal rains) during the electromagnetic vibration process.

Crystal rains usually lead to the uneven refined structure; therefore, it is necessary to restrain them. Owing to the difference in susceptibility between

Please cite this article in press as: X. Li et al., Effects of the simultaneous imposition of electromagnetic and magnetic forces on the solidification structure of pure Al and Al–4.5 wt.%Cu alloy, J. Mater. Process. Tech. (2007), doi:10.1016/j.jmatprotec.2007.04.128

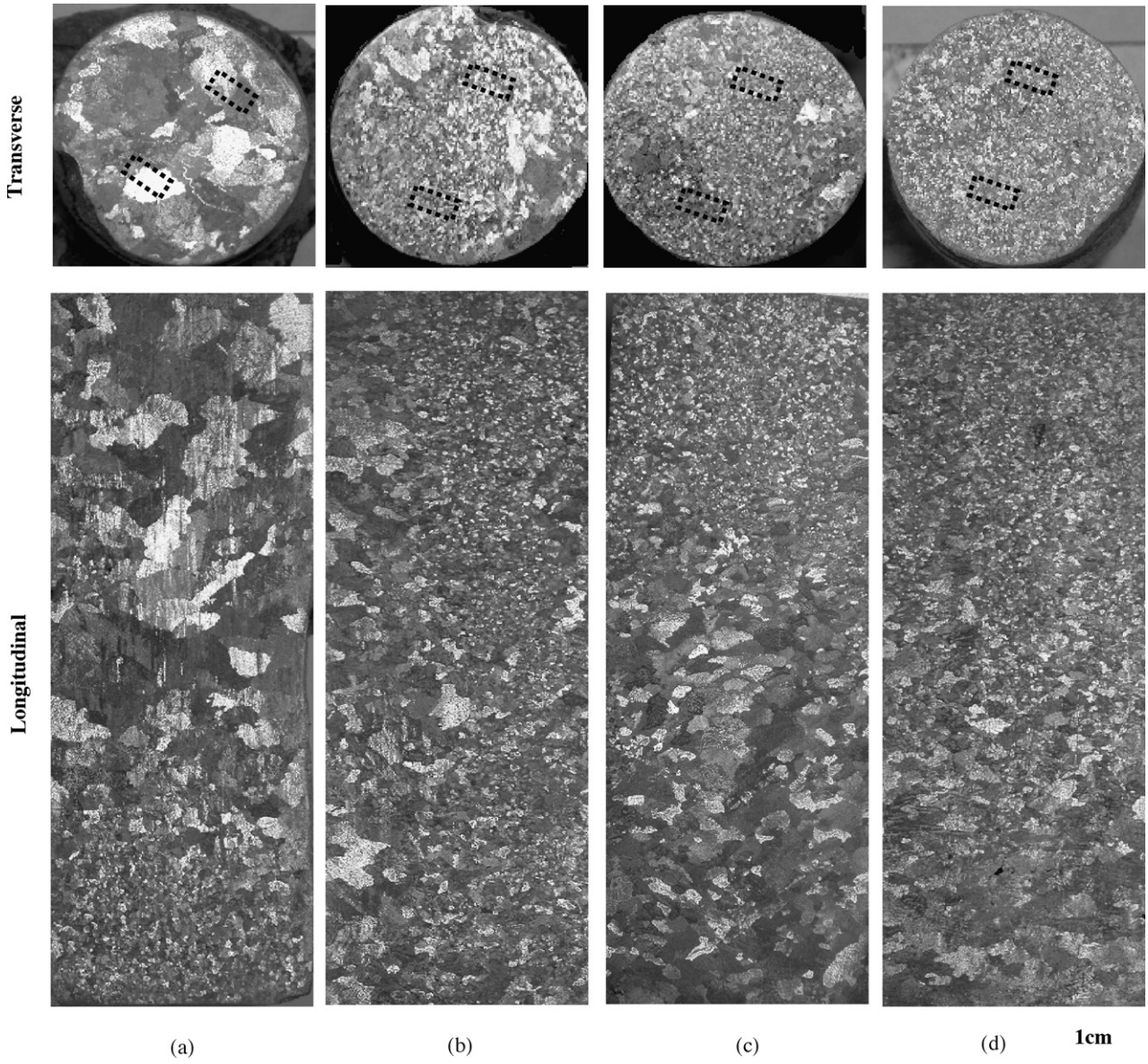

Fig. 7. Effect of the electromagnetic and magnetic forces on the structures under the same electric current density of 10 A with the frequency of 50 Hz (a) $B = 0.8$ T and $B_z\,dB_z/dz = 6.4\ T^2/m$, $I = 10$ A; (b) $B = 2$ T and $B_z\,dB_z/dz = 16.2\ T^2/m$, $I = 10$ A; (c) $B = 4$ T and $B_z\,dB_z/dz = 64.4\ T^2/m$, $I = 10$ A; (d) $B = 8$ T and $B_z\,dB_z/dz = 244.6\ T^2/m$, $I = 10$ A.

the liquid and the solid of the pure Al ($0 < \chi_L < \chi_S$), an upward effective magnetic force is applied on the solid Al when the sample is laid in a positive gradient magnetic field ($z > 0$). The magnetic force may restrain crystal rains and improve the distribution of the refining grains on the sample. Fig. 4 shows the structure with the same electromagnetic force density and various magnetic forces. Comparison of the structures indicates that with the increase of the magnetic force, the distribution of refining grains changes greatly. Under the complex fields of $B = 0.5$ T, $B_z\,dB_z/dz = 0.95\ T^2/m$ and $I = 20$ A, the structure (a) was refined only at the bottom of the sample. When imposed of the fields of $B = 1.5$ T, $B_z\,dB_z/dz = 8.5\ T^2/m$ and $I = 6.5$ A, the structure (b) was refined on the whole sample. Under the fields of $B = 2$ T, $B_z\,dB_z/dz = 16.2\ T^2/m$ and $I = 5$ A, the structure (c) was not refined at the margin of the sample. The structure was refined only on the top of the sample by the application of the fields of $B = 6$ T, $B_z\,dB_z/dz = 150\ T^2/m$ and $I = 1.6$ A (d). Indeed the above results prove that the application of the magnetization force has changed the distribution of the refined grains significantly. Moreover, it can be found that the application of the gradient field of $B = 1.5$ T, $B_z\,dB_z/dz = 8.5\ T^2/m$ has resulted in the refinement on the whole sample. Fig. 5 shows the structures solidified under complex fields of the gradient magnetic field of $B = 1.5$ T, $B_z\,dB_z/dz = 8.5\ T^2/m$ and alternating electric fields with various electric current densities. It can be observed that all samples were refined completely and with the increase of the current density, a decrease in size and increase in number of Al grains took place. This indicates that the gradient field of $B = 1.5$ T, $B_z\,dB_z/dz = 8.5\ T^2/m$ has offered a right magnetic force; as a consequence, crystal rains are restrained partly and part crystal grains fall and act as nucleuses of heterogeneous nucleation during the solidification process. Thus, the refining structure will be formed on the whole sample.

Since crystal rains have influenced the distribution of the refined grains; in order to investigate the effect of the electromagnetic force on the structures, it is necessary to eliminate the effect of crystal rains on the structure. From Fig. 4, it can be learned that the magnetic force under the gradient magnetic field of $B = 10$ T, $B_z\,dB_z/dz = 400\ T^2/m$ is enough to restrain crystal rains completely, therefore the structures under the gradient magnetic field of $B = 10$ T, $B_z\,dB_z/dz = 400\ T^2/m$ and various electric currents (Fig. 6) were investigated. Comparison of the structures in different conditions indicates that with the increase of the electric current, the size of Al grains decreased and the depth of

Please cite this article in press as: X. Li et al., Effects of the simultaneous imposition of electromagnetic and magnetic forces on the solidification structure of pure Al and Al–4.5 wt.%Cu alloy, J. Mater. Process. Tech. (2007), doi:10.1016/j.jmatprotec.2007.04.128

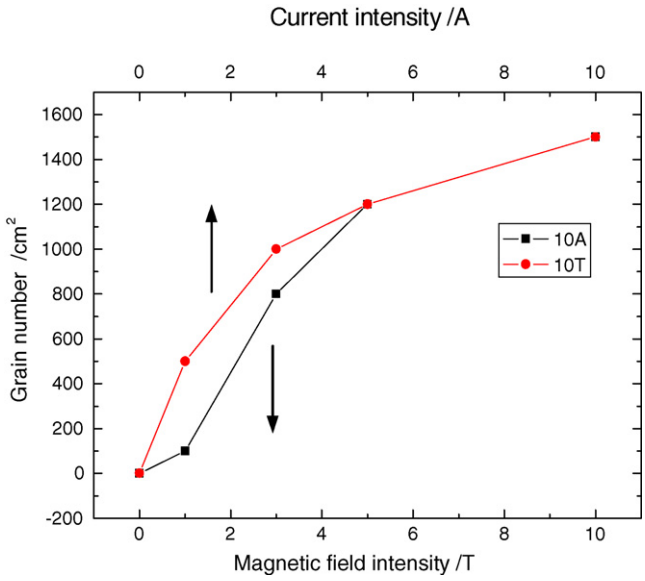

Fig. 8. The grains number on the transverse section at 2 mm position from the electrode as a function of current and magnetic field intensity.

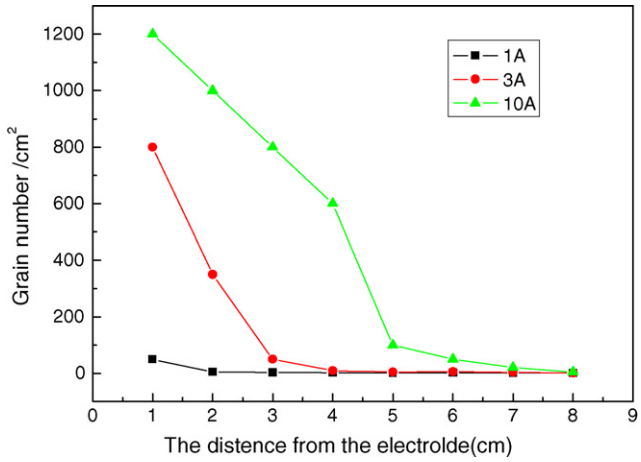

Fig. 9. The grains number on the longitudinal section as a function of the distance from the electrode under a gradient magnetic field of $B = 10\,T$, $B_z\,dB_z/dz = 400\,T^2/m$ and various current intensities.

refinement zone increased. This means that with the increase of the electromagnetic force density, the refining effect is enhanced.

Fig. 7 shows the structures solidified under complex fields of a certain alternating current of 10 A and various gradient magnetic fields. From the structures on the transverse sections, it can be observed that with the increase of the electromagnetic force, the size of the grains decreases. From the structures on the longitudinal sections, it can be learned that with the increase of the magnetic force, the distribution of refined grains was changed and the refining zone moved upward. This indicates that magnetic force and electromagnetic force should be responsible for the change of structure at the same time and agrees with the results in Figs. 4–6. In order to describe quantitatively the refinement, the average grain number per cm^2 of the sample was counted. Fig. 8 shows the grains number on the transverse section at 2 mm position from the electrode as a function of electrical magnitude and magnetic field intensity. It can be learned that with the increase of the electromagnetic force density, the number of the grain per the 1 cm^2 increases. Fig. 9 shows the grain number on the longitudinal section as a function of the distance from the electrode under the gradient magnetic field of $B = 10\,T$, $B_z\,dB_z/dz = 400\,T^2/m$ and various current intensities. It can be learned that with the increase of the distance from the electrode, the number of the grain per the 1 cm^2 decreases and the size of the grain increases; and with the increase of electric current, the number of the grain per the 1 cm^2 increased and the size of the grain decreased.

3.2. Al–4.5 wt.%Cu alloy

In order to investigate effects of the electromagnetic force and the magnetic force on the growth of dendrite, the microstructures of the Al–4.5 wt.%Cu alloy under complex fields were studied. Fig. 10 shows the microstructures on the transverse section at 2 mm from the electric pole. It can be noticed that under a single field (i.e. the magnetic field of 10 T or the current of 10 A), there are not obvious effects on microstructure [(b) and (c)]. However, simultaneous imposition of the magnetic field and the electric field, the microstructure was refined obviously. It can be observed that at lower electromagnetic force densities, complex fields changed the originally columnar dendritic structure into equiaxed ones (d); and at higher intensities, the irradiated structure was composed of fine fragmented dendrites (e) that continued to disintegrated into

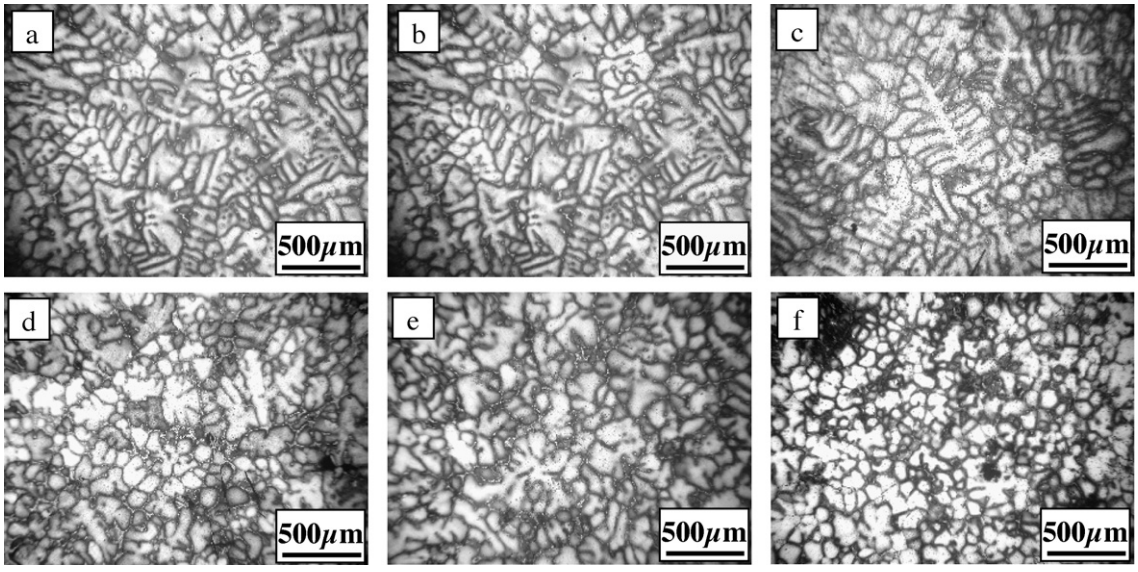

Fig. 10. Effect of an electromagnetic force on the solidification microstructure of Al–4.5 wt.%Cu alloy on the transverse section at the position 2 mm from the electric poles: (a) $B = 0\,T$, $I = 0\,A$; (b) $B = 0\,T$, $I = 10\,A$; (c) $B = 10\,T$, $I = 0\,A$; (d) $B = 10\,T$, $I = 1\,A$; (e) $B = 10\,T$, $I = 5\,A$; (f) $B = 10\,T$, $I = 10\,A$.

Please cite this article in press as: X. Li et al., Effects of the simultaneous imposition of electromagnetic and magnetic forces on the solidification structure of pure Al and Al–4.5 wt.%Cu alloy, J. Mater. Process. Tech. (2007), doi:10.1016/j.jmatprotec.2007.04.128

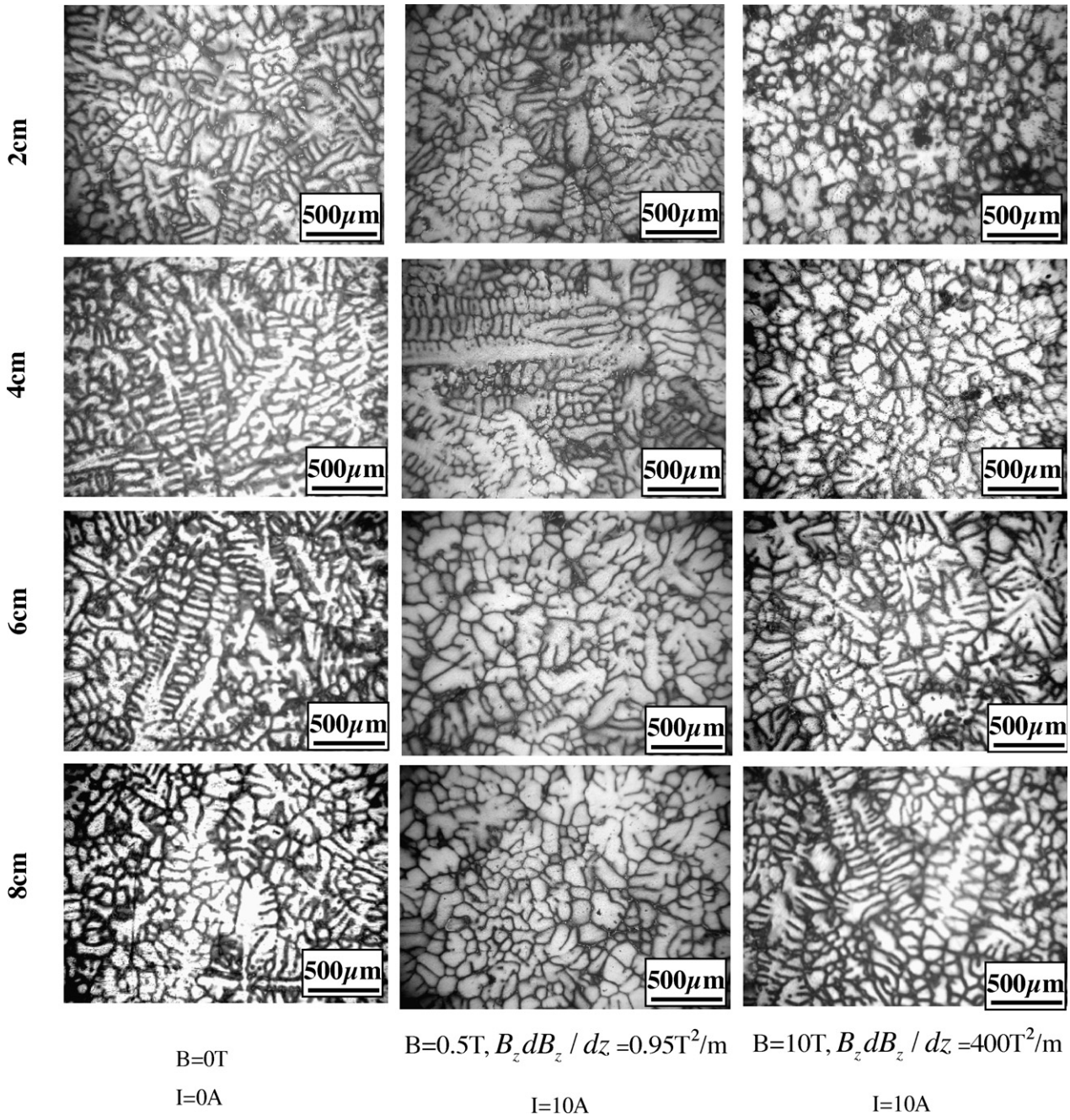

Fig. 11. Effect of the simultaneous imposition of electromagnetic and magnetic forces on the microstructure of Al–4.5 wt.%Cu alloy at various positions from the electric poles.

isolated grains as the current density was increased further (f). Fig. 11 shows the microstructures on longitudinal sections and it can be observed that the equiaxed and isolated structures were gained at the bottom of the sample under complex fields of $B = 0.5$ T, $B_z\, dB_z/dz = 8.5$ T^2/m and $I = 10$ A, which is similar to pure Al and should be attributed to crystal rains during the electromagnetic vibration. Imposed of complex fields of $B = 10$ T, $B_z\, dB_z/dz = 400$ T^2/m and $I = 10$ A, the refined structure was gained at the top of the sample and with the increase of the distance from the electric pole, the refining effect became weak. It can be observed that the isolated grains became large at the position of 4 cm and that the structure at 6 cm was composed of the large size equiaxed ones. When the depth increased to 8 cm, the structure became columnar dendrites. This indicates that the electromagnetic force is capable of breaking the dendrites of the Al–4.5 wt.%Cu alloy and the magnetic force could affect the distribution of the refined grains in the sample by restraining crystal rains.

4. Discussion

4.1. Refining mechanism

The refining mechanism should be attributed to the formation of the cavities during the electromagnetic vibrations [1]. The simultaneous imposition of a static magnetic field and an alternating current results in the induction of a vibrating electromagnetic field. When the electromagnetic vibrations are imposed in the molten metal, cyclic forces are induced which behaves as periodic forces of compression and tension and put the liquid into oscillatory motion. As a consequence, cavities can

Please cite this article in press as: X. Li et al., Effects of the simultaneous imposition of electromagnetic and magnetic forces on the solidification structure of pure Al and Al–4.5 wt.%Cu alloy, J. Mater. Process. Tech. (2007), doi:10.1016/j.jmatprotec.2007.04.128

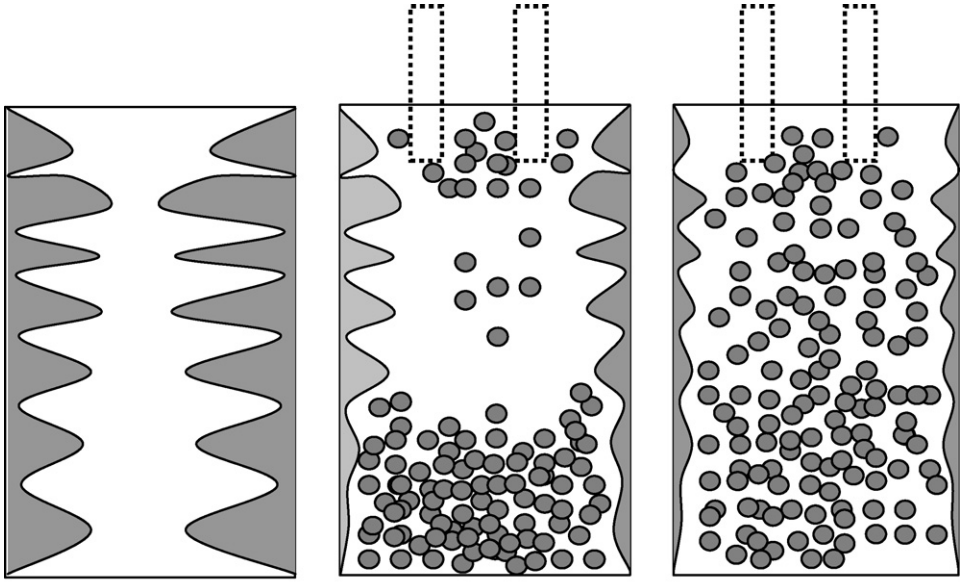

Fig. 12. Sketch map of crystal rains forming during the electromagnetic vibration and being restrained by the application of the magnetic force: (a) without fields; (b) the formation of crystal rains during the electromagnetic vibration; (c) restraint of crystal rain by the application of the magnetic force.

be formed. These cavities may then grow by absorbing gas or vapor during the tension period of the cyclic force and releasing a part of it during the compression period, and finally collapse to produce powerful shock waves by involution and jetting. Cavities was shown to be capable of building pressures of more than a thousand atmospheres in the ultrasonic experiment and the pressures can raise melting point many tens of degrees [5]; as a result, the vibration promotes nucleation in undercooled metals in this way and breaks the dendrite. Although Alfven and Magneto-acoustic waves can be propagated by the above complex fields; the measuring results in liquid metal showed that the pressure by the above waves was less than 1 atm [4]. The change in the equilibrium melting point (ΔT_P) from the change in applied pressure (ΔP) is quite small, i.e., on the order of 10^{-2} K/atm [6]. Hence, the pressure produced by the above waves has little influence on the melting point and nucleation. Consequently, it is reasonable to attribute the refinement of grains and the break of dendrites to the formation of the cavities.

4.2. Improving refining structure by controlling crystal rains

Above experimental results indicate that the magnetic force has influenced the distribution of the refined grains significantly. This should be attributed to the change of the effective gravitation under a gradient magnetic field. When imposed of above complex fields on the top of the sample, the nucleation will occur here firstly. Owing to the difference of the densities between the liquid and solid Al ($\rho_L < \rho_S$), the crystal nucleuses on the top will fall towards the bottom and the heterogeneous nucleation will occur at the bottom of the sample. Thus, the refined structure will produce at the bottom as shown in Fig. 12(b).

In our experiments, we used vertical coils, in which fields have an axial symmetry. We consider the case of the particle on the axis of the coil where only a vertical component B_z of the field exists. In this case, the vertical force F_z is

$$\vec{F}_z = \frac{\chi}{\mu_0} B_z \frac{\mathrm{d}B_z}{\mathrm{d}z} \tag{1}$$

where χ is the susceptibility; $B_z\,\mathrm{d}B_z/\mathrm{d}z$ the vertical component of the gradient magnetic field on the axis of the coil; z the distance above the center of the coil; μ_0 the permeability of the free space, and its value is $4\pi \times 10^{-7}$ H/m. The upward magnetic force produces at the positive gradient magnetic field ($z > 0$) for paramagnetic substance and at the negative gradient magnetic field ($z < 0$) for diamagnetic one. For the magnetic property of Al is paramagnetic and the susceptibility difference between the liquid and solid ($\chi_S > \chi_L$), the upwards magnetization force produces at the position $z > 0$. The effective magnetic force as following:

$$\vec{F}_V = (\chi_S - \chi_L)\frac{1}{\mu_0} B_z \frac{\mathrm{d}B_z}{\mathrm{d}z} \tag{2}$$

where χ_S and χ_L are the susceptibilities of the solid and liquid Al, respectively.

The effective gravitation without the field is

$$\vec{G}_V = (\rho_S - \rho_L)\vec{g} \tag{3}$$

Thus, the total force F acting on Al particles under a gradient magnetic field is

$$F = \vec{G}_V - \vec{F}_V = (\rho_S - \rho_L)\vec{g} - (\chi_S - \chi_L)\frac{1}{\mu_0} B_z \frac{\mathrm{d}B_z}{\mathrm{d}z} \tag{4}$$

This equation indicates that the effective gravitation is modified under a gradient magnetic field. Therefore the application of the

Please cite this article in press as: X. Li et al., Effects of the simultaneous imposition of electromagnetic and magnetic forces on the solidification structure of pure Al and Al–4.5 wt.%Cu alloy, J. Mater. Process. Tech. (2007), doi:10.1016/j.jmatprotec.2007.04.128

gradient magnetic field can restrain crystal rains and change the distribution of the refined grains [Fig. 12(c)].

5. Conclusions

1. During the simultaneous imposition of a static magnetic field with a magnetic flux density B and an alternating electric field with a current density J, a vibrating electromagnetic body force with a density of "$F = J \times B$" will be induced in the liquid. The application of electromagnetic vibration may lead into the formation and collapse of cavities, which will result in the refinement of grains and the break of dendrites.
2. For a long sample, if the electromagnetic force is imposed at the top, the refined grains will fall and form crystal rains; consequently, the refined structure may be gained only in the bottom of the sample. The application of a magnetic force can restrain crystal rains and control the refining structure effectively. The experimental result indicates that an appropriate magnetic force can enhance the structure to refine and improve the distribution of the refined grains.
3. In the case of the complete elimination of crystal rains, the effect of the electromagnetic force density on structure is investigated. The results show that with the increase of the electromagnetic force density, the size of the refined grains decreases and the depth of the refining zone increases.
4. For the Al–4.5 wt.%Cu alloy, it can be observed that with the increase of the electromagnetic force density, the columnar dendritic structure is changed into equiaxed ones that continued to disintegrate to isolated grains.

Acknowledgments

This work is supported by the European Space Agency through the IMPRESS project and the Natural Science Foundation of China (nos. 50234020, 50225416 and 59871026). One of the authors (LX) is also grateful for an Egide/Eiffel Doctorate Scholarship.

References

[1] C. Vives, Metall. Trans. B 27 (1996) 457–464.
[2] A. Rajdai, Kamiah, T. Nishio, Metall. Trans. A 29 (1998) 1477–1484.
[3] S. Kawai, Q. Wang, K. Iwai, S. Asai, Mater. Trans. JIM 42 (2001) 275–280.
[4] T. Kameyama, K. Sugiura, K. Iwai, S. Asai, Trans. Mater. Res. Soc. Jpn. 12 (2003) 255–258.
[5] H.E. Vatne, E. Nes, Scripta Metall. Mater. 30 (1994) 309–312.
[6] M.C. Flemings, Solidification Processing, McGraw, 1974.

Please cite this article in press as: X. Li et al., Effects of the simultaneous imposition of electromagnetic and magnetic forces on the solidification structure of pure Al and Al–4.5 wt.%Cu alloy, J. Mater. Process. Tech. (2007), doi:10.1016/j.jmatprotec.2007.04.128

Résumé

Dans cet article, des effets d'un champ magnétique élevé statique (jusqu'à 12T) sur la transformation liquide-pleine d'interface de l'alliage monophasé, la transformation de phase et la croissance eutectique ont été étudiés. D'ailleurs, des effets de la force magnétique sur la distribution de la phase et de la structure de raffinage pendant le procédé électromagnétique de vibration sont également étudiés.

L'Al-Cu, le hypo- Al-Ni, Bi-Manganèse et les alliages hypereutectic sont employés pour étudier des effets du champ magnétique sur les dendrites et la rangée, la transformation d'interface et la forme cellulaires. Les résultats indiquent que le champ cause l'interface être déstabilisée et irrégulier et favorisent la transformation planaire-cellulaire et cellulaire-dendritique. Le champ a une grande influence sur la morphologie cellulaire et de dendrite de rangée. En effet, le champ cause la déformation grave dans la rangée cellulaire et dendritique

Investigations sur des croissances de l'alliage eutectique lamellaire eutectique (Al2Cu-Al et Pb-Sn) et de tige (Bi-MnBi) sous une exposition élevée de champ magnétique qu'un champ magnétique élevé s'est dégénéré la structure lamellaire dans onduleuse à une basse vitesse de croissance et a changé le rapport préféré d'orientation. Cependant, le champ a augmenté la croissance de la fibre de MnBi le long de la direction de solidification et a augmenté l'espacement de fibre.

On l'a constaté que le champ a la transformation de phase de composés de MnBi/Mn1.08Bi. En conséquence, un champ 10T magnétique a soulevé la température de transformation de phase environ 20K. Le champ a changé la morphologie de phase de MnBi pendant la transformation de phase. Avec le changement de la morphologie, la propriété magnétique change de manière significative.

La distribution des grains de raffinage et de la phase primaire a été changée sensiblement en employant une force magnétique.

Abstract

In this paper, effects of a static high magnetic field (up to 12T) on liquid-solid interface transformation of the single phase alloy, the phase transformation and eutectic growth have been investigated. Moreover, effects of magnetic force on the distribution of the phase and refined structure during the electromagnetic vibration process are also studied.

Al-Cu, Al-Ni, Bi-Mn hypo- and hypereutectic alloys are used to study effects of the magnetic field on the dendrites and cellular array, interface transformation and shape. Results indicate that the field causes the interface to be destabilized and irregular and promotes the planar-cellular and the cellular-dendritic transformation. The field has a great influence on the cellular and dendrite array morphology. Indeed, the field causes severe distortion in the cellular and dendritic array

Investigations on growths of the lamellar eutectic (Al_2Cu-Al and Pb-Sn) and rod eutectic (Bi-MnBi) alloy under a high magnetic field show that a high magnetic field has degenerated the lamellar structure into a wavy one at a low growth speed and changed the preferred orientation relationship. However, the field has enhanced the growth of the MnBi fiber along the solidification direction and increased the fiber spacing.

It is found that the field has promoted the MnBi/$Mn_{1.08}$Bi compounds phase transformation. As a result, a 10T magnetic field has raised the phase transformation temperature about 20K. The field has changed the MnBi phase morphology during the phase transformation. Along with the change of the morphology, the magnetic property changes significantly.

The distribution of the refined grains and the primary phase was changed significantly by using a magnetic force.

Keyword: high magnetic field; single phase alloy; eutectic alloy; phase transformation; directional solidification.